

# **An investigation into ground improvement using geogrid encased stone columns**

**By**

**Joel Gniel**

**Bachelor of Civil Engineering (Hon. I)**

**A thesis submitted for the degree of Doctor of Philosophy**

**Department of Civil Engineering**

**Monash University, Australia**

**April 2009**

Under the Copyright Act 1968, this thesis must be used only under the normal conditions of scholarly fair dealing. In particular no results or conclusions should be extracted from it, nor should it be copied or closely paraphrased in whole or in part without the written consent of the author. Proper written acknowledgement should be made for any assistance obtained from this thesis.

# Table of contents

---

List of figures .....	viii
List of tables .....	xi
List of symbols .....	xii
Executive summary .....	xiii
Statement of originality .....	xv
Acknowledgements .....	xvi
Publications .....	xvii

<b>1</b>	<b>Introduction .....</b>	<b>1</b>
1.1	Background .....	1
1.2	Ground improvement.....	2
1.3	Conventional stone columns .....	3
1.4	Geosynthetic encased columns .....	3
1.5	Research hypothesis .....	5
1.6	Research aims .....	6
1.7	Discussion.....	6
1.7.1	Group and isolated column behaviour .....	6
1.7.2	Partial encasement .....	7
1.7.3	Method of overlap .....	7
1.7.4	Material properties.....	8
1.8	Methodology .....	8
1.8.1	Small-scale testing .....	9
1.8.2	Replication of small-scale test results.....	9
1.8.3	Medium-scale testing.....	9
1.8.4	Scaled-up numerical modelling.....	10
1.9	Organisation of thesis .....	10
<b>2</b>	<b>Literature review.....</b>	<b>12</b>
2.1	Ground improvement.....	12
2.1.1	Deep compaction .....	12
2.1.2	Consolidation.....	13
2.1.3	Stiffening columns.....	14
2.2	Conventional stone columns .....	15
2.2.1	Overview .....	15
2.2.2	History of use .....	17

2.2.3	Installation methods.....	17
2.2.4	Application.....	21
2.2.5	Aggregate size and density.....	24
2.3	Assessment of conventional stone column behaviour.....	24
2.3.1	Small-scale laboratory testing.....	24
2.3.2	Field and full-scale testing.....	31
2.3.3	Assessment of settlement reduction .....	34
2.3.4	Assessment of column capacity.....	44
2.4	Geosynthetic reinforced stone columns.....	46
2.4.1	Overview .....	46
2.4.2	Reinforcement methods .....	46
2.4.3	Geosynthetic reinforcement in horizontal layers.....	47
2.4.4	Geotextile encased columns (GECs) .....	50
2.4.5	Geogrid encased stone columns .....	56
2.5	Summary.....	59
2.6	Proposed research.....	60
<b>3</b>	<b>Small-scale laboratory tests .....</b>	<b>62</b>
3.1	Background .....	62
3.2	Apparatus design, construction and operation .....	63
3.2.1	Testing considerations .....	63
3.2.2	Cell construction.....	64
3.2.3	Cell operation .....	68
3.2.4	Formation of column and geogrid encasement .....	69
3.2.5	Sample loading.....	70
3.3	Materials .....	71
3.3.1	Kaolin clay .....	71
3.3.2	Quartz sand.....	77
3.3.3	Geogrid .....	81
3.4	Cell calibration.....	86
3.4.1	Components of cell friction.....	86
3.4.2	Summary .....	87
3.5	Test procedure.....	87
3.5.1	Slurry preparation .....	88
3.5.2	Cell preparation .....	88
3.5.3	Initial consolidation .....	88
3.5.4	Column construction.....	89
3.5.5	Column installation.....	91
3.5.6	Loading of column groups .....	92
3.5.7	Loading isolated columns .....	92
3.5.8	Test completion .....	93

3.6	Results of simulated column group tests .....	93
3.6.1	Test program .....	93
3.6.2	Sample properties .....	94
3.6.3	Vertical stress-strain behaviour .....	96
3.6.4	Column radial expansion .....	102
3.6.5	Stress concentration .....	104
3.6.6	Time rate of consolidation .....	104
3.7	Results of isolated column tests .....	108
3.7.1	Test program .....	108
3.7.2	Sample properties .....	109
3.7.3	Column loading .....	110
3.7.4	Column capacity .....	111
3.7.5	Column radial expansion .....	112
3.8	Method of overlap .....	113
3.8.1	Test program .....	114
3.8.2	Sample properties .....	114
3.8.3	Overlapped encasement behaviour .....	115
3.8.4	Summary .....	117
3.9	Discussion .....	118
3.9.1	Partial encasement .....	118
3.9.2	Comparison of group and isolated column behaviour .....	119
3.9.3	Influence of geogrid stiffness .....	120
3.9.4	Method of overlap .....	121
3.9.5	Vertical drainage .....	121
<b>4</b>	<b>Numerical modelling of small-scale test results .....</b>	<b>122</b>
4.1	Background .....	122
4.2	Modelling of small-scale tests .....	123
4.2.1	Kaolin .....	123
4.2.2	Modelling sand .....	128
4.2.3	Modelling geogrid .....	130
4.2.4	Modelling of group column tests .....	131
4.2.5	Modelling of isolated column tests .....	139
4.3	Summary .....	141
<b>5</b>	<b>Medium-scale laboratory tests .....</b>	<b>142</b>
5.1	Background .....	142
5.2	Materials .....	143
5.2.1	Columns .....	143
5.2.2	Geogrid .....	146
5.3	Column testing .....	149
5.3.1	Test schedule .....	149

5.3.2	Encasement construction.....	150
5.3.3	Column construction.....	151
5.3.4	Column loading .....	153
5.3.5	Instrumentation.....	155
5.3.6	Tank test.....	155
5.4	Test results .....	157
5.4.1	Typical test behaviour.....	157
5.4.2	Modes of column failure .....	158
5.4.3	Secugrid Q6 encasement (biaxial geogrid) .....	162
5.4.4	14/10 mm gravel and Combigrid tests .....	172
5.4.5	Secugrid R6 geogrids (uniaxial geogrids).....	175
5.4.5	Tensar TX 160 geogrid .....	180
5.5	Summary and discussion .....	182
5.5.1	Biaxial geogrids (Secugrid Q6 range) .....	182
5.5.2	Uniaxial geogrids (Secugrid R6 range).....	184
5.5.3	Other tests.....	184
5.5.4	Future research .....	185
<b>6</b>	<b>Extrapolation to full-scale columns .....</b>	<b>186</b>
6.1	Background.....	186
6.2	Base model.....	187
6.2.1	Clay.....	187
6.2.2	Stone column.....	189
6.2.3	Column installation.....	193
6.2.4	Effect of column diameter.....	193
6.2.5	Effect of mesh size.....	195
6.2.6	Loading of the unit-cell.....	196
6.2.7	Base model performance.....	196
6.3	Parametric study.....	197
6.3.1	Primary parametric study.....	197
6.3.2	Secondary parametric study .....	199
6.3.3	Results of primary parametric study.....	200
6.3.4	Results of secondary parametric study .....	207
6.4	Discussion.....	208
6.5	Summary.....	210
<b>7</b>	<b>Research findings and practical applications.....</b>	<b>212</b>
7.1	Research summary .....	212
7.1.1	Background .....	212
7.1.2	Research aims.....	213
7.1.3	Components of research.....	213
7.1.4	Methodology and observations .....	214

7.2	Discussion.....	220
7.2.1	Group and isolated columns.....	220
7.2.2	Partial encasement.....	220
7.2.3	Full-length encasement.....	221
7.2.4	Method of overlap.....	222
7.2.5	Geogrid properties.....	224
7.2.6	Practical applications.....	225
7.2.7	Construction methods.....	229
7.2.8	Cost.....	233
7.3	Further research.....	233
7.3.1	Scope of further research.....	234
7.3.2	Scope of proposed testing.....	235
7.3.3	Instrumentation.....	237
<b>8</b>	<b>Conclusions.....</b>	<b>239</b>
	<b>References .....</b>	<b>242</b>

## **Appendices**

Appendix A.1: small-scale test objectives and considerations

Appendix A.2: cell manufacture, instrumentation and safety

Appendix A.3: weld testing of mesh

Appendix A.4: cell calibration

Appendix B.1: PLAXIS soft soil model

Appendix C.1: medium-scale tests – load-compression and hoop strain results

Appendix D.1: primary parametric study – parameters

Appendix D.2: primary parametric study – charts

Appendix D.3: secondary parametric study – charts

## List of figures

---

Figure 2.1: Typical vibroflot (source: Keller Grundbau GmbH) .....	18
Figure 2.2: Vibro-replacement method .....	19
Figure 2.3: Vibro-displacement method.....	20
Figure 2.4: Bottom-feed method .....	21
Figure 2.5: Typical stone column shape following installation .....	22
Figure 2.6: Experimental and extrapolated test results, after Craig and Al-Khafaji (1997).....	28
Figure 2.7: Conical zone of influence under circular footing, after Muir-Wood et al. (2000).....	29
Figure 2.8: Greenwood curves, after Greenwood and Kirsch (1983) .....	35
Figure 2.9: Circular approximation of a stone column's zone of influence .....	36
Figure 2.10: Unit-cell idealisation of a stone column installed in soil.....	37
Figure 2.11: Priebe design curves, after Priebe (1995) .....	40
Figure 2.12: Horizontal reinforcement of granular columns.....	48
Figure 2.13: Installation of GECs using the replacement method.....	51
Figure 2.14: Installation of GECs using the displacement method .....	52
Figure 2.15: Geogrid encased column installation .....	56
Figure 2.16: Conventional welding of horizontal geogrid ribs .....	58
Figure 2.17: Excavated geogrid encased stone column.....	59
 Figure 3.1: Sketch of adopted consolidation cell design.....	 67
Figure 3.2: Consolidation cells used in model column testing.....	67
Figure 3.3: Concept of slurry consolidation within the cell .....	69
Figure 3.4: Concept of simulated column group loading and isolated column loading .....	70
Figure 3.5: e-log pressure behaviour of kaolin slurry .....	73
Figure 3.6: Moisture content – undrained shear strength relationship for kaolin clay .....	76
Figure 3.7: Void ratio – undrained shear strength relationship for kaolin clay .....	76
Figure 3.8: Shear stress – displacement relationship for kaolin clay .....	77
Figure 3.9: Mohr-Coulomb failure envelope for kaolin clay .....	77
Figure 3.10: Particle size distribution for Grade 8/16 sand.....	78
Figure 3.11: Shear stress – displacement relationship for Grade 8/16 sand.....	79
Figure 3.12: Mohr-Coulomb failure envelope for Grade 8/16 sand.....	80
Figure 3.13: e-log pressure behaviour of Grade 8/16 sand derived from oedometer testing .....	81
Figure 3.14: Load-strain relationship for fibreglass mesh.....	83
Figure 3.15: Load-strain relationship for aluminium mesh.....	84
Figure 3.16: Welded seam of a fibreglass mesh.....	89
Figure 3.17: Column constructed with a half circumference of fibreglass mesh overlap .....	90
Figure 3.18: Frozen sand column with 75% fibreglass encasement.....	90
Figure 3.19: Installation of a frozen model sand column.....	91



Figure 3.20: Vertical stress-strain relationship for column group tests.....	97
Figure 3.21: Approximate vertical strain reduction for column group tests .....	98
Figure 3.22: Extruded aluminium mesh (50% encased column).....	100
Figure 3.23: Extruded fibreglass mesh (75% encased column) .....	101
Figure 3.24: Extruded meshes, 100% fibreglass (top) and 100% aluminium (bottom) .....	102
Figure 3.25: Photographs of extruded group column samples.....	103
Figure 3.26: Comparison of consolidation time rate for group column tests.....	105
Figure 3.27: Clay ingress into column cross-sections, GC-4 (left) and GC-6 (right) .....	106
Figure 3.28: Vertical stress-strain relationship for isolated column tests.....	112
Figure 3.29: Photographs of extruded isolated columns .....	113
Figure 3.30: Vertical stress-strain relationship for group columns with overlapped encasement.....	116
Figure 3.31: Extruded mesh of group column with overlapped encasement (GC-11).....	116
Figure 3.32: Vertical stress-strain relationship for isolated column with overlapped encasement .....	117
Figure 4.1: e-log pressure behaviour of Soft Soil model compared to kaolin tests.....	126
Figure 4.2: Rate of primary consolidation in numerical models compared to oedometer tests .....	127
Figure 4.3: Rate of primary consolidation in numerical models compared to large cell test.....	127
Figure 4.4: e-log pressure behaviour of Hardening Soil model compared to sand tests .....	129
Figure 4.5: Axisymmetric model of cell geometry at various stages of testing .....	132
Figure 4.6: Numerical compression behaviour compared to fibreglass encased test results.....	133
Figure 4.7: Numerical compression behaviour compared to aluminium encased test results .....	134
Figure 4.8: Comparison of numerical and measured radial column expansion .....	135
Figure 4.9: Calculated hoop forces in fibreglass mesh using numerical analysis .....	136
Figure 4.10: Calculated hoop forces in aluminium mesh using numerical analysis .....	136
Figure 4.11: Comparison of numerical consolidation time rates to column test results.....	139
Figure 4.12: Numerical compression behaviour compared to isolated column test results .....	140
Figure 5.1: Particle size distribution of 20/50 mm rubble.....	144
Figure 5.2: Set up of large shear box .....	145
Figure 5.3: Particle size distribution of 14/10 mm gravel.....	146
Figure 5.4: Concept of machine and cross-machine direction .....	147
Figure 5.5: Photographs of the different geogrid products used for encasement construction .....	148
Figure 5.6: Encasement sleeve used for column test No. 2.....	151
Figure 5.7: Compacted column prepared for test No.2, comprising 20/50 mm rubble.....	152
Figure 5.8: Column wrapped with plastic film to retain 14/10 mm gravel (test No. 15) .....	153
Figure 5.9: Compressive column test in Amsler apparatus.....	154
Figure 5.10: Strain gauge attached to the upper section of the encasement.....	155
Figure 5.11: Encased column prepared for tank testing.....	156
Figure 5.12: Circumferential strain behaviour for a typical column test.....	158
Figure 5.13: Failure mode 1 (test No. 6) .....	159

Figure 5.14: Failure mode 2 (test No. 15).....	160
Figure 5.15: Failure mode 3 (test No. 4).....	160
Figure 5.16: Load-compression behaviour of columns encased with Secugrid 60/60.....	162
Figure 5.17: Strain and load measurements for columns encased with Secugrid 60/60.....	163
Figure 5.18: Partial cutting of horizontal ribs.....	164
Figure 5.19: Load-compression behaviour of Secugrid 80/80 columns.....	165
Figure 5.20: Strain and load measurements for columns encased with Secugrid 80/80.....	165
Figure 5.21: Load-compression behaviour of large diameter column (Secugrid 80/80).....	167
Figure 5.22: Load-compression behaviour of columns encased with Secugrid 120/120.....	168
Figure 5.23: Strain and load measurements for columns encased with Secugrid 120/120.....	168
Figure 5.24: Load-compression behaviour of columns encased with Secugrid Q6 geogrids.....	171
Figure 5.25: Strain and maximum load for columns encased with Secugrid Q6 geogrids.....	171
Figure 5.26: Failed geotextile encased columns, test No. 5 (left) and test No. 7 (right).....	173
Figure 5.27: Load-compression behaviour of columns constructed from 14/10 mm gravel.....	174
Figure 5.28: Strain and maximum load for columns constructed from 14/10 mm gravel.....	174
Figure 5.29: Load-compression behaviour of columns constructed from Secugrid R6 encasement ...	177
Figure 5.30: Strain and maximum load for columns constructed from Secugrid R6 encasement .....	177
Figure 5.31: Location of strain gauges in tests with different amounts of overlap.....	179
Figure 5.32: Load-compression behaviour of column constructed from TX 160 encasement.....	181
 Figure 6.1: Compressibility of numerical CIS model compared to oedometer test results.....	 188
Figure 6.2: Summary of one-dimensional consolidation tests undertaken on rockfill.....	190
Figure 6.3: Comparison of Mohr-Coulomb model to Hardening Soil model in small-scale test.....	192
Figure 6.4: Comparison of cell behaviour for constant column and cell diameter approaches.....	195
Figure 6.5: Impact of mesh size on strain behaviour of unit-cell.....	195
Figure 6.6: Behaviour of lightly compacted stone column installed in CIS.....	197
Figure 6.7: Example chart of strain reduction plotted against replacement ratio.....	201
Figure 6.8: Example chart of hoop forces generated in geogrid encasement.....	202
Figure 6.9: Hoop forces for partially encased columns.....	202
Figure 6.10: Axial strain reduction versus pressure for encased columns in base model .....	206
 Figure 7.1: Reducing the step in differential settlement.....	 228
Figure 7.2: Partial encasement for sites with layered stratum.....	229
Figure 7.3: Replacement installation of geogrid encased stone columns.....	231
Figure 7.4: Prefabricated geogrid sleeves (welded).....	232
Figure 7.5: Displacement installation method during site trial .....	232

## List of tables

---

Table 2.1: Prominent design methods used for assessment of settlement reduction.....	44
Table 3.1: Objectives of small-scale modelling.....	63
Table 3.2: Atterberg limits for kaolin Grade HR1F.....	72
Table 3.3: Particle size distribution of kaolin Grade HR1F.....	72
Table 3.4: Consolidation properties of kaolin slurry.....	74
Table 3.5: Minimum and maximum dry density of Grade 8/16 sand.....	79
Table 3.6: Compressibility parameters for Grade 8/16 sand.....	81
Table 3.7: Summary of soaked properties of fibreglass and aluminium mesh.....	86
Table 3.8: Tests performed to assess encased group column behaviour.....	94
Table 3.9: Kaolin clay properties for column group testing.....	95
Table 3.10: Sand column properties for column group testing.....	96
Table 3.11: Average vertical strain reduction for column group tests.....	99
Table 3.12: Maximum radial expansion of group columns.....	103
Table 3.13: Moisture content of group column samples following test completion.....	107
Table 3.14: Tests undertaken to assess encased isolated column behaviour.....	108
Table 3.15: Kaolin clay properties for isolated column tests.....	109
Table 3.16: Sand column properties for isolated column tests.....	110
Table 3.17: Tests performed to assess the method of overlap.....	114
Table 3.18: Kaolin clay properties for overlapped encasement tests.....	115
Table 3.19: Sand column properties for overlapped encasement tests.....	115
Table 4.1: Kaolin properties used in numerical modelling.....	124
Table 4.2: Sand properties used in numerical modelling.....	128
Table 4.3: Properties of fibreglass and aluminium mesh used for numerical modelling.....	130
Table 5.1: Minimum and maximum dry density of 20/50 mm rubble.....	144
Table 5.2: Secugrid technical data supplied by the manufacturer.....	147
Table 5.3: Properties of columns prepared for testing.....	149
Table 5.4: Results of column tests.....	161
Table 6.1: Properties of CIS used in numerical model.....	188
Table 6.2: Properties of lightly compacted stone column material used in numerical model.....	192
Table 6.3: Unit-cell geometry for constant column and cell diameter approaches.....	194
Table 6.4: Parameters investigated in the primary study.....	198
Table 6.5: Properties of soil models used in the secondary parametric study.....	200
Table 6.6: Summary of the impact of parameters on encased column behaviour.....	209
Table 7.1: Proposed future laboratory and site testing.....	235

## List of symbols

---

Symbols commonly used throughout this thesis are set out below:

$A_c$	Cross sectional or surface area of soil (clay)
$A_r$	Replacement ratio
$A_{sc}$	Cross sectional or surface area of stone column
$A_t$	Total surface area supported by one stone column
$C_c$	Compression index
$C_r$	Recompression/swelling index
$c_u$	Undrained cohesion
$\delta_{treated}$	Settlement of stone column treated soil
$\delta_{untreated}$	Settlement of untreated soil (clay)
$D_e$	Effective diameter of stone column
$D_{sc}$	Diameter of stone column
$e$	Void ratio
$EA$	Elastic axial stiffness
$E_{column}/E_{sc}$	Young's modulus of stone column
$E_{soil}/E_c$	Young's modulus of soil (clay)
$K_{a,c}$	Active earth pressure coefficient – soil (clay)
$K_{a,sc}$	Active earth pressure coefficient – stone column
$K_{p,c}$	Passive earth pressure coefficient – soil (clay)
$K_{p,sc}$	Passive earth pressure coefficient – stone column
$L$	Length of stone column
$\nu$	Poisson's ratio
$n$	Improvement factor
$\eta$	Stress concentration ratio
$\varphi_{sc}$	Internal angle of friction of stone column aggregate
$\varphi_c$	Internal angle of friction of soil (clay)
$\sigma_{v,t}$	Vertical stress applied to stone column treated soil
$\sigma_{v,c}$	Vertical stress in soil (clay)
$\sigma_{v,sc}$	Vertical stress in stone column
$\rho_{min}$	Minimum dry density
$\rho_{max}$	Maximum dry density
$s$	Centre to centre spacing of stone columns
$s_u$	Undrained shear strength
$t_{90}$	Time taken to complete 90% consolidation
$u$	Excess pore pressure

## Executive summary

---

Conventional stone columns are commonly used as a form of ground improvement in soft soils, for the support of lightly and moderately loaded structures such as embankments. However, their use in very soft and extremely soft soils is limited by the low stiffness and minimal confinement provided by the soft soil. To extend their use to such soft soils, a method of geotextile encasement has recently been developed, providing additional circumferential confinement. The technique has been used on numerous projects throughout Europe and more recently in South America. Although geotextile encasement provides a practical form of ground improvement, its use can be limited in some cases by excessive settlements, resulting from the adopted materials and installation practices. To investigate the potential benefits of using a stiffer encasement than geotextile (and to broaden the appeal of geosynthetics in ground improvement), the use of geogrid encasement is investigated.

The research presented in this thesis was used to investigate practical aspects of geogrid encasement including developing effective and efficient methods of encasement construction and assessment of encased column performance. The research was undertaken using a four-stage approach comprising small-scale laboratory testing, numerical simulation of small-scale tests, medium-scale laboratory testing and scaled-up numerical modelling of full-scale columns. Small-scale testing was undertaken on isolated and simulated group columns to investigate whether the full-length of the column needed to be encased, the impact of geogrid stiffness and methods of constructing the encasement. Numerical modelling was undertaken using the PLAXIS software package and was initially used to reproduce the small-scale test results. Following this, the models were scaled up to investigate the impact of different parameters on full-scale encased column behaviour. Medium-scale testing of unconfined columns was used to investigate methods of encasement construction including the suitability of different geogrids and stone column aggregates.

The research indicates that geogrid encasement can be constructed at relatively low cost and most effectively by constructing sleeves with a full circumference of overlap, fixed in position using cable ties. The technique relies on interlock between the overlapped section

of geogrid and protruding aggregate to provide a level of fixity similar to welding. Biaxial geogrids provide the stiffest and most reliable encasement material, particularly when used with typical stone column aggregates.


Based on the results of modelling and testing, geogrid encased columns are expected to reduce untreated settlements by between 50% and 95%, depending on properties such as geogrid stiffness, column density, soil stiffness and encased length. By progressively increasing the replacement ratio, geogrid stiffness and the encased length of a column, the stiffness of the treated soil mass may be steadily increased. Although the research indicates that geogrid encasement is likely to provide a stiffer alternative to geotextile, site testing is recommended to confirm some aspects of performance, including installation techniques.

## Statement of originality

---

This thesis contains no material which has been accepted for the award of any other degree or diploma in any university or other institution and affirms that to the best of my knowledge, the thesis contains no material previously published or written by another person, except where due reference is made in the text.

I certify that I have made all reasonable efforts to secure copyright permissions for third-party content included in this thesis and have not knowingly added copyright content to my work without the owner's permission.



JOEL GNIEL

## Acknowledgements

---

First and foremost I wish to thank my two supervisors, Assoc. Prof. Malek Bouazza and Dr Chris Haberfield. Their support and friendship has been very much appreciated.

The research presented in this thesis was funded by an Australian Research Council Linkage Grant and by NAUE GmbH and Frankipile Australia Pty Ltd (Keller Ground Engineering). Their support is gratefully acknowledged, particularly the valuable assistance provided by Professor Georg Heerten and Mr Henning Ehrenberg of NAUE.

The university staff have been of valuable assistance, especially those in the Civil Engineering workshops and laboratories involved with designing and constructing test apparatus and providing support for laboratory tests. In particular, I wish to thank Mike Leach, Alan Taylor and Carl Hemmings. Jenny Manson provided a valuable guide through the maze of postgraduate paperwork. Theresa Andrejack of Drexel University also provided assistance in the laboratory during her visit to Australia.

I also wish to thank Golder Associates Pty Ltd for their support, particularly in providing me with the opportunity to undertake postgraduate studies and helping me to attend several overseas conferences.

Finally, I wish to thank my wife, Kate, for her unconditional support, encouragement and assistance.



## Publications

---

The following papers were published as part of the research set out in this thesis:

- Gniel, J. & Bouazza, A. (2007) Methods used for the design of conventional and geosynthetic reinforced stone columns. Proceedings of 10th Australia New Zealand Conference on Geomechanics, Brisbane, Australia. pp. 72 – 77.
- Gniel, J. & Bouazza, A. (2008) Numerical modelling of small-scale geogrid encased sand column tests. Proceedings of 2nd International Workshop on Geotechnics of Soft Soils – Focus on Ground Improvement, Glasgow, Scotland.
- Gniel, J. & Bouazza, A. (2008) Model tests on geogrid encased stone columns. Proceedings of 4th European Conference on Geosynthetics, Edinburgh, Scotland.
- Gniel, J. & Bouazza, A. (2008) Predicted site behaviour of geogrid encased stone columns. Proceedings of 8th Young Geotechnical Professionals Conference, Wellington, New Zealand.

This paper was awarded the Don Douglas Youth Fellowship, presented to the Australian Geomechanics Society member who was judged to present the best paper by a delegate from Australia. The award recipient receives financial assistance to attend the International Young Geotechnical Engineers Conference (iYGEC) in Cairo, Egypt, 2009.

- Gniel, J. & Bouazza, A. (In Press) Improvement of soft soils using geogrid encased stone columns. Geotextiles and Geomembranes (2008), doi:10.1016/j.geotexmem.2008.11.001.

Several papers have also been prepared for journal publication and are in various stages of submission and review.

# **1 Introduction**

---

Sites comprising soft soils with poor engineering properties lend themselves to a range of ground improvement techniques. Some of these techniques have been practiced for many years, with aspects such as design and construction being well established. Other methods are relatively new and are continually being developed and improved. Ground improvement of soft cohesive soils using conventional stone columns has been a relatively new innovation, becoming popular in the last forty years. In this time, the technique has become widely used on many projects to support lightly and moderately loaded structures, but is generally not suited to very soft and extremely soft soils.

To extend the use of stone columns to soils of very low strength, geosynthetic reinforcement has been investigated, with a method of geotextile encasement being recently developed. The technique has become established in the last decade and its use has generally been limited to western Europe, with the exception of a project recently completed in South America. As a result, there is opportunity for researchers to better understand encased column behaviour and to better identify sites to which the technique may be suited. This may include investigating alternative geosynthetics and in particular, increase our understanding of the interaction between geosynthetic, column material and surrounding soil. Further research may also help to develop more efficient, practical and effective ways to implement the technique, reducing costs and broadening its appeal within the construction industry.

The research presented in this thesis is based on a program of laboratory testing and numerical modelling undertaken on geogrid encased stone columns. Geogrid encasement may provide an alternative to the now established method of geotextile encasement. The scope of the research is described in the following sections.

## **1.1 Background**

In recent years, increased infrastructure growth in urban and metropolitan areas has resulted in a dramatic rise in land prices and a shortage of suitable sites for development.

The building industry has therefore looked to develop available land, which has often comprised sites with poor ground conditions previously considered to be too expensive to develop. These types of sites include land in low-lying areas, often comprising geologically recent marine and estuarine deposits. Such deposits are generally characterised by undesirable geotechnical properties for foundations, including variable thickness, low strength and high compressibility. A range of ground improvement techniques have been employed to artificially improve the soil properties at these sites. Nevertheless, the construction industry continues to seek less expensive and more effective ways to undertake ground improvement. Some of the different methods of ground improvement available to engineers are described in the following section.

## **1.2 Ground improvement**

Ground improvement has been used for thousands of years to improve the engineering properties of weak soils. A significant increase in research and understanding has been gained in the last sixty years, mostly associated with the development of more sophisticated machinery and an increased understanding of soil behaviour. Of the extensive literature presented on the subject, Mitchell and Jardine (2002) provide a relatively concise definition of ground improvement, which they describe as:

*“the controlled alteration of the state, nature or mass behaviour of ground materials in order to achieve an intended satisfactory response to existing or projected environmental and engineering actions”*

The ground can be improved by many different techniques including densification through blasting, vibration and compaction, pre-compression, electro-osmosis, drainage, drying, heating, freezing, addition of admixtures including lime and cement, installation of stiffening columns and several other methods. The research described in this thesis focuses on ground improvement using conventional and geosynthetic encased stone columns.

### **1.3 Conventional stone columns**

The vibrating probe used for densification of granular material was developed in the mid 1930s. Using this technique, the void ratio of granular materials is reduced by vibrating the probe into the ground at predetermined intervals, forcing rearrangement of soil particles into a closer packed configuration. Often, the cylindrical cavities that remain after densification are backfilled with granular material to further stiffen the soil mass.

The properties of cohesive soils do not lend themselves to compaction through vibration alone, and therefore vibro-densification was not considered suitable for use in such soils. However, during the late 1950s, it was found that by adding granular material to the cavity left from using vibro-densification in cohesive soils, a stiffer soil mass could be achieved. The composite soil mass is characterised by improved stiffness, stability and time-settlement behaviour when compared to the untreated soil.

Unlike end-bearing piles, which bypass weak soil layers by transferring load to a more rigid founding layer, conventional stone columns improve the properties of weak soil. When the composite soil mass is loaded, columns interact with the surrounding soil, with load exchanged between the two materials in general accordance with their relative stiffness, column spacing and size. Conventional stone columns are commonly constructed using coarse gravel and coarser crushed rock aggregates compacted to a range of different densities, depending on site conditions and installation method. The composite soil mass is generally suited to supporting lightly and moderately loaded structures such as embankments.

### **1.4 Geosynthetic encased columns**

Geotextile encased columns have been a recent innovation, developed in the last decade for use on sites with very soft soils, where undrained shear strengths may be less than 5 kPa. These soils are typically of such low strength that they are unable to provide the confinement required to support conventional stone columns. In such soils, conventional columns tend to slump or bulge excessively when installed and loaded. In the past, piling or other forms of rigid foundations have been used to bypass such soils. However, in

many cases, geotextile encased columns now provide a more efficient and economical solution for the support of lightly and moderately loaded structures.

Being stiffer than conventional stone columns, encased columns need to be founded on a more rigid layer and may also require a geogrid reinforced bridging layer at the surface. As encased columns are loaded, radial expansion acts to mobilise hoop forces in the geotextile. This provides confinement to the column which increases column stiffness and limits the settlement of the composite soil mass. To date, the technique has been used on a number of projects to reduce settlement, reduce consolidation time and increase stability.

The use of geotextile, however, is limited to certain column materials and installation methods. Sand and fine gravel are typically used as backfill materials because coarser aggregates can damage the geotextile. In addition, to minimise the potential damage caused to the geotextile encasement, columns receive little compaction during installation. Finally, hoop strains in the order of 1% to 4% are required to mobilise the hoop forces in the encasement, resulting in significant radial expansion of the columns during loading. These combined factors can result in greater settlements than desired for some projects.

Recent research has been extended to study other geosynthetics, such as geogrid, for use as an encasement material. Although geogrid may be of lower strength than geotextile in some cases, geogrid is generally more robust and may enable columns to be compacted to a greater extent than geotextile. Furthermore, geogrid generally requires lower tensile strains than geotextile to mobilise tensile forces, providing a greater initial stiffness. These properties may enable a column with increased stiffness to be constructed (when compared to geotextile encasement). The use of geogrid encasement may also be compatible with coarser aggregates such as crushed rock, providing an alternative to materials such as sand and fine gravel.

The study of geogrid encasement has only recently been undertaken, with limited research conducted to date to investigate whether the technique provides a suitable alternative to geotextile. A summary of the research used to design, construct, install and assess the performance of conventional and geosynthetic encased stone columns is set out in a literature review, presented in Chapter 2 of this thesis.

## 1.5 Research hypothesis

The research presented in this thesis investigates the hypothesis that geogrid encasement can provide an alternative to the current practice of encasing sand columns with geotextile. In addition, geogrid encasement may offer benefits by using coarse crushed rock aggregates rather than fine gravels and sands and may also offer a stiffer alternative to geotextile encasement.

Should geogrid encasement provide a suitable alternative to geotextile encasement, the technique may broaden the overall appeal of ground improvement using geosynthetic encasement. This practice will be most relevant to projects where structures are to be founded on very soft and extremely soft soils.

To determine whether geogrid encasement can provide a suitable alternative to geotextile encasement, several theoretical and practical aspects were investigated. These comprised:

- Investigating whether geogrid can be practically used to construct encasement and whether it is then suited to encasing granular materials. This component required testing of typical stone column aggregates encased with different types of geogrid.
- Developing effective and economical methods for constructing and installing geogrid encased stone columns on site. Any technique used to construct encasement needs to be cost effective and easily performed on site. Encasement installation needs to be compatible with existing stone column installation techniques.
- Assessing the likely performance of geogrid encased stone columns. For the technique to be practical and useful, an understanding of the likely performance and limitations are required.
- Investigating the impact that different soils, column aggregates and geogrid properties have on encased column behaviour. The behaviour of encased columns is likely to vary depending on different material properties and site conditions. An understanding of the way in which these properties impact column behaviour is therefore required.

## **1.6 Research aims**

Based on the research hypothesis, the objectives of the study are primarily aimed at investigating the practical aspects of geogrid encased stone column behaviour including construction and performance. The aims of the research therefore comprise the following:

- (i) To investigate if the method of encasing stone columns with geogrid can provide a suitable alternative to geotextile encasement.
- (ii) To investigate the types of soil, column aggregate and geogrid that may be benefited using the technique.
- (iii) To investigate the likely performance of geogrid encased stone columns and the properties that have the greatest impact on column behaviour.
- (iv) To investigate practical methods of column construction.

## **1.7 Discussion**

To develop a suitable scope of research that fulfils the aims of the study, several aspects of encased column behaviour were considered. Those aspects considered to be of particular importance to this study are described in the following sections.

### **1.7.1 Group and isolated column behaviour**

Group column applications form the majority of stone column projects and therefore group column testing is considered paramount to understanding encased column behaviour. Much of the research previously published on both conventional stone columns and geosynthetic encased columns has focussed on the behaviour of isolated columns. This is most likely because isolated columns are generally more easily tested and assessed. However, isolated column testing does not satisfactorily replicate the conditions present in group column applications, particularly the confinement provided by adjacent columns. Therefore, research should focus on simulating group column behaviour and investigating the performance of group columns.

### **1.7.2 Partial encasement**

The current practice of geotextile encasement comprises circumferentially encasing the full length of the column (from top to toe). This is also true for the limited number of tests undertaken on geogrid encased stone columns. However, it is well documented that bulging occurs in the upper section of columns during loading. It is therefore considered that in many instances, full-length encasement may not be necessary for an encased column to perform adequately. A significant improvement in stone column performance, when compared to a non-encased column, may be achieved by encasing only the bulge zone and not the entire length of the column.

A study of partial encasement may help to reduce the amount of geogrid required for particular applications, providing a potential cost saving. In addition, partial encasement may be effective on sites comprising layered soils, where a very soft soil may overlie a soil of greater stiffness. Further research into partial encasement may provide valuable insight into encased column behaviour.

### **1.7.3 Method of overlap**

Geogrid encasement has previously been constructed by rolling geogrid into a cylindrical sleeve and then mechanically welding the narrow section of overlap. The technique generally provides geogrid encasement with adequate strength in the hoop direction for supporting vertical column loads. However, the technique requires the availability of a large welding frame. The length of column encasement is therefore limited to the length of the welding frame. Furthermore, the cost of shipping and mobilising such equipment to site can be cost prohibitive (Heerten 2006). The cost of prefabricating encasement off-site may also be prohibitive. Research into alternative techniques for constructing geogrid encasement would appear to be warranted. The “method of overlap” may provide such an alternative.

Encasement constructed using the method of overlap would comprise a geogrid sleeve overlapped by a certain percentage of the circumference (say a minimum of a half circumference). When filled with stone column aggregate, interlock from aggregate protruding between the geogrid ribs in the section of overlap may prevent the encasement from unravelling. Although the technique requires testing, it may provide an alternative to



welding. It may also provide a simple method for encasement construction on site, thereby reducing costs compared to welding.

#### **1.7.4 Material properties**

In previous research, properties such as the friction angle of stone column aggregate, replacement ratio (the percentage of soil replaced by stone column material) and soil stiffness have been shown to significantly affect conventional stone column behaviour. Such properties are likely to affect geogrid encased stone column behaviour in a similar manner. In addition, other properties such as geogrid stiffness, strength and aperture shape, and the stiffness and size of column aggregate are likely to influence encased stone column behaviour. The impact of these properties requires further investigation. The interaction between different sized aggregates and the overlapped section of different types of geogrids may also be important.

### **1.8 Methodology**

Research into the behaviour of geogrid encased stone columns, including the four components set out in Section 1.7, was undertaken using a four-stage approach. This comprised (i) small-scale laboratory testing of encased columns, (ii) numerical simulation of the small-scale tests, (iii) medium-scale testing of columns constructed from geogrid and typical stone column aggregates, and (iv) scaled-up numerical modelling to investigate full-scale column behaviour.

In the conception stages of the research, site testing of encased columns was proposed in place of the program of medium-scale testing. However, due to the difficulty in sourcing an appropriate site to conduct the full-scale tests, a program of medium-scale tests was undertaken in its place. In hindsight, undertaking medium-scale tests in place of the site trial was probably beneficial, as encasement construction methods and geogrid selection were significantly refined through the program of tests that were undertaken. A brief summary of the scope of the four stages of research is provided in the following sections.

### **1.8.1 Small-scale testing**

Small-scale testing was undertaken to investigate encased column behaviour in a controlled environment. Testing was undertaken on model sand columns measuring about 310 mm high and 55 mm in diameter, installed in very soft clay. The impact of properties such as encasement stiffness and encasement length on the behaviour of columns during consolidation were investigated. The impact of creep settlement on encased column behaviour was not investigated in this thesis.

Small-scale testing was also used to investigate the effectiveness of the method of overlap. Testing predominantly focussed on simulating group column behaviour, although isolated columns were also tested.

### **1.8.2 Replication of small-scale test results**

Numerical modelling was undertaken to simulate the results of the small-scale tests, providing insights into encased stone column behaviour, including the development of hoop forces in the geogrid encasement. Numerical modelling was undertaken using the well established, geotechnical finite element software, PLAXIS, described in greater detail in later chapters.

### **1.8.3 Medium-scale testing**

Medium-scale testing comprised unconfined compression tests undertaken on geogrid encased stone columns measuring 0.86 m high and about 0.24 m in diameter. Columns were constructed from geogrid and aggregates considered typical of stone column material. The tests were initially undertaken to assess whether adequate encasement fixity could be achieved using the method of overlap. The scope of testing was then broadened to include the impact of different geogrids (with different strength, stiffness and geometric properties), different amounts of overlap and different aggregates on encased column behaviour. The aggregates used in testing comprised medium to coarse crushed rock gravel and coarser-sized crushed rock, considered typical of stone column material. The impact of rounded gravels such as river gravels were not investigated in this thesis.

#### 1.8.4 Scaled-up numerical modelling

The same process used to numerically analyse small-scale tests was applied to model full-scale encased column behaviour. The scaled-up numerical analysis comprised a parametric study which was undertaken to investigate the impact of various column, geogrid and clay properties on encased column behaviour. The performance of geogrid encased stone columns in very soft clays was also assessed.

### 1.9 Organisation of thesis

This thesis is compiled as a series of chapters that generally describe and summarise the separate components of the research. The thesis is set out in the following chapters:

Chapter 1: Introduction

*A description of the research background and hypothesis, aims and methodology*

Chapter 2: Literature review

*A summary of the most significant and recent research undertaken by others on the subject of conventional and geosynthetic reinforced stone columns.*

Chapter 3: Small-scale laboratory tests

*A description of the design and development of the small-scale test apparatus, the test methodology and results, including discussion of test observations.*

Chapter 4: Numerical modelling of small-scale test results

*A summary of the numerical simulation of small-scale test results, including numerical modelling methodology.*

Chapter 5: Medium-scale laboratory tests

*A description of medium-scale test methodology and results, as well as discussion of test observations and materials suited to site trials.*

Chapter 6: Extrapolation to full-scale columns

*A summary of the full-scale parametric study used to assess the impact of different properties on encased column behaviour.*

Chapter 7: Research findings and practical applications

*A summary of the research findings from the four-stage approach, related to practical aspects of site construction and performance, including areas for future research.*

Chapter 8: Conclusions

*The conclusions of the research related back to the original aims*

## **2 Literature review**

---

### **2.1 Ground improvement**

Although ground improvement has been undertaken for centuries, considerable advances in understanding, design and methodology have occurred in the last sixty years, associated with rapid developments in technology. Throughout history, ground has been improved by various techniques including densification through blasting, vibration and compaction, pre-compression, electro-osmosis, drainage, drying, heating, freezing, addition of admixtures including lime and cement, addition of stiffening columns and numerous other methods. Some common methods of particular relevance to conventional stone column ground improvement are described in the following sections.

#### **2.1.1 Deep compaction**

Compaction is used to increase the density (reduce the void ratio) of soils with the aim of improving their engineering properties. A reduction in void ratio results in increased stiffness and strength, generally leading to an increase in bearing capacity and stability while reducing total and differential settlement under loading. This improvement is generally achieved using mechanical compaction.

In-situ deep compaction is suited to granular materials with a low percentage of fines. The most common forms of deep compaction are deep vibratory compaction, impact (dynamic) compaction and explosive compaction (blasting). Mechanical compactors and vibratory rollers are also frequently used to compact shallow soils, although the depth of influence of this equipment is limited. When using this type of equipment, deeper soils are generally excavated and replaced in thin layers.

Deep vibratory compaction has been used since the mid 1930s (Charles 2002) and is typically used to improve the behaviour of deep, loose sand deposits. A long torpedo-shaped probe is pushed into the ground and vibrated, compacting the surrounding soils. Pressurised water or air is often used with vibration to aid penetration. Depending on the

nature of the deposit and the size and power of the equipment used, the zone of improved soil typically extends between 1.5 m and 4 m from the vibrator (Mitchell 1981).

Impact compaction, also referred to as *dynamic compaction* or *heavy tamping* is achieved by repeatedly dropping heavy weights onto the ground surface from a crane or specialised rig. The weights are generally constructed from concrete or steel and vary in size depending on the crane size, ground conditions and degree of required compaction. Impact compaction is limited by the depth of influence that can be achieved by the equipment. The depth of influence is dependent on several factors including soil properties, water conditions and input energy per unit area (Mitchell 1981), the assessment of which can be subjective. In addition, the method can be limited by the amount of ground vibration induced by the tamping process, particularly for sites set in sensitive or populated areas.

Explosive compaction can provide a cheap and rapid alternative for compaction of loose, granular soils at depths beyond the reach of conventional compaction equipment (Gohl et al. 2000). The method generally comprises placing a charge at the required depth by drilling, vibrating or other means and then detonating the charge. The explosion causes compaction and densification of the surrounding soil and is particularly suited to either dry or saturated, clean sands (Mitchell 1981).

### **2.1.2 Consolidation**

Ground improvement by consolidation, or preloading, involves static loading of soil with the aim of increasing density through a reduction in void ratio. The method is most suited to highly compressible soils that undergo a large reduction in volume under increased effective stress. Fine grained, cohesive soils such as saturated soft clays, silts, organic clays and peats are often characterised by this. Consolidation of these soils under static loading generally results in a significant reduction in volume, resulting in increased stiffness and undrained shear strength.

The consolidation behaviour of these soils is typically highly plastic. As such, most consolidation and strength gain associated with preloading is unlikely to be reversed upon removal of the load. Methods for estimating the increase in undrained shear strength under applied static load have been presented by many authors including Bjerrum (1972).

This strength gain can be utilised for stability during future loading and construction. Furthermore, additional primary consolidation may only occur when the soil is subjected to a higher effective stress than experienced during preloading.

Preloading is also commonly adopted to limit secondary consolidation or creep. Creep settlements in the order of 10 mm/year may occur in thick deposits of soft and very soft soil, which can be detrimental to the structures founded on them. Bjerrum (1972) showed that creep settlement could be significantly reduced by using a surcharge pressure greater than the vertical stress applied by the proposed structure (over-consolidating the soil). This surcharge is typically removed at the completion of primary consolidation and prior to construction. Although the mechanics of creep are still not well understood, the method of preloading has been used successfully on many projects to reduce the rate of creep settlement. However, in the author's experience, the magnitude of creep settlement reduction can be difficult to accurately assess and can vary dramatically between different soil types.

Cohesive soils develop excess pore pressures when loaded that may take months, years or decades to dissipate because of their low permeability. For these soils, it is common for preloading to be combined with the use of prefabricated vertical drains (PVDs or wick drains) to accelerate the consolidation process. The use of preloading is governed by the volume of preload required, the cost of haulage, time constraints, bearing capacity and settlement tolerances. For sites where large volumes of fill material are not available or suitable, other methods such as vacuum consolidation, jacking systems and lowering of the water table have been successfully used in the past to induce consolidation and settlement (Mitchell and Jardine 2002).

### **2.1.3 Stiffening columns**

For some sites, stiffening columns provide a more suitable and economical form of ground improvement. Stiffening columns are generally used in soft cohesive soil and may include lime or cement stabilised columns, jet grouted columns, vibro-concrete columns and vibro-compacted stone columns, some of which are discussed in this section.

For deep in-situ soil mixing, the treatment is typically extended to a stiff underlying stratum, although columns can be founded within soft soil (floating), particularly for

projects where stability is the primary objective. Soil is mixed with an admixture of lime or cement using an auger or “egg-beater” shaped tool. The tool is initially screwed down to the founding level and then the rotation is reversed, at which point admixture is pumped through the hollow stem of the tool to the base of the hole. The rotation of the tool forces the admixture to blend with the soil. The tool is raised at a predetermined rate while admixture is continually fed, forming a stiffened column. The strength of the column increases as the admixture sets over a period of days and weeks. Typical column sizes range from about 0.5 m to 1.0 m in diameter and up to 10 m deep, although much larger columns have been used on specific projects (Mitchell 1981). In most cases, column spacing ranges from about 1.5 m to 3.0 m.

Jet grouted columns, vibro-concrete columns and lime/cement stabilised columns have high stiffness compared to the untreated surrounding soil. As a result, design of these columns is often treated similarly to that of piles, where structural capacity, end bearing and shaft friction may all be considered. There is some conjecture as to whether this method, or perhaps a technique using weighted properties of the soil-column unit, be adopted for aspects of design. Both appear to provide a reasonable design basis. In contrast, the behaviour of vibro-compacted stone columns is dependent on both the column material and the stiffness and confinement provided by the soil in which the column is installed. This makes assessment of the technique more complicated.

Although stone columns were originally adopted to improve the properties of loose, granular soils, their use in cohesive soils is now widely practiced. The technique has been established more recently than many other forms of ground improvement and as a result, design methods developed in the last forty years are still being improved. Recent innovations include reinforcing columns with geosynthetics to extend their use to sites with increasingly soft soils, an innovation that forms the basis of this thesis.

## **2.2 Conventional stone columns**

### **2.2.1 Overview**

For granular soils, vibration and compaction result in densification as particles rearrange themselves into a closer-packed configuration (lower void ratio). For fine, cohesive soils,



the impact of vibration and compaction is limited due to the relatively low permeability. Therefore, alternative techniques including the installation of stone columns are commonly adopted to improve the engineering properties of cohesive soils. Stone columns installed in cohesive soils act to create a composite material with lower compressibility, higher strength and higher permeability than the natural soil alone. Stone columns may be used in compressible cohesive soils to:

- (i) Improve bearing capacity.
- (ii) Reduce the magnitude of total and differential settlement.
- (iii) Improve stability.
- (iv) Reduce lateral spreading.
- (v) Increase the rate of consolidation (act as vertical drains).

Stone columns can either be founded on a stiffer underlying stratum or less commonly within the weak material as *floating* columns. Although column capacity is limited by the practicality of installation length, columns that extend to a stiffer layer are generally favoured because they have better load-settlement behaviour than floating columns. Furthermore, columns are rarely used in isolation, except perhaps for supporting small pad or strip footings. Column groups are most commonly adopted to support light to moderately loaded structures such as embankments, abutments, large storage tanks and in urban developments including land reclamation. In contrast to this, and probably for reasons of simplicity, much of the reported testing has been undertaken on isolated columns. As a result, the behaviour of isolated columns is relatively well established. The behaviour of isolated columns and column groups during loading are described in the following sections.

#### 2.2.1.1 Isolated column behaviour

When loaded, the stone column is forced downwards, creating shear stresses at the interface between the column and surrounding natural soil. This results in the dissipation of load with depth along the column and higher loads in the upper section of the column. When the confining pressure and stiffness of the natural soil is insufficient to support this load, the backfill within the column fails in shear, resulting in column *bulging*. This bulging can reach a state of plastic equilibrium and does not necessarily result in column failure (Goughnour 1983).

#### 2.2.1.2 Column group behaviour

Assuming that stone column treated soil is loaded using a relatively rigid footing and that columns are founded on a rigid stratum, loading forces the stone column and surrounding soil to settle by equal amounts. Since the stone is considered relatively incompressible compared to the natural soil, the stone column expands radially into the surrounding soil in response to its axial shortening. The soil is then forced to change volume in response to column shortening. Although additional confinement is provided by the radial expansion of adjacent columns, expansion may be greater in the upper section of the stone column where the lateral confining pressure and stiffness of the surrounding soil is lower. During loading, vertical stress is continually transferred between the column and natural soil in proportion to the relative stiffness of each material. Consolidation acts to increase column confinement and soil stiffness, continuing until equilibrium between the column and surrounding soil is reached.

#### 2.2.2 History of use

Hughes and Withers (1974) reported that stone columns were first used in 1830 by French military engineers in Bayonne, France. The columns were constructed on soft estuarine deposits to support the foundations of heavy ironworks. The columns measured 2 m in length, 0.2 m in diameter, supported 10 kN each and were constructed by driving stakes into the ground, removing the stakes and backfilling the holes so formed with crushed limestone. The technology was not further developed until about 1935, when the vibrating probe for compaction of granular soils was created. Development of the probe has been attributed to both Johann Keller and Serzey Steueman of Germany (Barksdale and Bachus 1983). Modern techniques for the construction of compacted stone columns in soft cohesive soils were developed in Germany in the late 1950s and concurrently in Japan (Mitchell 1981). Since then, stone columns have been used extensively around the world.

#### 2.2.3 Installation methods

A number of construction practices have been developed and adopted for the installation of stone columns in soft cohesive soils. Methods generally involve partial replacement of

a soft soil layer with cylindrical columns of stone aggregate. The base of the column typically penetrates a stiffer underlying stratum, although this is not always the case.

#### 2.2.3.1 Equipment

The column of stone aggregate is formed using a vibrating probe called a *vibroflot*. The vibroflot is generally torpedo shaped, ranges in diameter from 300 mm to 460 mm (Barksdale and Bachus 1983; Greenwood and Kirsch 1983), and is between 2 m and 5 m long (Baumann and Bauer 1974; McKelvey and Sivakumar 2000). A photograph of a typical vibroflot is presented in Figure 2.1. Eccentric weights mounted within the casing of the vibroflot are driven electrically or hydraulically and provide lateral vibration and vertical force. Fins mounted on the sides of the vibroflot prevent rotation during use. The vibroflot is generally suspended from a crane or special purpose rig. Follower tubes are placed above the probe to provide driving force and support for holes of greater depth.



**Figure 2.1:** Typical vibroflot (source: Keller Grundbau GmbH)

The vibroflot is generally pushed, jetted or vibrated into the layer of soft soil, forming a hole slightly larger in diameter than the vibroflot itself. The hole is then backfilled with stone aggregate. Compaction is performed with the vibroflot in lifts ranging between 0.3 m and 1.2 m (Barksdale and Bachus 1983). When flushing or jetting water is used in conjunction with the vibroflot to remove soil and form the hole, the process is referred to as *vibro-replacement*. When water is not used, the process is referred to as *vibro-displacement*. Each of these methods are discussed in the following sections.

### 2.2.3.2 Vibro-replacement

Vibro-replacement or the *wet process* involves jetting a hole into the ground with the vibroflot to the proposed toe depth of the column. The jets are generally positioned at the conical nose of the vibroflot and along its length. After reaching the required depth, the hole formed by the vibroflot is flushed and then backfilled in lifts with stone aggregate. The method of vibro-replacement is best suited to sites comprising soft to firm soils, with undrained shear strengths ranging between 15 kPa and 50 kPa and high groundwater levels (Munfakh et al. 1987). For soft soils, the vibroflot is generally left in the unsupported hole with water flowing throughout the installation to maintain stability. The flowing water also acts to wash out fines from the hole as the vibroflot is pushed into the ground. Stone aggregate is then tipped from the surface into the hole and compacted in lifts by lowering and raising the vibroflot. Columns ranging in diameter from 0.5 m to 1.0 m are formed using this process (Mitchell 1981; Mckelvey and Sivakumar 2000). Replacement techniques can also be used on dry sites, where an auger rig may be used to excavate the column holes in advance of the vibroflot, as shown in Figure 2.2.

The main disadvantage of the wet process is the large volume of waste water generated, which may impact the surrounding environment. Environmental regulations and site conditions may restrict the disposal of the water arising from the holes, which generally contains significant amounts of suspended soil. Sediment ponds, ditches and drainage are used on site to control the surface flow of the waste water and maintain an adequate surface for trafficking during the construction period.

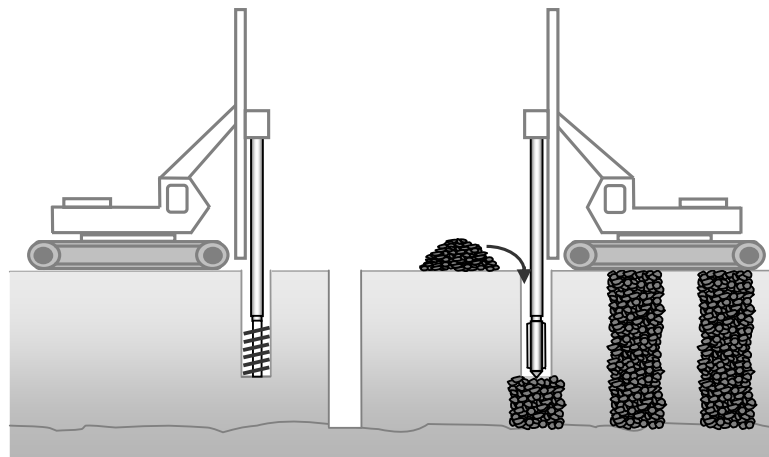


**Figure 2.2:** Vibro-replacement method

### 2.2.3.3 Vibro-displacement

Vibro-displacement or the *dry process* uses compressed air forced through the conical nose of the vibroflot to facilitate penetration. The process is cleaner than vibro-replacement. Once the vibroflot has reached the required depth, it is removed and granular material is placed in the hole in lifts and compacted by lowering the vibroflot back into the hole, as shown in Figure 2.3.

The process is dependent on the unsupported hole remaining open and stable during the compaction process and is therefore suited to stiffer soils and a low groundwater table. The method is suited to firm soils with undrained shear strengths ranging from 30 kPa to 60 kPa (Greenwood and Kirsch 1983; Munfakh et al. 1987). As it is a displacement process, column diameters are generally smaller than for vibro-replacement, with diameters in the range of 0.4 m to 0.8 m being common (McKelvey and Sivakumar 2000).

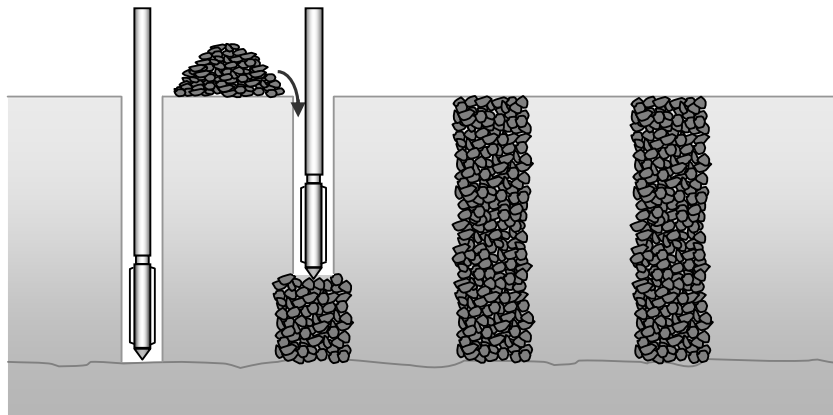


**Figure 2.3:** Vibro-displacement method

### 2.2.3.4 Bottom-feed methods

In recent years, the use of the bottom-feed method has become more common. Tubes placed next to or within the vibroflot allow stone aggregate to be fed from the ground surface down to the tip of the vibroflot where it can be compacted in lifts. This allows the vibroflot to remain in the hole for the duration of column installation, providing support to surrounding soil and preventing collapse, as shown in Figure 2.4.

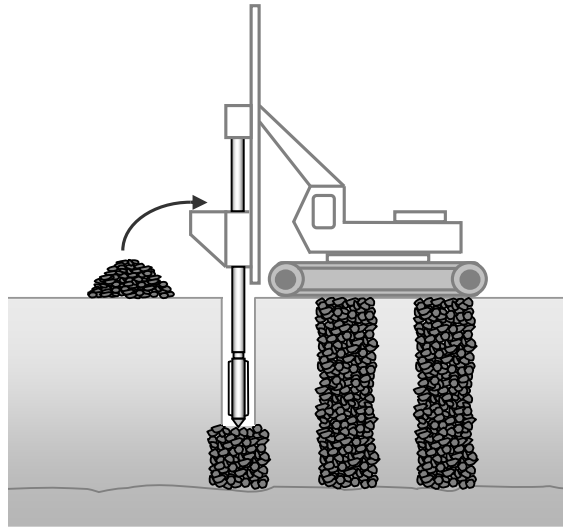


**Figure 2.4:** Bottom-feed method

Due to the support provided to the surrounding soil, the bottom-feed method can be used on sites with very soft soils and high groundwater tables. The technique is most commonly used in Europe.

#### **2.2.4 Application**

Stone columns have often been regarded as being suited to improving the behaviour of soils with undrained shear strengths ranging from about 15 kPa to 50 kPa (Mitchell 1981; Barksdale and Bachus 1983; Greenwood and Kirsch 1983; McKelvey and Sivakumar 2000). Below this strength, the natural soil has generally been considered to provide insufficient lateral confinement to stone columns, particularly for the case of isolated columns, where radial bulging may occur.

However, discussions with various contractors in both Australia and Europe have indicated that stone columns can and have been used in soils with undrained shear strengths as low as 5 kPa. In support of this, published case studies indicate that columns have been successfully used in soils with strengths as low as 6 kPa (Raju 1997), although a high level of site supervision was required. Furthermore, in soils of such low strength, practical aspects of column installation become paramount, including soil stability and site trafficking. Nevertheless, the once commonly accepted lower boundary of 15 kPa appears to be conservative. It is difficult to determine exactly why the strength of 15 kPa was

adopted as a lower bound, except that it probably corresponded well with the bulging failure of isolated columns and the strength required to easily mobilise and move equipment across site.

In soils with shear strengths less than about 5 kPa, the confining pressure from the surrounding soil is unable to support the conventional column shape. As a result, stone aggregate tends to heap during installation, forming a roughly conical shape (Wehr 2008). The shape of the cone is probably influenced by the soil stiffness at depth, the technique used to install the column and the internal friction angle of the stone aggregate. The general shape of such columns is illustrated in Figure 2.5.

Stone columns generally range in diameter from 0.4 m to 1.2 m depending on installation method, aggregate size, soil stiffness and other characteristics specific to the site. Columns with larger diameters have been used in the past for specialised applications including off-shore projects. Although somewhat unreliable, the post-installation column diameter is generally estimated by assuming a compacted relative density and measuring the volume of stone used for each column. This is of particular importance for quality control and design confirmation.

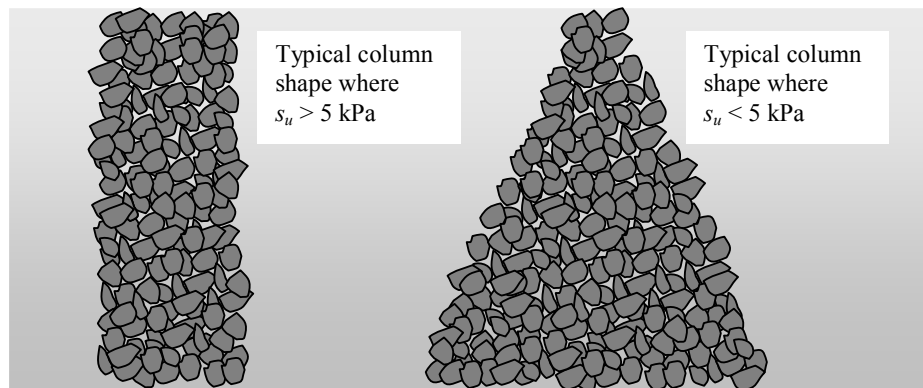


**Figure 2.5:** Typical stone column shape following installation

Columns can be installed on square and triangular grids at spacings ranging from about 1.5 m to 3.5 m (Mitchell 1981). Barksdale and Bachus (1983) report that a minimum centre to centre column spacing of about 1.5 m is imposed because of potential construction problems associated with soil stability and support. However, this spacing is dependent on in-situ soil stiffness, column diameter, column length and groundwater conditions. Based on current construction practices, smaller spacings and stone column walls (where columns are placed directly next to each other for the support of strip

footings) can often be constructed if required, although the cost associated with such closely spaced columns may not be economical.

For columns spaced evenly over a large area, the column *replacement ratio* can be defined as the total cross sectional area of the columns only, divided by the total area of the treated ground (loaded footprint), assuming the cross-sectional area of the column does not vary significantly with depth. For small footings, the replacement ratio can be defined as the cross-sectional area of one column divided by the total loaded area supported by one column. Hence:

$$\text{replacement ratio} = A_r = \frac{A_{sc}}{A_t} \quad (2.1)$$

Where  $A_t$  is the loaded footprint area,  $A_{sc}$  is the cross-sectional area of stone column(s).

Stone columns are generally installed at a replacement ratio ranging from about 10% to 35%. Within this range, the reduction in settlement of treated to untreated soils is generally between 20% and 50%. There are no defined upper and lower limits to the depth that stone columns can be installed, although constructability and economics become an issue for longer columns. Columns are generally founded on a stiffer underlying stratum and are typically within the range of 3 m to 15 m long (McKelvey and Sivakumar 2000). Barksdale and Bachus (1983) report that for columns greater than about 10 m long, other deep foundation options become more competitive economically. Depths of between 20 m and 30 m have previously been obtained in Japan, Europe and North America.

Granular columns accelerate the rate of consolidation for cohesive soils by providing a shorter horizontal drainage path for water being squeezed out of the natural soil. The consolidation rate is dependent on the column size and spacing, installation method, smearing and other factors.

Following construction, a bridging layer of sand or gravel is usually placed above the columns. The layer acts to distribute stresses more evenly on to the stone column treated soil and acts as a drainage blanket for water collected in the stone columns. The layer of sand is generally at least 300 mm thick and is often supported by geosynthetic material to provide additional stiffness to the bridging layer.



### **2.2.5 Aggregate size and density**

Aggregates used for stone columns typically comprise crushed rock that is uniformly graded and ranging from about 10 mm to 75 mm in size. Larger aggregate has been used for the dry method and for deeper holes to help stone reach the base of the hole. For bottom feed systems, the maximum particle size is limited by the size of the feeder tube and typically ranges from about 10 mm to 40 mm (Greenwood and Kirsch 1983). Stark and Yacyshyn (1991) provide grading sizes for aggregate suited to each installation technique. Cheung (1998) reports on using a 65 mm gap graded crushed rock with about 20% of material passing a 4.75 mm sieve for construction of stone columns. The finer gravel and sand was used to prevent voids forming in the column that could allow clay infiltration and therefore reduce the efficiency of the column to act as a vertical drain. Aggregate is typically compacted to a relative density of between 60% and 100%, depending on compactive effort.

## **2.3 Assessment of conventional stone column behaviour**

Laboratory testing, case studies, analytical modelling and numerical modelling have all been used to develop methods for assessment of stone column behaviour. Most techniques have either been developed to assess the capacity of an isolated column or to assess the reduction in settlement associated with the use of stone column groups.

### **2.3.1 Small-scale laboratory testing**

Laboratory testing has been used extensively since the early 1970s to investigate stone column behaviour. As is the case with many forms of modelling, small-scale laboratory testing is subject to scale effects. Centrifuge testing can be used to at least partially overcome these scale effects, although the cost associated with the technique is generally prohibitive. As a result, most laboratory testing has been undertaken with the understanding that scale effects may result in differences between model and site behaviour. Contrary to this, many authors have used small-scale testing successfully to predict the behaviour of stone columns at full-scale. Small-scale modelling is still being used today, particularly for ongoing research into geosynthetic reinforcement of stone

columns. Some of the pioneering research undertaken in the last forty years using small-scale laboratory testing is discussed in the following sections.

#### 2.3.1.1 Hughes and Withers

Hughes and Withers (1974) assumed the stone aggregate in isolated columns was confined by the lateral pressure provided by the surrounding soil. This assumption was used to direct their testing program and develop an analytical design method. A series of small-scale tests using staged loading of isolated stone columns installed within a consolidated bed of kaolin clay were undertaken. The columns measured 150 mm in length and ranged from 12.5 mm to 38 mm in diameter. The clay bed was confined, ensuring that drainage occurred as the column was loaded with a small footing. Radiographs of lead shot markers embedded within the clay were used to measure radial column expansion. Results were compared to tests performed on untreated kaolin clay.

From their results, the authors concluded that (i) model columns acted independently when placed more than 2.5 diameters apart, (ii) model columns increased the rate of consolidation by a factor of 4 and reduced settlement by a factor of about 6, (iii) at failure, a length corresponding to about four column diameters expanded radially at the top of the column and was referred to as the *bulging zone* (iv) the capacity of a column was primarily governed by the lateral reaction of soil surrounding the bulging zone. Based on these observations, the authors idealised the mechanism of column bulging as cylindrical cavity expansion in clay, similar to the behaviour of clay in a pressuremeter test. They assessed that the ultimate vertical stress,  $\sigma'_{v,sc}$ , a column could support as it bulged laterally could be expressed as:

$$\sigma'_{v,sc} = \frac{(1 + \sin \phi'_{sc})}{(1 - \sin \phi'_{sc})} (\sigma_{rl}) \quad (2.2)$$

Where  $\phi'_{sc}$  is the effective angle of internal friction of the column material and  $\sigma_{rl}$  is the radial resistance of the surrounding soil, given by:

$$\sigma_{rl} = \sigma'_{ro} + 4c_u + u \quad (2.3)$$

Where  $\sigma'_{ro}$  is the lateral effective stress in the bulging zone and  $u$  is the excess pore pressure. Since the column is considered to be effective in reducing excess pore pressure,  $u$  is typically zero.

The idealisation of cylindrical column bulging as cavity expansion may be overly simplified because bulging was typically confined to the upper section of the column. As a result, spherical cavity expansion theory may provide a better model. However, column capacity assessed using this theory has often compared favourably to the results of field testing and laboratory testing undertaken by others, including the laboratory testing undertaken as part of the research presented in this thesis.

#### 2.3.1.2 Charles and Watts

Charles and Watts (1983) investigated the behaviour of stone column groups founded on a rigid stratum. The problem was simplified for laboratory testing to an isolated column surrounded by an annulus of clay, confined within a “rigid” tube. The medium-scale model tests were performed on 600 mm high granular columns in a 1 m diameter oedometer cell.

A program of five tests was carried out on samples with varied column diameters to assess the impact on settlement. The clay used in the testing comprised reworked boulder clay with an average undrained shear strength of 30 kPa. The results of the testing indicated that (i) the compressibility of the clay was 10 times greater than the gravel for a given vertical stress, (ii) stone column behaviour was complex and dependent on column diameter, and (iii) vertical compression of the cell decreased with increasing column diameter.

Charles and Watts concluded that in order to achieve a significant reduction in compressibility (which was deemed to be about 33%), a replacement ratio of at least 30% was required. Compared to the body of published data on typical stone column performance, this reduction in compressibility is considered low for the adopted replacement ratio, perhaps a result of scaling error.

### 2.3.1.3 Craig and Al-Khafaji

Craig and Al-Khafaji (1997) investigated the effects of replacement ratio on the settlement response of stone column groups. Laboratory tests were carried out using a centrifuge test chamber to reduce the scale effects normally associated with model testing. The centrifuge chamber measured 325 mm in diameter and 200 mm in height. Cowden clay with an undrained shear strength of about 26 kPa was used. Four tests were conducted on samples using replacement ratios of 10%, 20%, 30% and 40%. Full depth sand columns of 10 mm diameter were installed on a triangular grid within the test chamber at a spacing corresponding to the required replacement ratio. The columns were installed using a vibrating engraving tool which simulated full-scale construction.

Results of the investigation indicated that (i) tests took significantly longer using smaller replacement ratios than higher replacement ratios, a likely result of the longer drainage path between smaller columns, (ii) settlements decreased significantly with an increasing replacement ratio, (iii) settlement was larger at the centre of the chamber, most likely due to side wall frictional effects, and (iv) the stiffness of the stone columns was estimated to be 7 times greater than the clay.

A graph of settlement reduction plotted against replacement ratio, together with a theoretical extrapolation, were presented by the authors and is presented in Figure 2.6. The results confirm the generally accepted range of settlement reduction associated with increased replacement ratio. However, the extrapolated results are questionable, particularly for the case of  $A_r=1$ , where the total area would be replaced by granular column material. On an intuitive basis, given the stiffness of compacted granular material compared to soft clay, the ratio of treated settlement to untreated settlement is expected to be closer to 0 than 0.2.

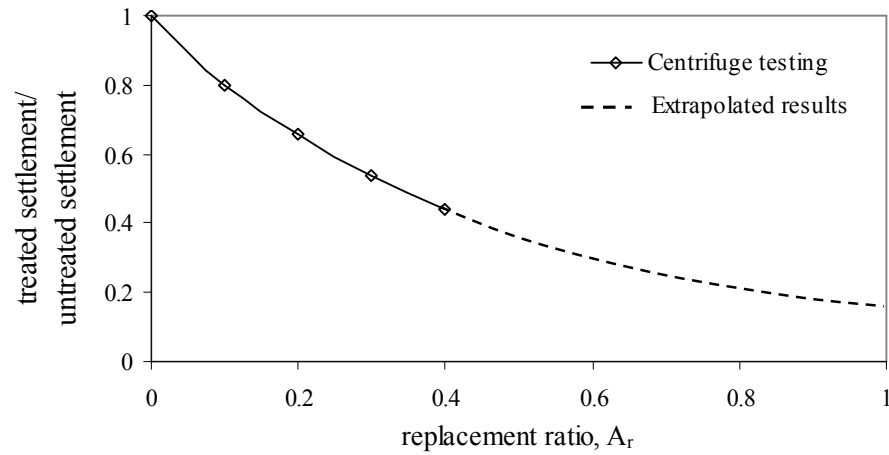


**Figure 2.6:** Experimental and extrapolated test results, after Craig and Al-Khafaji (1997)

#### 2.3.1.4 Muir-Wood, Hu and Nash

Muir-Wood et al. (2000) investigated the effect of varying column diameter, column spacing and column length on load transfer within groups of stone columns beneath a rigid foundation. Tests were carried out in a cylindrical tank measuring 300 mm in diameter. Kaolin was consolidated from slurry to form clay with undrained shear strengths ranging between 8 kPa and 23 kPa. Model columns were formed by removing the clay with a small auger and replacing the cavity with sand. Column groups with varying replacement ratios and toe depths were tested by loading them with a rigid circular footing measuring 100 mm in diameter. Numerical analysis was also undertaken to further investigate the primary mechanisms of stress and soil deformation.

The results of the investigation indicated that there was significant interaction between a footing and individual columns within a group. As a result, the load-settlement response of columns in different locations under the footing was different. Observation of column failure indicated that (i) a diagonal shear plane may form through a column subjected to high stress and low lateral restraint, (ii) columns that were short enough to allow significant load to be transmitted to the base penetrated the underlying material, and (iii) a slender column may deform like a laterally loaded pile due to lateral movement of clay beneath the model footing. From observations of the depth of bulging and location of shear planes, it was concluded that the zone of influence of a small footing on the underlying treated ground was roughly a conical zone as presented in Figure 2.7.

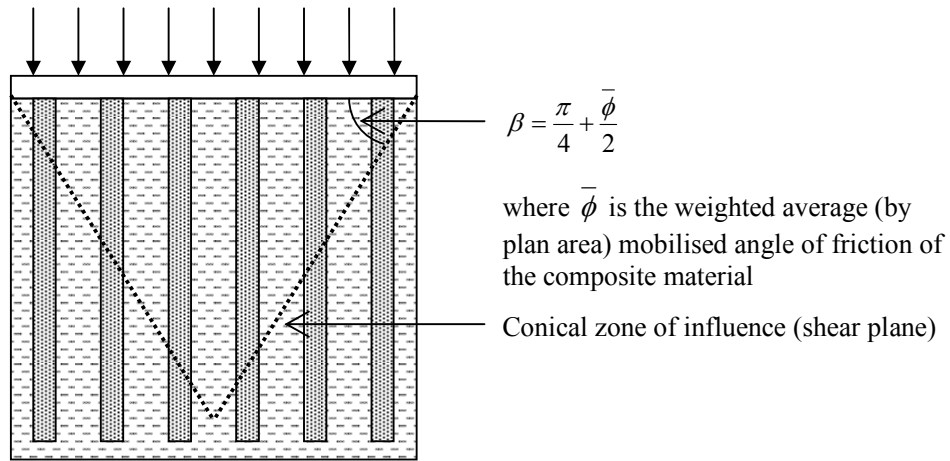


**Figure 2.7:** Conical zone of influence under circular footing, after Muir-Wood et al. (2000)

The investigation also indicated that increased column confinement towards the centre of the footing resulted in loads being pushed to greater depths, where stresses and stiffness were generally higher. It was therefore considered that assessment of column capacity near the centre of a footing, using cavity expansion theory like that of Hughes and Withers (1974), was likely to be conservative and should consider the increased stress and stiffness in soil at depth.

Although the investigation gave valuable insight into the interaction of individual columns beneath a small footing, it did not replicate the presumed oedometric like conditions likely beneath the centre of a wide, uniformly loaded area such as an embankment. As a result, their work is probably more valuable in assessing column behaviour near the perimeter of a wide loaded area. Given that most stone column applications comprise large column groups where oedometric conditions are likely, column group research would benefit from simulating these conditions.

#### 2.3.1.5 Sivakumar and McKelvey

Research undertaken at Queens University, Belfast, investigated the behaviour of sand columns using a series of laboratory tests that focussed on the impact of column reinforcement, installation method, replacement ratio and column length (McKelvey et al. 2004; Sivakumar et al. 2004; Sivakumar et al. 2002).

Samples of kaolin slurry were consolidated to form clay with an undrained shear strength of about 30 kPa. This was achieved in a one-dimensional loading chamber measuring 100 mm in diameter and 500 mm in height. Following completion, holes measuring 32 mm in diameter were formed in the clay using a small auger. The holes were filled with sand columns by compacting sand into the hole in layers. Results of this method were compared to a second technique where saturated columns were frozen in a mould, removed and then placed in the hole. Columns were installed as both floating and full depth columns to investigate the effect of depth on column capacity. The effect of wrapping columns in geotextile was also investigated. The composite material was then placed in a triaxial cell and tested to failure under undrained conditions.

Results of the testing indicated that the capacity of sand columns significantly increased when installed to full depth. For the method of frozen column installation, results (in terms of capacity and time-rate of consolidation) were significantly more consistent than for the method of in-situ compaction. This was probably a result of inconsistencies with in-situ compaction and the possibility of clay mixing with sand during installation. Full length columns with circumferential geotextile encasement showed a substantial increase in capacity when compared to non-encased columns.

In 2004, further tests were carried out on model sand columns using a transparent material that simulated clay behaviour and allowed the observation of column deformation during loading. Due to the high compressibility of the material, a large chamber measuring 1.2 m high and 0.413 m in diameter was used to consolidate a sample to about 0.5 m high. Three sand columns measuring 25 mm in diameter were installed on a triangular grid. Columns were loaded at constant displacement beneath a 100 mm diameter circular plate and column lengths were varied with each test. Tests were also conducted on kaolin clay using different column configurations to investigate the effect of varying the ratio of column length to diameter ( $L/D$  ratio).

The laboratory test results indicated (i) column bulging was not symmetrical about the vertical axis, being reduced in areas closest to adjacent columns, (ii) short columns ‘punched’ into underlying material, (iii) no obvious deformation occurred in the lower sections of longer columns, suggesting little load was transferred to the base of these columns, and (iv) columns had a limiting length/diameter ratio somewhere between 6 and

10, beyond which there was little increase in capacity although some reduction in settlement.

Their work was valuable for assessing isolated column behaviour, particularly for enabling the direct observation of column deformation during loading as opposed to the destructive techniques of column excavation used previously (at test completion). However, their work primarily focussed on isolated columns and small column groups, and did not capture the behaviour of large column groups beneath wide, uniformly loaded areas.

### **2.3.2 Field and full-scale testing**

Case studies and full-scale testing of stone columns have further contributed to the understanding of their behaviour. Some of these studies are discussed in the following sections.

#### **2.3.2.1 Hughes, Withers and Greenwood**

Hughes et al. (1975) sought to confirm their analytical design approach for assessing column capacity (based on cavity expansion theory) by testing a full-sized stone column. The column was constructed as part of a stone column project on Canvey Island in the Thames estuary (UK). Soil properties were assessed from detailed site investigation data and used to predict the capacity of the column.

The stone column was formed by wet jetting a vibroflot into the ground and installing the column by compacting gravel in layers. The column was installed to a depth of 10 m and was founded on a stiff underlying clay. The column was loaded with a cylindrical plate equal in diameter to that of the column. Column capacity was about 30% higher than predicted using their analytical approach. The column was excavated upon completion of the test to observe the deformed shape. The radial deformation was similar to the shape predicted from model testing with bulging confined to the upper section of the column. The difference in load capacity was attributed to a larger column diameter than expected following excavation.



In addition to testing, the authors introduced a method for calculating the critical length ( $L_c$ ) of an isolated column, defined as the shortest column length that can carry the load regardless of settlement. The critical length was assessed as the point where end bearing and shaft friction are equal, estimated using an adaptation of the general bearing capacity equation:

$$p_{sc} = \overline{c_c} A_{s,sc} + N_c c_c A_{sc} \quad (2.4)$$

Where:

$p_{sc}$  is the ultimate column load

$N_c$  is the appropriate bearing capacity factor (taken as 9 for a long column)

$A_{s,sc}$  is the column surface area (equal to  $\pi D_{sc} L_c$  where  $D_{sc}$  is the column diameter)

$c_c$  and  $\overline{c_c}$  are average cohesion along the column length and cohesion at the critical length, respectively.

#### 2.3.2.2 McKenna, Eyre and Wolstenholme

McKenna et al. (1975) presented a case study of the construction of a 9 m high trial embankment overlying soft alluvium in Southwest England. The trial embankment was 189 m long and 70 m wide with batter slopes at 3H:1V. Stone columns were constructed beneath a 30.5 m long section of the embankment. The stone columns were 0.9 m in diameter, installed on a triangular grid at 2.45 m centres and were founded on medium dense sand at a depth of 11.3 m below ground level. The columns were constructed from 38 mm nominal sized crushed limestone using the vibro-replacement method and were overlain by a drainage blanket 0.46 m thick.

After constructing the embankment to 7.9 m in height, a 60 m long section failed and further construction was stopped. After analysing pore pressure and settlement data, the authors concluded that there was little difference in the behaviour of the treated and untreated soil and the use of stone columns was abandoned. The authors concluded that infiltration of clay fines into the voids of the coarse gravel aggregate and remoulding during installation prevented the stone columns from working effectively. However, Greenwood (1991) noted from published data that the columns appeared to be acting as vertical drains and that most stress was transferred to the base of the columns. Greenwood

postulated that the stone columns acted as friction piles and failed by punching into the underlying material (the columns were of insufficient length). Based on the published data, this appears to provide a more plausible explanation for the observed column behaviour.

#### 2.3.2.3 Greenwood

Greenwood (1991) reported on the use of stone columns for numerous applications, including for reducing settlements at the south approach to the Humber Bridge. The bridge is founded on soft organic clays. Stone columns were used beneath the highest approach embankments to stiffen the underlying soils. Stone columns approximately 0.78 m in diameter were constructed on 2.25 m triangular grids to a depth of about 9 m. The columns were founded on stiff boulder clay. Final settlements were approximately 1.3 times less than the untreated ground, which closely matched values calculated using elastic and empirical methods for the observed modular ratio of 5.

#### 2.3.2.4 Raju

Raju (1997) reported on the use of stone columns used to reinforce very soft cohesive soils at the Kinrara and Kebun interchanges along the Shah Alam Expressway in Malaysia. The site investigation indicated that undrained soil strengths were as low as 6 kPa. Vibro-replaced stone columns were used to limit settlements beneath embankments ranging between 2 m and 10 m in height. Stone columns were typically between 1.0 m and 1.2 m in diameter and installed on grids ranging between 1.5 m and 2.5 m. The stone columns were installed to a maximum depth of 17 m and founded on a stiff stratum.

Monitoring indicated that stone column settlements (at completion of primary consolidation) at the Kinrara and Kebun sites were 4 times less and 2.5 times less than for the untreated ground, respectively. Based on these results, Raju concluded that it was possible to install stone columns in cohesive soil with undrained shear strengths less than 15 kPa, although the process was not routine and required close supervision.

### 2.3.2.5 Clemente and Davie

Clemente and Davie (2000) presented the findings of field tests undertaken at four electric power generation facilities where stone columns were installed to reduce the foundation settlements. Results were compared to published theoretical and empirical data, showing that stone columns provided a greater settlement reduction than expected (although some scatter was present in the results). Based on the field data collected, Clemente and Davie concluded that existing empirical and theoretical data provided a useful tool for the preliminary assessment of settlement reduction using stone columns. However, full-scale testing should be incorporated in projects to confirm design.

Their research raises an interesting observation, and that is the majority of published case studies report settlement reduction by comparing measured treated settlement to theoretical untreated settlement. Although theoretical methods may be based on laboratory testing of samples taken from site, the behaviour of the actual soil deposit can vary significantly from the laboratory sample. It is quite common for theoretical-based estimates to vary significantly from measured settlements, often giving an overestimation of compressibility. If measured treated settlement is compared to theoretical untreated settlement, the quoted settlement reduction may be overstated. Care should therefore be taken when presenting results from field studies. The type of settlement being compared (whether it is measured or calculated) should be clearly stated and measured treated settlements should be compared to measured untreated settlements where possible.

### 2.3.3 Assessment of settlement reduction

A number of analytical techniques used for assessment of stone column behaviour have been developed over the last forty years based on empirical, semi-empirical and theoretical approaches. Many of these techniques have assessed the reduction in settlement associated with the use of stone columns. Most of these methods have attempted to express this reduction in terms of an improvement factor,  $n$ , defined as the settlement of untreated soil divided by the settlement of treated soil, where:

$$n = \frac{\rho_{untreated}}{\rho_{treated}} \quad (2.5)$$

The settlement of untreated soil is typically measured in field trials or calculated using a method such as one-dimensional consolidation theory. Several of the most common methods used to assess settlement reduction associated with the use of stone columns are described in the following sections.

### 2.3.3.1 Greenwood method

Greenwood (1970) was one of the first authors to introduce design curves for assessing settlement reduction associated with the use of stone columns. The curves represented the settlement reduction as a function of column spacing and undrained cohesion of the natural soil. The curves were based on an entirely empirical approach for stone column groups placed under widespread loads in uniform soft clays. Later, Greenwood and Kirsch (1983) presented updated curves as a function of area ratio for comparison to other techniques. A reproduction of these curves is presented in Figure 2.8.

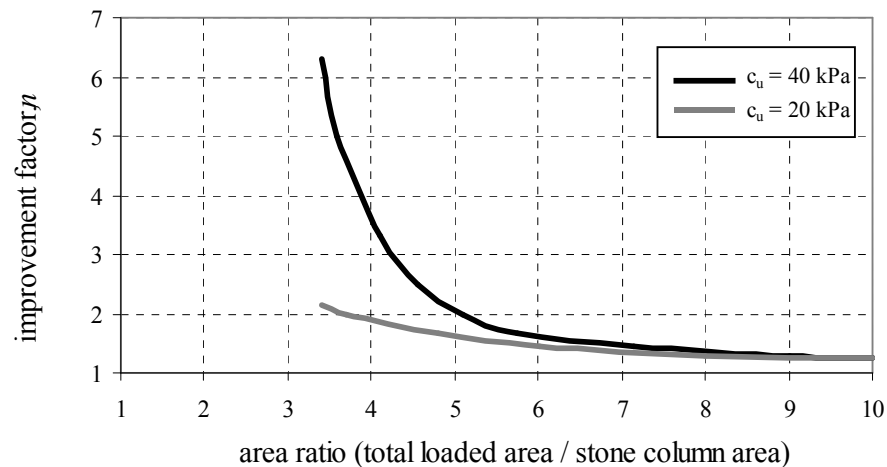


**Figure 2.8:** Greenwood curves, after Greenwood and Kirsch (1983)

The curves have limited use as a design tool because they are based on a limited number of case studies and have been outdated by more sophisticated design techniques. They are therefore more suited to preliminary assessment of stone column performance. For soft soils where  $c_u \approx 20$  kPa, the curves compare favourably with results obtained from more sophisticated methods. However, it seems counter-intuitive that the improvement factor for stiffer soils, where  $c_u \approx 40$  kPa, should be significantly greater than for soft soils. Although a stiffer soil would provide greater confinement to a column and therefore

increased stiffness, the relative stiffness of the column to surrounding soil is still likely to be less than for a softer soil. Therefore, it is reasonable to suggest that, at least intuitively, there should be a much smaller difference between the behaviour of columns in stiff and soft soil. In support of this, Barksdale and Bachus (1983) report that the curve for the stiffer soil tends to overestimate settlement reduction.

### 2.3.3.2 Unit-cell idealisation

For projects with large plan areas, stone columns are generally installed on either square or triangular grids. Stone columns arranged in a triangular geometric pattern are generally considered as having an equivalent hexagonal shaped zone of influence on the surrounding soil. For stone columns arranged in a square geometric pattern, this zone of influence is usually modelled as square shaped. For simplicity in both cases, the zone of influence can be approximated as a circle with the same area (Barksdale and Bachus 1983), as shown in Figure 2.9. For columns arranged on a triangular grid, the effective diameter of the approximated circle is  $1.05s$ , where  $s$  is the centre to centre spacing of the columns. For columns arranged on a square grid, the effective diameter is  $1.13s$ .

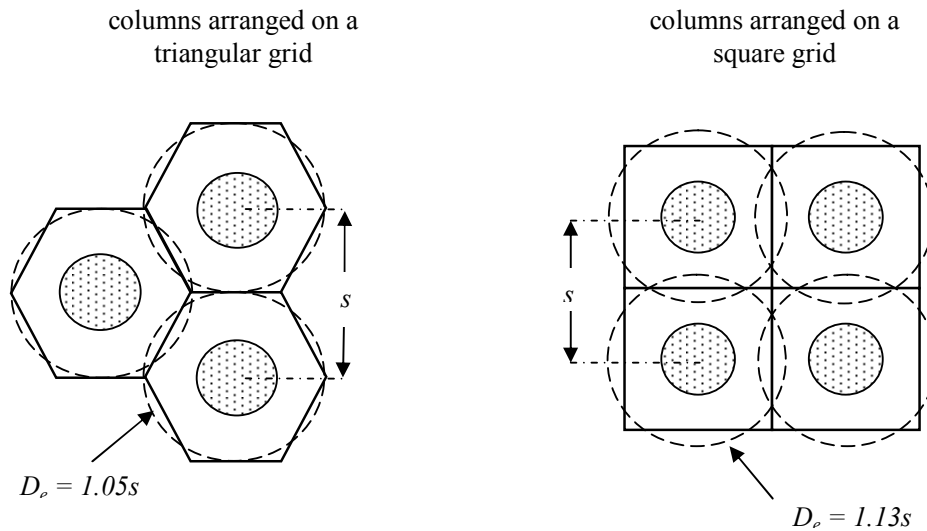


**Figure 2.9:** Circular approximation of a stone column's zone of influence

The stone column and approximated circular area of surrounding soil within its zone of influence are referred to as a *unit-cell*. The stone column is central to the unit-cell boundary as shown in Figure 2.10. The unit-cell can be adopted to simplify column group

behaviour beneath a wide, uniformly loaded area to that of a single column. The unit-cell has formed the basis of numerous analytical approaches used to assess column behaviour.

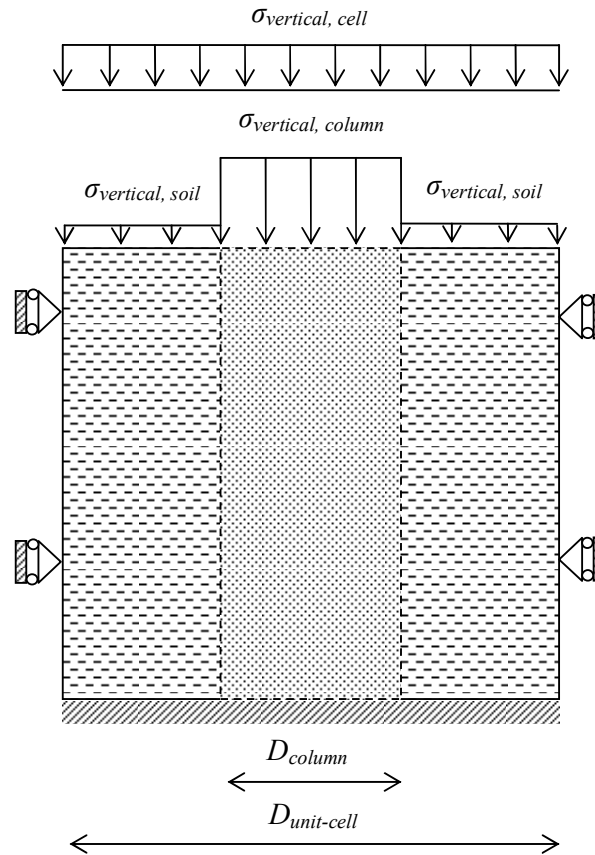


**Figure 2.10:** Unit-cell idealisation of a stone column installed in soil

Unit-cell idealisation is based on the following assumptions:

- (i) a roller boundary condition applies at the cell perimeter, allowing vertical settlement but no lateral movement of soil beyond the cell boundary.
- (ii) a fixed boundary condition applies at the base of the cell, replicating columns founded on a rigid stratum.
- (iii) load is applied to the cell through a rigid footing so that the vertical settlement of the column and surrounding soil are equal.

### 2.3.3.3 Equilibrium method

The *Equilibrium Method* is based on the concept that stresses from applied foundation loads are shared between the stone columns and natural soil in proportion to the relative stiffness of each material, the column spacing and column diameter. The stress concentration ratio,  $\eta$ , is defined as the ratio of vertical stress in the stone column ( $\sigma_{v,sc}$ ) to the vertical stress in the natural soft soil ( $\sigma_{v,c}$ ) where:

$$\eta = \frac{\sigma_{v,sc}}{\sigma_{v,c}} \quad (2.6)$$

For the case of rapid loading under undrained conditions, stress concentration will not occur until some time after loading and the magnitude of this ratio will increase as the soil approaches a fully drained state. Mitchell (1981) reported that the value of  $\eta$  fell within the range of 2 to 6 with values of 3 and 4 being typical. Goughnour (1983) reported that a value of 2 was adopted in practice in the United States. The value of  $\eta$  is usually determined from load cell measurements taken from field tests.

By assessing the forces on the stone column and surrounding natural soil resulting from foundation loading, the force on the unit-cell can be expressed as:

$$(A_{sc} + A_c)\sigma_{v,t} = A_{sc}\sigma_{v,sc} + A_c\sigma_{v,c} \quad (2.7)$$

Where  $\sigma_{v,t}$  is the average vertical stress applied to the cell (or bearing pressure) and  $A_c$  and  $A_{sc}$  are the cross-sectional areas of the natural soil and stone column, respectively.

Using equation 2.7, the stress in the stone column and natural soil can be defined as follows:

$$\sigma_{v,sc} = \frac{\eta\sigma_{v,t}}{[1 + (\eta - 1)A_r]} \quad (2.8)$$

$$\sigma_{v,c} = \frac{\sigma_{v,t}}{[1 + (\eta - 1)A_r]} \quad (2.9)$$

The stress in the clay,  $\sigma_{v,c}$ , can then be used to calculate the overall settlement of the unit cell by using one-dimensional consolidation theory or similar. Barksdale and Bachus (1983) introduced design curves for estimating the improvement factor for a range of stress concentration ratios and replacement ratios using elastic theory. It is important to note that the vertical column stress can be limited by the bearing capacity of the founding layer and this should be considered in calculation.

The equilibrium method provides a simple and practical process for estimating stone column settlement. The method was commonly used to estimate stone column settlement in Japanese practice during the 1980s (Barksdale and Bachus 1983). However, it does require an accurate assessment of the stress concentration ratio, which generally requires a site test. This can be a time consuming and expensive undertaking, requiring instrumented columns and the consolidation of a small trial area of treated ground.

#### 2.3.3.4 Priebe method

Priebe (1976) proposed a method for assessing settlement reduction based on the unit-cell concept. Balaam and Booker (1985) describe his work as a combination of elastic theory and Rankine earth pressure theory. In his model, the stone column was assumed to be in plastic equilibrium and the natural soil was idealised as an elastic material. Stone columns were assumed to be incompressible and settlement of the natural soil was related to vertical shortening and radial expansion of the column. The column was deemed to expand radially when the lateral pressure in the column was greater than the passive confinement provided by the surrounding soil. Radial expansion was related to cavity expansion theory and soil stiffness. A summation of the vertical strain in discrete horizontal slices was used to assess the overall settlement performance of the column.

Priebe generated a series of design curves where the soil improvement factor,  $n$ , was plotted against the area ratio,  $A_t/A_{sc}$ , for a range of granular materials. An example of these design curves is presented in Figure 2.11.



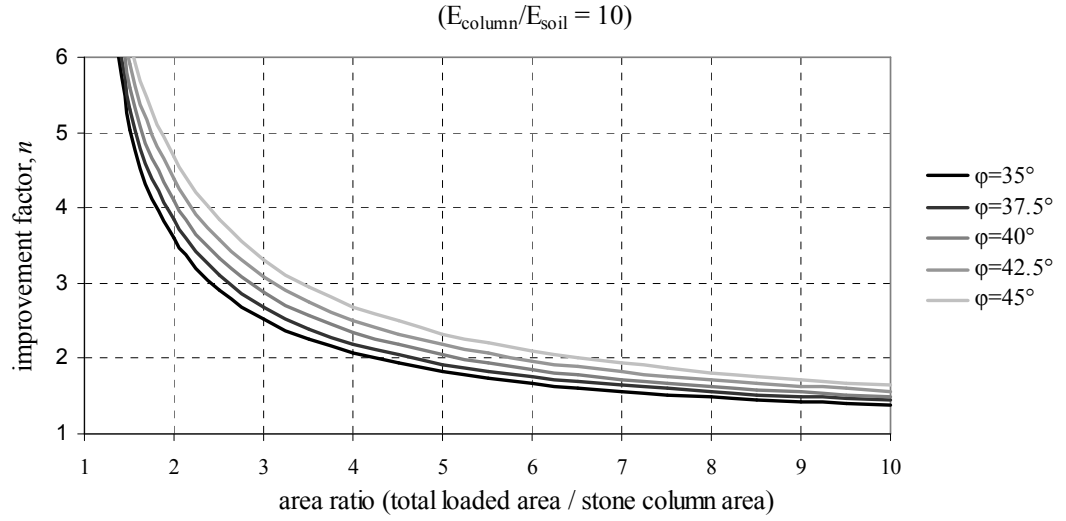


**Figure 2.11:** Priebe design curves, after Priebe (1995)

Using this method, a conventional calculation for untreated soil settlement is performed and divided by the improvement factor,  $n$ , where:

$$n = 1 + A_r \frac{\frac{1}{2} + f(\nu_c, A_r)}{K_{a,sc} \cdot f(\nu_c, A_r)} \quad (2.10)$$

and

$$f(\mu, A_r) = \frac{1 - \nu_c^2}{1 - \nu_c - 2\nu_c^2} \cdot \frac{(1 - 2\nu_c)(1 - A_r)}{1 - 2\nu_c + A_r} \quad (2.11)$$

Where  $\nu_c$  is the Poisson's ratio of the natural soil and  $K_{a,sc}$  is the active earth pressure coefficient of the stone aggregate defined by:

$$k_{a,sc} = \tan^2 \left( 45^\circ - \frac{\phi_{sc}}{2} \right) \quad (2.12)$$

Following criticism of his method including that it did not consider column-soil modular ratio or the initial stresses associated with overburden, Priebe (1995) presented a revised version of his method. In the updated method, various additions are made including consideration of column compressibility, modular ratio of the column and soil, and

confinement provided to the columns from overburden. In addition, the method is adapted to individual and strip footings founded on a finite number of stone columns.

The Priebe method has been used extensively in industry as a design tool for assessing settlement reduction. The relatively simple technique of applying a reduction factor to conventional consolidation calculations has made the method quite popular. Although Barksdale and Bachus (1983) reported that his method tended to overestimate the reduction in settlement that can be achieved, particularly for stress concentration ratios between 3 and 5, the updated method appears to adequately address this.

#### 2.3.3.5 Numerical methods

Numerical methods are arguably the most theoretically robust approach to modelling stone column reinforced ground, being capable of modelling soils and geometry more realistically than other techniques. Numerical methods can consider non-linear, elastic-plastic material behaviour, soil interaction, complex geometry and interface slip. In addition, with advances in the sophistication of computer software packages such as FLAC and PLAXIS, plane-strain, axisymmetric, two dimensional and three dimensional problems can all be modelled.

Early work modelling stone column treated ground using finite element methods was undertaken at the University of Sydney in the late 1970s. Balaam et al. (1977) used finite element and finite difference methods to model fully penetrating and floating columns under flexible footings in elastic and elasto-plastic materials. The solutions were obtained from the analysis of a simplified unit-cell, rather than a three-dimensional assessment which is considerably more complex. From their work, they concluded that when the ratio of column spacing to column diameter was greater than 5, the reduction in settlement compared to untreated ground was negligible. They found that the difference in settlement reduction between plastic and elastic models was less than 6%. They also showed that decreasing the spacing between columns led to significant increases in consolidation rate. A series of design curves for predicting settlement reduction and consolidation rate were presented.

Balaam and Booker (1981) used unit-cell idealisation to investigate the magnitude and rate of settlement for a simulated group of fully penetrating stone columns under a rigid raft

footing. They modelled the load-settlement behaviour through the transition from an undrained to a drained state. They also showed that the simplification of the unit-cell from a hexagonal or square plan area to a circle with equivalent area produced negligible errors. An analytical solution was presented for estimating stone column settlement reduction and the shear forces and bending moments acting on the rigid raft footing.

Balaam and Poulos (1983) compared the results of elastic finite element analysis to other design methods available at the time, including those of Greenwood and Priebe. Their work indicated that results varied significantly between design methods. However, their numerical results were in close agreement with the analytical design solution developed by Priebe (1976), for lower modular ratios. A comparison of their numerical results to a laboratory test showed close agreement.

Balaam and Booker (1985) developed an analytical approach termed *interaction analysis*, using previous linear-elastic theory that had been extended to consider plastic deformation at the top of the column under high stresses. The method was based on elasto-plastic finite element analyses. The method was used to show that stone columns were more effective at 2.5 m spacing than predicted by Greenwood's empirical curves for soft clay. It also showed that the difference in error between plastic and elastic models was most significant when column spacing was small and the modular ratio between column and soil was high. Their results were presented as a series of correction factors to existing elastic solutions with modular ratios in the range of 10 to 40.

Han and Ye (2001) used numerical modelling to produce a simplified method for assessing improvement in consolidation rate associated with stone columns. Pulko and Majes (2005) extended the work of Balaam and Booker to consider confined yielding of the column material according to dilatancy theory. Their work considered factors including column length and spacing, initial stress state, applied load, material properties and closely matched results from elastic-plastic finite element analysis. Tan and Oo (2005) and Tan et al. (2008) produced methods for converting finite element axisymmetric models to plane-strain models. Their work focussed on realistically modelling column stresses, settlement reduction and consolidation rate for the plane-strain case and provides practical guidance for those modelling typical stone column problems.

Numerous other authors have presented results of numerical modelling that closely reflect results reported from laboratory testing, large scale testing and case studies. Nevertheless, numerical modelling can be time consuming and requires an experienced engineer to undertake the assessment. Even with advances in sophisticated and user-friendly software leading to a reduction in setup and calculation time, most projects are unlikely to have the scope at a preliminary design stage to undertake a thorough numerical assessment. Approximate or simplified analytical methods derived from numerical modelling have the benefit of being simpler to implement while maintaining a more robust theoretical approach than analytical and empirical techniques.

#### 2.3.3.6 Other methods

Other methods used to estimate the settlement reduction for stone column treated ground include the De Beer-Van Impe method (1983). Early steps in this technique were similar to those used by Priebe (1976). Rigid plastic behaviour was used to model the stone columns and elastic behaviour was adopted for the surrounding soil. The problem was considered in two dimensions (plane-strain), where stone columns were replaced by an equivalent stone wall.

A method for analysing settlement reduction by using a ring of plastic soil surrounding the stone column, in place of the more simple elastic approaches, was presented by Wallays et al. (1983). Although the approach may consider a more realistic soil response, particularly for higher stress conditions, the method generally requires assistance from spreadsheets that may be cumbersome to apply if being used on a one-off basis.

Goughnour and Bayuk (1979) and later Goughnour (1983) used the *Incremental Method* to provide an analytical solution to assess group column settlement. For this technique, the unit-cell model was used in conjunction with an incremental and iterative, elastic-plastic solution with similar assumptions made to those of Priebe (1976). The unit-cell was divided into small horizontal elements and the vertical strains and stresses acting on each element were calculated. It was assumed that no shear stresses acted along the interface between the stone column and surrounding soil, hence lateral and vertical stresses acting on the cell were principal stresses. Both elastic and plastic responses were considered, giving a theoretically robust response to treated soil behaviour. If stresses and strains were low then the stone column behaved elastically. However, for most cases the

column bulged, behaving plastically over some of its length. Although calculations were complex and required iteration, Goughnour (1983) went some way to improving this by providing design charts for simplification.

#### 2.3.3.7 Summary

Although many of the methods used to assess settlement reduction associated with the use of stone columns vary in their theoretical robustness, most techniques could play some role in design. Some of the more prominent techniques and their suitability to design of stone column performance are summarised in Table 2.1.

**Table 2.1:** Prominent design methods used for assessment of settlement reduction

assessment method	theoretical robustness	difficulty of application	suited to:	
			preliminary design	detailed design
Greenwood curves (Greenwood and Kirsch 1983)	low	low	✓	
Equilibrium method*	medium	medium	✓	✓
Priebe method (Priebe 1995)	medium	medium	✓	✓
Incremental method (Goughnour 1983)	high	medium - high	✓	✓
Numerical methods	high	high		✓

\* provided a site test is undertaken to measure stress concentration ratio

### 2.3.4 Assessment of column capacity

Methods are also available for assessment of column capacity as described below.

#### 2.3.4.1 Cavity expansion theory

As outlined earlier, Hughes and Withers (1974) used cavity expansion theory to approximate the capacity of an isolated column installed in soft clay. The limiting failure

stress as the stone column bulges is given by equation 2.2. Although only the upper section of a column generally bulges during loading, idealising the column as an infinitely long expanding cylinder appears to yield reasonable results.

#### 2.3.4.2 Mitchell

Mitchell (1981) used results derived from cavity expansion theory and empirical data from others to show that the allowable vertical stress,  $\sigma_{v,sc}$ , on an isolated column in soft clay, with undrained shear strength,  $s_u$ , can be expressed by:

$$\sigma_{v,sc} = \frac{25s_u}{FOS} \quad (2.13)$$

Where  $FOS$  is the factor of safety. A  $FOS = 3$  is typically adopted for design.

#### 2.3.4.3 Barksdale and Bachus

Barksdale and Bachus (1983) used cavity expansion equations proposed by Vesic (1972) to present the following relationship for the ultimate capacity of an isolated column installed using vibro-replacement, where

$$q_{ult} = c_u N_c \quad (2.14)$$

Where  $q_{ult}$  is the ultimate stress the stone column can carry and  $N_c$  is a bearing capacity factor for the stone column, where  $18 \leq N_c \leq 22$ . The value of  $N_c$  is semi-empirical and is dependent on the compressibility of the soil surrounding the column. For soils with a high stiffness, the upper bound ( $N_c=22$ ) should be adopted. For soils with low stiffness such as organic or very soft clays, the lower bound ( $N_c=18$ ) should be adopted. Although recognising its conservatism, the authors suggested that the capacity of an isolated column be used as an estimate of the capacity of small groups of columns under a rigid footing.

## **2.4 Geosynthetic reinforced stone columns**

### **2.4.1 Overview**

The design and construction of vibro-replaced and vibro-displaced stone columns has been well established for nearly forty years. However, the technique is generally not adopted in very soft and extremely soft soils (where  $s_u \leq 5$  kPa) due to the lack of lateral confinement provided by the surrounding soil. Use of columns in such soils may result in detrimental column bulging or formation of conical shaped columns (refer Section 2.2.4) during installation.

Sites comprising very soft soils are generally located in low-lying coastal and estuarine regions, where groundwater levels are close to the surface. The soils are typically geologically very recent and are likely to be normally or near-normally consolidated. Access to these sites with heavy machinery can be difficult, often requiring barge construction or use of extensive bridging layers. Conventional piling has traditionally been adopted as a foundation solution at such sites, with load being transferred to a stiffer underlying layer, bypassing the weak layer.

Although piles provide an effective load transfer option, the cost of the technique can be prohibitive, especially for projects with large areas requiring treatment. Other than costs associated with construction and installation of the piles themselves, costs can also include construction of a stiffened raft and pile caps to transfer load to the piles. In addition, some sites can be sensitive to noise and vibration, which may be an issue with driven piles. The use of geosynthetic reinforcement was investigated to provide an alternative to piling and to extend the use of stone columns to very soft soils. Initial research on the technique began in the 1980s. Significant development in the field occurred in the early 1990s and implementation has become more widespread only in very recent times.

### **2.4.2 Reinforcement methods**

Research in the field of geosynthetic reinforcement has generally followed one of the three following directions:

- (i) Geosynthetic reinforcement of stone columns using horizontal layers of geogrid placed in the upper section of a column to reduce bulging.
- (ii) Geotextile encased columns (GECs) – circumferential encasement of predominantly sand columns using a geotextile sleeve.
- (iii) Geogrid encased stone columns – circumferential encasement of stone columns using a geogrid sleeve.

A summary of the development and use of each technique is presented in the following sections.

### **2.4.3 Geosynthetic reinforcement in horizontal layers**

As set out earlier, columns tend to expand laterally as they are loaded. The magnitude and location of this radial expansion is dependent on whether the column acts in isolation or as part of a group, in addition to the physical properties of the column and surrounding soil. Although radial expansion can contribute to the lateral confinement of adjacent columns, excessive expansion (bulging) can lead to column failure. Experiments, generally on isolated columns, have shown that bulging typically occurs in the upper section of the column, where lateral confinement is lower. Based on this, research has focussed on placing geosynthetic material in horizontal layers within the *bulge zone* of the stone column to provide resistance to lateral deformation. This resistance is provided by interaction and interlocking between the reinforcement and the granular column material. This concept is illustrated in Figure 2.12.

Some of the earliest work investigating geosynthetic reinforced granular material can be attributed to Gray and Al-Refeai (1986). Their work focussed on comparing the stress-deformation response of sand reinforced with fabric layers and random fibres. Although their work did not concentrate on stone columns, they concluded that fibre reinforcement of a granular trench in soft clay could significantly increase bearing capacity.

Madhav et al. (1994) reported that the performance of an isolated stone column could be improved by reinforcing the upper part of the column with horizontal layers of geogrid. A series of small scale tests were used to show that the capacity and stiffness of a column increased with an increasing number of reinforcement layers. The authors reported that the column stiffness was increased as shear stresses were mobilised at the interface of the



granular material and the reinforcement. Materials with higher frictional resistance were shown to develop greater shear stresses and therefore provide greater resistance to bulging. An analytical method for assessing the ultimate capacity of a reinforced column, based on the approach adopted by Hughes and Withers (1974), was presented.

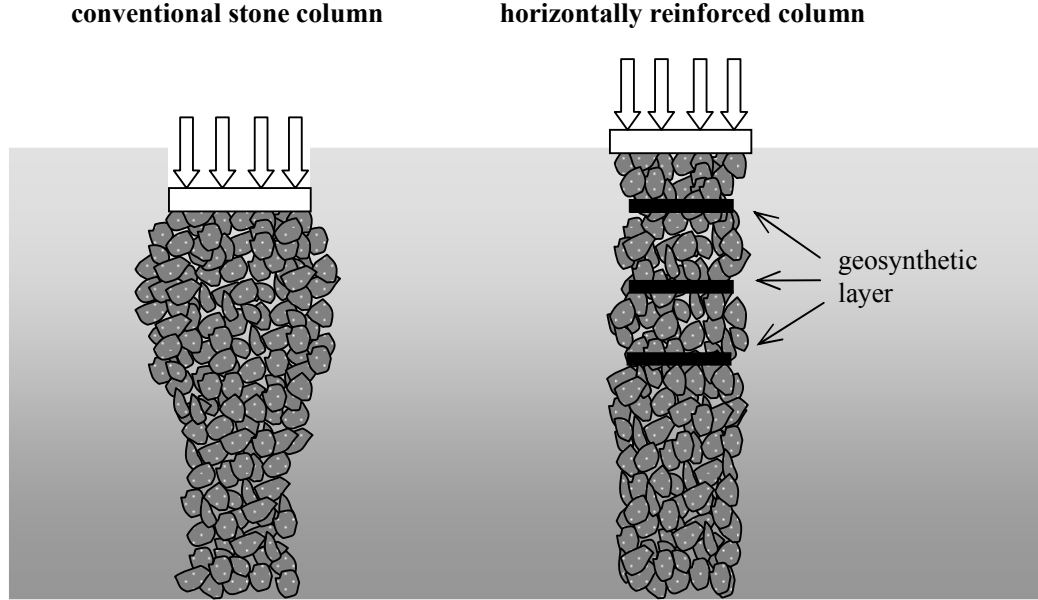


**Figure 2.12:** Horizontal reinforcement of granular columns

Cai and Li (1994) conducted experiments in a large triaxial cell (300 mm diameter) to investigate the use of horizontal reinforcement. A sand column measuring 42.5 mm in diameter was installed in the triaxial cell, using steel mesh to simulate geogrid reinforcement. The sand column was loaded with a circular plate using a constant rate of displacement. The experiments were designed to investigate three parameters, (i) the depth below the base of the loading plate to the first layer of geogrid, (ii) the vertical spacing of the geogrid, and (iii) the number of layers of geogrid.

Results of the investigation showed that the maximum column capacity occurred when:

$$\frac{u_f}{(d_f - d_p)} = 0.5 \quad (2.15)$$

Where  $u_f$  is the depth below the loading plate to the first layer of geogrid,  $d_f$  is the loading plate diameter, and  $d_p$  is the column diameter.

The spacing of the layers of geogrid,  $\Delta z$ , reached an optimum value when:

$$\frac{\Delta z}{d_p} = 0.5 \quad (2.16)$$

Tests indicated that the optimum number of geogrid layers was about 4, above which there was little additional increase in column capacity. The results corresponded well with other analyses undertaken using numerical methods.

Sharma (1998) conducted a parametric study of geogrid reinforced stone columns using a finite element model that was initially validated against a field trial on an isolated stone column. Horizontal layers of geogrid were then modelled within the column. A range of geogrid moduli, layer numbers and spacings were assessed in the study. Based on this research, Sharma concluded that the inclusion of geogrid layers facilitated a more effective transfer of lateral stresses into the surrounding soil. This was achieved by redistributing lateral deformation in the upper section of column over a greater length, limiting localised bulging and increasing column capacity. Sharma found that little further improvement in capacity occurred when layers of geogrid were placed at less than about half a column diameter spacing.

Sharma et al. (2004) attempted to confirm previous numerical modelling by undertaking a series of laboratory tests on stone columns reinforced with horizontal layers of geogrid. Fourteen load tests were conducted on full penetrating sand columns measuring 60 mm in diameter and installed in a 300 mm thick bed of clay. The number of geogrid layers and spacings were varied in each of the models. The results of the laboratory investigation confirmed that the inclusion of geogrid layers improved the capacity of stone columns and reduced lateral bulging.

Although testing and numerical modelling of horizontal geosynthetic reinforcement has indicated that significant increases in column capacity may be gained, it would appear difficult to adapt the technique to site installation. This may offer some explanation for the lack of published information regarding its use for ground improvement projects.

#### **2.4.4 Geotextile encased columns (GECs)**

Although the concept of GECs was formulated in the 1980s, the technique was not developed further until the early 1990s (Huesker Synthetic GmbH). The method involves encasing a granular column with a sock constructed from geotextile, which acts to confine the column in the same manner as a confining ring in an oedometer test (Alexiew et al. 2003). As the column is subjected to vertical load, it expands radially, mobilising tensile hoop forces within the geotextile. Circumferential strains in the order of 1% to 4% are typically required to mobilise these forces (Alexiew et al. 2005). Radial expansion of the geotextile and column densification cause some vertical settlement.

GECs behave in a similar manner to piles in that they transfer load from the surface to an underlying rigid stratum. However, due to radial expansion and densification of the column during loading, significant axial shortening of the column occurs. This results in settlement and subsequent strength gain in the surrounding soil. In addition, the surrounding soil provides a confining pressure that acts to increase column capacity. The method can therefore be considered as a ground improvement technique, although the surrounding soil is not improved to the same extent as for conventional stone columns.

##### **2.4.4.1 Column properties**

Design strength and time dependent strain behaviour of the geotextile are important for foundation design. Sudden loss of radial support through failure of the encasement would result in additional stress being proportioned to the soil, further settlement and the possibility of exceeding serviceability conditions. Huesker developed Ringtrac<sup>®</sup>, a seamless geotextile sock possessing a high modulus, low creep, high permeability and resistance to unfavourable chemical and biological environments. As the geotextile is susceptible to puncturing from typical stone column aggregates (e.g. coarse crushed rock gravel), sand and fine gravel are generally used to construct the column.

##### **2.4.4.2 Installation**

A replacement or displacement technique may be used to install GECs in very soft and extremely soft soils. Both techniques are described in the following section.

*Replacement method:* An open-toe, thin-walled steel tube (casing) equal in diameter to the geotextile sock is pushed from the surface down to the underlying founding layer. The soil within the casing is excavated using an auger. The geotextile is then placed inside the casing and filled from the surface. Fill generally comprises sand and fine gravel. After the geotextile sock has been filled, the steel casing is raised around the encased column, leaving it in-situ. The column may receive light compaction by vibrating the casing as it is raised. Upon loading, lateral column stresses result in radial expansion and geotextile strain, providing confinement to the column. This installation method is illustrated in Figure 2.13.

*Displacement method:* Steel casing is vibrated down to the founding layer. The casing has two mechanised flaps at the base which are held closed during driving, causing displacement of the surrounding soft soil. The geotextile is then placed and filled inside the casing in the same manner as for the replacement method. As the casing is raised, the flaps at the base are forced open allowing it to be raised around the encased column. This installation method is illustrated in Figure 2.14. The displacement method is most commonly used for construction and is preferred for very soft soils.

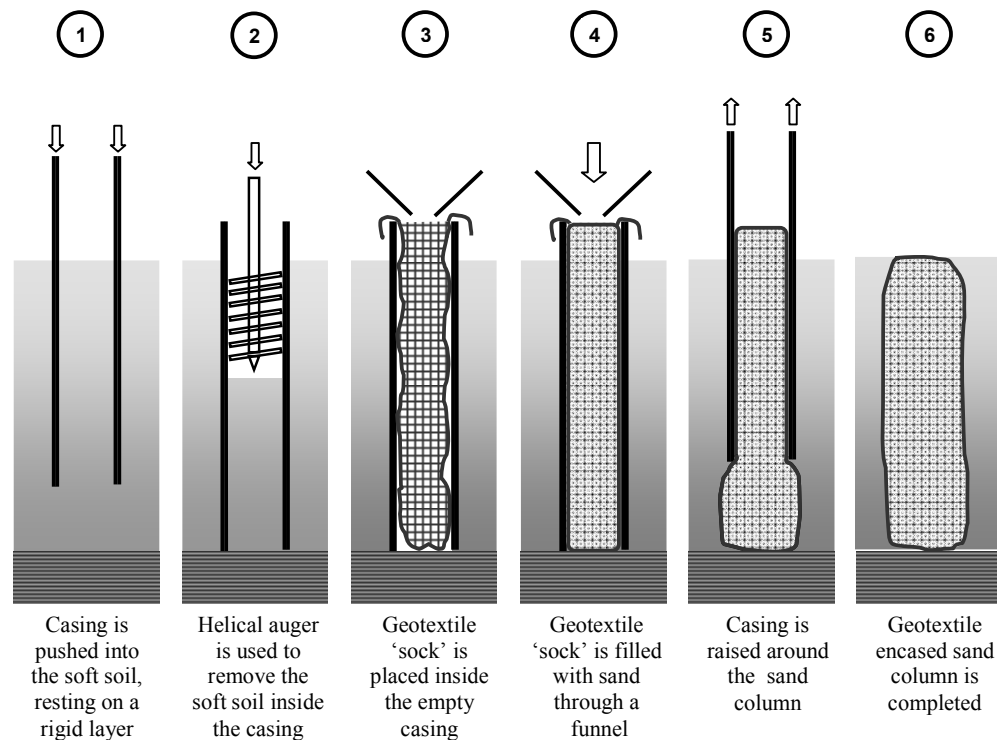


**Figure 2.13:** Installation of GECs using the replacement method

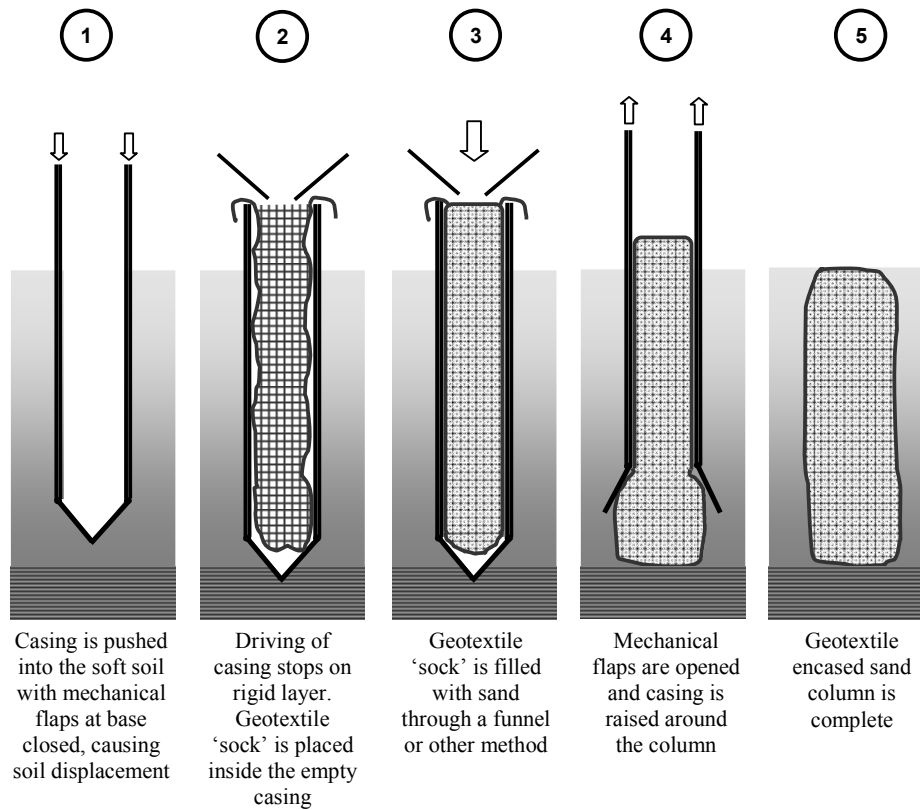


**Figure 2.14:** Installation of GECs using the displacement method

#### 2.4.4.3 Application

Sidak et al. (2004) reports that geotextile encased columns were used in Austria as early as 1992 by ground improvement contractor Keller Grundbau GmbH. However, the encased columns were not used to provide support under vertical loading, rather to provide drainage and flood protection.

It is estimated that following the first application of the Ringtrac<sup>®</sup> system for ground improvement in about 1995, more than 15 projects have been completed throughout Germany, Sweden and the Netherlands using the technique (Alexiew et al. 2005; Raithel et al. 2005). In addition, De Mello et al. (2008) reports on the first use of GECs in South America.

Alexiew et al. (2003) reported that the typical diameter of GECs is about 0.8 m. Columns are generally installed on a triangular grid with axial spacing ranging between 1.7 m and 2.4 m, equating to a replacement ratio of between 10% and 20%.

Raithel and Kempfert (2002) reported on the use of GECs for a dike foundation on river sludge along the Elbe River, Hamburg, Germany in 2001. The 2.4 km long dike was constructed as part of a 140 hectare land reclamation project for an airplane dockyard plant site. The site comprised contaminated river sludge ranging in undrained shear strength from 0.4 kPa to 10 kPa, overlying a bearing layer between 4 m and 14 m below surface level. About 60,000 GECs were installed to the underlying bearing layer using the vibro-displacement method. Work was predominantly undertaken from offshore pontoons resting directly on the soft soil. The columns were installed at replacement ratios ranging between 10% and 20%. The dike was constructed to a maximum height of about 7 m in a nine month period. The maximum settlement beneath the dike was about 1.2 m, corresponding to an improvement ratio of between 2.5 and 4. The technique was observed to significantly increase the undrained shear strength of the river sludge.

Nods (2002) reported on the use of GECs for limiting settlements along a section of embankment forming part of the Antwerp to Amsterdam high speed railway.

#### 2.4.4.4 Design methods

Van Impe and Rouck (1985) recognised that stone columns could still be used in very soft soils such as silts and hydraulic fills when wrapped in geotextile, which would provide the necessary confinement to the column. The initial steps in developing a procedure for the design of GECs were proposed by Van Impe (1989). His analytical procedure assessed the required tensile strength of the geotextile for given load conditions, allowing a geotextile of suitable strength to be adopted. However, the method did not consider the strain behaviour of the geotextile under loading and therefore, the radial deformation and settlement of the column could not be estimated.

Raithel and Kempfert (1999; 2000) presented an analytical design procedure using unit-cell idealisation based on established procedures by Priebe (1995) and elastic cavity expansion equations by Ghionna and Jamiolkowski (1981). Using their method, the difference in lateral stress between the non-encased stone column and surrounding soil during loading was calculated using Rankine earth pressure theory, allowing the assessment of the geotextile tensile force required to bring the cell to equilibrium. The tensile stiffness modulus of the geotextile,  $J$  (kN/m), was then incorporated, defined by the stress-strain behaviour of the geotextile. This enabled calculation of the geotextile

circumferential strain and therefore assessment of column radial expansion during loading. The radial expansion of the column was related to axial column shortening by assuming no volume change within the column material, allowing a calculation of cell settlement.

The procedure is complex and solved iteratively using computer software. More details regarding the derivation of the method are presented in Raithel and Kempfert (1999; 2000) and Raithel et al. (2005). The design procedure is well established and currently used in conjunction with numerical modelling for design of the Ringtrac<sup>®</sup> system. Raithel et al. (2005) also present information on installation methods and previous projects where GECs have been implemented.

#### 2.4.4.5 Other research

Zhigang et al. (2001) used finite element modelling, laboratory testing and field testing to investigate the effect of wrapping crushed stone columns with geonet and needle-punched geotextile. The work was primarily used to investigate the effectiveness of the geotextile in increasing the rate of consolidation in the surrounding clay, but was also used to investigate the role of the geotextile in limiting bulging. Model tests were undertaken in the laboratory in a chamber measuring 1.0 m in diameter and 1.3 m deep. Stone columns measuring 0.16 m in diameter were installed in the chamber and loaded. Field trials comprised the staged construction of a 6 m high embankment over a grid of columns measuring about 2.4 m long, 0.2 m in diameter and spaced at 1.5 m centres. The results of the finite element modelling and experiments were in close agreement, with less than 10% difference. From this, the authors concluded that the geotextile prevented the ingress of clay fines into the column during consolidation, increasing the effectiveness of the column to act as a drain. The geonet also reduced column bulging.

Ayadat and Hanna (2005) carried out a series of small-scale experiments on reinforced stone columns, focussing on their use in collapsible soils. Sand columns measuring 23 mm in diameter were installed in a 390 mm diameter consolidation chamber with varying depths of penetration. The stone columns were encased with geotextile of varying stiffness. The collapsible soil was subject to wetting by raising the water level inside the consolidation chamber and columns were loaded under constant strain. Following testing, the authors concluded that the capacity of the encased columns was increased with increased geotextile stiffness and by greater penetration into the collapsible soil.

Analytical solutions were presented for estimating both the capacity of an encased stone column and the reduction in settlement associated with the use of encasement. The theoretical approach reflected experimental trends but underestimated the magnitude of the experimental values.

Murugesan and Rajagopal (2007) conducted small-scale experiments on isolated stone columns encased with geotextile. The columns were installed by a displacement method in a bed of extremely soft clay measuring 210 mm in diameter and 500 mm high. The columns were instrumented with strain gauges and loaded with a small footing under a constant rate of displacement. The column diameter and stiffness of the geotextile were varied in the tests. A small number of tests were also conducted on partially encased columns. Results of the testing indicated that the hoop stresses within the geotextile were greatest near the surface, decreasing with depth as column confinement increased. The impact of the encasement was less for larger diameter columns, with hoop stresses being lower. Partially encased columns were observed to behave similarly to fully-encased columns up to a certain pressure, suggesting that for isolated columns, encasement of just the bulge zone may be an effective method of increasing capacity. Numerical modelling was used to further investigate the results from testing (Murugesan and Rajagopal 2006). The modelling concentrated on isolated columns but was also extended to group behaviour beneath an embankment.

#### 2.4.4.6 Summary

GECs provide an option for improvement and reinforcement of very soft and extremely soft soils. Although the technique may result in significant settlement associated with radial column straining and densification, it is an effective method of accelerating consolidation, increasing stability and reducing post construction settlements. The use of GECs on numerous projects has enabled the confirmation of design, installation and performance, leading to industry confidence in the technique. Furthermore, laboratory testing of columns has been undertaken to investigate aspects including consolidation rate and encasement stiffness. However, like previous laboratory testing of conventional stone columns set out earlier in this Chapter, much testing has focussed on the behaviour of isolated columns. The technique is limited to using sand as a column backfill material which may be expensive and difficult to source in some cases. Also, the stiffness of the



reinforced soil is less than that provided by other techniques including soil mixing, which may lead to problems associated with long-term creep settlement.

#### 2.4.5 Geogrid encased stone columns

Research into the use of geogrid encased stone columns began in the mid 1990s and has been the focus of German company NAUE GmbH (Heerten and Ewert 2004; Heerten et al. 2004). The method comprises encasing a stone column in a sleeve of geogrid, as illustrated in Figure 2.15. The method is similar to GECs, except that geogrid is used in place of geotextile and due to the robustness of the geogrid, typical stone column aggregates can be used as backfill material in place of sand. In contrast to GECs, geogrid encased stone columns are still in the early stages of development, with little testing of the technique having been undertaken to date.

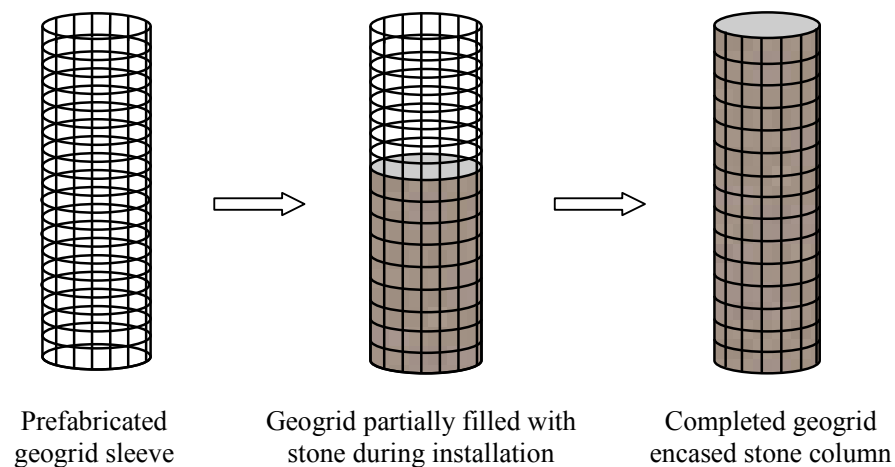


**Figure 2.15:** Geogrid encased column installation

The principles of geotextile and geogrid encased column behaviour are very similar. Both systems utilise hoop forces generated within the geosynthetic material to provide lateral restraint to the column in addition to that provided by the surrounding soil. However, the geogrid is typically stiffer than geotextile (especially during initial loading), generating a more rigid response. The geogrid is also likely to be used in conjunction with typical stone aggregates such as coarse crushed rock gravel, rather than sand. Finally, the increased robustness of the geogrid is likely to enable a greater compactive effort to be

used during installation, resulting in a denser column. These factors may produce a stiffer column response under loading when compared to GECs, lending the technique to its own unique set of applications.

#### 2.4.5.1 Small-scale laboratory testing

Although many authors have investigated the behaviour of soil reinforced with layers of geogrid, Al-Joulani and Bauer (1995) were one of the first to investigate its application for encasement of stone columns. Their work concentrated on testing samples of aggregate wrapped with two types of geogrid in a triaxial apparatus. The geogrids were formed in a cylindrical shape measuring 225 mm in diameter and 450 mm high and filled with compacted aggregate. Columns were loaded under a constant rate of axial displacement until geogrid failure occurred. From their research, they concluded that capacity was significantly increased when compared with non-encased columns.

Malarvizhi and Ilamparuthi (2007) used small-scale laboratory testing coupled with finite element modelling (using the geotechnical software PLAXIS – described in more detail in Chapter 4 of this thesis) to investigate the behaviour of isolated geogrid encased stone columns. Amongst other observations, they concluded that the Soft Soil model and Mohr Coulomb model within PLAXIS could adequately represent the behaviour of the soft clay and stone column aggregate used in testing.

#### 2.4.5.2 Large-scale testing and site trials

Paul and Ponomarjow (2004) investigated analytical solutions for the calculation of encased column capacity, based mostly on the unit-cell approach adopted by Raithel and Kempfert (1999). Their work was supplemented by laboratory and field testing which included large-scale testing of encased stone columns under laboratory conditions. This was followed by field testing to investigate installation techniques (Trunk et al. 2004).

The laboratory tests comprised static loading experiments on free-standing columns measuring 0.6 m in diameter and 1.88 m high (but up to 3 m high in some cases). Several types of geogrid and aggregate combinations were tested. Secugrid<sup>®</sup>, comprising a mechanically bonded geogrid was used with coarse stone aggregate. Combigrd<sup>®</sup>,

comprising a combined geogrid and geotextile sleeve was used with fine aggregate to confine the material within the column. The horizontal geogrid ribs were mechanically welded using about 30 mm of overlap to form the cylindrical sleeve, as presented in Figure 2.16. Results of the testing indicated that during loading, circumferential strains of about 2% were measured prior to failure, although failure generally comprised column buckling (due to the unconfined state). Deformation behaviour and capacity of the encased columns were observed to lie between those of conventional non-encased stone columns and vibro concrete columns. The Young's modulus of the fully-encased columns were back-calculated to generally be in the range of 15 MPa to 18 MPa, but up to 80 MPa in some cases.



**Figure 2.16:** Conventional welding of horizontal geogrid ribs

Field trials were aimed at optimising the installation technique, including varying the column diameter, varying the compactive effort used and incorporating a stiff overlying layer in the installation. It is understood that the columns were installed using the bottom feed method. Geogrid was welded into a cylindrical sleeve with a closed toe and placed around the outside of the vibroflot prior to installation. The vibroflot was used to push the geogrid sleeve to the target depth, where the column was then filled with stone aggregate in lifts and compacted.

Excavation of columns at completion showed that little structural damage occurred to horizontal ribs during the installation process, particularly when horizontal ribs were placed on the inside of the encasement. In this case, horizontal ribs were located on the inside of the sleeve to prevent them being torn away from the vertical ribs as the encasement was being pushed into the ground. An excavated column is presented in

Figure 2.17. The field trials also indicated that the backfill material (stone aggregate) could be installed with a high relative density.



**Figure 2.17:** Excavated geogrid encased stone column

## **2.5 Summary**

Conventional stone columns are commonly adopted to improve the engineering properties of soft to firm cohesive soils for the support of lightly and moderately loaded structures such as embankments. Much work has been undertaken over the last forty years to investigate conventional stone column behaviour through small-scale laboratory testing, site testing and theoretical methods.

Much of the physical testing has focussed on assessing the capacity and radial expansion behaviour of isolated stone columns, even though group behaviour generally has more practical significance. This is probably due to the relative simplicity of testing and assessing isolated column behaviour compared to group behaviour. The typical behaviour of isolated columns is hence relatively well established and well documented. When loaded, columns tend to bulge near the surface where the lateral confining stresses and stiffness in the surrounding soil may be lower.

The behaviour of a column within a group is not as well understood. Very little work has been undertaken to assess the radial expansion of a full-scale column within a large group, probably due to the destructive nature of such an investigation. Small-scale testing of model column groups has shown that the magnitude of bulging is significantly reduced by

confinement from adjacent columns. This behaviour is also expected in the oedometric like conditions that may occur beneath the centre of a wide, uniformly-loaded area like an embankment. However, for this case, it is generally considered that radial expansion will be greater in the upper section of the column, where confining stresses and stiffness in the surrounding soil are lower.

It is also generally accepted that conventional stone columns are not suited to soils with undrained shear strengths less than about 5 kPa. Below this strength, the stiffness of the soil is generally insufficient to adequately confine the column. Mobilisation of construction equipment and trafficking in soils of such low strength can also be problematic.

To extend the use of stone columns to extremely soft soils, geosynthetic reinforcement has been adopted to provide the necessary confinement to the column. The most successful reinforcement technique to date has comprised encasing the full length of a sand column in geotextile, providing radial confinement to the column through the generation of hoop forces in the geotextile during loading. The technique has been used on numerous projects throughout Western Europe and South America.

The concept of geogrid encasement has been a relatively new development, with the technique likely to provide a stiffer column response than GECs (particularly under initial loading), thereby further reducing vertical settlement. Being a relatively new development, geogrid encasement has not been well researched and further investigation is required to confirm its suitability to a range of stone column applications.

## **2.6 Proposed research**

The research that forms the basis of this thesis investigates the suitability of geogrid encased stone columns to applications in very soft soils. Given that isolated column loading is rarely adopted in practice and that column groups are used for most site applications, the research will primarily focus on simulating column group behaviour. However, some isolated column testing will be undertaken to compare encased column behaviour to the well documented behaviour of conventional isolated columns. Furthermore, floating columns will not be considered in this thesis as they are rarely used on site (at least in Australia) and are not likely to be compatible with geogrid encasement.

Based on the bulging behaviour of isolated columns and limited testing of partially encased isolated columns (Murugesan and Rajagopal 2007), sufficient column confinement for certain applications may be achieved through partial encasement of only the upper section of a column. This concept will be investigated for isolated columns and extended to group columns, given that the radial expansion of a column within a group is likely to be greater near the surface than at depth. Should the technique of partial encasement prove effective for column groups, it could potentially provide a significant cost saving on large projects.

Finally, the technique of mechanically welding the horizontal geogrid ribs to form a cylindrical geogrid sleeve (the technique adopted in recent German trials and set out previously) requires shipment of a heavy and bulky welding frame to site. It is expected that shipment will be time-consuming and prohibitively expensive, except perhaps for very large projects where the additional costs can be absorbed. To find a cheaper and more practical technique for constructing geogrid encasement on site, an alternative technique to welding will be investigated.

The study is based on a four-stage approach comprising:

- (i) Small-scale laboratory testing of model geogrid encased sand columns using custom-made, enlarged consolidation cells.
- (ii) A numerical simulation of small-scale tests to supplement the laboratory test results.
- (iii) Medium-scale laboratory testing of geogrid encased stone columns to investigate a practical method of encasement construction (other than welding) and the impact of material properties on encased column behaviour.
- (iv) Full-scale numerical modelling to investigate the impact of different geogrid, column aggregate and soil properties on full-scale encased column behaviour.

### 3 Small-scale laboratory tests

---

Small-scale laboratory tests were undertaken to investigate various aspects of geogrid encased column behaviour, including:

- comparison of group column behaviour to isolated column behaviour,
- the impact of partial encasement (encasing just the upper section of the column) on column behaviour,
- an alternative method to welding when constructing the geogrid encasement, and
- the impact of geogrid stiffness on encased column behaviour.

Details of the design and construction of the test apparatus, test procedure and test results are provided in this chapter.

#### 3.1 Background

In geomechanics, laboratory model testing is a common and relatively inexpensive method of investigating engineering behaviour without the cost and inconvenience associated with site testing (full-scale testing). Laboratory model testing cannot generally replicate the unique soil properties or stress conditions found at a particular site, although centrifuge testing can address the latter to some extent. Nevertheless, small-scale geotechnical models have been used successfully in the past to predict full-scale behaviour, and this is also true for conventional stone column studies. Many previous authors, such as Hughes and Withers (1974), have used small-scale testing to predict full-scale stone column behaviour and to develop design techniques.

On this basis, a method of testing was developed to investigate the behaviour of small-scale geogrid encased stone columns. Although trends observed in small-scale tests are identified and discussed later in this chapter, the results of small-scale testing were not intended to be used for direct interpretation of full-scale column behaviour. The aim of this testing was primarily to measure aspects of small-scale encased column behaviour that could then be simulated numerically. Numerical methods were then used to scale-up columns and investigate the impact of different material and geometric properties on full-scale column behaviour. Numerical modelling is described in later chapters.

### 3.2 Apparatus design, construction and operation

In this study, a method was established for testing small-scale geogrid encased sand columns. Emphasis was placed on scaling down encased column properties. In developing a suitable test apparatus, emphasis was placed on making the apparatus as large as possible while remaining economical to construct and operate. In addition, the test procedure was to be reliable and easily repeated. This section describes the design, development and manufacture of the apparatus used in the small-scale testing program. Design considerations and instrumentation requirements are also discussed.

#### 3.2.1 Testing considerations

Laboratory model testing was proposed on the basis that a sample of consolidated kaolin clay adequately represented a soft natural soil deposit. In addition, it would appear reasonable that a sand column installed in the clay could provide a reasonable small-scale model of a stone column. An initial requirement of testing was that the apparatus consolidated kaolin slurry to the consistency of very soft clay, in which the model columns were to be installed. Secondly, the cells were required to apply a vertical surcharge load to the columns. The final cell design was governed by the objectives of this study, which are summarised in Table 3.1 and described in detail in Appendix A.1.

**Table 3.1:** Objectives of small-scale modelling

	<b>Objectives</b>	<b>Comments</b>
(i)	Investigating column group behaviour, simulated using unit-cell boundary conditions.	2 No. steel cells proposed to expedite testing. 155 mm internal diameter. 51 mm diameter column proposed, resulting in $A_r$ of 11%.
(ii)	Investigating isolated column behaviour, with columns loaded using a small footing equal in diameter to the column.	Perspex cell proposed, 143 mm internal diameter. 51 mm diameter column proposed.
(iii)	Using staged loading of model columns to represent the staged construction commonly used in stone column projects.	Different to constant displacement techniques generally used in scaled laboratory testing. Maximum cell pressure of about 350 kPa.



	Objectives	Comments
(iv)	Investigating partial encasement – whether the full-length of the column needs to be encased.	Tests proposed using encasement of the upper 25%, 50%, 75% and 100% column length. 310 mm high columns.
(v)	Investigating the impact of geogrid properties (namely stiffness and strength).	Fibreglass and aluminium mesh proposed with different properties.
(vi)	Investigating method of alternative construction of geogrid sleeves.	Comparing overlapped mesh behaviour to mesh welded with epoxy-resin.
(vii)	Reducing various aspects of model testing by an appropriate scale factor.	Including column length, diameter, particle size, mesh aperture size, etc.
(viii)	Measuring stress concentration – ratio of column stress to soil stress.	Considered an important design parameter. Instrumentation required.

### 3.2.2 Cell construction

#### 3.2.2.1 Design requirements

The consolidation cells were required to fulfil several criteria, comprising:

- Acting as an oedometer to initially consolidate kaolin slurry to the consistency of very soft clay.
- Being of suitable size to consolidate kaolin slurry in an economical timeframe.
- Following column installation, being capable of further loading the columns using either unit-cell loading to simulate group column behaviour or isolated column loading (using a small footing equal in diameter to the column).
- Being of adequate diameter to maintain a column spacing of at least  $2.5D$  for isolated columns, and a replacement ratio of  $10\% < A_r < 35\%$  for column groups (based on a column diameter of 51 mm).
- Having sufficient instrumentation to measure excess pore pressure in the kaolin clay and sample compression during loading.

- Producing reliable and repeatable results.
- Being constructed from readily available materials to expedite construction.
- A design that could be constructed at the Monash Civil Engineering Workshop.

### 3.2.2.2 Preliminary design

Cell dimensions were based on the design requirements and the compressibility of kaolin slurry. The preliminary cell design was similar to those adopted by previous researchers including Hughes and Withers (1974) and McKelvey et al. (2004). The cell comprised a thin-walled, large diameter cylinder in which the slurry was placed in preparation for consolidation. A piston was used to load the slurry while enabling two-directional cell drainage from the top and base of the cell.

A number of techniques for loading the piston were investigated, including using:

- air pressure applied directly to the top of the piston.
- air pressure applied through an inflatable rubber diaphragm.
- dead weights applied directly to the piston.
- a hydraulic jacking system.

The option of dead weights was immediately discarded due to the impractically large (and potentially unsafe) weight needed to generate the required surcharge load. A jacking system and associated load frame were seen as being too costly and time-consuming to construct. The option of using an inflatable rubber diaphragm to apply the load was considered favourable, as it would prevent air from passing around the piston and coming in direct contact with the slurry. This would eliminate the need for the piston to be sealed with an O-ring, thereby eliminating the resistance associated with the seal during loading. However, given the high compressibility of the proposed slurry, a custom-made diaphragm was required, making this option prohibitively expensive. Although there was inherent resistance in load transfer, the option of sealing the piston with O-rings and then applying surcharge load using air pressure was chosen as being the most practical and economical design to construct and operate.

The use of this approach was accompanied by measurement to quantify friction and reduce it where practical. Side-wall friction in the cell was identified as a problem that affected testing in two ways:

- (i) Shear stresses developed at the interface between the slurry and the cell reduced load transferred to the base of the cell, invalidating the one-dimensional assumption.
- (ii) Friction between the side-wall of the cell and the O-rings of the piston reduced the efficiency of the piston to transfer load to the sample.

Based on research undertaken by Gachet et al. (2003), who showed that lubrication significantly reduced cell resistance, the use of lubricant was investigated to reduce side-wall friction. This was undertaken following construction of the cells.

#### 3.2.2.3 Detailed design

Detailed design was undertaken in consultation with the Monash University Civil Engineering Workshop, to ensure that the correct tolerances and clearances were applied to the cell design. A series of detailed drawings were developed for Workshop use during construction. As a result of the cells operating at an internal pressure of up to about 350 kPa, the cells were designed as pressure vessels, in general accordance with Australian Standard AS1210 – 1997 ‘Pressure Vessels’. A sketch of the final cell design is presented in Figure 3.1.

#### 3.2.2.4 Cell Manufacture and Instrumentation

Three consolidation cells were manufactured. The first cell was constructed from Perspex and used to test isolated columns. The second type of cell, of which two were made, was constructed from stainless steel and used to simulate group column behaviour using unit-cell idealisation. The design and construction of the three cells was completed over a period of about 12 months. The construction materials and process used in manufacturing are summarised in Appendix A.2, along with details on instrumentation and aspects of operational safety. A photograph of the three cylinders in operation is presented in Figure 3.2. The Perspex cell is located to the right of the frame.

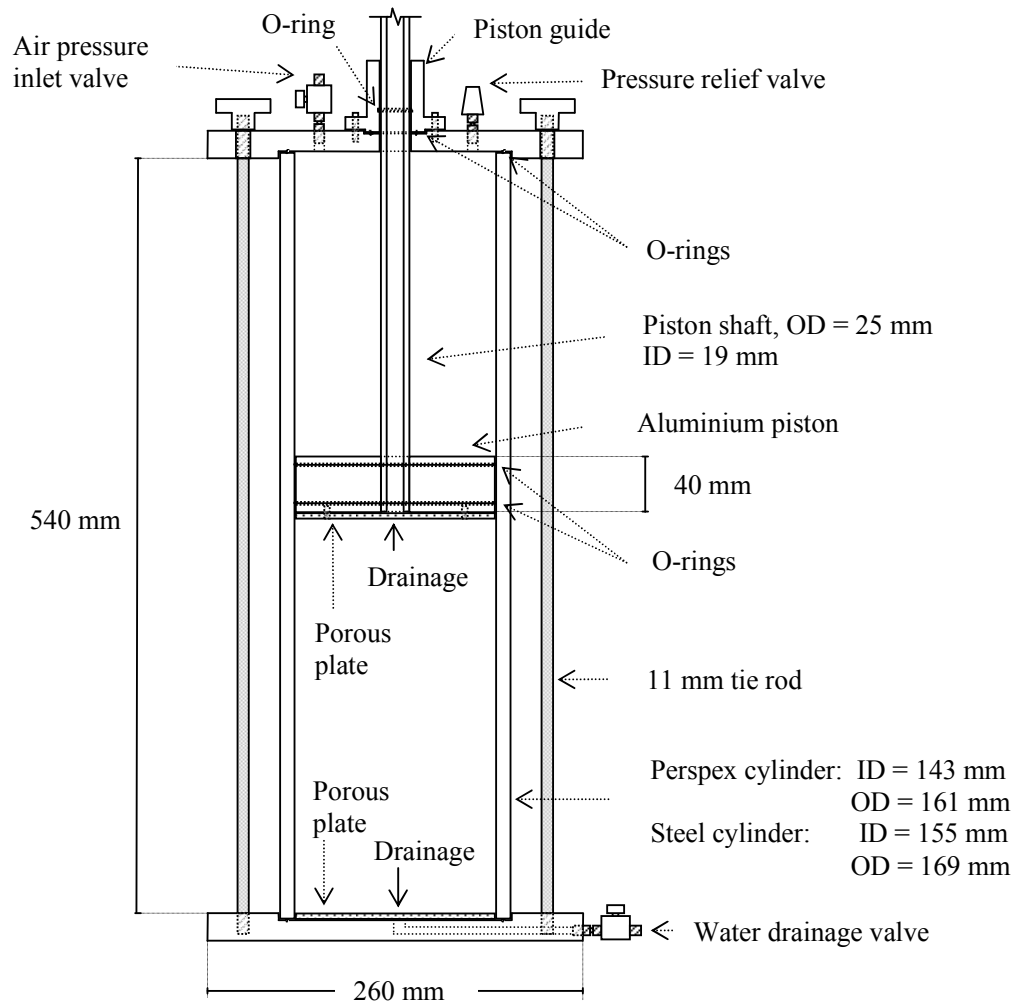


**Figure 3.1:** Sketch of adopted consolidation cell design



**Figure 3.2:** Consolidation cells used in model column testing

### 3.2.3 Cell operation

Load was applied to the kaolin slurry by pressurising the chamber above the piston with air, driving the piston downwards. Water drained through the groove within the piston shaft and through the groove in the base plate, causing consolidation. The water level was kept above the level of the piston at all times to maintain saturation. The concept of sample consolidation is illustrated in Figure 3.3. To prevent slurry ‘squeezing’ around the piston and coming in contact with pressurised air, a double O-ring system was adopted. Resistance was reduced between the side-wall of the cell and piston O-rings by boring and polishing the inner surface of the cell. Furthermore, a thin layer of lubricant was applied to the internal surface of the cell prior to being filled with slurry. The effect of lubrication is discussed later in this chapter.

#### Steel cell

The air pressure supplied to the upper chamber of the cell was measured using calibrated gauges with an accuracy of about  $\pm 5$  kPa. The actual pressure applied to the kaolin slurry was measured using two pore pressure transducers mounted to the side of the cell. For each load stage, the load resistance was assessed as being the difference between air pressure supplied to the cell and excess pore pressure within the slurry. The resistance was also measured during cell calibration and is described later in this chapter.

#### Perspex cell

The pressure supplied to the upper chamber of the cell was measured using a calibrated air pressure gauge with an accuracy of about  $\pm 2$  kPa. Pore pressure transducers were not used because of the potential weakness introduced into the Perspex cylinder. As a result, pore pressures within the kaolin were not measured. However, load resistance was measured during calibration, enabling assessment of pressure applied to the slurry. The calibration process is described later in this chapter.

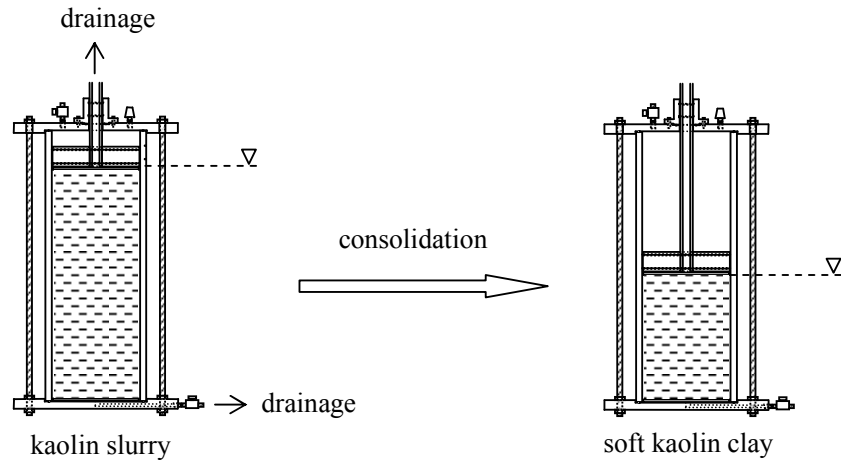


**Figure 3.3:** Concept of slurry consolidation within the cell

#### 3.2.4 Formation of column and geogrid encasement

Previous researchers have encountered difficulty when attempting to compact a column in-situ, particularly when using a displacement technique. In such cases, repeatability of column density and permeability has been difficult to achieve (Sivakumar et al. 2004). A replacement technique using prefabricated columns was therefore adopted to provide a more reliable and repeatable method of column installation. The method of prefabricated frozen sand columns, described by Sivakumar et al. (2004) was used. Although this method is not an installation technique that is used on site, it was considered to provide a suitable method of sample preparation.

Using this technique, the column was compacted to the required relative density (of about 90%) within a plastic mould before being saturated, frozen, and extruded. The frozen column measured 50.5 mm in diameter. A thin-walled aluminium tube measuring 51 mm in diameter was then pushed into the clay sample, creating a cylindrical cavity at its centre that extended to the base of the cell. The frozen column was then placed in the cavity, with the slightly smaller column diameter (compared to the cavity) aiding installation.

Fibreglass and aluminium meshes were used to replicate geogrid in small-scale. The process of mesh selection was based primarily on geogrid geometry, namely aperture size. The mesh was shaped into a cylindrical sleeve and bonded using epoxy-resin adhesive to replicate the welded geogrid encasement that has been adopted for site construction in the

past. In some cases, the mesh was overlapped by either a half circumference or full circumference (without bonding) to investigate an alternative method of fixing the encasement in position. Where encased columns were used in testing, the mesh sleeve was placed inside the plastic mould prior to being filled with sand. Further details regarding mesh properties and encased column construction are presented later in this chapter.

### 3.2.5 Sample loading

Following installation, the columns were loaded either as simulated group columns using unit-cell idealisation or as isolated columns. Both methods are described in the following sections and are illustrated in Figure 3.4.

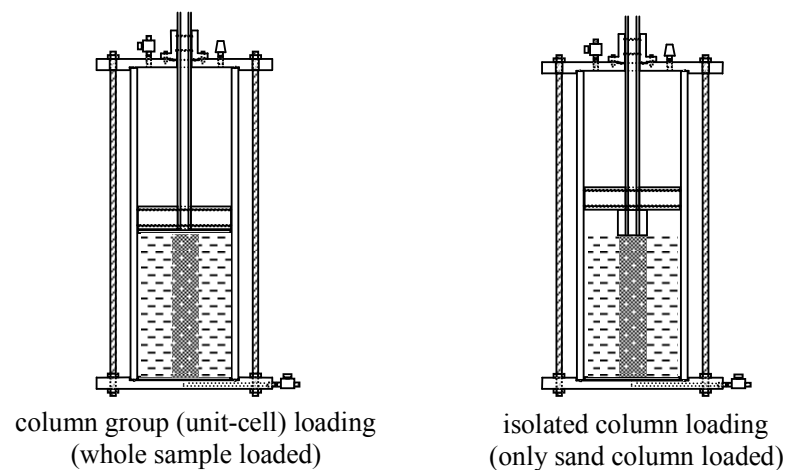


**Figure 3.4:** Concept of simulated column group loading and isolated column loading

#### 3.2.5.1 Column group loading

The piston used to consolidate the kaolin slurry was also used to further load the column-clay sample as a unit-cell. After the column had been installed and thawed (which was ensured by leaving the sample for about 3 hours prior to loading), the cell was loaded by about 4 kPa above the pre-consolidation pressure of the clay. This nominal loading enabled a small amount of additional consolidation to occur, allowing the sand column and clay to be in intimate contact. Furthermore, reductions in column density that may have occurred during freezing or installation may have been recovered, although no

attempt was made to confirm this. Loading was then advanced in increments ranging from about 15 kPa to 70 kPa, depending on percent encased length. The sample was allowed to undergo consolidation under each load stage. Samples were subjected to a maximum pressure of about 350 kPa.

#### 3.2.5.2 Isolated column loading

A small steel footing measuring 51 mm diameter (equal in diameter to the sand column) and 50 mm high was fixed to the underside of the piston. A porous plate was attached to the underside of the footing, allowing vertical drainage through the footing. The column was loaded in increments of about 10 kPa (depending on percent encased length) until failure. As above, samples were allowed to undergo consolidation under each load stage.

For pressures less than 200 kPa, the O-rings surrounding the piston and within the piston guide were removed to eliminate resistance in the loading mechanism. A load plate was then attached to the top of the piston shaft, enabling the column to be loaded with weights. The use of weights was considered to be more accurate for lower pressures, as load stages could be advanced in smaller increments and friction was negligible. For surcharge pressures greater than 200 kPa, the weight required to load the piston became too large to be supported by the cell. Therefore, the cell was adapted to load the column with air pressure. This comprised re-attaching O-rings to the piston and piston guide so that air pressure could be sealed within the upper chamber of the cell.

### 3.3 Materials

The following section describes the engineering properties and behaviour of materials selected for use in small-scale laboratory tests.

#### 3.3.1 Kaolin clay

To investigate the behaviour of geogrid encased stone columns, very soft samples of clay were required in which to install the columns. The samples were required to be homogeneous and provide consistent, repeatable behaviour. In addition, the



compressibility of the clay needed to reflect a natural soft soil deposit. Based on these requirements, kaolin was adopted. Commercially available kaolin clay has been used extensively in geotechnical laboratory research for many years and its properties are well suited to the production of compressible, homogeneous clay samples. Powdered kaolin (Grade HR1F, supplied by Unimin Australia Ltd.) was used for the small-scale testing component of this research.

#### 3.3.1.1 Atterberg limits

The liquid limit and plastic limit of Kaolin Grade HR1F were measured in general accordance with Australian Standards AS1289.3.1.1 and AS1289.3.1.2, respectively. Atterberg limits for the kaolin are presented in Table 3.2.

**Table 3.2:** Atterberg limits for kaolin Grade HR1F

<b>Parameter</b>	<b>Value</b>
Plastic Limit (%)	29
Liquid Limit (%)	62
Plasticity Index (%)	33

#### 3.3.1.2 Particle size distribution

Particle size distribution testing by sedimentation was undertaken on samples of kaolin Grade HR1F by the supplier. Results of particle size distribution testing are presented in Table 3.3, indicating that kaolin comprised mostly clay.

**Table 3.3:** Particle size distribution of kaolin Grade HR1F

<b>Parameter</b>	<b>Value</b>
Approximate clay fraction (<0.002 mm)	86%
Approximate silt fraction	11%
Approximate fine sand fraction	3%

### 3.3.1.3 Consolidation behaviour

Samples of kaolin slurry were prepared at different initial moisture contents to select a slurry with a viscosity that enabled it to be poured into the consolidation cell. Based on these tests, slurry with an initial moisture content of 115% was considered appropriate and practical. This corresponded to an initial moisture content of about 1.8 times the liquid limit. Slurries with lower initial moisture contents were found to be difficult to handle and had an increased occurrence of visible air bubbles entrapped within the slurry matrix. One-dimensional consolidation tests were then undertaken on the slurry to measure its compressibility (in general accordance with Australian Standard AS1289.6.6.1).

Results from two consolidation tests undertaken on kaolin slurry with an initial moisture content of 115% are plotted in the e-log pressure plane and presented in Figure 3.5. Engineering properties derived (in part) from these tests are presented in Table 3.4. Results indicated a similar compressibility to natural soft clays.

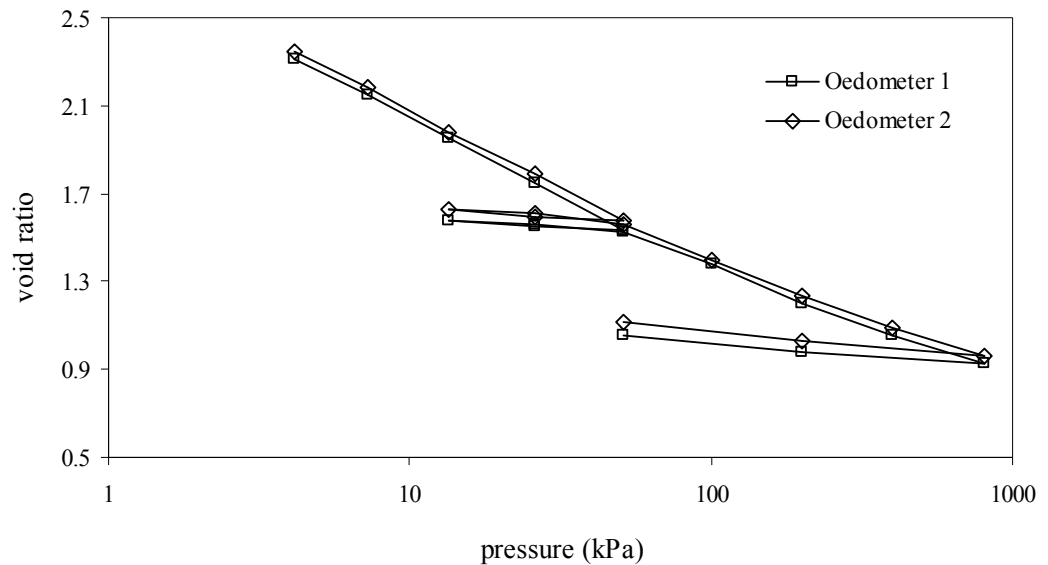


**Figure 3.5:** e-log pressure behaviour of kaolin slurry

**Table 3.4:** Consolidation properties of kaolin slurry

Parameter	Value
Specific gravity	2.64
Initial moisture content (%)	115
Initial void ratio, $e_0$	3.04
Average Compression Index, $C_c$	0.80
Average Recompression Index, $C_r$	0.09

The saturated density of kaolin after being consolidated at a vertical stress of 54 kPa (corresponding to a moisture content of 62%) was approximately 1620 kg/m<sup>3</sup>.

#### 3.3.1.4 Permeability

Determination of the permeability of kaolin clay was important for designing a suitable and economical test schedule. It was also a key parameter required for numerical modelling, the results of which are presented in Chapter 4. Permeability was calculated indirectly from consolidation tests. The coefficient of consolidation was first calculated from assessing time-settlement data obtained from oedometer tests undertaken on kaolin clay.

The coefficient of consolidation,  $c_v$ , was calculated using the following well-established equation:

$$c_v = \frac{T_{90} H_{dr}^2}{t_{90}} \quad (3.1)$$

Here,  $T_{90}$  is a time factor taken as 0.848 for 90% consolidation.  $H_{dr}$  is the length of the drainage path. For two-directional drainage (standard oedometer test),  $H_{dr}$  is taken as the initial height of the sample divided by two.  $t_{90}$  is the time taken to complete 90% consolidation, determined using Taylor's square root of time fitting method (Taylor 1948) and further described by Holtz and Kovacs (1981).

The coefficient of permeability,  $k$ , was obtained indirectly from the consolidation tests using the following relationship (e.g. Holtz and Kovacz 1981):

$$k = \frac{c_v \rho_w g a_v}{1 + e_0} \quad (3.2)$$

Where  $e_0$  is the void ratio at the start of the time readings for a given load increment,  $\rho_w$  is the unit weight of water (taken as  $10 \text{ kN/m}^3$ ),  $g$  is acceleration due to gravity (taken as  $9.81 \text{ ms}^{-2}$ ) and  $a_v$  is the coefficient of compressibility calculated using the following equation:

$$a_v = \frac{e_1 - e_2}{\sigma'_2 - \sigma'_1} \quad (3.3)$$

Where  $e_1$  and  $e_2$  are the initial and final void ratio, respectively, for a given load stage.  $\sigma'_1$  and  $\sigma'_2$  are the initial and final effective stress, respectively, for a given load stage.

Calculated permeability was found to vary depending on stress, which ranged from 4 kPa to 801 kPa. Permeability ranged from  $7.4 \times 10^{-9} \text{ m/s}$  to  $6.62 \times 10^{-11} \text{ m/s}$ , with an average of approximately  $9.2 \times 10^{-10} \text{ m/s}$ .

### 3.3.1.5 Shear strength and moisture content

An essential component of this research was to install sand columns in a homogeneous bed of clay with a low undrained shear strength. As geosynthetic encasement is typically adopted in very soft and extremely soft soils, an undrained shear strength of about 5 kPa was targeted. A custom-built consolidation cell (measuring 100 mm high) was used to produce samples of consolidated kaolin over a range of moisture contents for strength and moisture testing. Consolidated samples measured between 30 mm and 60 mm high and were tested using a combination of laboratory vane shear and pocket penetrometer tests. The tests were used to investigate the relationship between moisture content and undrained shear strength, presented in Figure 3.6. The relationship between void ratio and undrained shear strength is presented in Figure 3.7. The figures also include data from the small-scale column tests undertaken as part of this research and outlined later in this chapter.

The strength and moisture testing indicated that a saturated bed of consolidated kaolin with an undrained shear strength of about 5 kPa was achieved at a moisture content of about 62% (equating to a void ratio of 1.64). Based on oedometer tests, a vertical pressure

of about 54 kPa was required to consolidate a sample of kaolin from an initial void ratio of 3.04 to 1.64. It follows that a vertical pressure of 54 kPa is required to consolidate kaolin slurry to the target undrained shear strength of 5 kPa.

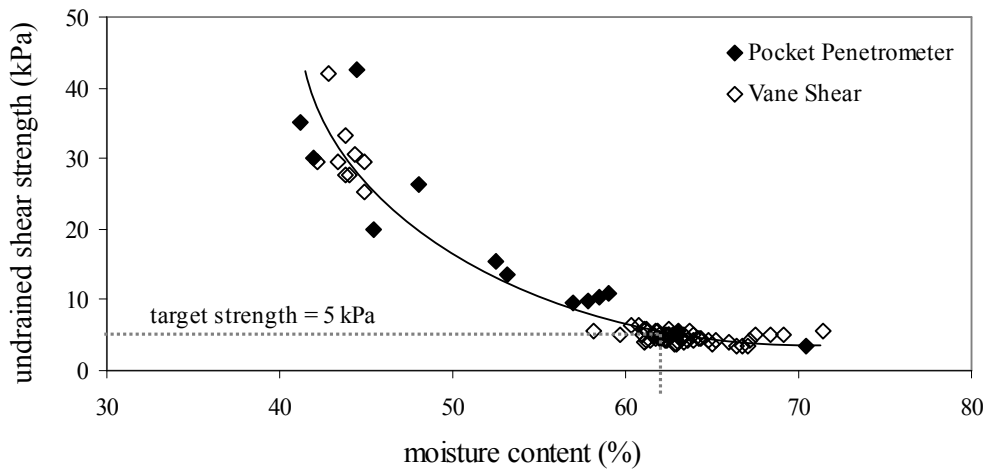


**Figure 3.6:** Moisture content – undrained shear strength relationship for kaolin clay

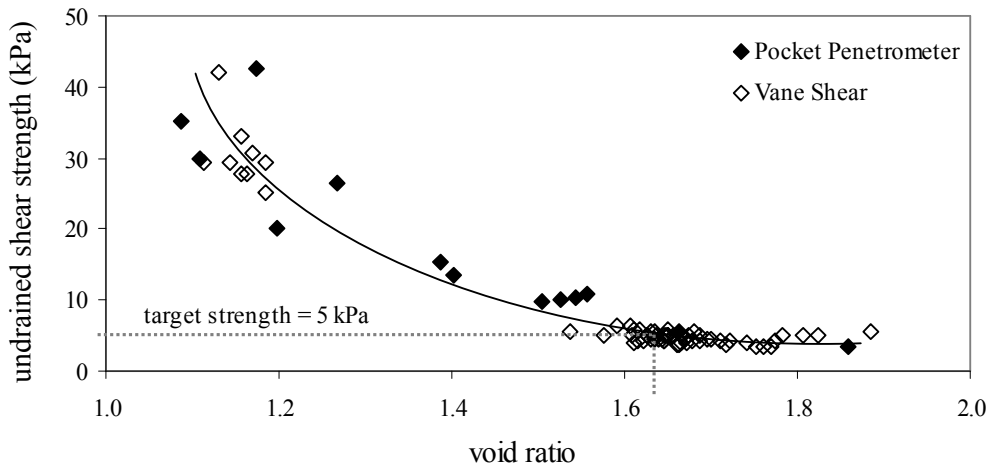


**Figure 3.7:** Void ratio – undrained shear strength relationship for kaolin clay

#### 3.3.1.6 Shear box testing

Shear box testing was undertaken to measure the drained shear strength properties of the kaolin clay. Testing was undertaken in general accordance with Australian Standard AS1289.6.2.2 – 2000. Kaolin slurry was first consolidated in a consolidation cell using a 200 kPa surcharge to form samples of firm clay. The samples were then placed in a conventional shear box measuring 60 mm by 60 mm and loaded to failure. The shear

stress-displacement relationship for the kaolin under effective vertical stresses of 50 kPa, 100 kPa and 150 kPa is presented in Figure 3.8. The behaviour of kaolin was typical of firm cohesive soils, with little dilation across the range of vertical stresses. The peak shear stress for each test was plotted against normal stress to determine the Mohr-Coulomb failure envelope, shown in Figure 3.9. The angle of internal friction,  $\phi'$ , for the kaolin was measured to be approximately  $18^\circ$ .

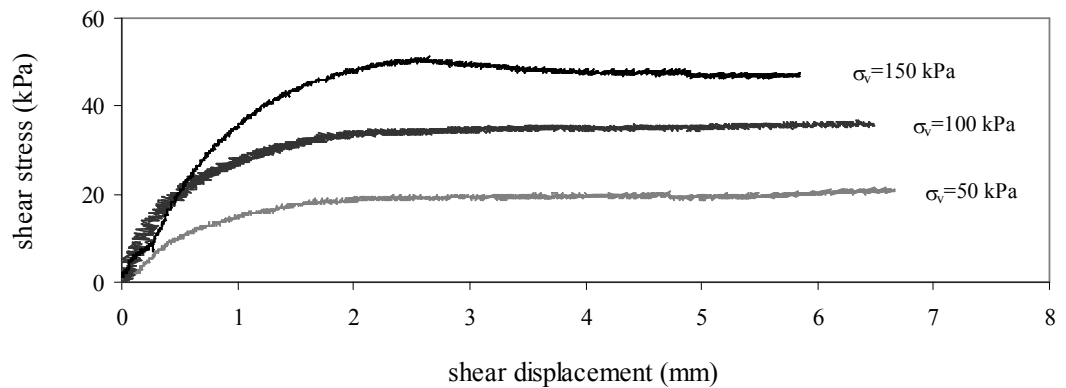


**Figure 3.8:** Shear stress – displacement relationship for kaolin clay

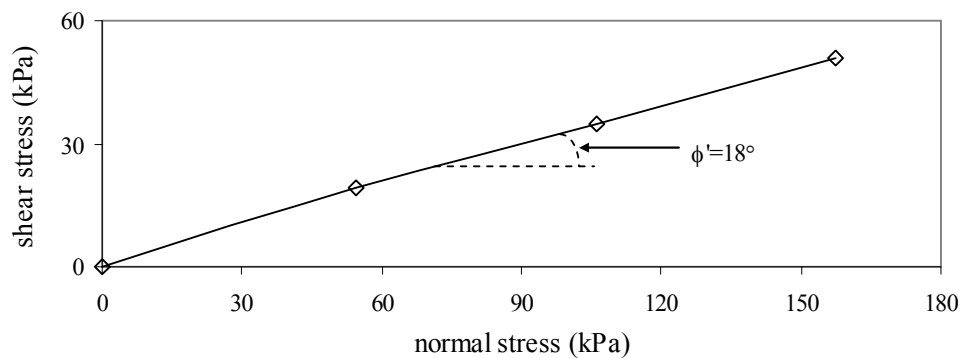


**Figure 3.9:** Mohr-Coulomb failure envelope for kaolin clay

### 3.3.2 Quartz sand

A commercially-available, poorly-graded sand with scaled properties (including particle size, particle shape and grading) similar to typical stone column aggregates was required to investigate the behaviour of geogrid encased model columns in the laboratory. Locally available commercial quartz sand (Grade 8/16, supplied by Unimin Australia Ltd.) was used for this purpose.

### 3.3.2.1 Particle size distribution

The granular material used to form stone columns generally ranges between 25 mm and 75 mm in diameter, is typically angular to sub-angular and in the author's experience, may have a friction angle ranging from  $35^\circ$  to greater than  $50^\circ$  depending on density. The model sand columns used to represent stone columns in the laboratory tests were scaled down from full-size by a factor of between 20 and 35. Therefore, sand with a nominal particle size in the range of 1 mm to 4 mm was required to create a suitable scale-model sand column. The particle size distribution of Grade 8/16 sand, measured from sieve analysis, is presented in Figure 3.10. The sand was poorly graded and had an average diameter of about 1.6 mm. The sand particles were typically sub-angular in shape and were considered a suitable small-scale representation of the stone aggregate used for full-scale stone columns.

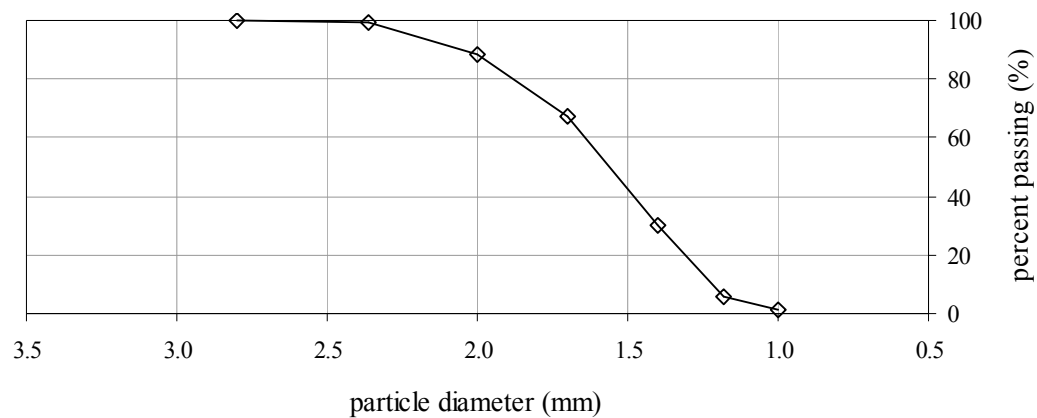


**Figure 3.10:** Particle size distribution for Grade 8/16 sand

### 3.3.2.2 Relative density

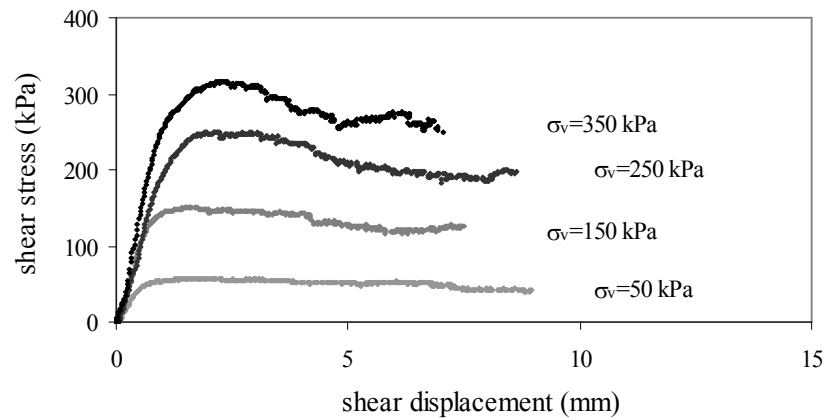
Depending on the method of installation, stone columns generally have a relative density between 60% and 100%. Density testing was undertaken on samples of Grade 8/16 sand in general accordance with Australian Standard AS1289.5.5.1 – 2000. Testing was undertaken to measure the minimum and maximum dry density of the sand to control compaction of model sand columns. Results of the testing are presented in Table 3.5.

**Table 3.5:** Minimum and maximum dry density of Grade 8/16 sand

Parameter	Value
Minimum dry density, $\rho_{\min}$ (kg/m <sup>3</sup> )	1390
Maximum dry density, $\rho_{\max}$ (kg/m <sup>3</sup> )	1650

### 3.3.2.3 Shear box testing

Shear box testing was undertaken to measure the internal angle of friction of Grade 8/16 sand. Samples were prepared for testing at a relative density of 90%. The shear stress-displacement relationship at vertical confining stresses of 50 kPa, 150 kPa, 250 kPa and 350 kPa is presented in Figure 3.11.

**Figure 3.11:** Shear stress – displacement relationship for Grade 8/16 sand

The behaviour of Grade 8/16 sand compacted to a relative density of 90% was typical of other dense sands, showing significant dilation that decreased with increasing confining stress. The peak and residual shear strength for each test was plotted against normal stress to measure the peak and residual failure envelopes, shown in Figure 3.12.



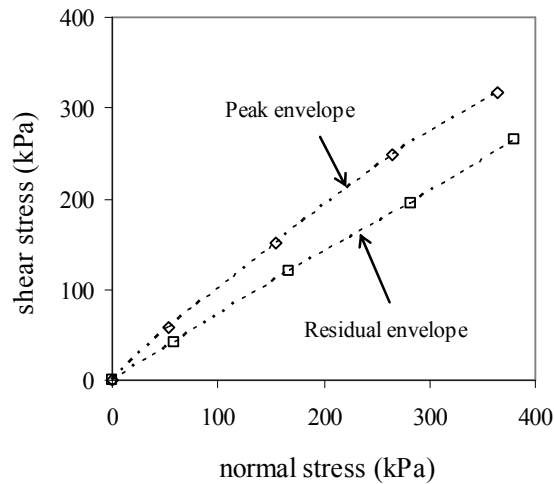


**Figure 3.12:** Mohr-Coulomb failure envelope for Grade 8/16 sand

The residual (or large strain) angle of internal friction,  $\phi'$ , for the sand was determined to be approximately  $35^\circ$ . The peak angle of internal friction ranged from about  $46^\circ$  at a vertical stress of 50 kPa to  $41^\circ$  at a vertical stress of 350 kPa. The measured peak angle of dilation,  $\psi$ , decreased from about  $11^\circ$  to  $6^\circ$  across the same stress range.

#### 3.3.2.4 Consolidation and compressibility

One-dimensional consolidation tests were undertaken on two samples of Grade 8/16 sand to measure compressibility under constrained conditions. These tests were also undertaken to obtain parameters that were used to develop a numerical model representing the sand material. The sand was compacted to a relative density of 90% inside an oedometer ring, filled with water and then conventionally loaded. Results from the two oedometer tests are plotted in the e-log pressure plane and presented in Figure 3.13. Parameters derived (in part) from the oedometer tests are summarised in Table 3.6.

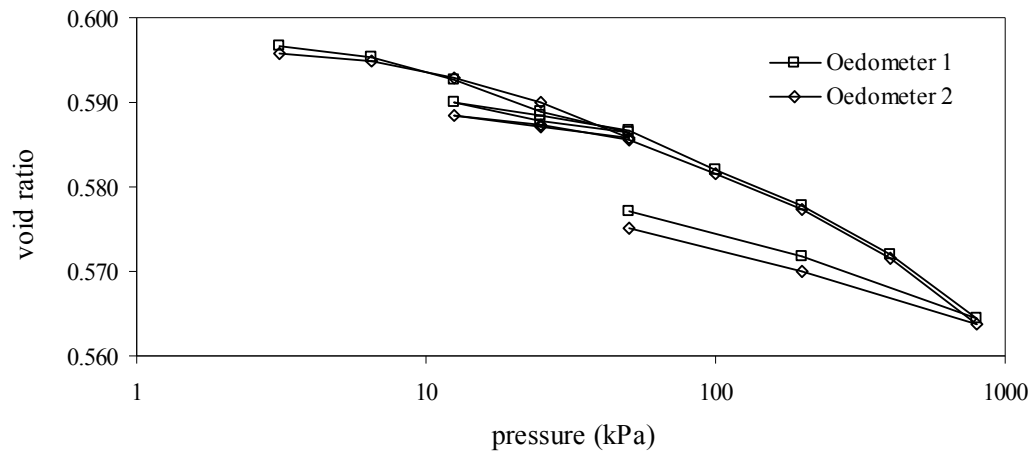


**Figure 3.13:** e-log pressure behaviour of Grade 8/16 sand derived from oedometer testing

**Table 3.6:** Compressibility parameters for Grade 8/16 sand

Parameter	Value
Initial void ratio, $e_0$	0.598
Compression Index, $C_c$	0.013
Recompression Index, $C_r$	0.007
Dry density ( $\text{kg/m}^3$ )	1620
Wet density ( $\text{kg/m}^3$ )	2020

### 3.3.2.5 Permeability

Determination of the permeability of Grade 8/16 sand was required for the development of a representative numerical soil model. Constant head permeability testing was undertaken on five samples of sand. The coefficient of permeability,  $k$ , was measured directly from the tests, and found to range between  $4.2 \times 10^{-2}$  m/s and  $4.6 \times 10^{-2}$  m/s, with an average of  $4.5 \times 10^{-2}$  m/s.

### 3.3.3 Geogrid

To investigate the behaviour of geogrid encased stone columns, a material that replicated the behaviour of geogrid in small-scale was required. Geometric properties, modulus and tensile strength were all considered when selecting a suitable material. Due to the

difficulty in sourcing a small-scale geogrid, readily available fibreglass and aluminium window mesh (“fly-wire”) was used. The mesh was considered geometrically suitable and although the scaled-up stiffness was likely to represent a material with greater stiffness than typical geogrid, the impact of stiffness was to be examined predominantly using numerical techniques (described in Chapters 4 and 6) rather than through small-scale laboratory testing.

#### 3.3.3.1 Mesh properties

Fibreglass and aluminium mesh were used in the testing. The fibreglass mesh comprises glass fibres bunched together to form strands which are woven into a biaxial mesh. The aluminium mesh comprises single aluminium strands woven into a biaxial mesh. Both meshes have a protective paint coating (applied by the manufacturer). Each mesh has similar geometric properties. The average strand diameter of the fibreglass mesh is about 0.2 mm, with an average aperture size of about  $1.35 \times 1.35$  mm. The average strand diameter of the aluminium mesh is about 0.3 mm, with an average aperture size of about  $1.25 \times 1.25$  mm. Based on the particle size distribution of the Grade 8/16 sand, the ratio of aperture size to average particle size is within the range that would generally be used in full-scale, about 1:1.

The two types of mesh also had different stiffness and tensile strength. They were therefore considered to provide contrast for investigating the impact of mesh stiffness and strength on column behaviour. The testing undertaken to define these parameters is discussed in the following sections.

#### 3.3.3.2 Uniaxial testing

A universal (tension compression) testing machine was used to test mesh samples measuring 200 mm long  $\times$  25 mm wide. Samples were placed into the upper and lower steel jaws and locked in place. The steel jaws were lined with a thin layer of latex rubber that prevented crushing of the strands while still maintaining adequate grip. Tensile load was then applied to the sample by pulling the jaws apart relative to each other, at a constant rate of 1 mm/min. A number of tests were undertaken to confirm that a consistent load-strain behaviour had been obtained.

### Fibreglass

Uniaxial tension tests were initially undertaken on 2 samples of fibreglass mesh. The tests indicated a linear load-strain relationship up until sample failure. Failure occurred by a simultaneous rupture of a number of strands at the centre of the sample. The load-strain relationship for the fibreglass mesh is presented in Figure 3.14. Results indicated that the maximum average load of 0.021 kN per strand occurred at a strain of about 4%. This equates to a tensile strength of about 13.5 kN/m width of mesh.

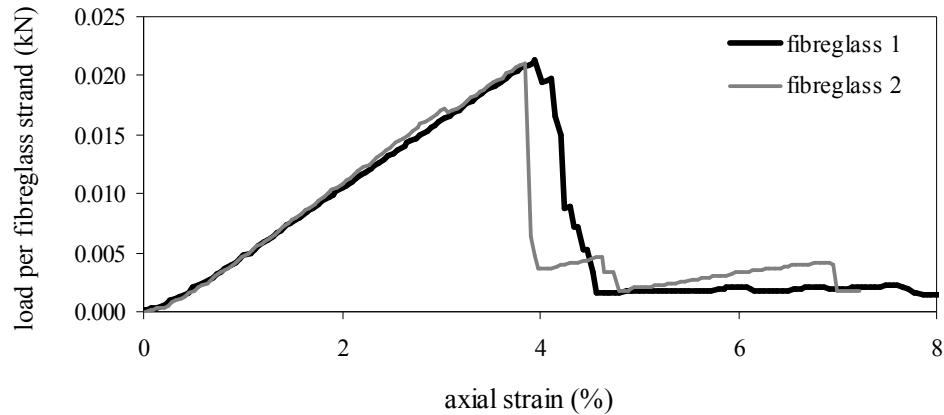


**Figure 3.14:** Load-strain relationship for fibreglass mesh

### Aluminium

Uniaxial tension tests were undertaken on 3 samples of aluminium mesh. The testing indicated an initial linear load-strain relationship, followed by creep prior to failure. Failure comprised a progressive rupture of individual strands, generally beginning at the centre of the sample. The load-strain relationship for the aluminium mesh is presented in Figure 3.15. Results indicated that the maximum average load of 0.014 kN per strand occurred at a strain of about 2%. This equates to a tensile strength of about 9.0 kN/m width of mesh.

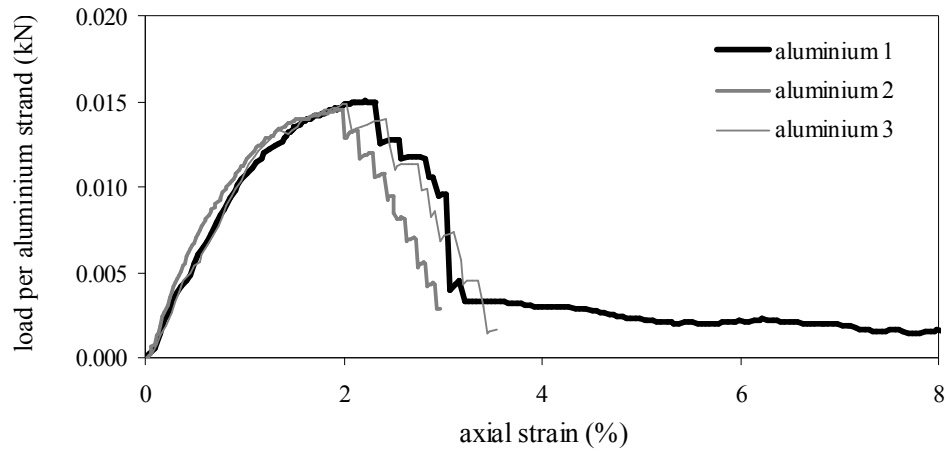


**Figure 3.15:** Load-strain relationship for aluminium mesh

A comparison of load-strain behaviour of the two mesh types indicates the aluminium mesh has a stiffer initial loading modulus. However, the tests indicated the tensile strength of the fibreglass mesh was significantly higher than the aluminium mesh. The tensile test results indicated the two meshes had sufficiently different properties to allow an assessment of the impact of geogrid properties on encased column behaviour (although the results of column testing set out later in this chapter indicate that this is not necessarily the case).

### 3.3.3.3 Weld testing

Additional uniaxial tension testing was undertaken to find a suitable adhesive for welding the mesh encasement. The tests were used primarily to investigate whether strength loss occurred across the weld. Soaked testing (in water) was then undertaken to investigate whether strength loss occurred with submersion. Further details and results of these tests are provided in Appendix A.3. The tests indicated that epoxy-resin was the most suitable adhesive for bonding the mesh, with the weld strength being at least equal to the mesh strength. However, 28-day soaked tests indicated that a loss in strength occurred in both the fibreglass and aluminium meshes. Although water-insensitive meshes were preferred, the strength loss did not significantly affect the mesh stiffness. Because the mesh properties were well defined by testing, both mesh types were retained for encased column testing.

#### 3.3.3.4 Summary of properties

The load-strain behaviour of the soaked fibreglass mesh was typically linear up to failure, which occurred at an axial strain of about 3.5%. In contrast, non-linear yielding was observed for the aluminium mesh when axial strains exceeded about 1%. The *elastic axial stiffness* of geogrid,  $EA$ , was used to define and compare geogrid stiffness.  $EA$  is a parameter that may be supplied by geogrid manufacturers and is determined from the linear section of the load-strain plot, derived from tensile testing. This parameter is important for comparing the stiffness of geogrids and is also used in numerical modelling.  $EA$  is calculated using the following relationship:

$$EA = \frac{F}{\Delta L / L} \quad (3.4)$$

Where  $F$  is the applied axial force per unit width of sample and  $\Delta L / L$  is the axial strain.

The test results indicate the  $EA$  of the aluminium mesh (600 kN/m) was double that of the fibreglass mesh (300 kN/m). These values are at the lower end of the  $EA$  typically associated with full-scale geogrids (which generally range between 200 kN/m and 4000 kN/m), although the scaled-up stiffness of the mesh is likely to represent a material of higher stiffness than the typical values for geogrid set out above.

As the impact of material properties (such as geogrid stiffness) were to be predominantly investigated using numerical techniques, the adopted meshes were considered to be suitable for the small-scale encased column testing. A summary of the properties for the fibreglass and aluminium meshes are presented in Table 3.7. As the tensile strains of the meshes are less than those typical of full-scale geogrids, tensile strengths at 1% and 2% strain are reported.

**Table 3.7:** Summary of soaked properties of fibreglass and aluminium mesh

Parameter	Value	
	Fibreglass	Aluminium
Maximum tensile strength (kN/m)	8.6	6.8
Tensile strength at 1% strain (kN/m)	1.6	5.8
Tensile strength at 2% strain (kN/m)	4.8	-
Strain at maximum tensile strength (%)	3.5	1.3
Strain at failure (%)	3.5	1.8
Aperture size (mm × mm)	1.35 × 1.35	1.25 × 1.25
Average strand diameter (mm)	0.2	0.3
Elastic axial stiffness, EA (kN/m)	300	600

### 3.4 Cell calibration

As set out earlier, the adopted cell design produced frictional effects in operation that could not be easily overcome. The manufacturing process, comprising boring and polishing of the Perspex and stainless steel cells was used to create a smooth internal surface, thereby reducing side-wall friction within the cell to some extent. However, due to the length of the sample, it was considered important to reduce friction as far as could be practically achieved so that load was distributed uniformly throughout the sample. The methods used to reduce side-wall friction are described in this section.

#### 3.4.1 Components of cell friction

Friction could impact the vertical stress-strain behaviour of samples within the cell in the following ways:

- Friction between the kaolin and internal surface of the cells during consolidation (side-wall friction) may produce shear stresses that restrict the vertical strain of the kaolin sample, reducing the stress transmitted to the base of the cell.
- Friction between the two O-rings on the piston and the internal surface of the consolidation cell may produce shear stresses that reduce the vertical pressure applied to the kaolin, such that the pressure applied to the kaolin is less than the pressure applied to the cell.

- Additional friction between the O-ring within the piston guide and the piston shaft may produce shear stresses that may reduce the vertical pressure applied to the kaolin, such that the pressure applied to the kaolin is less than the pressure applied to the cell.

The use of lubricants were investigated as a means of reducing the magnitude of side-wall friction acting in the cell. A lubricant spread evenly across the internal surface of the cell may:

- Reduce shear stresses acting between the sample and the internal surface of the cell, resulting in a more uniform vertical stress distribution in the kaolin sample.
- Reduce shear stresses between the piston O-rings and the internal surface of the cell such that pressure applied to the sample was closer to the cell pressure.

It was considered that the friction acting between the O-rings of the piston guide and the piston shaft could not be reduced in a cost effective manner. Testing was therefore undertaken to quantify the magnitude of the friction losses. Testing was also undertaken to quantify the magnitude of side-wall friction acting within the cells following the application of lubricants. Details of the testing undertaken in both the Perspex and stainless steel cells are provided in Appendix A.4.

### **3.4.2 Summary**

Results of calibration testing and consolidation testing in the Perspex and stainless steel cells indicated significant O-ring and side-wall friction. By applying silicone lubrication to the internal surface of each cell, side-wall friction was reduced to between about 10% and 15% of the applied load which considered satisfactory for the current study.

## **3.5 Test procedure**

The procedure adopted to test isolated and group columns in the three custom-built consolidation cells is described in this section.



### **3.5.1 Slurry preparation**

About 6 kg of powdered kaolin and 10 litres of water were mixed in a large mixing bowl continuously for about four hours using an electric mixer. This resulted in a kaolin slurry with moisture content of about 115%. The homogeneous mix was then left to sit for a further four hours, allowing air bubbles to rise to the surface.

### **3.5.2 Cell preparation**

Approximately 10 grams of silicone was spread evenly across the internal surface of each cell, providing a thin layer of lubrication that significantly reduced cell friction. Two calibrated pore pressure transducers were connected to the side-wall of each stainless steel cell by fastening them to the brass ports. The transducers and brass ports were then saturated with de-oxygenated water. The hole in the side-wall of the cell connecting the sample to the transducer was temporarily sealed with a rubber stopper to maintain saturation of the transducers while the cell was empty.

A porous plate that had been soaked in water was placed at the base of the cell and covered with filter paper. The cylinder was then placed on the base plate. The cell was filled with slurry via a funnel and tube such that the head of slurry within the cell was always above the toe of the tube. This helped to reduce agitation of the slurry and occurrence of air bubbles. After the height of slurry within the cylinder had risen above the location of the pore pressure transducers, the rubber stoppers were slowly removed, maintaining saturation of the transducers. At completion, the slurry height was approximately 480 mm.

### **3.5.3 Initial consolidation**

Filter paper was placed on top of the slurry and the remainder of the cell was filled with water. The piston (with saturated porous plate) was then pushed into the cell, filling the piston shaft with water. The piston was pushed downwards until it rested on the slurry. The taps on top of the piston shaft and at the base of the cell were then closed, providing a saturated system. The stringpot cable was extended and connected to the steel rod (attached to the piston shaft). The piston shaft was rotated such that the stringpot cable

was positioned directly above the drum. Pressure was applied to the upper chamber of the cell (about 65 kPa), generating an excess pore pressure of about 55 kPa in the slurry (the 10 kPa difference was due to side-wall friction and O-ring friction in the consolidation cell).

After measuring the pressure applied to the slurry using the pore pressure transducers, consolidation was commenced by simultaneously opening the taps connected to the base plate and piston shaft. The completion of consolidation was determined from pore pressure and settlement measurements. Settlement rates of less than 1 mm/day generally coincided with the end of consolidation as determined from log-time and square-root time methods and the complete dissipation of excess pore pressures. Both measurements were used to assess the completion of primary consolidation. Consolidation generally took about two weeks to complete. At completion, the piston was removed, allowing the kaolin clay to swell slightly.

#### **3.5.4 Column construction**

Cylindrical geogrid encasement was constructed using the following process:

- Forming fibreglass and aluminium mesh into cylindrical sleeves measuring 50.5 mm in diameter (with 10 mm of circumferential overlap). Mesh length was dependent on the percentage of encased column length being tested.
- Temporarily stitching the mesh along the overlapped section with cotton.
- Applying epoxy-resin along the length of overlap and then clamping it in place.
- Allowing the resin to achieve full bond strength over a period of 3 days.

A photograph of fibreglass mesh encasement, welded with epoxy-resin is presented in Figure 3.16. The welded seam is located along the mid-section of the column.

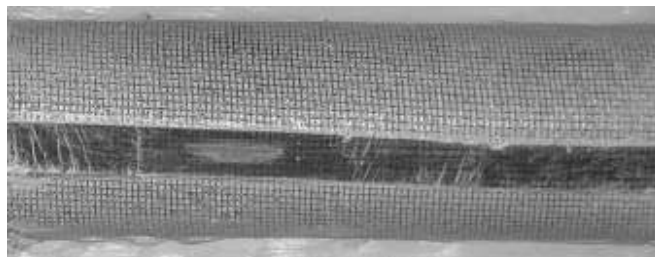


**Figure 3.16:** Welded seam of a fibreglass mesh

Where tests were undertaken to investigate the behaviour of columns encased with a sleeve comprising a half circumference of overlap (method of overlap rather than welding), the mesh was stitched at several locations in order to maintain the cylindrical shape. A photograph of a column prepared with a half circumference of overlap is presented in Figure 3.17. The overlapped section is in the bottom half of the frame, and although difficult to observe on the photograph, stitching is located along the mid-section of the column.

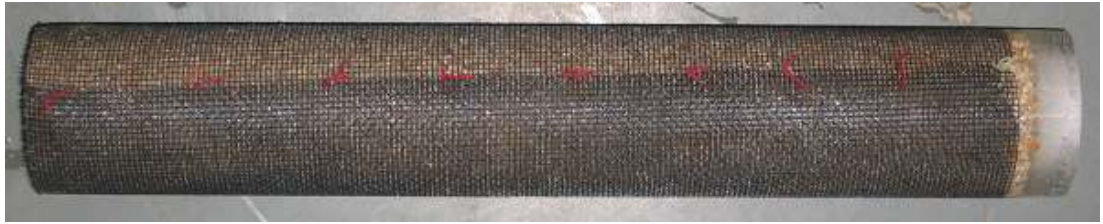


**Figure 3.17:** Column constructed with a half circumference of fibreglass mesh overlap

The frozen column technique described by Sivakumar et al. (2004) was adopted for model column construction and comprised the following process:

- Grade 8/16 sand was placed in a plastic mould measuring 50.5 mm in internal diameter (0.5 mm less than the cavity created for the column).
- The sand was compacted to the required relative density of about 90% using a hand-held, air-vibrated tool. Columns were compacted to a height equal to that of the unloaded, consolidated clay bed, generally about 310 mm.
- The mould was filled with water to completely submerge the sand.
- The column was frozen at a temperature of about  $-5^{\circ}\text{C}$  for at least 24 hours.

Where geogrid encased columns were tested, the mesh encasement was placed inside the plastic mould prior to filling the mould with sand. A photograph of an extruded frozen sand column with 75% fibreglass encasement is presented in Figure 3.18. The top of the column is located to the right of the frame.

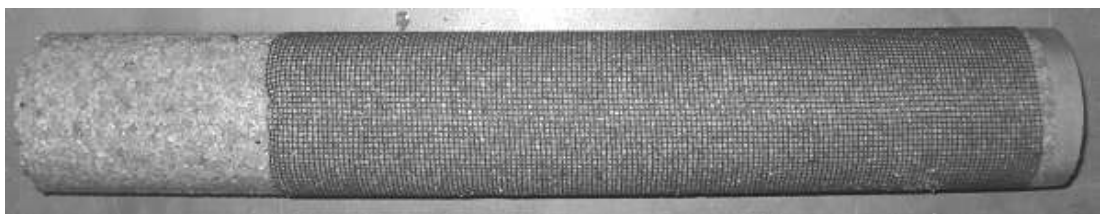


**Figure 3.18:** Frozen sand column with 75% fibreglass encasement

### 3.5.5 Column installation

A cavity was formed at the centre of the clay bed by pushing a thin-walled aluminium tube to the base of the cell. The method was similar to the way in which undisturbed tube samples are retrieved during drilled site investigations. Centrality was achieved by pushing the tube through a guide mounted to the top of the cell. The outside diameter of the thin-walled tube measured about 51.0 mm. The porous plate at the base of the cell was removed to prevent negative pressures forming in the cavity as the tube was slowly extruded (and subsequent collapse of soil). At completion, a smooth-walled cylindrical cavity equal in diameter to that of the thin-walled tube was formed. The sample retained within the thin-walled tube was used for strength and moisture testing.

After the column was removed from the freezer, it was allowed to thaw slightly, enabling the column to be extruded from the mould using minimal pressure. Following extrusion, the frozen column was placed in the cylindrical cavity formed at the centre of the clay. The slightly smaller diameter of the column relative to the cavity enabled the column to be pushed to the base of the cell with minimal disturbance of the surrounding clay. The column was then allowed to thaw at room temperature for about 3 hours before loading. This was about 3 times longer than required, as determined from a thawing trial undertaken on an unconfined column at room temperature. The column installation technique is demonstrated in Figure 3.19.



**Figure 3.19:** Installation of a frozen model sand column

### **3.5.6 Loading of column groups**

To replicate unit-cell boundary conditions, the piston was used to further load the sand column and surrounding soil. Following column installation, a saturated closed-cell condition was achieved using the same technique adopted for the initial consolidation stage. A pressure of about 59 kPa was then applied to the sample, 4 kPa above the pre-consolidation pressure of the clay. This nominal loading was undertaken to further consolidate the clay by a small amount, causing axial shortening of the column and radial expansion, and resulting in intimate contact between the sand column and surrounding clay. The method may also have helped to re-instate any loss of column density associated with freezing or installation. The sample was then consolidated by opening the two drainage taps. Under nominal loading, the sample was allowed to undergo complete consolidation, as estimated from pore pressure and settlement measurements.

Further load stages were undertaken using the same process. Load stages ranged from about 15 kPa to 70 kPa, depending on the percent encased length. Each test took between 6 and 8 weeks to complete, comprising about 5 load stages (unless mesh failure occurred prior to this). The maximum cell pressure was about 350 kPa, which was considered to be the maximum loading likely to be adopted on site.

### **3.5.7 Loading isolated columns**

Where footing pressures less than about 200 kPa resulted in column failure, the column was loaded with dead load rather than air pressure to eliminate O-ring friction. For this method, the 51 mm diameter footing was bolted directly to the base of the piston. A load plate was fixed to the top of the piston shaft and all O-rings in the system were removed. Weights were then placed on the load plate, applying pressure directly to the column. Columns were loaded in increments between 5 kPa and 20 kPa, depending on percent encased length. Column load was maintained for at least 24 hours before the next stage was applied, allowing any consolidation to be completed between stages. Where air pressure was used to load columns, O-rings were replaced, sealing the piston. Columns were loaded in increments between 20 kPa and 60 kPa, depending on percent encased length. As with columns loaded with dead weight, samples were kept at the same pressure for at least 24 hours.

### **3.5.8 Test completion**

At the completion of tests, samples were unloaded and left to swell for a period of about 24 hours. A layer of casting plaster about 20 mm thick was poured on to the top of the sample and allowed to set, providing a suitable platform on which to extrude the sample. The cylinder was then turned upside-down with the cast end placed on a cylindrical timber ram. Hand pressure was used to extrude the sample, a process aided by the weight of the cylinder and silicone lubrication. The samples were typically extruded with minimal effort or disturbance, confirming the effectiveness of the silicone lubrication. Extruded samples were placed in a Perspex frame in preparation for bisection.

Following extrusion, the height of the sample was measured to confirm that compression did not occur during extrusion (considered unlikely due to the stiffness of the samples following consolidation and effectiveness of silicone lubrication). Samples were then cut in half along the vertical axis to observe the deformed shape of the column. This was achieved by carefully removing the clay that surrounded the column using a wire cutting tool, exposing the interface between the clay and sand. The samples were photographed and the deformation profile along the length of the column was measured to an accuracy of about 0.5 mm, using vernier callipers and a measuring tape. Moisture content samples within the clay were taken at 10 locations to assess the reduction in moisture content associated with consolidation. Moisture content samples were taken at 5 different evenly-spaced heights within the clay sample, at distances of 35 mm (adjacent to the column) and 70 mm (outer cell boundary) from the central vertical axis of the cell.

## **3.6 Results of simulated column group tests**

The results of unit-cell tests undertaken to simulate and assess encased group column behaviour are discussed in this section.

### **3.6.1 Test program**

Column group tests were undertaken in the two stainless steel cells. Descriptions of each test are provided in Table 3.8. In each test, a full-length column measuring 51 mm in

diameter was installed at the centre of the cell. Where geogrid encasement was used, the mesh was welded into a cylindrical sleeve using epoxy-resin, as set out earlier.

**Table 3.8:** Tests performed to assess encased group column behaviour

test no.	cell	test type
GC-1	Steel cell #1	Kaolin consolidation test
GC-2	Steel cell #1	Sand column test
GC-3	Steel cell #2	Sand column test (duplicate)
GC-4	Steel cell #1	25% fibreglass encased sand column test
GC-5	Steel cell #2	50% fibreglass encased sand column test
GC-6	Steel cell #1	50% aluminium encased sand column test
GC-7	Steel cell #2	75% fibreglass encased sand column test
GC-8	Steel cell #2	100% fibreglass encased sand column test
GC-9	Steel cell #2	100% aluminium encased sand column test

### 3.6.2 Sample properties

#### 3.6.2.2 Kaolin clay

Slurry with an initial moisture content of 115% and a height of about 480 mm was used for testing. Although small variations in these properties occurred as part of sample preparation (refer Table 3.9), samples generally remained relatively consistent throughout the course of the testing program. A consolidation pressure (surcharge) of 55 kPa was targeted for the initial consolidation stage. However, due to the type of instrumentation used, the pressure applied to the sample could only be measured to an accuracy of about  $\pm 3$  kPa. The properties of the kaolin used for column testing are presented in Table 3.9.

Results show that the targeted undrained shear strength of about 5 kPa was generally obtained for each test. This was measured using a laboratory shear vane. The consistency of the properties of consolidated test samples set out in Table 3.9, indicate that the adopted consolidation technique was a reliable method of reproducing homogeneous clay samples.

**Table 3.9:** Kaolin clay properties for column group testing

test no.	kaolin slurry		consolidated kaolin clay			
	slurry	moisture	consolidation	unloaded	moisture	$s_u^*$
	height (mm)	content (%)	pressure (kPa)	height (mm)	content (%)	(kPa)
GC-1	477	118	51	311	64	-
GC-2	484	116	51	313	62	5.5
GC-3	475	117	55	306	62	5.7
GC-4	460 <sup>#</sup>	114	56	293	62	5.1
GC-5	475	116	55	317	67	3.7
GC-6	478	118	54	307	61	4.4
GC-7	480	115	54	315	63	3.8
GC-8	473	113	57	311	59	5.3
GC-9	481	115	56	317	63	5.0

<sup>#</sup> Some loss of slurry in initial loading due to O-ring breakage

\* Measured using a laboratory shear vane

### 3.6.2.2 Sand column

The properties of the sand columns used for testing are summarised in Table 3.10. The columns were constructed using the method of freezing, outlined earlier. A column measuring 50.5 mm in diameter was produced. Compacted columns were generally the same height as the unloaded consolidated clay sample. Upon freezing, columns were observed to expand in height by approximately 2 mm. The process tended to reduce the relative density of the column by between 3% and 4%. The unfrozen column densities are presented in Table 3.10.

Following installation and thawing, a further slight reduction in column density probably occurred due to the small difference between the column and cavity diameter. However, this was offset by the nominal loading applied after installation which increased column density, likely recovering the target relative density of 90%. Details of the nominal loading and associated settlements are presented in Table 3.10. The nominal loading indicated that up to 13 mm settlement occurred in some samples (although average settlements were generally significantly less). This value appeared to vary depending on the percent encased length and magnitude of load. Furthermore, in most cases the cell was



placed on its side to remove the thin-walled tube during column installation. This process often resulted in some movement of the clay sample within the cell and therefore nominal loading often comprised a re-seating component of settlement. Settlements measured during nominal loading were ignored when comparing test sample behaviour.

**Table 3.10:** Sand column properties for column group testing

test no.	sand column				nominal loading		
	initial height (mm)	relative density (%)	type	encased length (mm)	applied pressure (kPa)	pressure increase (kPa)	final height (mm)
GC-2	313	92	Non-encased	-	54	3	308
GC-3	306	93	Non-encased	-	59	4	295
GC-4	293	92	fibreglass	72	58	3	286
GC-5	317	92	fibreglass	159	55	1	304
GC-6	307	92	aluminium	153	55	1	302
GC-7	315	93	fibreglass	235	59	5	312
GC-8	311	91	fibreglass	311	59	2	310
GC-9	317	91	aluminium	317	59	3	314

### 3.6.3 Vertical stress-strain behaviour

For each sand column test, settlement was measured using the stringpot gauge. Settlement for each load stage was divided into primary and secondary (creep) settlement, determined from pore pressure and settlement measurements, as set out earlier. Throughout testing, creep settlements that occurred after the completion of primary consolidation were generally limited by immediately applying the following load stage. Although immediate application of the next load stage was not always possible, creep settlements were kept to less than 13% of the total settlement (with an average of 7%) in all column tests.

The primary consolidation for each test was divided by the consolidated sample height at completion of the nominal loading stage, giving vertical sample strain. Accumulated strains at the end of each load stage were used to develop vertical stress-strain curves for each column test. As the sample height at completion of nominal loading varied between samples, vertical strain (rather than settlement) enabled direct comparison of sample

compressibility. This allowed an assessment of the impact of varying encased column length and mesh stiffness. The vertical stress-strain relationships for column tests are compared in Figure 3.20.

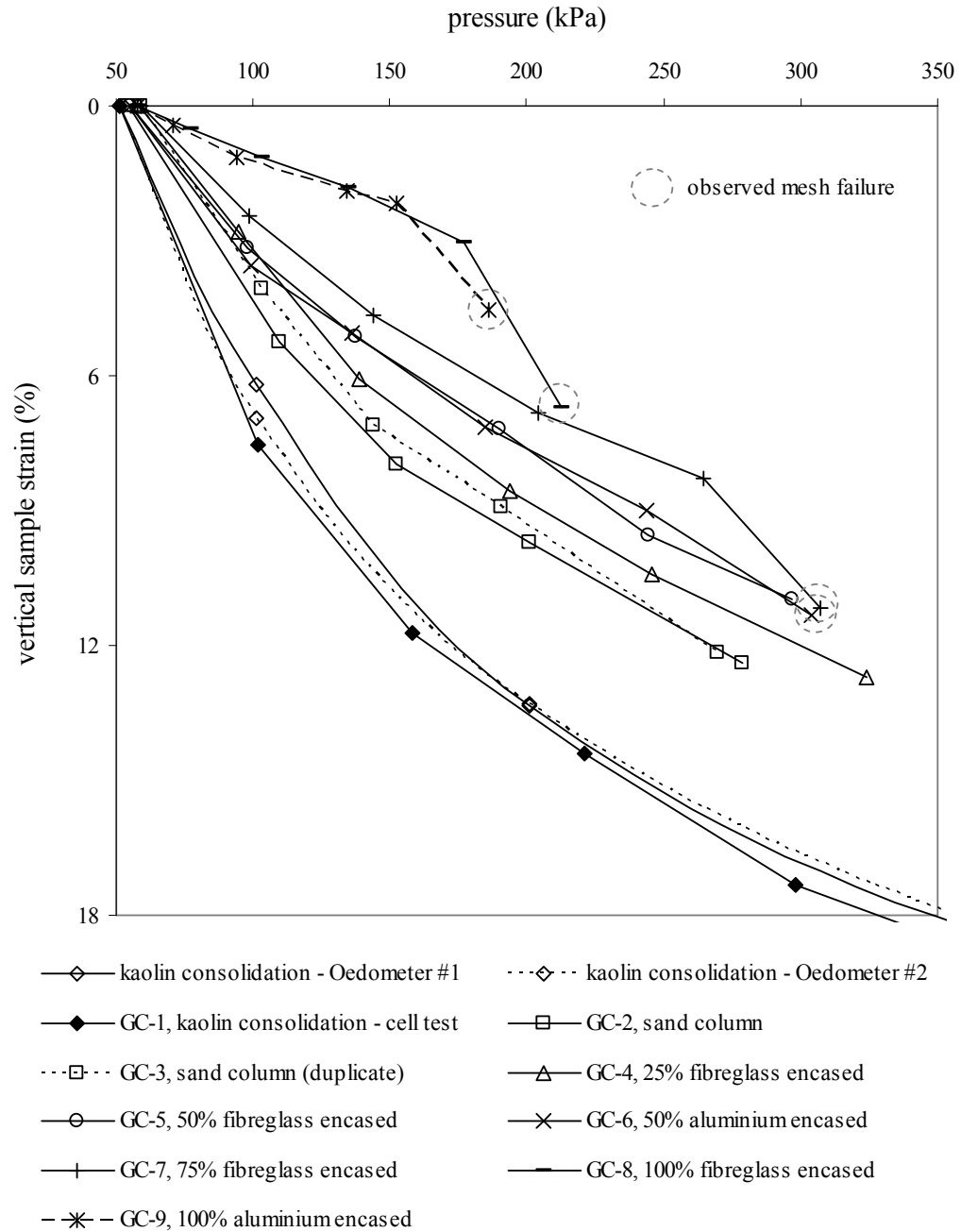


**Figure 3.20:** Vertical stress-strain relationship for column group tests

In Figure 3.20, the compressibility of the kaolin measured in the cell test slightly exceeded that measured in the oedometer tests, for pressures greater than about 50 kPa. This

indicated that the silicone lubrication acted very effectively in reducing side-wall friction. Results also indicated a trend of strain reduction with increasing percent encased length.

As loading of samples was commenced at slightly different pressures (ranging from 54 kPa to 59 kPa), the reduction in vertical strain for samples was compared by adjusting the starting pressure of each test to the same value. This was done by using 4<sup>th</sup> order polynomial equations to initially replicate the shape of the stress-strain curve of each column test, including the kaolin consolidation test. The polynomial equations were then used to adjust each stress-strain curve to a start pressure of 59 kPa. This resulted in a modified stress-strain curve that approximated the compressive behaviour of column tests. The kaolin consolidation test was used as the baseline value for which reductions in vertical strain were assessed. Approximate reductions in vertical strain for consolidation tests are presented in Figure 3.21. Test results are discussed in detail in following sections.

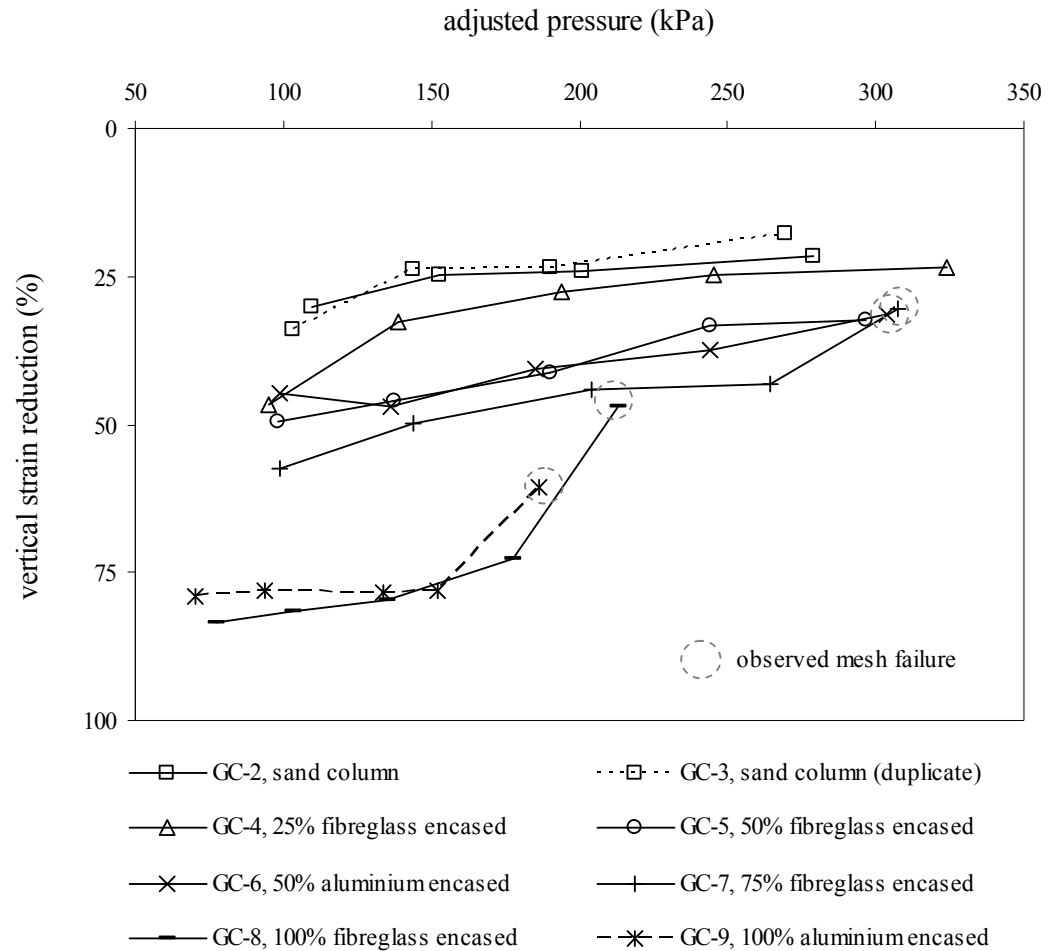


**Figure 3.21:** Approximate vertical strain reduction for column group tests

### 3.6.3.1 Non-encased columns

A non-encased column test was undertaken in each steel cell to confirm that each cell performed similarly. As observed in Figure 3.20, the two non-encased column samples (GC-2 and GC-3) displayed very similar compressibility. It was therefore concluded that the behaviour of Steel cell #2 closely matched that of Steel cell #1 and that the method of column installation produced samples of high repeatability.

The average vertical strain reduction for non-encased sand columns was about 25%, corresponding to an improvement factor,  $\eta$ , of about 1.3. This was within the range of results typical for stone column groups with a replacement ratio,  $A_r$ , of 11%. Vertical strain reduction was not constant across the range of applied stresses but was observed to decrease slightly with increasing pressure. This may be attributed to the clay becoming stiffer with ongoing consolidation, enabling it to support more of the vertical load, thereby reducing the impact of the stiffening column. The average vertical strain reduction of column group tests, across the range of applied stresses, are compared to untreated kaolin clay behaviour in Table 3.11. Reported values of strain reduction include results prior to encasement mesh failure only.

**Table 3.11:** Average vertical strain reduction for column group tests

test no.	test type	average vertical strain reduction (%)	improvement factor $\eta$	Cell stress at mesh failure (kPa)
GC-2	Non-encased	25	1.3	-
GC-3	Non-encased (duplicate)	25	1.3	-
GC-4	25% fibreglass encased	31	1.5	-
GC-5	50% fibreglass encased	41	1.7	-
GC-6	50% aluminium encased	40	1.7	304
GC-7	75% fibreglass encased	49	1.9	307
GC-8	100% fibreglass encased	79	5.0	213
GC-9	100% aluminium encased	78	4.6	186

### 3.6.3.2 Partially encased columns

As outlined in Table 3.11, columns with 25%, 50% and 75% fibreglass encasement achieved reductions in vertical strain of about 30%, 40% and 50%, respectively. There appeared to be little difference in behaviour between the 50% fibreglass encased and 50% aluminium encased columns, regardless of the significantly higher stiffness of the aluminium mesh. Strain reduction for partially encased columns was also observed to decrease with ongoing consolidation.

#### Mesh failure

Mesh failure was generally identified in testing by a significant increase in vertical strain for a given load stage, in addition to a rapid increase in pore pressure as greater load was supported by the clay. Following completion of the load stage, testing was terminated and the sample was bisected to confirm failure.

The 50% aluminium mesh (GC-6) was observed to have undergone plastic strain in several locations, with several horizontal strands in the upper section of the mesh having failed. The 50% fibreglass mesh (GC-5) remained intact. As both tests were terminated at similar surcharges, it was considered that the higher stiffness and lower tensile strength of the aluminium mesh contributed to the failure. A photograph of the failed aluminium mesh is presented in Figure 3.22. The top of the mesh is located to the right of the frame.

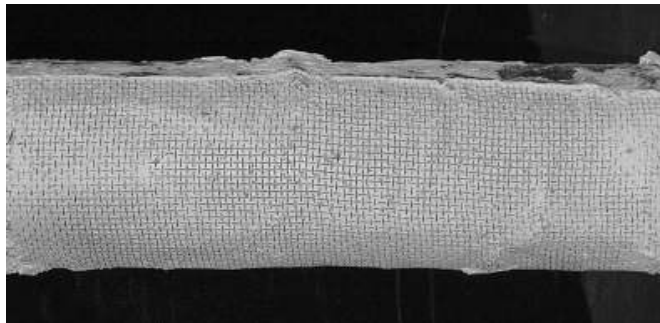


**Figure 3.22:** Extruded aluminium mesh (50% encased column)

The 75% fibreglass mesh (GC-7) was also observed to have failed, at a surcharge of 307 kPa. Broken strands were observed in the bottom 5 mm of the mesh, in the transition from the encased zone to the non-encased zone. In addition, broken horizontal strands were observed in a roughly vertical line through the middle of the mesh and in two approximately 50 mm long intersecting diagonal planes, stretching from the top of the

mesh. A photograph of the failed mesh is presented in Figure 3.23. The top of the mesh is located to the right of the frame.

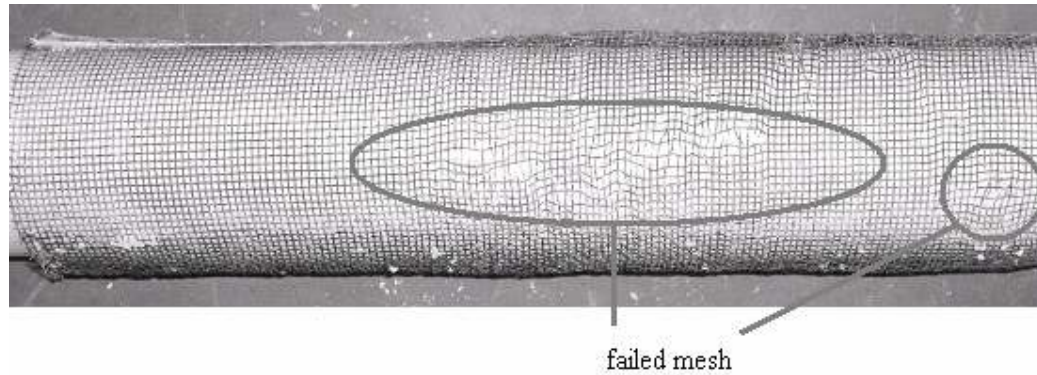


**Figure 3.23:** Extruded fibreglass mesh (75% encased column)

#### 3.6.3.3 Fully encased columns

Testing of 100% fibreglass encased and 100% aluminium encased columns reduced vertical strain by about 80% prior to mesh failure. As observed in earlier tests, strain reduction for the fibreglass mesh decreased with increasing surcharge, although not to the same extent as for partially encased columns. For the aluminium mesh, strain reduction remained constant across the range of applied surcharges. There appeared to be little difference between the behaviour of the fibreglass and aluminium encased columns, except perhaps a slightly stiffer response from the aluminium mesh at higher stresses.

##### Mesh failure

For the 100% fibreglass encased column test (GC-8), mesh failure occurred at a surcharge of about 213 kPa. This was a significantly lower pressure than for the 75% fibreglass mesh failure, perhaps indicating that for a given surcharge, hoop forces were higher for the fully encased test. The fibreglass strands failed in the upper section of the mesh, with strands breaking along intersecting diagonal planes in the upper 50 mm of the mesh. Some strands also failed through the middle section of the column.

The 100% aluminium encased column test (GC-9) failed at a surcharge of about 186 kPa, significantly less than the fibreglass test, most likely due to the higher stiffness and lower tensile strength of the mesh. The aluminium mesh was observed to have locally buckled in several locations along the column length, with plastic straining and broken horizontal

strands observed at numerous locations along the full length of the column. Photographs of the failed meshes are presented in Figure 3.24. The top of the mesh is located to the right of each frame.

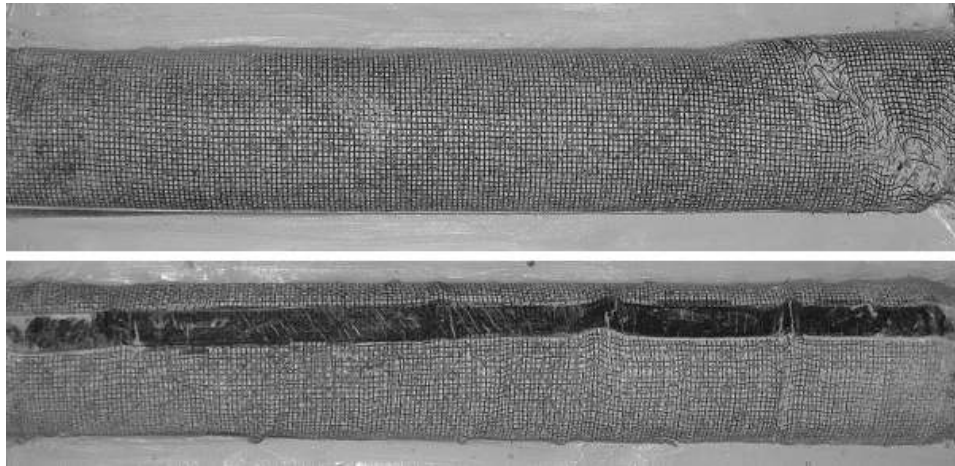


**Figure 3.24:** Extruded meshes, 100% fibreglass (top) and 100% aluminium (bottom)

#### **3.6.4 Column radial expansion**

Extruded samples were carefully bisected to measure column deformation. Radial deformation was measured to an accuracy of about 0.5 mm. Photographs of the extruded column cross-sections are presented in Figure 3.25.

Radial expansion of non-encased columns was relatively even along their length, with an average radial strain of about 5%. Column bulging was not observed and this was most likely due to the very small variation in lateral stress and stiffness within the clay sample, in addition to the one-dimensional load conditions.

For partially encased columns, the entire non-encased length was observed to bulge. Radial bulging increased in magnitude with increased encased length. A maximum radial strain of about 34% was observed for the 75% fibreglass encased column. The largest lateral deformations occurred directly beneath the base of the encasement. The maximum radial strains for non-encased and partially encased columns are presented in Table 3.12.

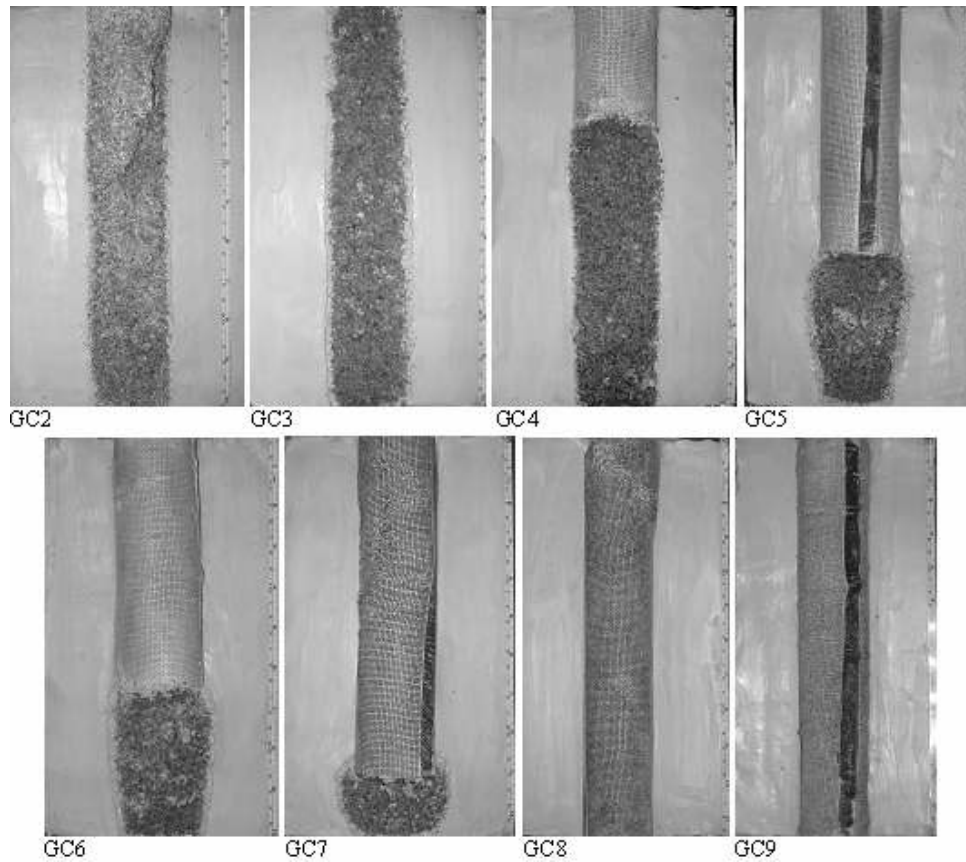


**Figure 3.25:** Photographs of extruded group column samples

**Table 3.12:** Maximum radial expansion of group columns

test no.	test type	maximum radial strain
		(%)
GC-2	Non-encased	9
GC-3	Non-encased (duplicate)	8
GC-4	25% fibreglass encased	21
GC-5	50% fibreglass encased	28
GC-6	50% aluminium encased	30
GC-7	75% fibreglass encased	34

Although the mesh was too fine to instrument with conventional strain gauges, the deformed shape of the clay in the areas of intact fibreglass mesh indicated radial straining between about 1% and 4%, generally within the range of strain observed during tensile testing of fibreglass mesh samples (prior to failure). For equivalent tests undertaken using



aluminium mesh, sections of failure and mesh buckling were more pronounced than for the fibreglass mesh, making comparison more difficult. However, in areas where the mesh remained intact, the radial strains were generally smaller than for fibreglass mesh. This was in line with expectations, given the lower failure strain of the aluminium mesh. Further assessment of mesh radial strain using numerical techniques is presented in Chapter 4.

### **3.6.5 Stress concentration**

The vertical stress applied to the top of the sand column was measured using a miniature pressure cell transducer mounted to the underside of the piston. Vertical column stress was measured for the non-encased (GC-3) and fully fibreglass encased (GC-8) column tests only. Although the intention was to measure stress at the top of the column and clay for all samples, including partially encased columns, the transducer wires and connections proved too delicate to support multiple testing. In fact, only the gauge used for the measurement of column stress was robust enough to support multiple testing.

In the 100% fibreglass encased test, a column stress of greater than 1000 kPa was measured prior to mesh failure, equating to a stress concentration ratio (ratio of column stress to surrounding clay stress) of greater than 10. For non-encased columns, the stress concentration ratio ranged between 2 and 3. The measurement of stress concentration demonstrated that full-length encasement dramatically increased column stiffness and strength.

### **3.6.6 Time rate of consolidation**

Although assessment of the time rate of consolidation was not a primary aim of this research, a significant amount of data was collected during column testing. Tests confirmed that columns acted as vertical drains, by shortening the drainage path through the clay and therefore accelerating the rate of consolidation.

Taylor's square root time method (Taylor 1948) was used to compare the time taken to complete 90% consolidation,  $t_{90}$ , for each load stage in each column test. In the kaolin cell test, the first load stage immediately followed the initial consolidation stage (where the

slurry was consolidated to a very soft clay using a surcharge of 51 kPa). For column tests, the first load stage followed nominal loading. In each test, the first load stage was generally followed by up to four subsequent stages. Although the surcharge pressure for each stage varied between tests, results were compared to identify trends in consolidation rate. The time taken to complete 90% consolidation for each load stage in each test is presented in Figure 3.26.

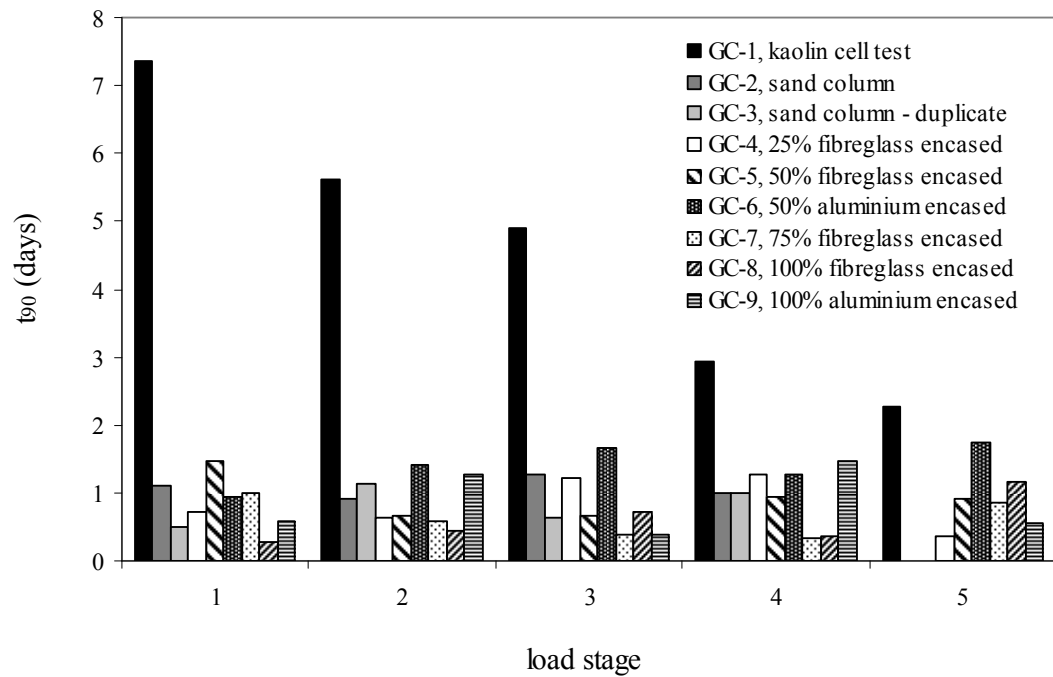


**Figure 3.26:** Comparison of consolidation time rate for group column tests

The kaolin cell test indicated that the time taken to complete 90% consolidation steadily decreased with ongoing loading (higher pressures). This time ranged from more than 7 days in the first load stage to less than 3 days in the fifth and final load stage. This reduction in consolidation time may be attributed to the increased stiffness of the clay sample achieved through progressive loading and consolidation. The addition of sand columns reduced consolidation time (in the first load stage) to about 1 day. This corresponded to a reduction factor of about 7 when compared to kaolin clay alone, suggesting that columns initially acted as very effective vertical drains.

In subsequent load stages, the time taken to complete 90% consolidation remained reasonably constant at an average of about 1 day, although the variability in time increased between tests. In the fifth and final load stage, this equated to a halving of the average

time taken to complete consolidation. Mesh encasement appeared to have little impact on the drainage behaviour of columns. This was expected, as the mesh aperture size was considered unlikely to provide an impediment for water flow into the column.

#### 3.6.6.1 Clay ingress

In contrast to the kaolin cell test, the time rate of consolidation for the sand column tests generally did not decrease significantly with progressive loading. Bisection of samples at test completion revealed significant ingress of clay into the model column cross-sections. In some cases, clay had penetrated the column by up to 6 mm, equating to about 40% of the cross-sectional area. Photographs of the cross-sections of two encased columns illustrating clay ingress are presented in Figure 3.27. The photographs are generally considered to be representative of all column tests. In the photographs, the loose sand at the centre of the columns was removed and sand that had been cemented by the clay ingress was retained.

It was considered that clay ingress may have significantly reduced the permeability of the column and therefore reduced the effectiveness of the column to act as a drain. In particular, ongoing consolidation may have caused continued migration of clay fines into the column and squeezing of clay into column voids. These effects may account for the time rate of consolidation staying reasonably constant over the duration of the column tests (refer Figure 3.26), rather than decreasing, as was observed for the untreated kaolin test. Further assessment of the time rate of consolidation using numerical methods is presented in Chapter 4.

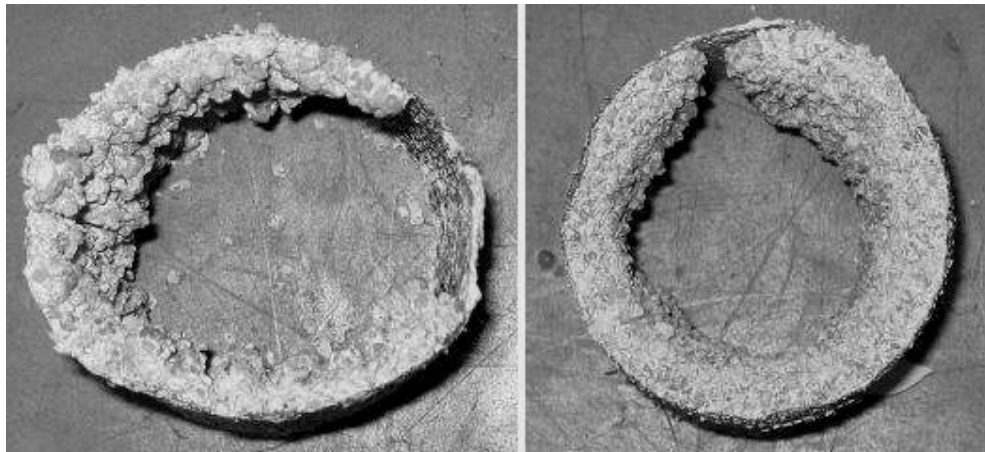


**Figure 3.27:** Clay ingress into column cross-sections, GC-4 (left) and GC-6 (right)

### 3.6.6.2 Moisture content

Following sample extrusion, moisture content testing was undertaken in the kaolin clay that surrounded the column. The tests were undertaken to confirm clay consolidation and compare moisture contents at different depths. Test samples were taken at ten locations within the clay. These corresponded to distances of 35 mm and 70 mm from the centre of the column, at five evenly distributed depths (generally 30 mm, 90 mm, 150 mm, 210 mm and 270 mm from the top of the sample). Average moisture contents for samples before and after testing are presented in Table 3.13 and indicate a significant reduction in moisture content for all samples at test completion. As observed in Figure 3.20, non-encased and partially encased tests were completed with the samples having undergone a similar vertical strain (generally due to the failure of mesh encasement). The final average moisture content of these samples were similar and confirmed that the samples had undergone a similar degree of consolidation.

**Table 3.13:** Moisture content of group column samples following test completion

test no.	test type	moisture content (%)	
		initial	test completion
GC-2	Non-encased	61.5	46.5
GC-3	Non-encased (duplicate)	62.0	48.0
GC-4	25% fibreglass encased	62.0	48.0
GC-5	50% fibreglass encased	66.5	46.5
GC-6	50% aluminium encased	61.5	46.5
GC-7	75% fibreglass encased	63.5	47.5
GC-8	100% fibreglass encased	59.0	53.5
GC-9	100% aluminium encased	62.5	58.5

Although only the average moisture content of samples is presented in Table 3.13, the moisture content was observed to vary along the column length. For partially encased columns, the moisture content below the level of encasement was up to 3% less than the upper encased sections. This indicated that more consolidation tended to occur in the bulge zone beneath the encasement.

Fully encased column tests were completed with samples having undergone less consolidation than for other column tests. This was reflected in the higher average final moisture content. The moisture content at the top of samples was up to 5% less than at the base of samples, most likely a result of mesh failure occurring, or being more prevalent in the upper section of the column. Furthermore, the moisture content directly adjacent to the column was about 3% less than near the cell boundary, indicating radial consolidation around the perimeter of the column.

### 3.7 Results of isolated column tests

The results of column tests undertaken to investigate the behaviour of isolated model sand columns are discussed in this section. Tests were undertaken in the Perspex cell.

#### 3.7.1 Test program

The program of isolated model column tests undertaken is outlined in Table 3.14. In all column tests, a full-length column measuring 51 mm in diameter was installed at the centre of the Perspex cell.

**Table 3.14:** Tests undertaken to assess encased isolated column behaviour

test no.	test type
IC-1	Kaolin footing test
IC-2	Sand column test
IC-3	Sand column test (duplicate)
IC-4	25% fibreglass encased sand column test
IC-5	50% fibreglass encased sand column test
IC-6	75% fibreglass encased sand column test
IC-7	100% fibreglass encased sand column test

### 3.7.2 Sample properties

#### 3.7.2.1 Kaolin clay

Slurry was prepared using the same process set out for column group testing (simulated using unit-cell idealisation). An initial consolidation pressure of 55 kPa was adopted for tests, measured to an accuracy of about  $\pm 2$  kPa. The properties of the kaolin clay used for testing of isolated columns are summarised in Table 3.15.

**Table 3.15:** Kaolin clay properties for isolated column tests

test no.	kaolin slurry		consolidated kaolin clay			
	slurry height (mm)	moisture content (%)	consolidation pressure (kPa)	unloaded height (mm)	moisture content (%)	$s_u^{\#}$ (kPa)
IC-1	482	118	55	322	67	5.0
IC-2	476	115	55	311	63	5.1
IC-3	476	118	55	311	65	4.5
IC-4	478	118	55	308	64	4.5
IC-5	476	118	55	315	67	4.1
IC-6	477	114	55	315	62	4.6
IC-7	480	117	55	317	65	3.7

<sup>#</sup> Measured using a laboratory shear vane

#### 3.7.2.2 Sand column

The properties of the sand columns used for tests are summarised in Table 3.16. The columns were constructed and installed using the same process adopted for group column tests. Column densities prior to freezing are presented.

**Table 3.16:** Sand column properties for isolated column tests

test no.	height (mm)	relative density (%)	encased length (mm)
IC-2	311	90	-
IC-3	311	94	-
IC-4	308	92	78
IC-5	315	93	159
IC-6	315	91	237
IC-7	317	92	317

### 3.7.3 Column loading

Column testing was undertaken using incremental loading. Upon application of each load stage, an immediate (undrained) settlement was typically observed, followed by time-dependent consolidation. This consolidation was completed prior to the application of the following load stage, typically corresponding to at least a 24 hour loading period. The first load stage comprised application of the footing and therefore column settlement was due to the weight of the footing and associated load apparatus. Under this initial light loading, settlement was generally considered to be a result of sample disturbance and column re-densification (as was the case for group column tests under nominal loading), and therefore column strain for the first load stage was ignored.

Moisture content testing was undertaken on the clay extruded from the inside of the thin-walled tube (clay that had been removed and replaced by the sand column during column installation) and compared to the moisture content following test completion. Results indicated a reduction in moisture content consistent with consolidation. It was therefore considered that drained, or at least partially drained loading occurred in the clay immediately surrounding the bulge zone of the column in the load stages prior to failure. However, failure in the final load stage was generally rapid and was therefore considered to comprise an undrained state.

#### **3.7.4 Column capacity**

The vertical stress-strain relationship for column tests is presented in Figure 3.28. The vertical strain, comprising elastic and consolidation column settlements was measured using the stringpot gauge. Failure comprised rapid (undrained) radial expansion of the non-encased section of columns, resulting in large vertical settlements.

For non-encased columns, tests indicated an average capacity of about 80 kPa, equating to almost a three-fold increase when compared to kaolin clay. This compared favourably to the theoretical prediction of about 90 kPa, using cavity expansion equations proposed by Hughes and Withers (1974). Furthermore, the behaviour of the two non-encased column tests closely matched each other, indicating that the method of column installation and testing produced repeatable results.

Column capacity was observed to increase with some consistency from the non-encased state to the 50% encased state. Capacity was approximately 110 kPa and 135 kPa for the 25% and 50% encased column tests, respectively. Capacity increased significantly to about 200 kPa for the 75% encased column. For these tests, the vertical strain at failure was typically between 3% and 4%. Failure comprised bulging of the column below the level of encasement. For the non-encased and 25% encased column tests, this included visible uplift of the clay above the bulge zone. Mesh failure was not observed in any test.

The 100% fibreglass encased column test was not loaded to failure due to the high pressures required to do so. At a maximum vertical stress of 676 kPa, the fully encased column displayed a much stiffer response than the partially encased columns. This was most likely because bulging and therefore column failure was prevented by the mesh. Based on column group testing and radial strain measurements, it was assessed that a significantly higher vertical stress was required to cause mesh failure.



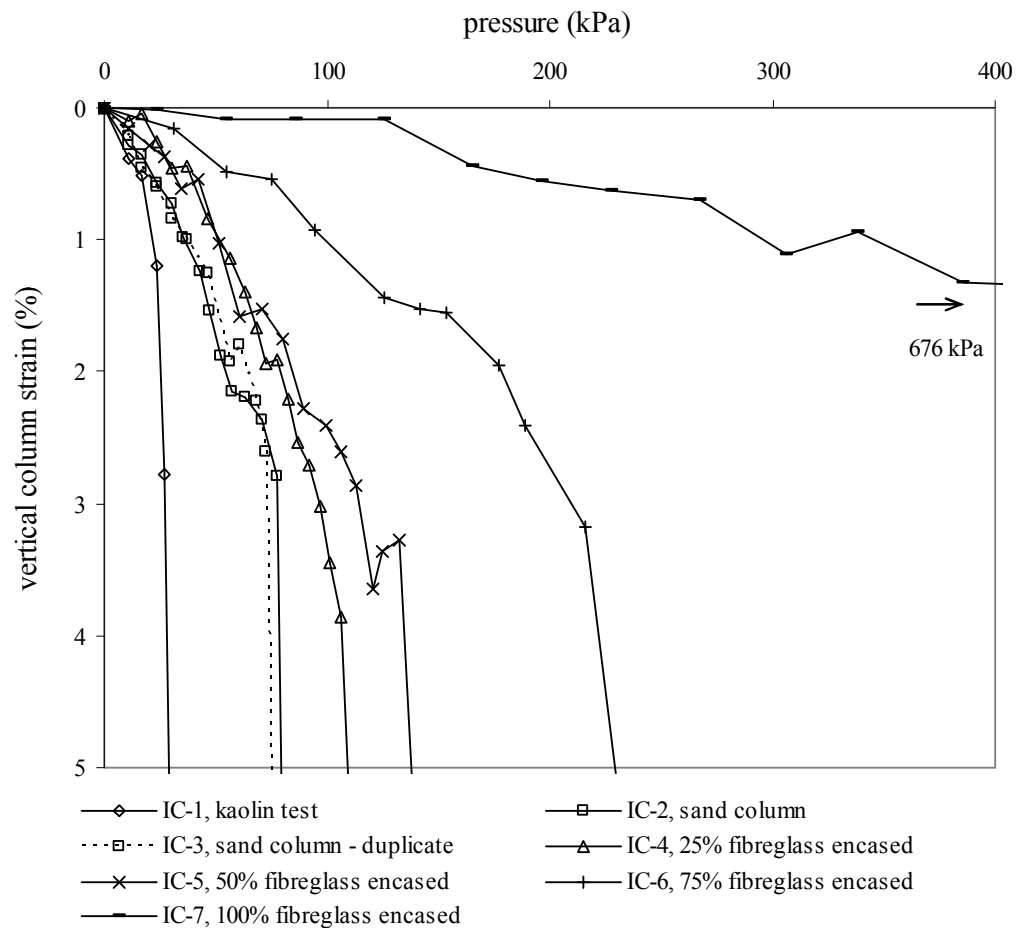


**Figure 3.28:** Vertical stress-strain relationship for isolated column tests

### 3.7.5 Column radial expansion

The duplicate sand column tests were observed to bulge in the upper section of the column, confined to a length of about 1.5 diameters. This confirmed the observations of previous authors including Hughes and Withers (1974), who showed that column bulging tended to occur in the upper section of isolated columns.

For partially encased columns, bulging occurred directly below the encasement, confined to a length of about 2 column diameters. As the magnitude of bulging was measured following column failure, comparison of this to other tests was generally not meaningful. However, the magnitude of isolated column bulging for partially encased columns was generally less than for group columns, even though it was measured after failure. This was most likely due to the lower column settlements and lower column loads experienced in isolated column testing. Photographs of sample cross-sections following extrusion are

presented in Figure 3.29. Column bulging is visible beneath the level of encasement. Further comparisons between group and isolated column behaviour are made later in this chapter.

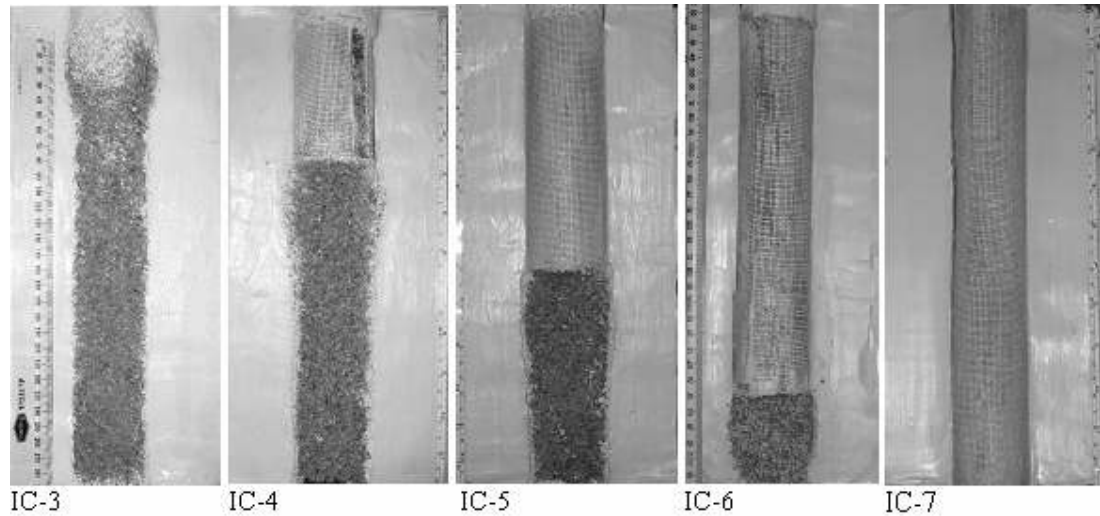


**Figure 3.29:** Photographs of extruded isolated columns

### 3.8 Method of overlap

An aim of this research was to investigate an alternative technique to geogrid welding that could be adopted to fix cylindrical encasement in position. As set out earlier, the method of overlap was proposed. For model column tests, the method of overlap generally comprised overlapping the mesh encasement by either a half or full circumference. The method relied on sufficient interlock between sand grains and the overlapped section of mesh being achieved, preventing the mesh from unravelling during loading. It was considered that this type of encasement construction may provide a level of fixity similar to welding. The sand particle size and mesh aperture size were selected to give an accurate small-scale representation of full-scale materials used in encased column construction. The results of small-scale testing undertaken to investigate the method of overlap are discussed in this section.

### 3.8.1 Test program

Two group column tests simulated using unit-cell idealisation and one isolated column test were undertaken on fully encased columns using the method of overlap. In each test, the clay bed and sand column were prepared using the same technique as for welded columns. A description of the three tests is presented in Table 3.17.

**Table 3.17:** Tests performed to assess the method of overlap

test no.	cell	test type
GC-10	Steel #1	100% fibreglass encased sand column test, 0.5× circumference overlap and stitched in place
GC-11	Steel #2	100% fibreglass encased sand column test, 0.5× circumference overlap, no stitching
IC-8	Perspex	100% fibreglass encased sand column test, 1× circumference overlap, no stitching

In test GC-10, the overlapped encasement was held in a cylindrical shape by stitching it in place with cotton at approximately 30 mm intervals along the length of the sleeve. During column loading, the stitching appeared to introduce areas of increased stress, with mesh strands tearing at stitched locations. Because on this, the mesh encasement used in the two following tests (GC-11 and IC-8) was not stitched, rather held in place within the plastic mould as it was filled with sand. When these frozen columns were extruded from the mould and installed, the encasement did not unravel, eliminating the need for stitching.

### 3.8.2 Sample properties

Kaolin and sand column samples were prepared in the same manner as welded column tests. The properties of the kaolin clay and sand columns are presented in Table 3.18 and Table 3.19, respectively.

**Table 3.18:** Kaolin clay properties for overlapped encasement tests

test no.	kaolin slurry		consolidated kaolin clay			
	slurry	moisture	consolidation	unloaded	moisture	$s_u^*$
	height (mm)	content (%)	pressure (kPa)	height (mm)	content (%)	(kPa)
GC-10	478	117	52	285 <sup>#</sup>	63	4.6
GC-11	479	117	54	313	64	4.4
IC-8	481	117	55	311	62	5.0

<sup>#</sup> Upper 25 mm of the sample was removed due to disturbance during unloading

\* Measured using a laboratory shear vane

**Table 3.19:** Sand column properties for overlapped encasement tests

test no.	height (mm)	relative density (%)	encased length (mm)
GC-10	285	93	285
GC-11	313	91	313
IC-8	311	92	311

### 3.8.3 Overlapped encasement behaviour

Columns constructed with overlapped encasement were loaded in the same manner as welded columns. The vertical stress-strain behaviour of the two group column tests with overlapped encasement are compared to the behaviour of the welded fibreglass encased column test in Figure 3.30. Results show similar compressibility in all three tests up to failure, indicating a similar stiffness. The mesh that was overlapped without stitching (GC-11) failed at a similar surcharge pressure to the welded test (GC-8). Extrusion of this sample indicated that the mesh had failed by breakage of horizontal strands in a diagonal plane stretching about 40 mm from the top of the column. This mode of failure was similar to the failure mode of the welded column and indicated a similar level of fixity had been achieved using the method of overlap. A photograph of the extruded overlapped mesh with visible failure plane is presented in Figure 3.31. The top of the column is located to the right of the frame.

The results for the mesh that was overlapped and stitched (GC-10) are less clear. As the second load stage for this test was relatively large, it is difficult to assess at what stress the failure occurred. Also, the test was continued beyond mesh failure to observe whether the column would behave as a non-encased column (which it did with progressive loading). The shape of the column and condition of the mesh after extrusion were therefore quite distorted. However, it was determined from examination of the mesh that failure occurred and propagated from the stitched locations in the lower half of the column. As the surcharge pressure at failure was significantly less than for the other fully-encased tests, the stitching was assessed to have contributed to the mesh failure.

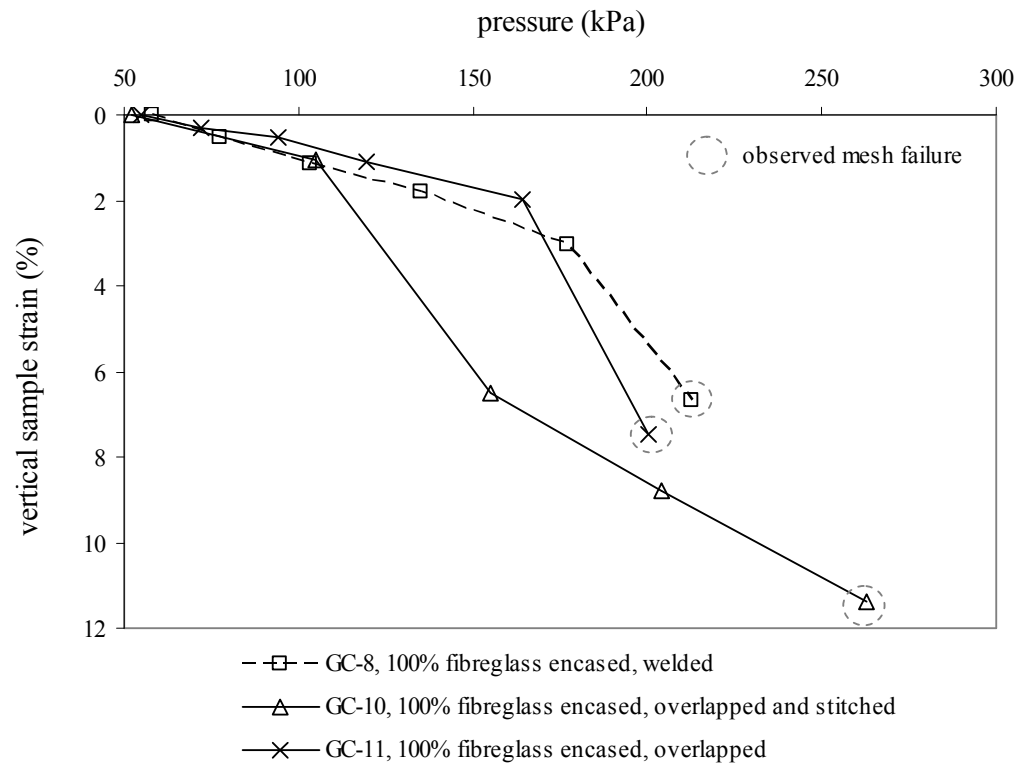


**Figure 3.30:** Vertical stress-strain relationship for group columns with overlapped encasement

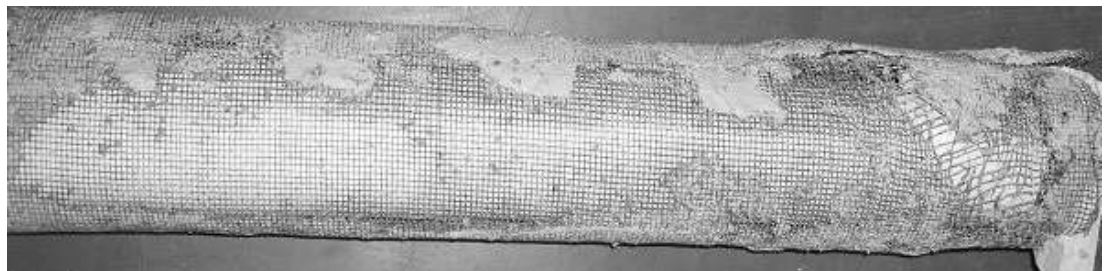


**Figure 3.31:** Extruded mesh of group column with overlapped encasement (GC-11)

For the isolated column test (IC-8), the encasement was overlapped by a full circumference. The vertical stress-strain relationship for the column with overlapped encasement is compared to the column with welded encasement in Figure 3.32. In both tests, failure of the mesh could not be achieved due to the high pressures required to do so. The behaviour of both columns was similar, with a slightly lower compressibility (and therefore higher stiffness) observed for the column with overlapped encasement. This is consistent with the greater thickness of the overlapped column encasement.

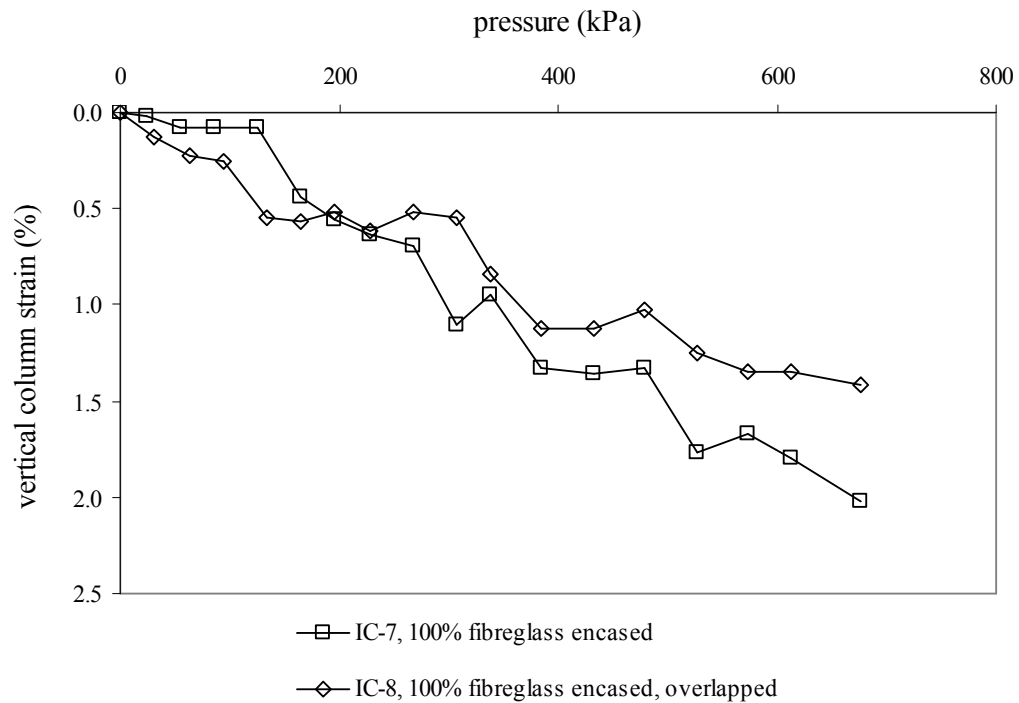


**Figure 3.32:** Vertical stress-strain relationship for isolated column with overlapped encasement

### 3.8.4 Summary

Tests on columns with encasement constructed from overlapped mesh indicate that the interlock achieved between the sand grains and the overlap section provide a level of fixity similar to welding. There appears to be little difference between the behaviour of columns with a full circumference of overlap compared to a half circumference of overlap, except perhaps a slightly stiffer response. The use of stitching to hold the overlapped mesh in place during column compaction appears to have a detrimental effect on column capacity, creating points of weakness in the encasement.

The method of overlap appears to provide an alternative method of forming cylindrical encasement, at least in small-scale. Whether the level of fixity achieved in small-scale tests can be translated to full-scale materials is examined in Chapter 5, where the results of unconfined compression tests conducted on medium-scale columns are presented.

### **3.9 Discussion**

The following section examines the results of small-scale testing. Comment is also made on the suitability of the technique to full-scale applications, where appropriate.

#### **3.9.1 Partial encasement**

Partial encasement appears to provide an effective method for progressively reducing column settlement and increasing column stiffness. For both group and isolated columns subjected to a given pressure, column strain (and settlement) was steadily reduced by progressively increasing the encased length. The unit-cell loading adopted to simulate group column behaviour resulted in the clay settling by the same amount as the column, although most column settlement was probably a result of axial shortening (and radial expansion) rather than significant volume change. This led to a significant increase in sample stiffness (both column and clay). For isolated column tests, this was realised by an increase in column capacity with increased encased length, particularly for columns with greater than 50% encasement.

Although the mesh was too fine to practically instrument, surcharge loads were obviously transmitted to the mesh as hoop forces, evidenced by the radial strains that were measured. Failure was also observed in the 50% aluminium and 75% fibreglass group tests, indicating that the tensile capacity of the mesh had been exceeded. These failures suggested that the mesh encasement in columns with greater percent encased length attracted greater stress, given that they occurred at similar surcharge pressures to tests with less encasement.

Although the small-scale tests were subject to scale errors, preliminary findings indicate that a progressive increase in stiffness can be achieved by increasing the percent encased

length. This aspect of partial encasement may provide a design solution for some of the following applications:

- To soften the “step” in differential settlement that often occurs between areas of untreated soil (such as motorway embankments) and rigid structures (such as piled bridge abutments). This could be achieved by progressively increasing the encased length on the approach to the rigid structure.
- Projects where greater settlement control is required than can be provided by conventional stone columns.
- To reduce the number of stone columns used on a project while delivering the same reduction in vertical settlement, providing a cost saving.
- Sites with layered stratum, such as a geologically recent deposit of extremely soft clay overlying an older deposit of firm clay.

Further assessment of encased columns, mesh failure and the suitability of partial encasement to full-scale applications is presented in later chapters, where numerical methods are used to investigate encased column behaviour.

### **3.9.2 Comparison of group and isolated column behaviour**

The primary difference between isolated and group column behaviour was that isolated columns failed whereas group columns did not (with the exception of the mesh encasement). For group columns, the constrained boundary condition provided additional confinement to the column, preventing radial failure and providing a shorter drainage path in the surrounding clay. This constrained boundary enabled columns to expand laterally and in a plastic state without failing. Where present, the mesh encasement acted to reinforce the column by transmitting surcharge loads to mesh hoop forces, reducing radial expansion and reducing vertical strain (increasing column stiffness). Cell loading could therefore be continued up to and beyond mesh failure, if required.

For isolated columns, failure comprised rapid radial bulging of the column below the encasement. For non-encased and 25% encased columns, this was accompanied by visible uplift of the clay above the bulge zone. Failure was therefore considered to be governed by the undrained shear strength of the clay surrounding the non-encased section of the column. For partially encased columns, failure of the sample occurred before stresses in



the mesh encasement could reach tensile capacity. For fully-encased columns, the stresses required to cause mesh failure were greater than the capacity of the test apparatus. As such, mesh failure was not reached in any test.

Based on the small-scale tests, the use of full-length geogrid encasement appears capable of extending the use of stone columns to extremely soft soils in the same way geotextile encasement has been used in the past. Full-length encasement appears suited to both group column or isolated column applications.

Given the constrained conditions likely in large group column applications, partial encasement could be adopted without detrimental bulging failure. Furthermore, the confinement provided to the non-encased section of full-scale columns in soft clay is likely to exceed that achieved in model tests. This is because the soil stiffness and lateral earth pressure in natural soft soil deposits increase significantly with depth, unlike the model tests. However, the use of partial encasement in isolated column applications would need to be treated with caution. The failure of isolated columns is likely to be governed by the undrained shear strength of soil surrounding the non-encased section of the column. A reliable measurement of this strength would be required to make a reasonably confident estimate of column capacity.

As site testing was not available to confirm the preliminary findings of small-scale testing, alternative confirmation work was undertaken as part of this research. This included medium-scale testing on unconfined, encased columns undertaken to investigate the performance of real geogrid encasement. Results of this testing are presented in Chapter 5. A full-scale parametric study using numerical techniques was also undertaken to investigate the impact of column and soil properties on column behaviour. The results of this study are presented in Chapter 6.

### **3.9.3 Influence of geogrid stiffness**

The behaviour of columns encased with aluminium mesh appear to differ little from the behaviour of columns encased with fibreglass mesh, except perhaps a slightly stiffer response from the aluminium mesh at higher stresses. Although the stiffness of the aluminium mesh was twice that of the fibreglass, it was considered that there was insufficient contrast between the two. In addition, the scaled stiffness of both meshes

probably represented a material with greater stiffness than the range typically associated with geogrids.

To compare the behaviour of columns encased with geogrids of different stiffness, materials with a greater contrast in stiffness are probably required. Furthermore, tests would benefit from being of larger scale, where the impact on settlement and deformation would be more pronounced. Results of a numerical study and medium-scale testing used to assess the impact of mesh stiffness on encased column behaviour (amongst other things) are presented in later chapters.

#### **3.9.4 Method of overlap**

The method of overlap used in small-scale tests comprised constructing the encasement by overlapping the mesh sleeve with at least a half circumference of sacrificial mesh. Interlocking between the sand grains and the overlapped section of mesh provided a level of fixity similar to bonding the mesh with epoxy-resin, for both isolated columns and group columns simulated using unit-cell idealisation. Although the tests were undertaken at relatively small-scale, by extrapolation it would appear reasonable to assume that the interaction could be reproduced in full-scale, providing an alternative to welding the geogrid on site. Column tests using real geogrid and typical stone column aggregates were undertaken to confirm this, as part of the research that forms this thesis. Results of these tests are presented in Chapter 5.

#### **3.9.5 Vertical drainage**

Although assessment of the time rate of consolidation was not a primary component of this research, data was collected as part of small-scale column testing. Tests indicated that columns acted as effective vertical drains, significantly reducing the time required to consolidate column-clay samples. However, the ability of columns to act as drains appeared to decrease with time, a likely result of observed clay ingress into the column cross-section with ongoing consolidation. This observed ingress behaviour is also likely to affect columns installed on site, and although it is outside the scope of research outlined in this thesis, warrants further investigation.

## **4 Numerical modelling of small-scale test results**

---

Numerical analysis is often used in geotechnical engineering to model test results, leading to a better understanding of the engineering problem at hand and more accurate prediction of material behaviour. Numerical analysis is probably the most theoretically robust approach to assessing geotechnical problems because the technique can combine highly non-linear soil models with complex geometry and interface properties.

In this research, numerical analysis was used to model the results of small-scale tests, providing insights into encased column behaviour. Soil models were calibrated to the behaviour of materials measured in simple laboratory strength and deformation tests. These soil models were then combined to investigate column test behaviour. As the mesh used in the small-scale tests is too fine to practically instrument, numerical analysis was used to investigate the development of mesh hoop forces. This supplemented the observations of mesh failure and the conclusions made earlier in Chapter 3.

The numerical analysis described herein was undertaken using the 2D finite element modelling software package “PLAXIS”. This chapter provides background on the adopted numerical modelling technique and comparison of the numerical analysis to laboratory test results.

### **4.1 Background**

PLAXIS Version 8 was used to undertake the numerical modelling. The PLAXIS software was developed in the late 1980s at the Technical University of Delft and has subsequently been updated and improved. The package is used by many practicing geotechnical engineers world-wide and comprises robust computational procedures that have been well tested over many years. The particular version of PLAXIS used in this research was designed to analyse two-dimensional deformation and stability problems, with the capacity to simulate non-linear and time-dependent soil/rock behaviour in plane-strain or axisymmetric conditions. The package comprises user-friendly, Windows based

software with a CAD based graphical input system that allows input of soil layers, structures, geometry and loading sequences.

The package offers many advanced features. Some of particular relevance to modelling stone columns include:

- 4<sup>th</sup> order polynomial, 15-noded triangular elements which generally do not suffer from “locking” problems like lower order formulations may (Sloan and Randolph 1982).
- Tensile elements that can be used to simulate geogrid and enable assessment of tensile forces within the geogrid.
- Advanced soil models which simulate elastoplastic soil behaviour, including the Hardening Soil model and Soft Soil model, set out later in this chapter.
- Staged construction, allowing realistic simulation of construction installation procedures including excavation and replacement of soil modules and staged loading.
- Consolidation analysis which enables generation of excess pore pressure in low-permeability soil during loading and dissipation of excess pore pressure with time.

## **4.2 Modelling of small-scale tests**

As group column behaviour was considered to be of most practical significance, numerical modelling focussed on group column tests, although some consideration was also given to isolated column tests. To replicate the laboratory column test results, numerical models that adequately reproduced the behaviour of the test materials were first required. This was achieved by calibrating the numerical material models to the behaviour of the laboratory tests used to measure material strength and compressibility. The processes used to model the clay, sand and geogrid are described separately in the following sections. Details of the relevant PLAXIS soil models are also included.

### **4.2.1 Kaolin**

As described in Chapter 3, kaolin was used to create homogeneous samples of very soft clay. Shear box and conventional oedometer tests were used to measure the strength and

compressibility characteristics of the kaolin, respectively. The relevant kaolin properties are summarised in Table 4.1.

**Table 4.1:** Kaolin properties used in numerical modelling

parameter	unit	value
Angle of internal friction	°	18
Dilation	°	0
Saturated unit weight	kN/m <sup>3</sup>	16.2
Initial void ratio	-	3.04
Compression index, $C_c$	-	0.80
Recompression index, $C_r$	-	0.09
Permeability	ms <sup>-1</sup>	$9.2 \times 10^{-10}$

#### 4.2.1.1 Soft Soil model

The kaolin constitutive model was created using the PLAXIS Soft Soil model, described by Vermeer and Brinkgreve (1998). This advanced soil model is suited to simulating normally consolidated and slightly over-consolidated soft soils. It models logarithmic compression behaviour (stress dependent stiffness) and can distinguish between load phases and unload/reload phases. In addition, pre-consolidation stresses and over-consolidation can be incorporated into the model. Further details of the model are provided in the PLAXIS User Manual (Brinkgreve and Broere 2004) and a brief summary of the salient features is provided in Appendix B.1.

#### 4.2.1.2 Rationale

Although a numerical model should generally be calibrated against a controlled test, preferably where both strength and deformation are measured (like a triaxial test), triaxial testing was not undertaken for the following reasons:

- The time required to undertake several multiple-staged, drained triaxial tests on kaolin clay.
- An enlarged oedometer cell was used to load sand columns in the small-scale testing component of this research. A numerical model based on the

compressibility measured in standard oedometer tests was therefore likely to adequately replicate kaolin clay behaviour.

Furthermore, to measure the compressibility of soils on projects where stone columns may be used, one-dimensional consolidation tests are often undertaken. This is because they are relatively quick and cheap to perform and reflect the plane-strain conditions that occur beneath wide, uniformly loaded areas. Calibration of numerical modelling to conventional oedometer tests was therefore considered to be a reasonable approach.

#### 4.2.1.3 Methodology

The geometry of the conventional oedometer tests undertaken on very soft kaolin clay (outlined in Chapter 3) was modelled in axisymmetric half-space using a fine mesh constructed from 15-noded triangular elements. Standard fixities (no displacement perpendicular to the boundary) were applied to the cell perimeter and a closed consolidation boundary was applied to both sides of the cell, preventing radial drainage from the boundary. Consolidation analysis was undertaken, enabling assessment of pore pressure dissipation. Load was applied through a rigid horizontal plate placed directly above the sample. Because the slurry did not demonstrate classical soil behaviour until it had undergone some consolidation, the initial properties of the model (including height, void ratio and stress history) were adjusted to reflect kaolin consolidated at a pressure of about 6 kPa. The same increments of vertical stress used in the oedometer test were applied to the numerical model. An updated mesh was also adopted because large strains, and therefore large nodal displacements, were likely. Sample deformation and time rate of consolidation were calculated for each load stage.

#### 4.2.1.3 Results

The e-log pressure relationship obtained from the PLAXIS analysis is compared to the behaviour measured in oedometer tests in Figure 4.1. Results indicate that the compressibility of the numerical model closely matches that of the oedometer tests, particularly across the range of vertical stresses relevant to laboratory testing (50 kPa to 350 kPa). Although the shear test was not modelled numerically, it was considered that

the Mohr-Coulomb failure criteria used in the Soft Soil model would adequately model kaolin shear behaviour.

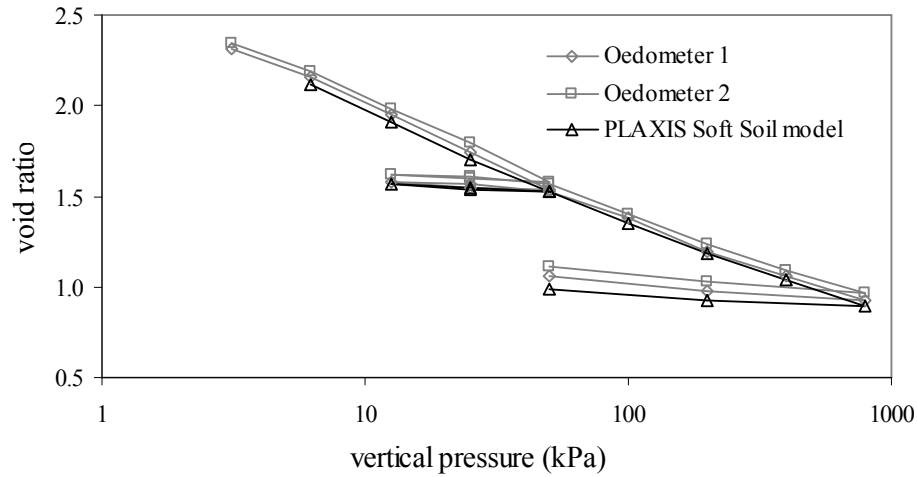


**Figure 4.1:** e-log pressure behaviour of Soft Soil model compared to kaolin tests

The time taken to dissipate excess pore pressure was calculated for each load stage. Consolidation rate was primarily affected by soil permeability. Initially, a permeability of  $9.2 \times 10^{-10}$  m/s was adopted in the clay model, based on the average permeability assessed from oedometer tests (refer to Section 3.3.1.4). The kaolin was modelled as an isotropic material, with the same permeability adopted in the vertical and horizontal directions. To investigate the influence of permeability on consolidation time, two numerical models with different permeability were used. ‘Soft Soil model 1’ assumed a permeability of  $9.2 \times 10^{-10}$  m/s and ‘Soft Soil model 2’ assumed a permeability of  $1.4 \times 10^{-9}$  m/s. The results of the numerical assessment are compared to laboratory test results in Figure 4.2.

Results indicate that the time taken to consolidate ‘Soft Soil model 1’ was greater than for ‘Soft Soil model 2’ and matched the results of the oedometer tests more closely. However, there was significant variation in the test results, particularly for the range of vertical stresses relevant to column testing (50 kPa to 350 kPa). This variability was probably a result of the thin samples used in conventional oedometer testing. Although there was reasonable correlation between the numerical and test results, it was decided to refine the value of permeability based on consolidation tests undertaken on a thicker sample of kaolin.

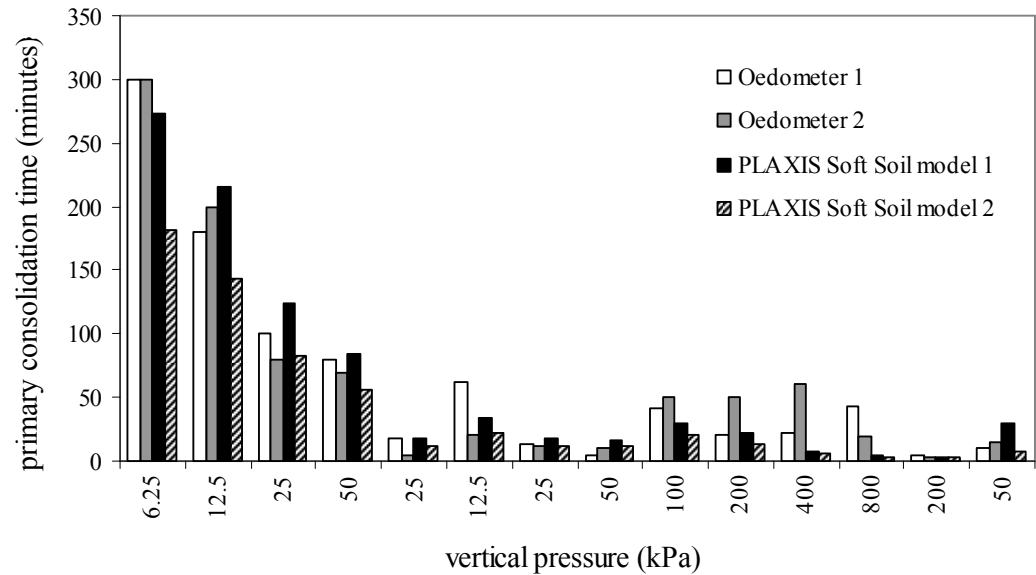


**Figure 4.2:** Rate of primary consolidation in numerical models compared to oedometer tests

The kaolin cell test (GC-1) comprised consolidation of a much thicker sample of clay (about 480 mm), and in the authors experience, provided data of greater reliability to which the numerical model could be calibrated. The geometry of Steel cell #1 was modelled in axisymmetric half space, in the same way the smaller, conventional oedometer cell was modelled. Additional details on this modelling process are provided later in this chapter. The calculated consolidation time for the two models was then compared to the time taken for each load stage of the kaolin cell test. The results are presented in Figure 4.3.

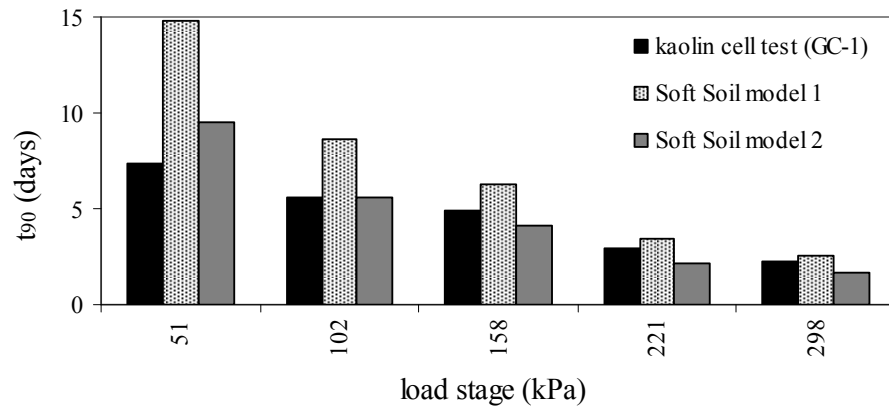


**Figure 4.3:** Rate of primary consolidation in numerical models compared to large cell test



The results indicate that better correlation was achieved with the numerical model of higher permeability (Soft Soil model 2). As the kaolin cell test was considered more reliable and more representative of column tests, the permeability of  $1.4 \times 10^{-9}$  m/s was adopted for further modelling of kaolin clay.

#### 4.2.2 Modelling sand

Conventional oedometer testing and shear box testing were also used to measure the compressibility and strength of sand. The relevant sand properties are summarised in Table 4.2.

**Table 4.2:** Sand properties used in numerical modelling

parameter	unit	range/value
Peak angle of internal friction	°	40 - 43
Angle of dilation at peak	°	8 - 10
Saturated unit weight	kN/m <sup>3</sup>	20.2
Initial void ratio	-	0.60
Compression index, $C_c$	-	0.013
Recompression index, $C_r$	-	0.007
Average permeability	ms <sup>-1</sup>	$4.5 \times 10^{-2}$

##### 4.2.2.1 Hardening Soil model

The PLAXIS Hardening Soil model, described by Schanz et al. (1999), was used to model the sand. This soil model is capable of simulating the behaviour of both stiff and soft soils, featuring stress dependent stiffness, elastic unloading and reloading and failure according to Mohr-Coulomb criteria. Its origins are based on the hyperbolic soil model proposed by Duncan and Chang (1970), but supersedes it in a number of ways, with the inclusion of plasticity theory, dilatancy and a yield cap. Some features of this advanced soil model include:

- Stress dependent stiffness, such that stiffness moduli increase with pressure.
- Compression hardening due to irreversible plastic straining in oedometric compression or isotropic loading.

- Shear hardening due to irreversible plastic straining as a result of primary deviatoric loading.

Further details of the Hardening Soil model, especially relating to its implementation, are provided in the PLAXIS User Manual (Brinkgreve and Broere 2004).

#### 4.2.2.2 Methodology

The sand oedometer tests were modelled using a similar process adopted for kaolin clay. However, as the sand was considered to drain immediately upon loading, time-dependent settlement analysis was not undertaken. Furthermore, no adjustment to the initial soil properties (as a result of kaolin not demonstrating classical soil behaviour until it had undergone some consolidation) was required. The vertical deformation for each load stage was calculated.

#### 4.2.2.3 Results

The e-log pressure relationship obtained from the PLAXIS analysis is compared to the behaviour of oedometer tests in Figure 4.4.

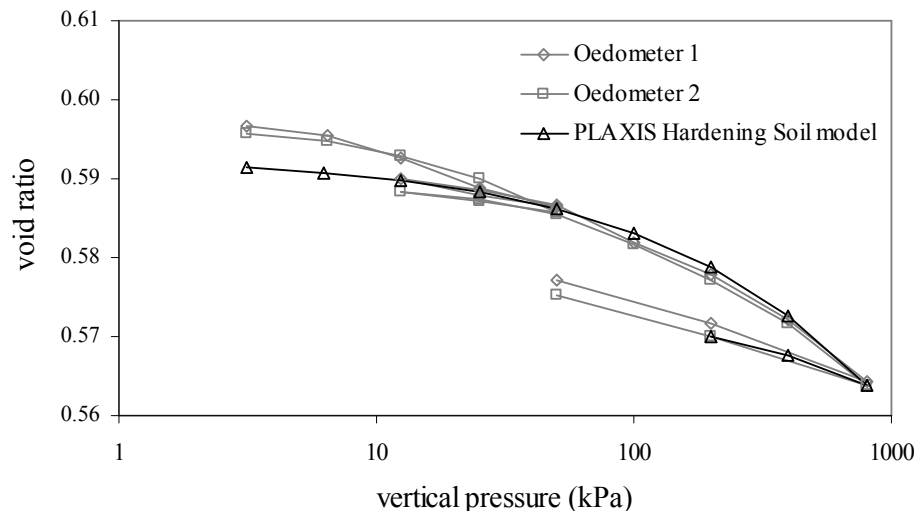


**Figure 4.4:** e-log pressure behaviour of Hardening Soil model compared to sand tests

Figure 4.4 indicates that divergence occurs between the numerical model and the oedometer tests at pressures less than about 25 kPa. Above this pressure, the numerical results closely match the compressibility of the sand. As sand columns were generally tested at cell pressures greater than 55 kPa, the observed divergence was considered to have little impact on model behaviour. The divergence may have been a result of parameter selection in the numerical model, compliance effects that were not adequately accounted for during initial loading of the laboratory test samples or a number of other reasons. However, as the divergence was considered to have little effect on the modelling for the range of applied surcharges, its cause was not further investigated. The Hardening Soil model, with parameters set out in Table 4.2, was considered to provide a reasonable representation of the behaviour of the sand.

#### 4.2.3 Modelling geogrid

The geogrid elements provided in PLAXIS were used to model the aluminium and fibreglass mesh as they were able to sustain tension forces. The elements can be used in axisymmetric models, enabling the calculation of hoop forces. To use the geogrid elements, the tensile strength and elastic axial stiffness of the geogrid,  $EA$ , are required as input parameters. For geosynthetics, these parameters are typically supplied by the manufacturer. For the fibreglass and aluminium mesh used in laboratory tests, properties were assessed from uniaxial tests outlined in Chapter 3, and are presented in Table 4.3.

**Table 4.3:** Properties of fibreglass and aluminium mesh used for numerical modelling

parameter	value	
	fibreglass	aluminium
Tensile strength (kN/m)	8.6	6.8
Elastic axial stiffness, $EA$ (kN/m)	300	600

Although elastic-perfectly plastic tensile elements can be used to model the geogrid in PLAXIS by defining a plastic yield stress, elastic elements were adopted. This was because laboratory tensile testing of the mesh indicated generally elastic behaviour up to the point of failure, with little load sustained following rupture. For numerical models, exceeding the tensile strength was considered to represent mesh failure, at which point the analysis was stopped.

#### **4.2.4 Modelling of group column tests**

As group column tests were considered to be of the most practical significance, numerical modelling was primarily aimed at reproducing group column test behaviour.

##### **4.2.4.1 Cell geometry**

After confirming that PLAXIS could satisfactorily model the behaviour of materials used in laboratory testing, PLAXIS was used to model the cell column tests described in Chapter 3. Initially, the steel cell geometry was modelled in axisymmetric half-space using the same procedure adopted for modelling oedometer tests. This resulted in a model with a width of 78 mm (half the width of the cell) and a height of about 375 mm, which corresponded to the slurry height consolidated at a pressure of 6 kPa. 15-noded triangular elements were used to construct the mesh. To simplify the modelling, side-wall friction in the cell was ignored. A closed consolidation boundary was applied to the vertical cell boundaries. A vertical geometry line was constructed 25.5 mm from the central axis of the model, representing the perimeter of the sand column that was to be installed. No interface was applied to the geometry line because of the boundary conditions imposed by the cell. This resulted in the clay and column settling by equal amounts, reducing shearing at the column-clay interface. The geogrid was modelled along this vertical geometry line, with the length dependent on the amount of encasement used in the test. The piston was modelled as a rigid plate element.

##### **4.2.4.2 Column installation and loading**

A 55 kPa downward pressure was applied to the model, reducing the sample height to about 310 mm at the completion of consolidation, in line with testing. The model was then unloaded and the clay zone adjacent to the central axis was replaced with sand, simulating column installation. To simulate pore pressure dissipation in the clay, the sand was modelled as an undrained material with a permeability of less than 5 orders of magnitude greater than kaolin (Tan 2007). This reduced the potential for numerical errors, and although it did not accurately reflect the permeability of the sand, it had little impact on results. This was because consolidation rate was primarily influenced by the permeability of the kaolin.

Although the nominal 4 kPa load (used to obtain intimate contact between the column and clay) was applied to the numerical model, the calculated settlements were much less than those observed in testing. This was probably because the modelling technique did not include the disturbance or re-seating created during column installation. For this reason, settlements associated with this nominal loading were ignored when comparing numerical and physical models. The numerical models were loaded using the pressure increments adopted in the laboratory column tests. An illustration of the cell and mesh geometry for the 50% fibreglass encased column sample, at various stages of loading, is presented in Figure 4.5. Figure 4.5 shows the initial state of kaolin (left), sand column and geogrid installation (middle), and sample loading (right).

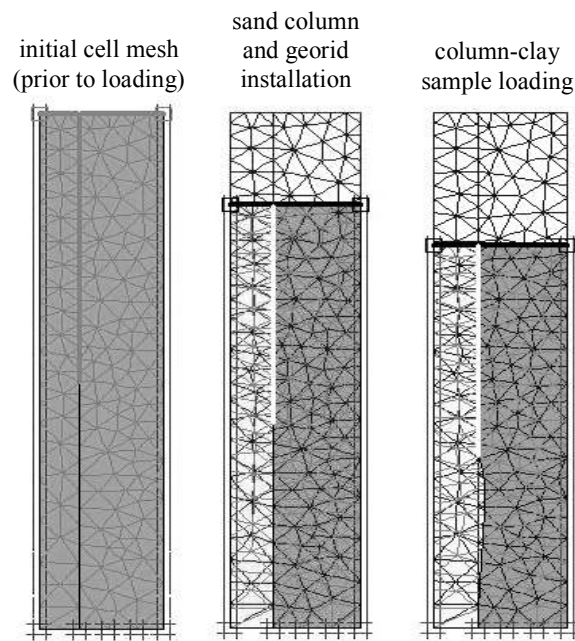


**Figure 4.5:** Axisymmetric model of cell geometry at various stages of testing

#### 4.2.4.3 Vertical stress-strain behaviour

Results of the laboratory testing indicated a significant reduction in vertical column strain with increasing encased length. The results of numerical modelling are compared to the behaviour of fibreglass encased column tests in Figure 4.6, and aluminium encased column tests in Figure 4.7. The results of the numerical analysis generally closely matched the laboratory test results.

As illustrated in Figure 4.6, the calculated vertical strain of the kaolin cell is marginally less than obtained from the test results. This confirms that the silicone lubrication was effective in reducing side-wall friction. For column tests, there are minor variations between laboratory test results and the numerical analysis. For the kaolin cell test (GC-1) and non-encased column test (GC-2), the calculated vertical strain is slightly lower than the measured value. This may be attributed to a number of different factors, of which the small percentage of creep included in the measured values is considered a significant influence. As the percent encased length is increased, the comparison between the numerical model and laboratory test results generally improves, particularly for columns encased with aluminium mesh. For the fully fibreglass encased column test (GC-8), the numerical model slightly overestimates the measured sample strain. This may indicate that the fibreglass encasement acted with greater stiffness than measured in uniaxial tensile tests. The numerical results closely match the measured values for the fully aluminium encased column test (GC-9).

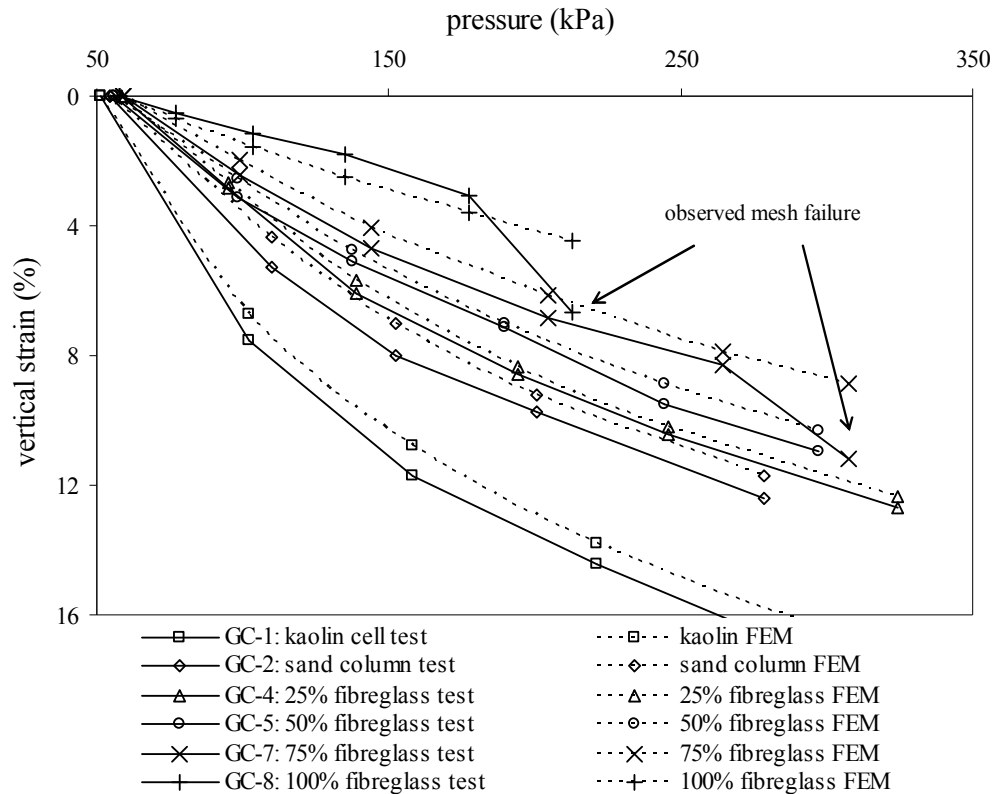


**Figure 4.6:** Numerical compression behaviour compared to fibreglass encased test results

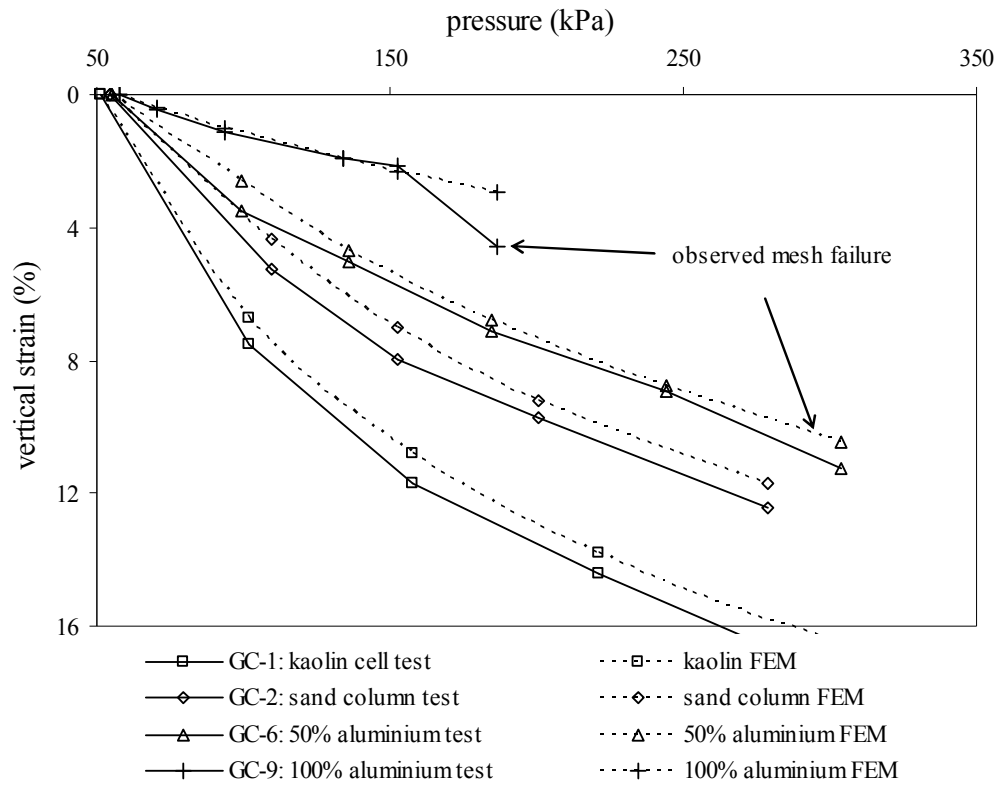


**Figure 4.7:** Numerical compression behaviour compared to aluminium encased test results

The results set out above generally indicate that numerical modelling is capable of reproducing the vertical strain behaviour of encased column tests.

#### 4.2.4.4 Radial column expansion

At the completion of column tests, samples were extruded and carefully bisected to observe the deformed shape along the length of the column. These deformations were then compared to those obtained from numerical analysis. Comparisons for non-encased and partially encased column tests are presented in Figure 4.8. The deformed shape of fully-encased columns are not presented because the meshes in the laboratory tests distorted significantly during failure, making meaningful comparison difficult.

As observed in Figure 4.8, the measured and calculated radial deformations are in close agreement for both encased and non-encased sections of the column. For some samples, particularly columns with a greater encased length (where the magnitude of expansion is greater), the numerical analysis slightly underestimates the magnitude of radial expansion.

This may be due to parameter selection (e.g. dilation of the sand) or perhaps the difficulty in defining the kaolin-sand boundary in extruded samples (because of kaolin ingress into the column during consolidation). However, discussions with other PLAXIS users and those involved with developing the PLAXIS software (Vermeer 2008) have indicated that the underestimation of lateral displacement is quite common when using some of the advanced soil models. The variation in lateral deformation between laboratory tests and numerical models is not considered to be significant.

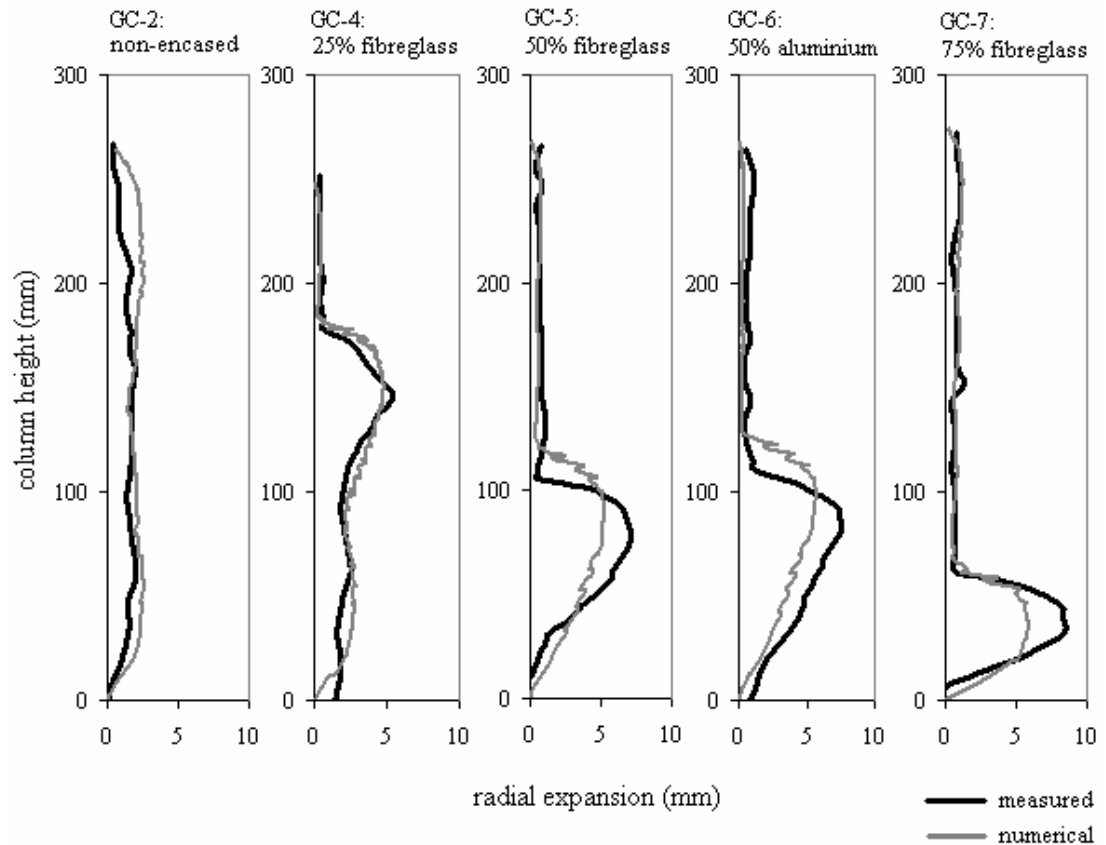


**Figure 4.8:** Comparison of numerical and measured radial column expansion

#### 4.2.4.5 Examination of mesh failure

As set out in Chapter 3, failure of the mesh used to encase the model sand columns was observed for 75% and 100% fibreglass encasement, and 50% and 100% aluminium encasement. Failure typically occurred in the upper section of the encasement, indicating that the tensile capacity of the mesh had been exceeded. Although no direct measurement of the hoop forces were made during testing, they were calculated numerically.



The results of this assessment are presented in Figure 4.9 and Figure 4.10, where hoop forces in the final load stage are compared to the capacity of the fibreglass and aluminium meshes, respectively.

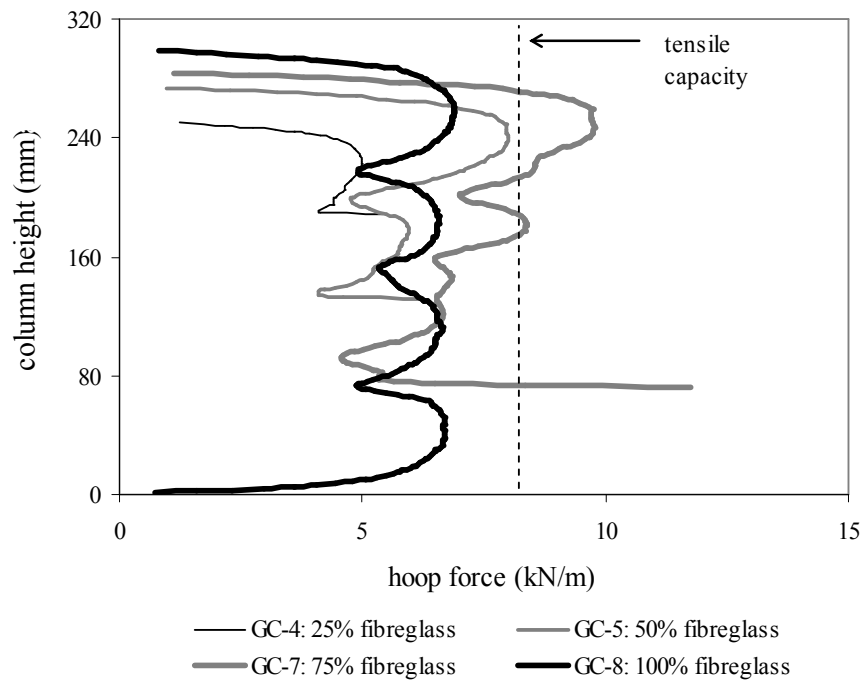


**Figure 4.9:** Calculated hoop forces in fibreglass mesh using numerical analysis

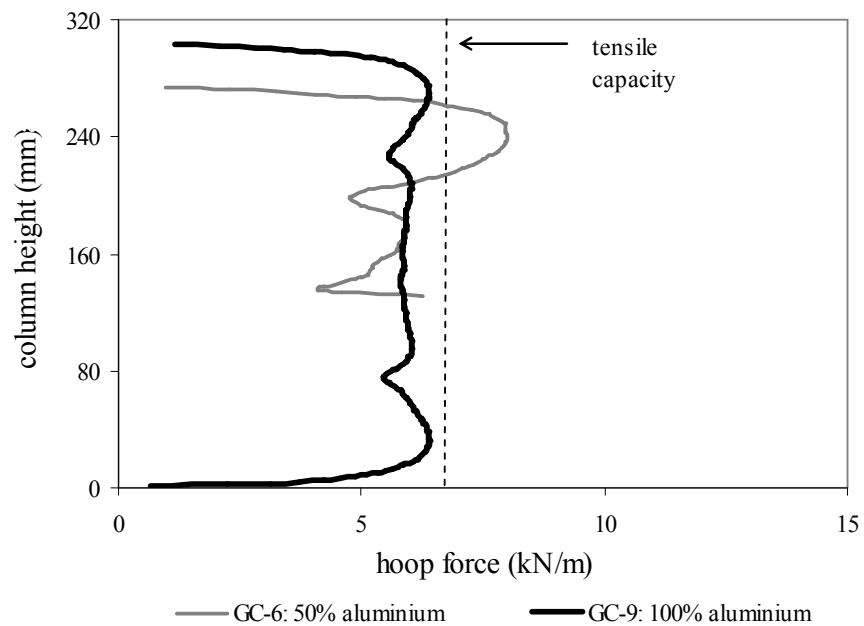


**Figure 4.10:** Calculated hoop forces in aluminium mesh using numerical analysis

With the exception of the 25% fibreglass encased column (GC-4), forces within the mesh encasement of all columns were calculated to be either close to, or in excess of the tensile capacity along at least some length of the encasement. Of these, only the mesh encasement in the 50% fibreglass encased column test (GC-5) did not fail. Furthermore, in partially encased column tests, hoop forces calculated numerically are generally highest in the upper section of the column. This correlates well with the observed encasement failures, where strand breakage was generally most prolific in the upper section of the column. Finally, for the 75% fibreglass encased column (GC-7), hoop forces in the transition zone at the base of the mesh are calculated to be much higher than the tension capacity of the mesh. This section of the mesh was observed to have failed in the laboratory test. These combined observations indicate that the numerical analysis undertaken provides a reasonably accurate model of the laboratory tests, including the performance of the mesh.

The following inferences may be drawn from the modelling:

- For partially encased columns, hoop forces are generally higher in the upper section of the encasement and in the transition zone from encased to non-encased section at the base of the encasement.
- Load appears to be distributed more evenly throughout the length of the fully-encased column, with hoop forces generally consistent along the full length of the encasement. This was apparent in both the fibreglass and aluminium encased columns, presented in Figure 4.9 and Figure 4.10, respectively.

From the small-scale test results presented in Chapter 3, it appears that for a nominated surcharge, columns with greater encased length attract greater peak hoop forces. This was based on the 75% fibreglass encased column failing whereas the 50% fibreglass encased column did not, even though both tests were terminated at similar pressures. Although this is investigated in greater detail in Chapter 6 (where full-scale numerical modelling of geogrid encased stone columns is undertaken), results of the modelling presented in Figure 4.9 indicate that the peak hoop forces in the 75% fibreglass encased column are only slightly higher than the 50% encased column. The modelling also indicates that the mesh encasement of the 50% fibreglass column was probably very close to failure.

#### 4.2.4.6 Cell drainage

The time taken to complete consolidation was measured for each load stage in each laboratory column test, using a combination of pore pressure and settlement measurements, as set out in Chapter 3. Consolidation time was calculated numerically using consolidation analysis in PLAXIS, which enabled simulation of excess pore pressure dissipation. The calculated consolidation times for all eight group column tests (GC-2 to GC-9) are compared to the measured values in Figure 4.11. The results from the kaolin cell test (GC-1) were omitted because they were used to calibrate the permeability of the kaolin numerical model.

With the exception of the 50% aluminium encased column test (GC-6) and some minor variability in other tests, the numerical results generally matched the time of consolidation measured for the nominal load stage and the following one or two load stages. As the number of load stages increased (and therefore the surcharge pressure and total consolidation), the comparison between numerical and measured results diverged and became more variable. In the latter load stages, the calculated consolidation times were generally less than the measured values, most significantly in the final load stage of each test. It is unlikely that this divergence was a function of the adopted numerical model. As outlined in Chapter 3, significant clay ingress was observed in the column cross-section following sample extrusion (refer Figure 3.27). This was likely to significantly reduce the permeability of the column and therefore the ability of the column to act as a vertical drain. This may account for the difference between numerical and measured consolidation times in the latter load stages. Further investigation of this was considered outside the scope of the present research.

The measured consolidation times for GC-6 were significantly higher than for other tests. Following test completion, examination of the brass porous plates indicated a significant amount of clogging, limiting the ability of the porous plate to drain water from the consolidating sample. This was considered to have adversely affected the measured consolidated rate.

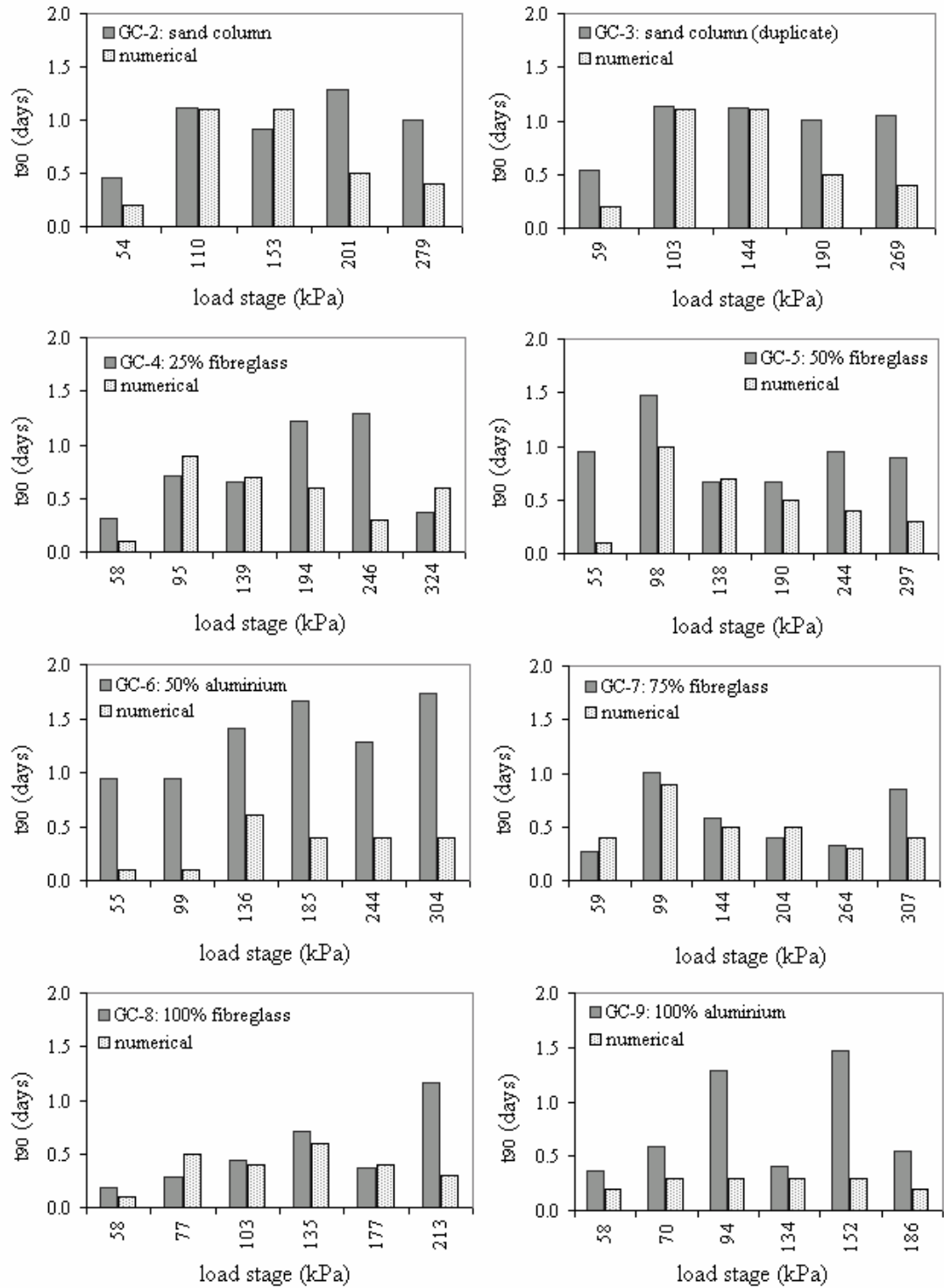


**Figure 4.11:** Comparison of numerical consolidation time rates to column test results

#### 4.2.5 Modelling of isolated column tests

The numerical modelling of isolated column tests was limited to investigating vertical column strain only. This is because the isolated column test program is of less practical

significance than group column testing, as set out in Section 1.7. Cell geometry was modelled in the same way as group column tests, but to model the Perspex cell diameter of 143 mm, an axisymmetric model width of 71 mm was adopted for the numerical analysis. The kaolin was consolidated with a surcharge of 55 kPa, assuming drained material properties. This resulted in a clay height of about 310 mm. Column installation was then modelled and the column was loaded using a plate element equal in radius to the column, simulating the small footing used in the laboratory tests.

Loading was undertaken in small increments, not necessarily corresponding to those used in laboratory tests. As at least some drainage occurred during the laboratory testing (as indicated by reduced clay moisture content measured adjacent to columns and observed time-dependent settlement), drained numerical analyses were undertaken. Loading was continued until column failure occurred, with vertical stress-strain curves plotted for each column test. These curves are compared to the laboratory test results in Figure 4.12.

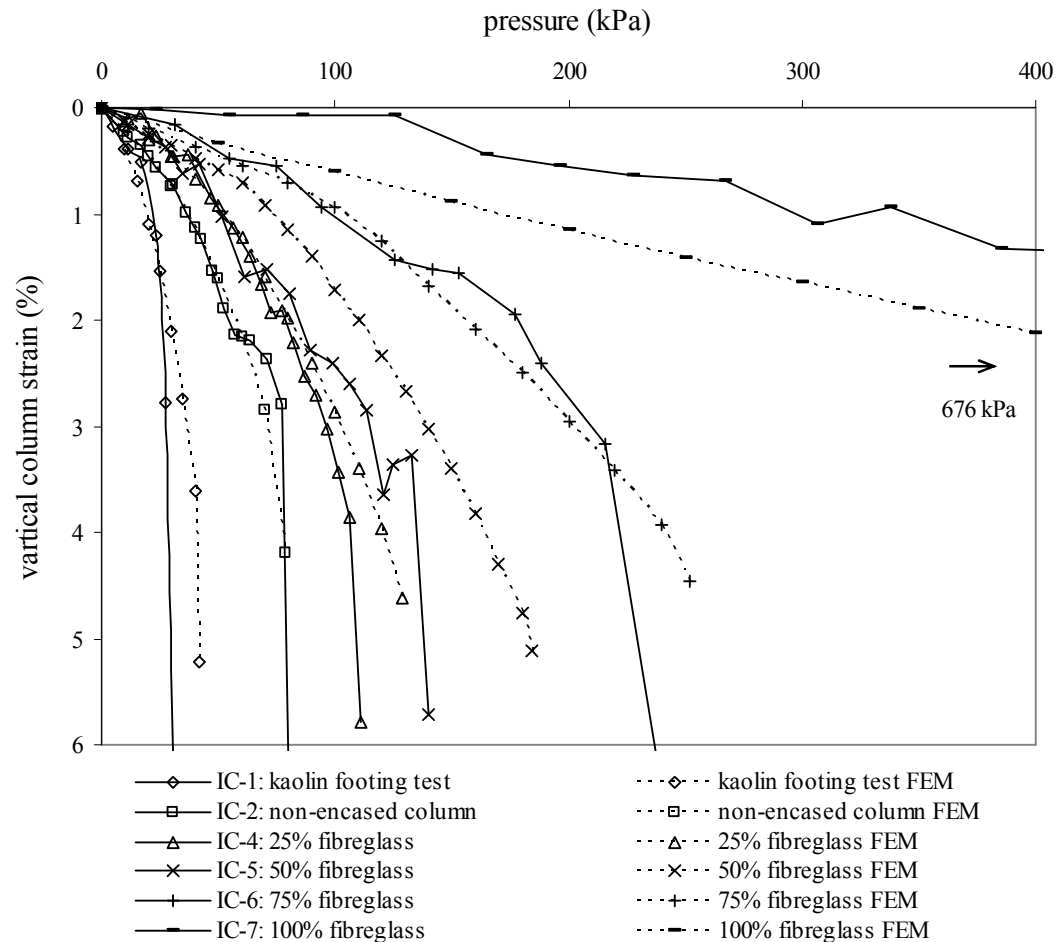


**Figure 4.12:** Numerical compression behaviour compared to isolated column test results

The results of the numerical analysis compare well with those measured in the laboratory. The general trend of increased column capacity with increased encased length observed in the laboratory tests (Chapter 3) is reproduced and the average failure strain of between 4% and 5% compares favourably with those measured in the laboratory tests. Although the strain for the fully-encased column (IC-7) is overestimated, the same observation was made for group column modelling. This further supports the contention that the fibreglass mesh acted with greater stiffness than measured in uniaxial testing, at least when columns were fully-encased.

### **4.3 Summary**

The adopted numerical modelling technique comprised:

- (i) Creating numerical soil models for test materials (sand and clay).
- (ii) Calibrating the model behaviour to simple laboratory strength and deformation test results including standard oedometer tests.
- (iii) Combining the models to simulate column tests, with consideration given to the method of column installation.

The numerical analysis of small-scale laboratory tests presented in this chapter indicates that numerical modelling is capable of reproducing small-scale encased column behaviour with reasonable accuracy. The numerical modelling process set out above simulated various aspects of encased column behaviour including column compressibility and lateral deformation. Although mesh strain was not measured during the laboratory tests, the hoop forces calculated from the numerical analysis provided a reasonable indication of mesh failure.

## 5 Medium-scale laboratory tests

---

Based on the success of the small-scale laboratory testing set out in Chapter 3, medium-scale laboratory testing was undertaken to investigate whether geogrid encasement is effective with full-scale materials. Several different geogrids and crushed rock aggregates were investigated. The scope of testing was primarily aimed at investigating whether the method of overlap provided an effective method of encasement construction with these materials. The impact of material and geometric properties (including geogrid stiffness and strength, amount of encasement overlap, column diameter and aggregate type) on encased column behaviour was also investigated. Medium-scale testing generally comprised unconfined compression loading of columns fully encased with geogrid.

The methodology used to undertake medium-scale testing is described in this chapter, together with results and discussion on the suitability of different materials to encased column applications.

### 5.1 Background

As set out in Chapter 2, medium-scale testing of geogrid encased stone columns has been previously undertaken at the Gropius Institute of the Hochschule Anhalt Technical College, Dessau. The work, which was described by Trunk et al. (2004), comprised unconfined compression tests on several geogrid encased columns measuring 1.88 m in height (but up to 3 m in some cases) and 0.6 m in diameter. Columns were constructed from various types of granular material and encased with Secugrid® and Combigrigrid® sleeves supplied by NAUE GmbH. The encasement was fixed in place by mechanically welding the overlapped section of geogrid. The columns were loaded in 50 kN stages. Stages were held static (although some dynamic testing was undertaken) for about 7 days before application of the following stage. Maximum column stresses of about 1400 kPa were measured prior to failure, which generally comprised column buckling at about 2% circumferential strain. Creep of the geogrid was not observed during testing.

The medium-scale testing undertaken as part of the research presented in this thesis differed from the work undertaken at Dessau in three important ways:

- (i) Columns were constructed from geogrid encasement that was formed using the method of overlap, rather than from being welded. Welding is not considered practical or economical for encasement construction on site, as set out in Chapter 2. In this study, the columns were generally overlapped by between 50% (0.5×) and 100% (1×) of the column circumference. The hoop strength and fixity of the encasement was generally dependent on the interlock provided by rock aggregate protruding between geogrid ribs in the section of overlap.
- (ii) Columns were smaller, particularly in height. Columns generally measured 0.86 m high and 0.24 m to 0.36 m in diameter. Smaller columns were used for a number of reasons, including:
  - Shorter columns were less likely to buckle (as occurred in Dessau) when loaded. Failure was therefore likely to be governed by the encasement strength, as would generally occur in the confined conditions on site.
  - Smaller columns reduced column construction time and the amount of materials required, increasing the number of columns (and therefore column types) that were tested.
  - The load frame used for testing was only capable of supporting columns with a diameter of less than about 0.5 m.
- (iii) As the stress-strain properties of the geogrid were not considered to be time dependent (no creeping of the geogrid was observed in Dessau tests), a constant displacement method was used to load columns rather than static loading. This significantly reduced test time, generally to a few hours or less, and increased the number of tests that were undertaken.

## **5.2 Materials**

The materials used in the testing of medium-scale geogrid encased stone columns are described in the following sections.

### **5.2.1 Columns**

Two types of crushed rock aggregate were used to test encased columns, “20/50 mm rubble” and “14/10 mm gravel”. The 20/50 mm rubble is considered representative of typical conventional stone column aggregate and was therefore used in the majority of



medium-scale tests. The smaller 14/10 mm gravel was used to test whether sufficient interlock (using the method of overlap) was achieved using smaller aggregates. Its use was therefore confined to a limited number of tests.

#### 5.2.1.1 20/50 mm rubble

The 20/50 mm rubble comprised angular crushed basalt rock typically graded between 20 mm and 50 mm. The product is produced locally (Melbourne, Australia) by Boral Ltd. The particle size distribution of the rubble is presented in Figure 5.1.

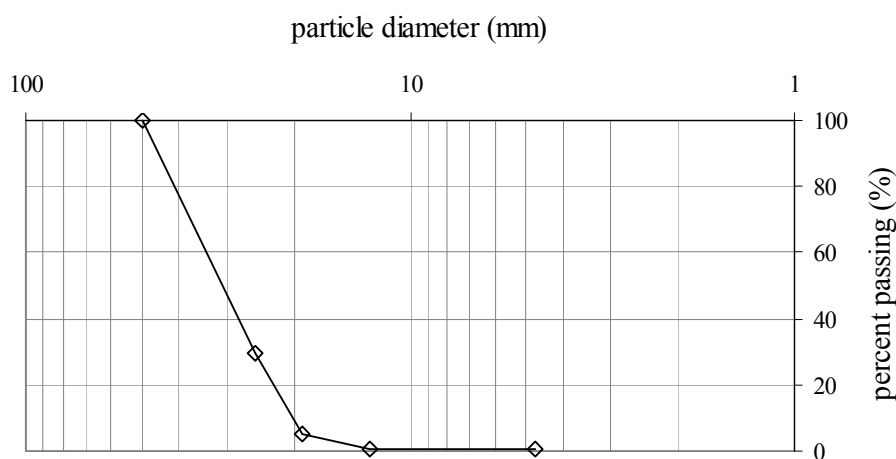


**Figure 5.1:** Particle size distribution of 20/50 mm rubble

Relative density testing was undertaken in general accordance with Australian Standard AS1289.5.5.1 to measure the minimum and maximum dry density of the rubble. Due to the coarse size of the aggregate it was compacted in a container measuring about 400 mm high and 300 mm in diameter. Minimum density was measured by hand placing aggregate in the container, with care taken not to significantly disturb or vibrate the surrounding material. Maximum density was measured by shaking the container on a vibrating plate until no measurable increase in density occurred (generally after about 10 minutes). The minimum and maximum dry densities are presented in Table 5.1.

**Table 5.1:** Minimum and maximum dry density of 20/50 mm rubble

Parameter	Value
Minimum dry density, $\rho_{\min}$ (kg/m <sup>3</sup> )	1470
Maximum dry density, $\rho_{\max}$ (kg/m <sup>3</sup> )	1630

For encased column testing, a relative density of between about 60% and 70% was targeted. This is at the low end of the range of typical conventional stone column relative densities set out in Chapter 2. It is considered to be a realistic relative density for columns installed using a replacement technique (where compaction would occur through vibration of the casing during installation, a technique similar to that used to install GECs and described in greater detail in Chapter 7). However, this value is difficult to measure in the laboratory tests with certainty. This is due to the irregular diameter of the column along its length, resulting from the variable size and shape of protruding rock aggregate.

Shear box testing was also undertaken to measure the internal angle of friction of the 20/50 mm rubble, although this was not used as part of any further analysis. The rubble was lightly compacted in a large shear box measuring 600 mm long by 200 mm wide and sheared under constant normal stresses of 50 kPa and 250 kPa. The peak friction angle measured in the shear box testing was about  $\phi=52^\circ$ . A photograph of the large shear box is presented in Figure 5.2.



**Figure 5.2:** Set up of large shear box

#### 5.2.1.2 14/10 mm gravel

Medium to coarse sized gravel was used to investigate whether the method of overlap was effective with smaller aggregates. 14/10 mm crushed basalt gravel (“Pakenham Blue

Metal”) was used for this purpose, supplied by CEMEX Australia (formerly Readymix). As the 14/10 mm gravel was only used for testing the method of overlap, no strength or density testing was undertaken. The particle size distribution of the gravel is presented in Figure 5.3.

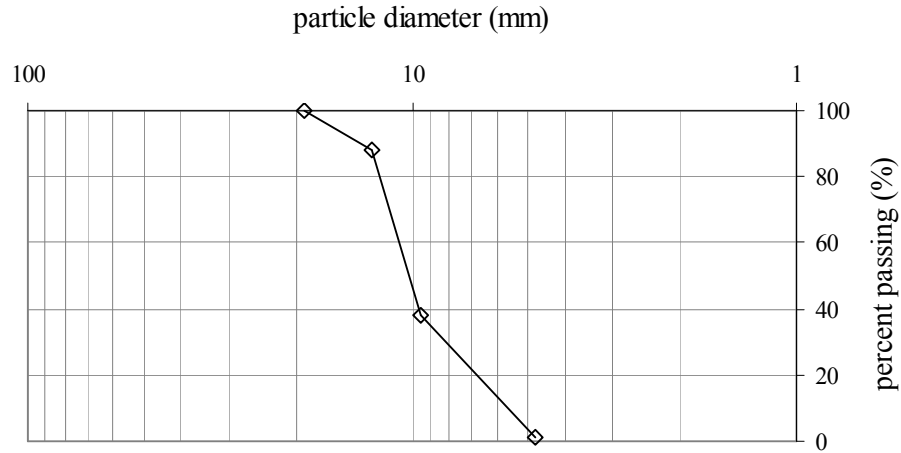


**Figure 5.3:** Particle size distribution of 14/10 mm gravel

### 5.2.2 Geogrid

Seven different geogrids were used in the medium-scale tests. These were used to assess which geogrids were best suited to the method of overlap and to investigate the impact of properties such as strength, stiffness and aperture spacing on encased column behaviour. Five of the seven geogrids used in medium-scale testing were Secugrid® (Secugrid) type geogrids, supplied by NAUE GmbH. The five Secugrid products comprised:

- Secugrid 60/60 Q6
- Secugrid 80/80 Q6
- Secugrid 120/120 Q6
- Secugrid 120/40 R6
- Secugrid 200/40 R6

Secugrid comprises monolithic polyester (PET) ribs that are mechanically welded to form a mesh. For biaxial geogrids (Q6 products) such as Secugrid 60/60 Q6, the mesh is typically square-shaped, with the strength in the machine direction (md) the same as the cross-machine direction (cmd). For uniaxial geogrids (R6 products) such as Secugrid 200/40 R6, the mesh is typically rectangular-shaped, with the strength in the machine

direction generally higher than for the cross-machine direction, although this may be changed to suit in some cases.

The concept of machine direction and cross-machine direction in the context of geogrid manufacture is illustrated in Figure 5.4. Technical data supplied by the manufacturer for the five Secugrid products used in testing is presented in Table 5.2. The typical load-strain behaviour of Secugrid products is presented in Appendix D.1.

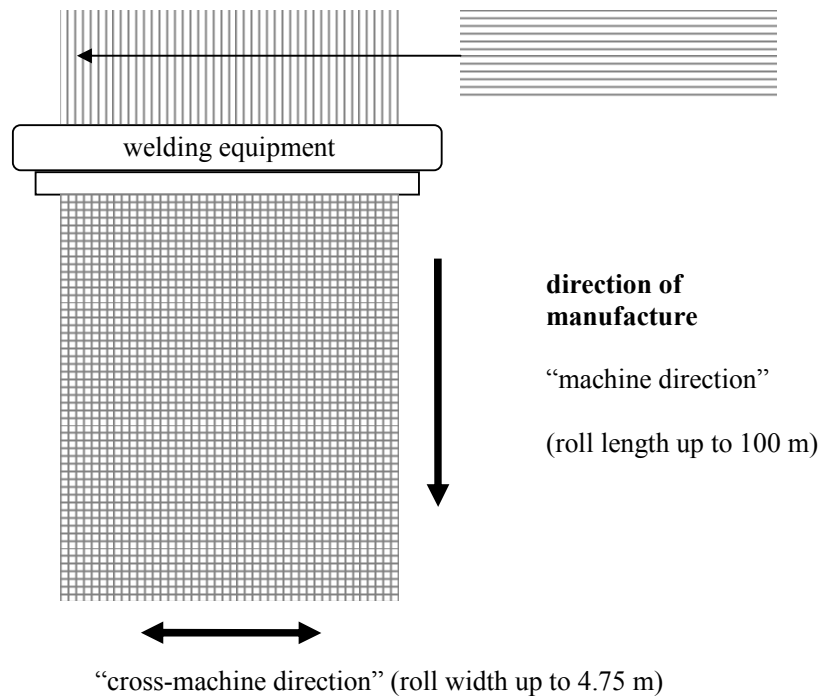


**Figure 5.4:** Concept of machine and cross-machine direction

**Table 5.2:** Secugrid technical data supplied by the manufacturer

technical data	unit	60/60 Q6	80/80 Q6	120/120 Q6	120/40 R6	200/40 R6
Material		Polyester/PET (transparent)				
Max. tensile strength*	kN/m	≥60/≥60	≥80/≥80	120/120	120/40	200/40
Elongation at nominal strength*	%	≤8/≤8	≤8/≤8	≤8/≤8	≤8/≤8	≤8/≤8
Tensile strength at 2% elongation*	kN/m	27/27	28/28	42/42	42/-	70/-
Tensile strength at 5% elongation*	kN/m	48/48	52/52	72/72	72/-	120/-
Mesh aperture spacing* <sup>#</sup>	mm×mm	32×31	31×30	27×27	71×27	71×25

\* strengths are presented as – machine direction / cross-machine direction

<sup>#</sup> measured from inside edge of each rib

The sixth geogrid used in testing comprised Combigrd<sup>®</sup> 60/60 Q6, also supplied by NAUE GmbH. Combigrd<sup>®</sup> (Combigrd) comprises a geogrid and geotextile composite, where a layer of geotextile is placed between the geogrid ribs aligned in the machine direction and cross-machine direction, prior to welding. Combigrd is suited to a range of applications including drainage and separation. In this case, it was used to retain fine aggregate that would otherwise have fallen out of the Secugrid mesh. For encasement applications, Combigrd develops its strength from the geogrid, not the geotextile. The strength properties of Secugrid 60/60 Q6, presented in Table 5.2, are considered representative of the Combigrd strength in such cases.

The final geogrid used in testing was the TX 160 geogrid (TriAx), manufactured by Tensar International and donated by Geofabrics Australia Pty Ltd, with the understanding that it was to be used for encasement construction. The geogrid is manufactured from a punched polypropylene sheet, with triangular shaped apertures formed. The ribs are significantly more slender than the other geogrids used in testing and junctions are integral rather than welded. The TriAx geogrid is typically used in applications such as roads to distribute loads more evenly through pavement materials. The radial stiffness of the geogrid at low strain (0.5%) is about 430 kN/m, which is at the low end of the range available for geogrid products and at least half the stiffness of the lowest strength Secugrid used in the scope of medium-scale testing. The TriAx geogrid was primarily used to investigate whether sufficient interlock could be achieved with the triangular aperture shape. It was also used to investigate the behaviour of encasement constructed from geogrid that did not comprise welded junctions. Photographs of columns encased with some of the geogrid products set out in this section are presented in Figure 5.5.

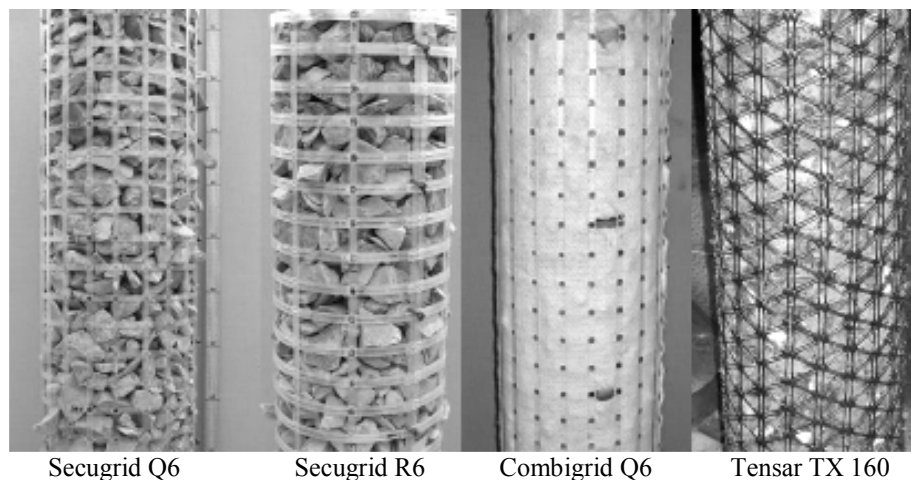


**Figure 5.5:** Photographs of the different geogrid products used for encasement construction

### 5.3 Column testing

The methods used to prepare and test medium-scale geogrid encased stone columns are described in the following sections.

#### 5.3.1 Test schedule

Nineteen fully-encased columns were prepared for testing, using combinations of different geogrids, encasement geometry and stone column aggregates. The properties of these columns are presented in Figure 5.3.

**Table 5.3:** Properties of columns prepared for testing

test no.	encasement type	aggregate type (mm)	column diameter (mm)	relative density (%)	geogrid overlap (%)	horizontal ribs
1	Secugrid 60/60 Q6	20/50	235	68	53	inside
2	Secugrid 60/60 Q6	20/50	235	76	53	inside
3	Secugrid 60/60 Q6	20/50	235	69	53	inside
4	Secugrid 60/60 Q6	20/50	235	69	53	outside
5	Secugrid 60/60 Q6*	14/10	235	-	53	outside
6	Secugrid 120/40 R6	20/50	250	65	64	outside
7	Combigrid 60/60 Q6	20/50	235	67	53	inside
8	Secugrid 120/40 R6	20/50	225	65	100	outside
9	Secugrid 60/60 Q6	20/50	235	61	100	outside
10	Secugrid 60/60 Q6	20/50	235	61	100	outside
11	Secugrid 80/80 Q6	20/50	235	61	100	outside
12	Secugrid 80/80 Q6	20/50	235	61	100	outside
13	Secugrid 200/40 R6	20/50	250	65	100	outside
14	Secugrid 80/80 Q6	20/50	360	65	78	outside
15	Secugrid 60/60 Q6 <sup>#</sup>	14/10	235	-	100	outside
16	Secugrid 60/60 Q6 <sup>#</sup>	14/10	235	-	100	outside
17	Tensar TX 160	20/50	235	-	100	-
18	Secugrid 120/120 Q6	20/50	235	64	100	outside
19	Secugrid 120/120 Q6	20/50	235	68	100	outside

\* geotextile sleeve was placed inside the geogrid encasement to retain gravel

<sup>#</sup> columns were encased with a thin plastic film to retain gravel

### 5.3.2 Encasement construction

Geogrid encasement was constructed by rolling a flat section of geogrid into a cylindrical sleeve. The diameter of the cylinder was about 0.24 m, although this varied slightly depending on the geometric properties of the geogrid used. The height of the encasement sleeve was kept constant at 0.86 m. Initially, about 50% of the column circumference was overlapped. However, testing indicated that this amount was inadequate in some cases and overlap was increased to 100% in later tests.

Encasement was initially constructed with horizontal ribs located on the inside of the sleeve and vertical ribs located on the outside. However, a greater capacity was measured in early tests when horizontal ribs were located on the outside of the column. Although this aspect of encasement construction was not further investigated, encasement was constructed with horizontal ribs located on the outside in subsequent tests.

Cable ties were used to fix the encasement sleeve in position and prevent it from unravelling during handling, particularly while the sleeve was being filled with aggregate and compacted. As the tests were unconfined, the ties were also likely to be required in the initial stages of loading to provide support until some radial expansion and interlock occurred. Once interlock occurred, the cable ties were considered unlikely to provide additional support, due to their much lower strength compared to the geogrid ribs. Tension testing of the ties indicated that their capacity was about 0.45 kN, about five times less than the weakest Secugrid ribs (Secugrid 60/60) used for encasement. Cable ties were used at six evenly-spaced locations along the length of the encasement, corresponding to an average spacing of about 170 mm. At this interval, their strength was about 3 kN/m, much lower than the weakest Secugrid strength of about 60 kN/m.

Early column testing indicated that the cable ties provided little support after initial loading. Where interlock was insufficient, circumferential slippage (unravelling) of the overlapped section generally caused failure of the ties. In such tests, either column failure occurred or further loading resulted in an adequate state of interlock being reached which enabled column testing to continue. If adequate interlock was achieved at the start of testing, little load was supported by the cable ties and they generally remained intact, occasionally even after failure of the encasement ribs.

After the encasement sleeve had been constructed, a plate of geogrid was attached to the base of the encasement using 8 cable ties spaced evenly around the perimeter. The base plate was used to retain the gravel in the column while it was being handled and transferred into the loading frame. It was considered to have little impact on the circumferential strength of the sleeve. A layer of geotextile was often placed on the base plate to prevent finer aggregate from falling out of the sleeve. Photographs of the encasement sleeve constructed for test No. 2 are presented in Figure 5.6. The type of construction adopted in this test was considered representative of most encasement sleeves.

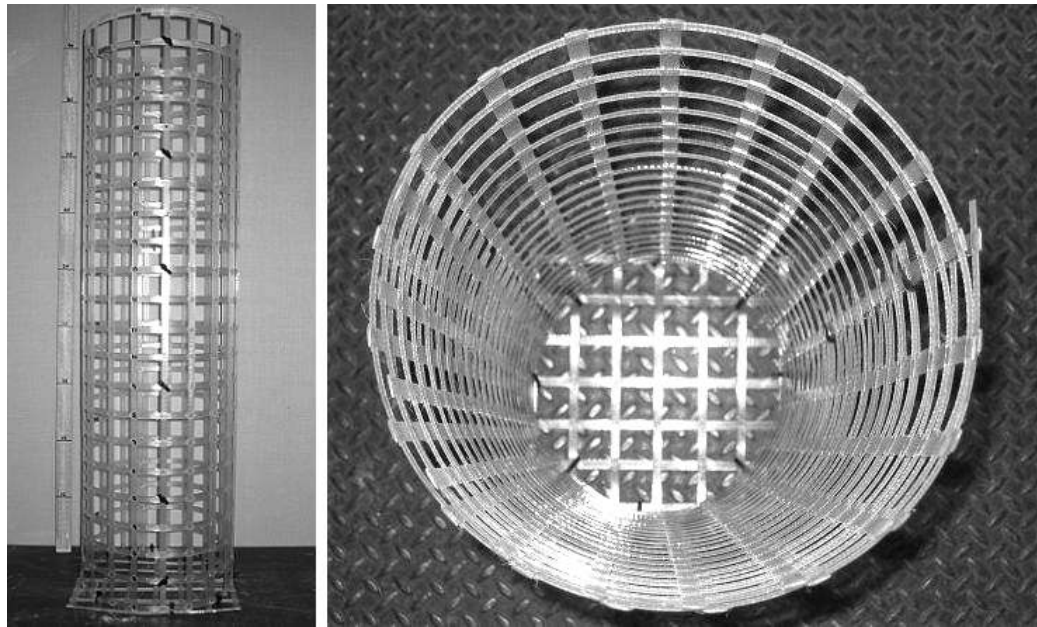


**Figure 5.6:** Encasement sleeve used for column test No. 2

Cable ties provided a useful method for temporarily fixing the cylindrical encasement in place. The technique was developed with site testing in mind. It is envisaged that when constructing full-scale encasement on site, cable ties may provide a practical method for fixing the sleeves in position. Cable ties spaced at about 0.5 m intervals along the length of the encasement could provide the temporary fixity required during installation.

### **5.3.3 Column construction**

The completed encasement sleeve was filled with 20/50 mm rubble in layers of about 200 mm. After the placement of each layer, the rubble was compacted by shaking the



encasement by hand for about 1 minute. Upon completion, the column was weighed to determine an approximate column density (volume was calculated using the internal diameter and height of the encasement). The adopted method of compaction generally resulted in a relative density between about 60% and 70%, which was the targeted level of compaction. The relative density of each column prepared for testing is presented in Table 5.3. A photograph of the compacted column prepared for test No. 2 is presented in Figure 5.7.



**Figure 5.7:** Compacted column prepared for test No.2, comprising 20/50 mm rubble

In three of the column tests, 14/10 mm gravel was used to investigate whether sufficient interlock occurred using smaller aggregates. In test No. 5, a geotextile insert (constructed from 151 GRK 3 geotextile, supplied by NAUE) was placed inside the geogrid sleeve to retain the gravel and prevent it from falling through the geogrid ribs. Although this method adequately retained the gravel, it reduced the ability of the gravel to protrude between the ribs and therefore develop interlock.

Based on this unsuccessful test, an alternative technique was used in test No. 15 and 16 to provide some limited confinement to the gravel. A single layer of thin, transparent plastic film (“Cling Wrap”, generally used in food preparation) was wrapped around the outside of the geogrid sleeve. The film had very low tensile strength (not measured) and was not considered to significantly affect the column strength. The column was then filled with

14/10 mm gravel using the same compaction technique adopted for columns constructed using 20/50 mm rubble. Density was not measured for these columns because the tests were used only to assess the ability of the smaller gravel to achieve interlock. Using the thin plastic film, the gravel was observed to protrude from between the ribs in the same way it did for 20/50 mm rubble tests. Photographs of the column prepared for test No. 15 are presented in Figure 5.8.

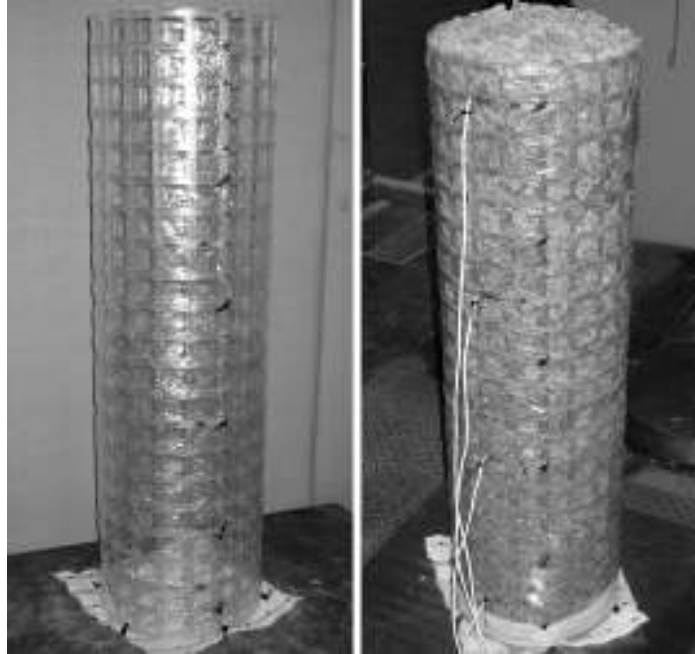


**Figure 5.8:** Column wrapped with plastic film to retain 14/10 mm gravel (test No. 15)

#### **5.3.4 Column loading**

Columns were tested using an Amsler compression test machine (Amsler), located in the Civil Engineering laboratories at Monash University, Clayton Campus. The Amsler comprises a base plate which is raised and lowered by a hydraulic piston. A sample is typically placed on the base plate. A cross-head is then fixed in place above the sample and the base plate is forced upwards at a controlled rate of displacement, compressing the sample against the cross-head. The force required to raise the piston is measured by load cells within the apparatus. The distance between the base plate and cross-head is measured using 2 No. Stringpot transducers (described in greater detail in Chapter 3) fixed at opposite sides of the base plate. A data acquisition system is used to record load and displacement at user-defined intervals.

For unconfined compression testing of encased columns, the columns were shifted on to the base plate using a scissor-lift. The cross-head was then lowered so that it was resting on top of the column but not applying any measurable load. During testing, the base plate was raised at a rate of 1-2 mm/min (corresponding to about a 1 hour test). In test No. 3, the rate of displacement was reduced to about 0.3 mm/min (corresponding to about a 6 hour test), to investigate whether the reduced rate had an impact on column capacity or geogrid hoop strain. No significant difference in column behaviour was observed when using the slower load rate, so the rate of 1-2 mm/min was adopted in subsequent tests. A photograph of a column being tested in the Amsler is presented in Figure 5.9.



**Figure 5.9:** Compressive column test in Amsler apparatus

During testing, the maximum displacement of the base plate (about 80 mm) was often exceeded. When this occurred, the column had to be unloaded by lowering the base plate to its original position. The cross-head was then lowered to rest on top of the column and column loading was re-commenced, producing an unload-reload cycle in the test. Although an unload-reload cycle was not desired because it made meaningful comparison of the axial compression and radial strain behaviour of tests difficult beyond the unload stage, it was considered an unavoidable part of testing when using the Amsler apparatus. The displacement of the initial load stage was increased in later tests (up to 120 mm) by manually lowering the cross-head on to the column before raising the piston.

### 5.3.5 Instrumentation

Strain gauges were attached to horizontal ribs to measure geogrid hoop strains. 4 No. strain gauges were generally attached to each encased column in the same plane vertically, but evenly spaced along the length of the column. Where 50% overlap was adopted in testing, strain gauges were attached to the non-overlapped section of the column. Where 100% overlap was adopted in testing, the strain gauges were located at the beginning of the overlapped section (as measured hoop strains were likely to decrease the further the gauges were placed from the beginning of the overlap). With this configuration, the measured hoop strains could be compared to those taken in the non-overlapped section of the columns.

To attach the strain gauges, the often textured surface of the geogrid ribs was sanded back to a smooth surface. An adhesive was then applied to the ribs and the gauges were attached and then connected to a data acquisition system. The general purpose strain gauges were manufactured by Vishay Intertechnology Inc. A photograph of the instrumented section of a column is presented in Figure 5.10.



**Figure 5.10:** Strain gauge attached to the upper section of the encasement

### 5.3.6 Tank test

The first medium-scale encased column test undertaken in the laboratory was a tank test (test No. 1), where an encased column was pushed into a 600 mm diameter tank filled with kaolin slurry. The tank test was initially adopted because it was thought that the method

of overlap may be ineffective in unconfined conditions (even with the use of cable ties). It was considered that a material like slurry may provide the lateral pressures required to confine the column during loading. The slurry also better reproduced the site conditions in which the columns would be installed, although the stiffness and confinement provided by the slurry was likely to be significantly lower than a natural soil.

The slurry was prepared at a moisture content of 90% and had an undrained shear strength of about 1 kPa, measured using a laboratory shear vane. The slurry was manufactured from the same powdered kaolin used in the small-scale laboratory testing, described in Chapter 3. A photograph of the tank test is presented in Figure 5.11.



**Figure 5.11:** Encased column prepared for tank testing

The instrumented column was loaded using a footing that measured 350 mm in diameter. Results indicated that the method of overlap worked effectively in providing encasement fixity. Based on this, and observations of column behaviour made during construction, an unconfined test (test No. 2) was undertaken to determine whether unconfined testing was also possible. Results of this unconfined test indicated that there was little difference between the confined and unconfined test behaviour, with the method of overlap working effectively in unconfined conditions.

Due to the time associated with preparing, undertaking and then dismantling the tank test (and the similarity in the behaviour of confined and unconfined column tests), unconfined testing was adopted for subsequent tests. This enabled a greater scope of testing to be undertaken in the allocated timeframe, including assessment of the behaviour of columns constructed from different materials.

## **5.4 Test results**

The results of medium-scale, encased stone column tests are described and discussed in the following sections. Graphs of column load versus column axial compression and geogrid hoop strain versus column axial compression for each test are presented in Appendix C.1.

### **5.4.1 Typical test behaviour**

As set out earlier, 19 tests were undertaken on geogrid encased stone columns. With the exception of test No. 1, columns were loaded in unconfined compression. In most column tests, loading initially caused axial compression of the stone aggregates. Relatively little circumferential strain was measured in the geogrid during this stage, at least when compared to the latter stages of loading.

As loading continued, aggregate particles protruded from the geogrid apertures, to a greater extent than at the beginning of the test. This indicates that the column was expanding radially, a process that acted to increase the interlock between the aggregate and the overlapped section of the column. This also coincided with a significant increase in measured circumferential strain, which indicates that the encasement was working to confine the aggregate. This can generally be considered as the point where geogrid hoop forces are mobilised. The increase in circumferential strain typically occurred at hoop strains of about 0.5%. This was significantly less than the 1% to 4% hoop strain required to mobilise the hoop forces in geotextile (GECs), as reported by Alexiew et al. (2005).

Axial compression and radial straining continued to occur as the column was further loaded, often punctuated by the sound of rock particles breaking and crushing. The circumferential (hoop) strains measured at different locations on the geogrid encasement

are plotted against axial strain in Figure 5.12. The initial stage of the test, where axial compression occurred without significant mobilisation of geogrid hoop forces, is highlighted. The results presented are for test No. 12, where encasement was constructed from Secugrid 80/80 Q6. These results comprise axial compression and circumferential strain measured prior to unloading the column and are considered representative of the behaviour of most column tests.

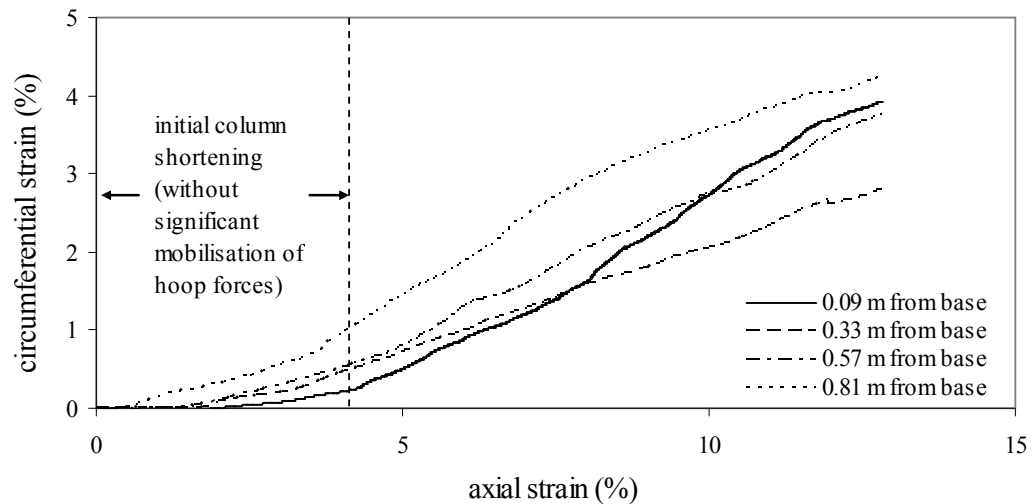


**Figure 5.12:** Circumferential strain behaviour for a typical column test

Cable ties often broke in the early stages of column loading, resulting in slight slipping or unravelling of the overlapped section of geogrid (and a reduction in measured geogrid strain) before the protruding rock interlocked with the geogrid again, providing fixity. Prior to column failure, the sound and frequency of rock crushing intensified. Circumferential strains generally increased roughly linearly with axial strain. The circumferential strain measurements for each column test are presented in Appendix C.1. Failure was observed to occur in one of three ways, described in the following section.

#### 5.4.2 Modes of column failure

The mode of column failure was generally dependent on the type of geogrid being used, the type of aggregate and the amount of overlap. Three modes of failure were identified in testing and are described separately in this section.

#### 5.4.2.1 Mode 1 – insufficient overlap, sufficient interlock

When an insufficient amount of overlap was used to form the geogrid encasement but the interlock between the aggregate and the geogrid ribs was adequate, the welded junctions of the geogrid generally sheared in the overlapped section. This caused vertical ribs to tear away from horizontal ribs or vice-versa, resulting in a loss of radial confinement and failure generally in the upper or mid section of the column. Photographs of test No. 6, where this failure mode was observed, are presented in Figure 5.13.



**Figure 5.13:** Failure mode 1 (test No. 6)

#### 5.4.2.2 Mode 2 – insufficient interlock

When interlock was insufficient, the overlapped section of geogrid encasement tended to slip until most of the circumferential load was supported by the cable ties. When these failed, the geogrid encasement generally unravelled with little damage occurring to the geogrid. This mode of failure generally occurred when 14/10 mm gravel was used in place of the 20/50 mm rubble. Photographs of test No. 15, where this mode of failure was observed, are presented in Figure 5.14.





**Figure 5.14:** Failure mode 2 (test No. 15)

#### 5.4.2.3 Mode 3 – sufficient overlap, sufficient interlock (desired failure)

When both overlap and interlock were sufficient, tension failure occurred in the horizontal ribs of the geogrid (circumferential direction). This was considered the desired failure mode because it indicated that the tensile capacity of the geogrid was being used. One or two ribs generally failed simultaneously, with ribs above and below this location progressively failing with ongoing loading. The ultimate tensile strain of the geogrid (and therefore tensile strength) was generally reduced in testing due to cutting of the ribs from the angular-shaped rock. This aspect is discussed later in this chapter. Photographs of test No. 4, where this type of failure occurred, are presented in Figure 5.15.

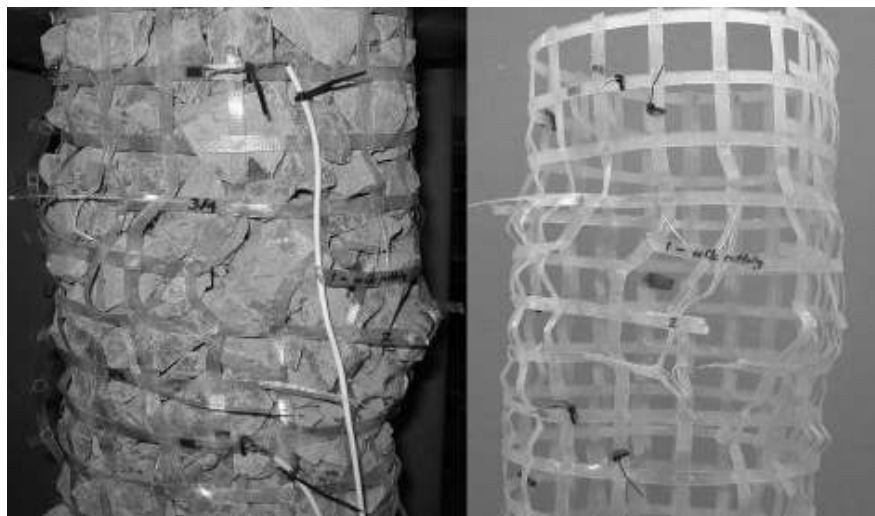


**Figure 5.15:** Failure mode 3 (test No. 4)

The results of the encased column tests, including mode of failure, failure load and circumferential (hoop) strain are presented in Table 5.4. Both maximum and average geogrid hoop strains are presented because both are considered important in assessing encasement performance. Due to the irregular shape of the granular fill and small column diameters, localised strains varied significantly along the length of the column and at different locations around the circumference of the column. Localised strains were obviously higher when rock was pressing directly against a rib.

**Table 5.4:** Results of column tests

<b>test no.</b>	<b>geogrid type</b>	<b>rock type (mm)</b>	<b>overlap (%)</b>	<b>failure mode (1,2,3)</b>	<b>max. load (kN)</b>	<b>ave. hoop strain (%)</b>	<b>max. hoop strain (%)</b>
1	Secugrid 60/60 Q6	20/50	53	3	66	3.0	4.1
2	Secugrid 60/60 Q6	20/50	53	1	73	2.5	2.8
3	Secugrid 60/60 Q6	20/50	53	1	65	3.2	4.4
4	Secugrid 60/60 Q6	20/50	53	3	84	3.0	3.9
5	Secugrid 60/60 Q6	14/10	53	2	26	0.5	0.7
6	Secugrid 120/40 R6	20/50	64	1	56	1.5	2.1
7	Combigrd 60/60 Q6	20/50	53	1	28	0.4	0.4
8	Secugrid 120/40 R6	20/50	100	1*	99	1.3	2.0
9	Secugrid 60/60 Q6	20/50	100	3	95	2.7	3.1
10	Secugrid 60/60 Q6	20/50	100	3	94	2.7	3.8
11	Secugrid 80/80 Q6	20/50	100	3	113	4.0	5.2
12	Secugrid 80/80 Q6	20/50	100	3*	105	4.0	4.9
13	Secugrid 200/40 R6	20/50	100	1	86	0.9	1.4
14	Secugrid 80/80 Q6	20/50	78	3	145	4.0	5.2
15	Secugrid 60/60 Q6 <sup>#</sup>	14/10	100	2	106	3.4	4.0
16	Secugrid 60/60 Q6 <sup>#</sup>	14/10	100	2	110	3.5	3.8
17	Tensar TX 160	20/50	100	3	51	-	-
18	Secugrid 120/120 Q6	20/50	100	3	128	4.0	5.4
19	Secugrid 120/120 Q6	20/50	100	3	125	4.2	4.7

\* Column buckling also occurred

<sup>#</sup> columns were encased with thin plastic film to retain gravel

As it was not practical or economical to instrument each horizontal rib (nor numerous locations on the same rib), the hoop strains at four locations were generally used to assess average hoop strain and therefore average hoop force. Maximum hoop strain generally gave an indication of the localised strain in the failure zone (although this was not always the case) and may provide a better measurement of capacity.

Axial strains (or column compression) at failure are not compared between tests because an unload-reload stage was included in several tests, making meaningful comparison difficult.

### 5.4.3 Secugrid Q6 encasement (biaxial geogrid)

The results of tests undertaken on columns constructed using 20/50 rubble and encased with Secugrid Q6 geogrid are discussed in this section.

#### 5.4.3.1 Secugrid 60/60 tests

The load-compression behaviour of 20/50 mm rubble columns encased with Secugrid 60/60 is presented in Figure 5.16.

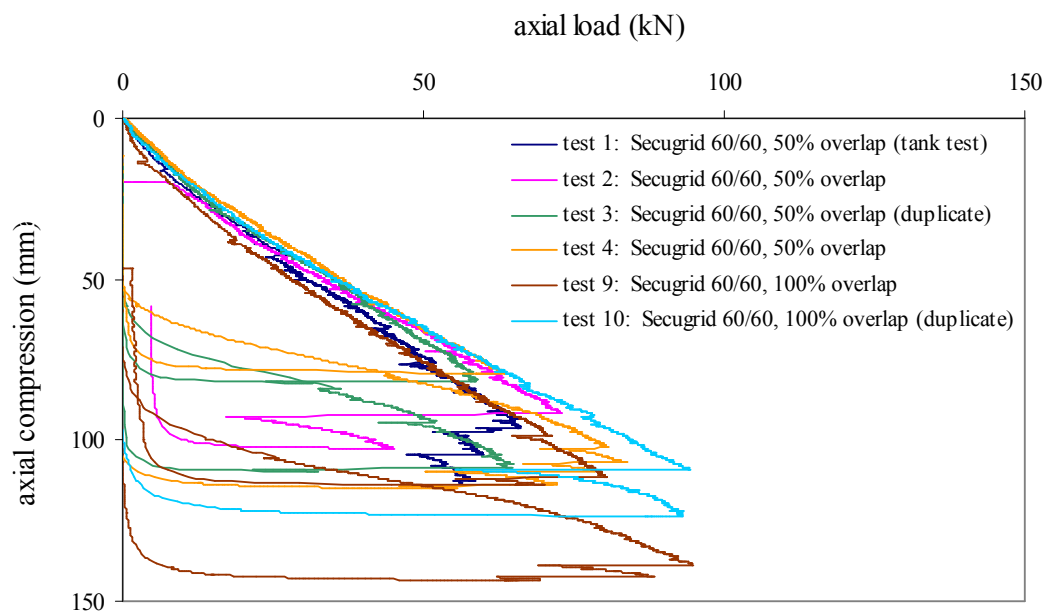


**Figure 5.16:** Load-compression behaviour of columns encased with Secugrid 60/60

All six column tests had a similar stiffness when loaded, indicating that both the aggregate and geogrid encasement behaved with some consistency. It is difficult to meaningfully compare the shape of each load-compression curve beyond about 80 mm compression because of the unload-reload stage. However, the initial stiffness of columns (prior to the unload-reload stage) and maximum load give a reasonable basis for comparing encased column behaviour. Figure 5.17 presents the maximum axial load reached in each test along with the average and maximum geogrid hoop strains measured in the geogrid encasement.

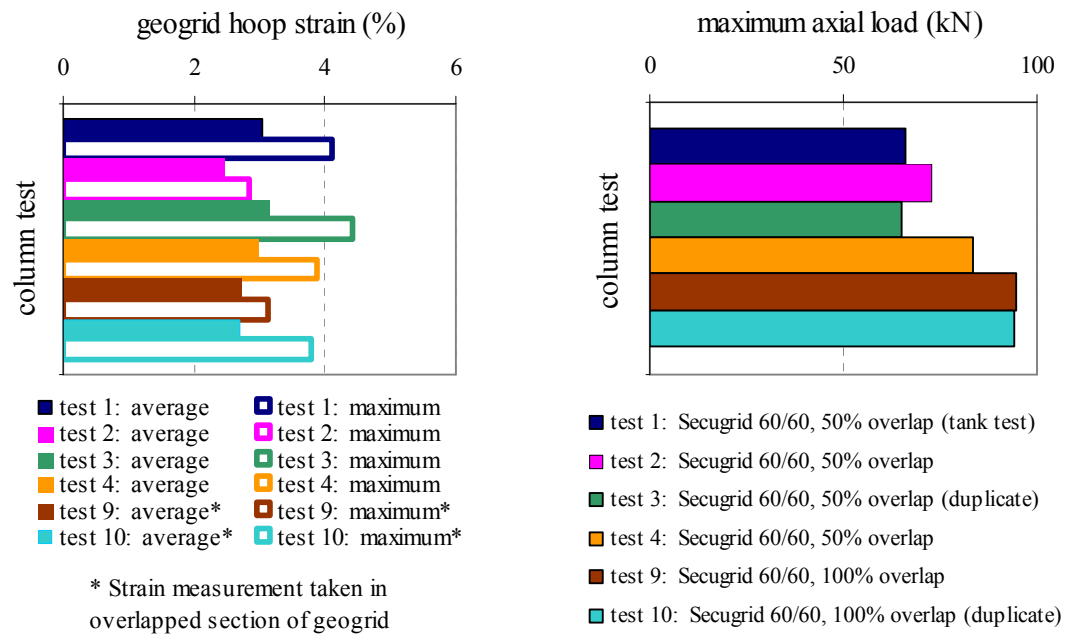


**Figure 5.17:** Strain and load measurements for columns encased with Secugrid 60/60

The results indicate that a greater load is supported by columns encased with 100% overlap compared to columns encased with 50% overlap. Columns with 100% overlap also failed in the desired manner (by horizontal ribs failing in tension), whereas for the 50% overlapped encasement, only test No. 1 (which was partially confined) and test No. 4 failed in this manner. Test No.2 and 3 failed by welds tearing in the section of overlap, generally indicating that there was insufficient overlap in these cases. The mode of failure is presented in Table 5.4.

These observations indicate that while 50% overlap may provide sufficient fixity in some cases, it can be achieved with greater certainty using 100% overlap.

It is also interesting to note that in test No. 4, the horizontal ribs were located on the outside of the encasement sleeve, whereas in test No.s 1 – 3, the horizontal ribs were located on the inside of the sleeve. The load supported by the column in test No. 4 was significantly higher than the previous three tests, perhaps indicating that the location of the horizontal ribs had some effect on column capacity. Although this aspect was not further investigated, columns tested subsequent to test No. 4 were generally constructed with the horizontal ribs located on the outside of the encasement sleeve.

Finally, the average hoop strains measured in the encasement at failure were generally about 3%, with little difference measured for columns constructed with 50% overlap and 100% overlap. For columns where horizontal ribs failed in tension, this strain was about half the capacity of the geogrid (about 6.2%), measured by uniaxial tension testing of the geogrid by the manufacturer. Examination of photographs, video footage and the mesh after failure indicate that the failed ribs had generally been at least partially cut by angular crushed rock pressing against the ribs during loading. Cutting may account for the reduced tension capacity of the geogrid and is examined in greater detail later in this chapter. A photograph of failed geogrid ribs from test No. 1 is presented in Figure 5.18 and highlights sections of partial cutting.

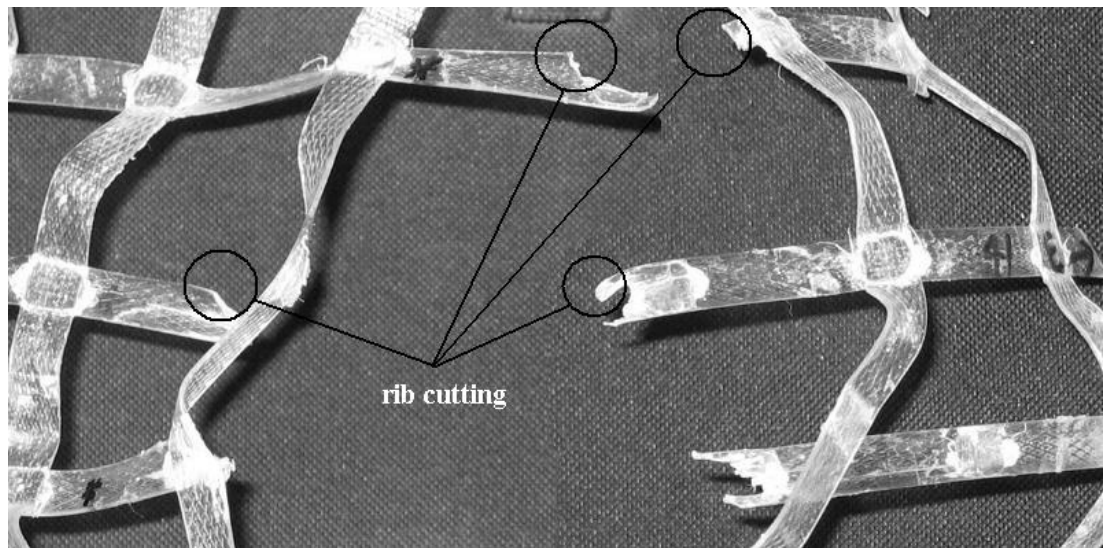


**Figure 5.18:** Partial cutting of horizontal ribs

### 5.4.3.2 Secugrid 80/80 tests

Two unconfined compression tests were undertaken on columns encased with Secugrid 80/80, using 100% overlap. Secugrid 80/80 Q6 is considered the preferred product (by the manufacturer) for encasement construction, as it is more readily manufactured and therefore more readily available. The load-compression behaviour of these columns is compared to columns encased with Secugrid 60/60 in Figure 5.19. Hoop strains and maximum loads are presented in Figure 5.20.

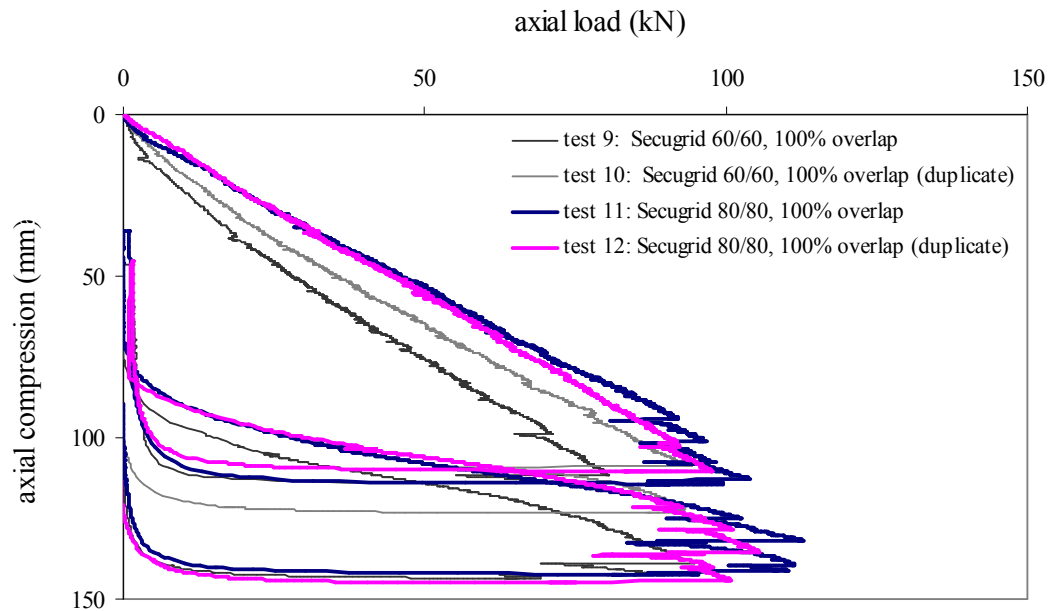


**Figure 5.19:** Load-compression behaviour of Secugrid 80/80 columns

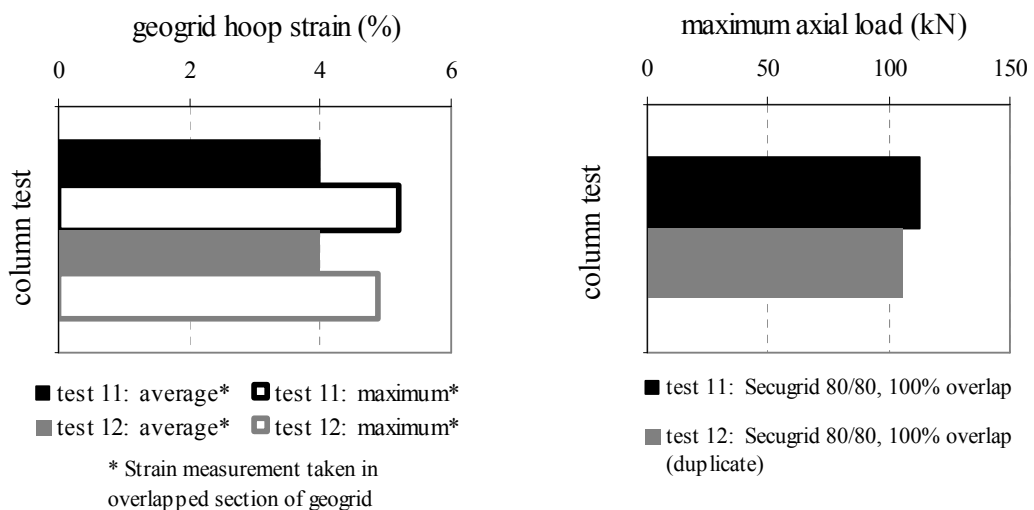


**Figure 5.20:** Strain and load measurements for columns encased with Secugrid 80/80

As indicated in Figure 5.19, the stiffness of columns encased with Secugrid 80/80 was greater than columns encased with Secugrid 60/60 (the height and radius of columns were similar, making this comparison possible using load-compression graphs). Columns also supported a significantly higher load before failure. Failure typically comprised tensile rupturing of the horizontal ribs near the beginning of the overlapped section (desired mode of failure). Column buckling was also observed during the loading of test No. 12. The average geogrid hoop strain at failure was about 4%, with maximum hoop strains of 5.2% measured. These average hoop strains were higher than the average of 3% measured for Secugrid 60/60 tests, indicating that Secugrid 80/80 probably had a greater resistance to cutting than Secugrid 60/60. As the ribs of Secugrid 80/80 have a greater cross-sectional area than Secugrid 60/60 (the ribs are generally wider, as indicated by the smaller apertures presented in Table 5.2), it follows that it would be more robust and more resistant to cutting.

#### Large diameter test

After observing various column failures during testing, it was evident that the geogrid junction strength played an important role in providing interlock. For encasement with insufficient overlap, junctions sheared and therefore their shear strength was crucial. It therefore followed that adopting a minimum number of junctions within the overlapped section may be more important than adopting a percentage of circumferential overlap. A test was undertaken on a column measuring 360 mm diameter to investigate the role of overlap in providing interlock.

The encasement for the larger diameter column was constructed with the same number of vertical ribs (and therefore welded junctions) used for the smaller diameter encasement constructed with 100% overlap. This comprised 21 vertical ribs in the section of overlap and corresponded to about 78% overlap. The behaviour of the larger diameter column during loading was then compared to the behaviour of smaller diameter columns with 100% overlap. The load-compression behaviour of the large and small diameter columns encased with Secugrid 80/80 are compared in Figure 5.21.

Although the modulus of both column types was similar (determined from analysis of the stress-strain behaviour), the larger diameter column had a significantly higher capacity (145 kN) when compared to the smaller diameter columns. This is most likely due to the greater area of aggregate in the column cross-section. The column failed by the horizontal

ribs in the non-overlapped section rupturing in tension, the desired failure mode and the same mode as the 100% overlapped columns. The average and maximum geogrid hoop strains were 4% and 5.2%, respectively, also similar to the 100% overlapped columns. This indicated that 21 vertical ribs of overlap (78% circumferential overlap) provided adequate fixity and a similar performance to the smaller diameter encasement constructed with 100% circumferential overlap.

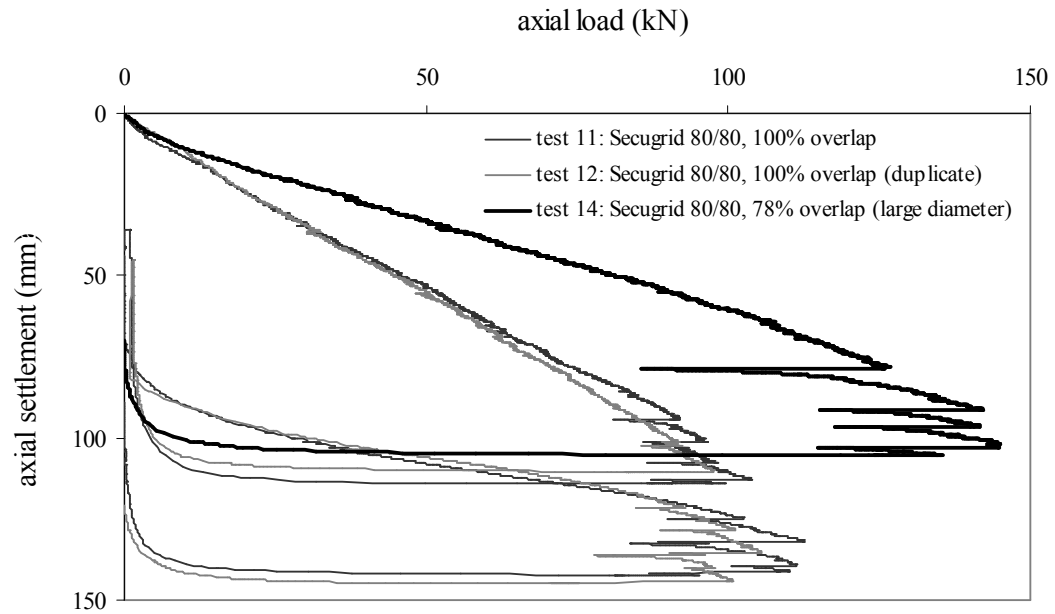


**Figure 5.21:** Load-compression behaviour of large diameter column (Secugrid 80/80)

It would therefore appear that encasement fixity may be dependent on a minimum number of vertical ribs (welded junctions) in the overlapped section. The strength of these welded junctions is also likely to be important for determining the minimum number required in the section of overlap. Further investigation of this aspect was considered outside the scope of the present study but should be included in any future research on geogrid encased stone columns.

#### 5.4.3.3 Secugrid 120/120 tests

Two tests were undertaken on columns encased with Secugrid 120/120 (100% overlap), a higher strength biaxial product developed recently. The load-compression behaviour of these tests is compared to the behaviour of the Secugrid 80/80 encased columns in Figure 5.22. Hoop strains and maximum loads are presented in Figure 5.23.



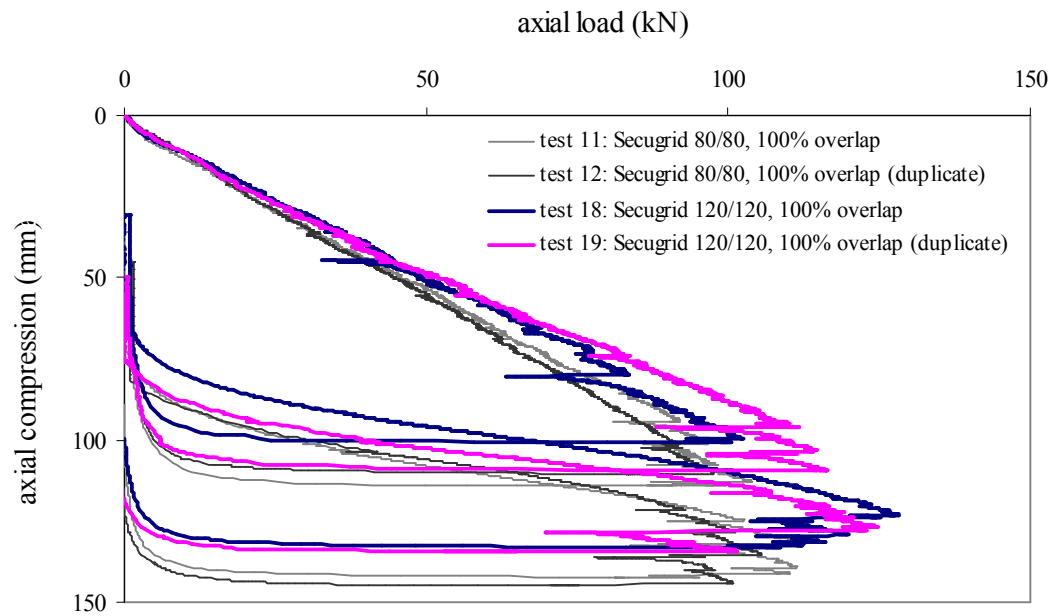


**Figure 5.22:** Load-compression behaviour of columns encased with Secugrid 120/120

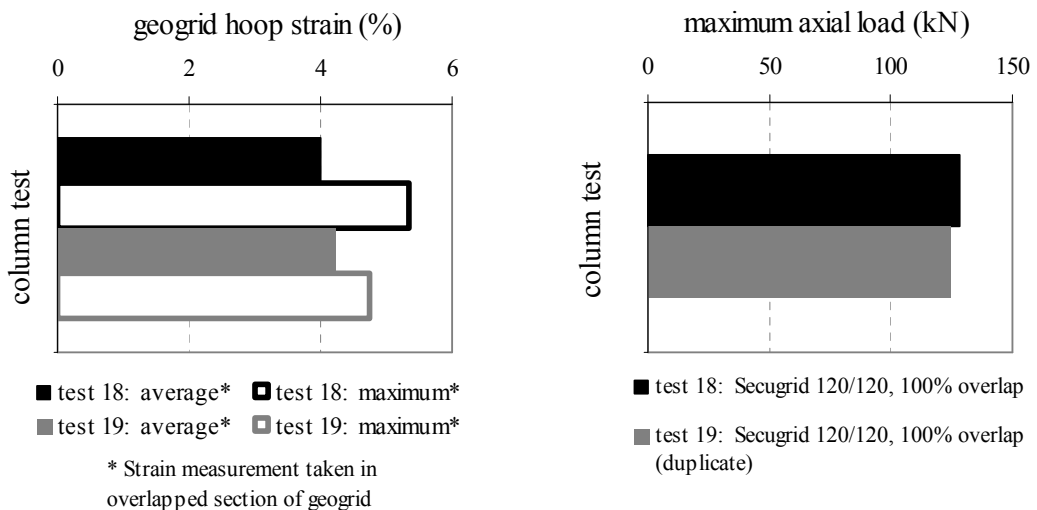


**Figure 5.23:** Strain and load measurements for columns encased with Secugrid 120/120

The stiffness and capacity of columns encased with Secugrid 120/120 were greater than both the Secugrid 80/80 and Secugrid 60/60 encased columns. Encasement failure comprised tensile rupturing of the horizontal ribs near the beginning of the overlap, the desired failure mode. This generally indicates that the column had sufficient overlap and interlock. The average hoop strain at failure was about 4%, with maximum strains of about of 5.4% measured. This was similar to the Secugrid 80/80 encasement, and less than the 6.2% at failure measured in uniaxial tension tests. Examination of failed

horizontal ribs at the completion of testing indicated partial cutting had occurred, as was the case for most other columns encased with biaxial geogrid. There appeared to be little increase in the tensile capacity of the geogrid encasement beyond that measured for the Secugrid 80/80 encasement, even though the rib cross-sectional area was greater. This may indicate that a limit to the cutting resistance had been reached, although a higher strength biaxial geogrid was not available to further test this hypothesis.

#### 5.4.3.4 Encased column stiffness

As set out at the beginning of this chapter, several geogrid encased column tests have previously been undertaken at the Gropius Institute of the Hochschule Anhalt Technical College, Dessau. Columns were constructed from welded Secugrid R6 encasement with a tensile strength of approximately 200 kN/m in the hoop direction. Results of testing, reported by Trunk et al. (2004), indicate that the Young's modulus of the columns ranged between about 15 MPa and 18 MPa. Maximum column stresses of about 1400 kPa and hoop strains of about 2% were measured prior to column failure, which generally comprised column buckling rather than tensile failure of the encasement.

To confirm that the results of medium-scale column tests presented in the present research were within the range reported in previous studies, they were compared to the Dessau test results. Maximum column stresses for the medium-scale columns were calculated by dividing the column load by the cross-sectional area. The average Young's modulus was calculated by dividing the column stress by axial strain for the linear section of loading (prior to about 80 mm axial compression). The results of this assessment are summarised below:

- Secugrid 60/60: Young's modulus = 13 to 15 MPa  
maximum stress  $\approx$  2100 kPa
- Secugrid 80/80: Young's modulus = 18 MPa  
maximum stress  $\approx$  2500 kPa
- Secugrid 120/120: Young's modulus = 20 MPa  
maximum stress  $\approx$  2900 kPa

The results indicate that the Young's modulus of the encased columns increases with increasing geogrid stiffness and strength. The stiffness of the Secugrid 120/120 encased columns was greater than that reported for several columns tested in Dessau, even though the geogrid used in the present study was generally of lower stiffness (at least in the hoop direction). However, the aggregates used to construct the columns in both studies were different and the results of medium-scale testing were generally within the range reported for the Dessau tests.

The circumferential strain behaviour of the encasement in the two studies was also similar, even though the medium-scale columns tested in the present research were not welded. For a column stress of 1400 kPa, a hoop strain of about 2% was measured in Dessau. For the medium-scale tests, strains of about 4% were measured for a column stress of between 2500 kPa and 2900 kPa. Hoop strain generally increased roughly linearly with column stress, with hoop strains of about 2% measured for column stresses of about 1500 kPa. The results indicate that there was consistency in the behaviour of geogrid encased columns tested in the two studies.

#### 5.4.3.5 Summary

Tests using 20/50 mm rubble encased with Secugrid Q6 geogrids indicate that a level of fixity similar to welding can be achieved using 100% circumferential overlap. However, a minimum number of welded junctions in the section of overlap may also produce a similar result. The load-compression behaviour of 20/50 mm rubble columns encased with different types of Secugrid Q6 geogrid is presented in Figure 5.24. Hoop strains and maximum loads are compared in Figure 5.25.

Where 100% overlap was adopted, columns failed by tensile rupturing of the horizontal ribs, considered to be the desired mode of failure. Although the strain of the ribs measured in laboratory uniaxial tension tests was about 6.2% at failure, this strain was not reached in any of the column tests. The reduction in capacity is attributed to partial cutting of ribs from the angular crushed rock pressing against them during loading. Hoop strains increased from an average of about 3% using Secugrid 60/60 to about 4% using Secugrid 80/80 and 120/120 geogrids. This increase is most likely a result of the greater cross-sectional area of geogrid ribs providing increased resistance to cutting.

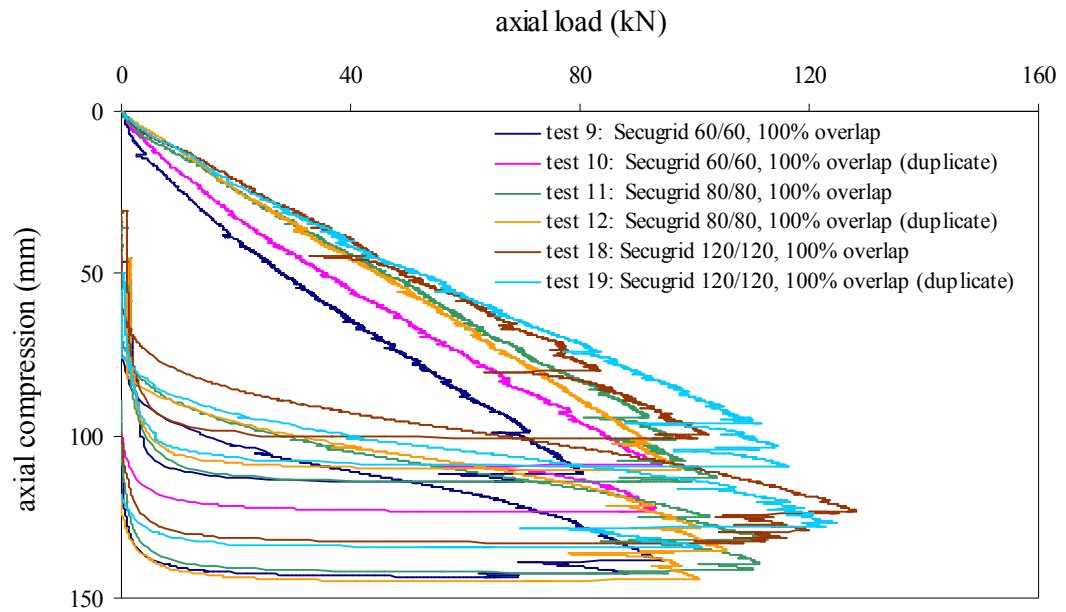


**Figure 5.24:** Load-compression behaviour of columns encased with Secugrid Q6 geogrids

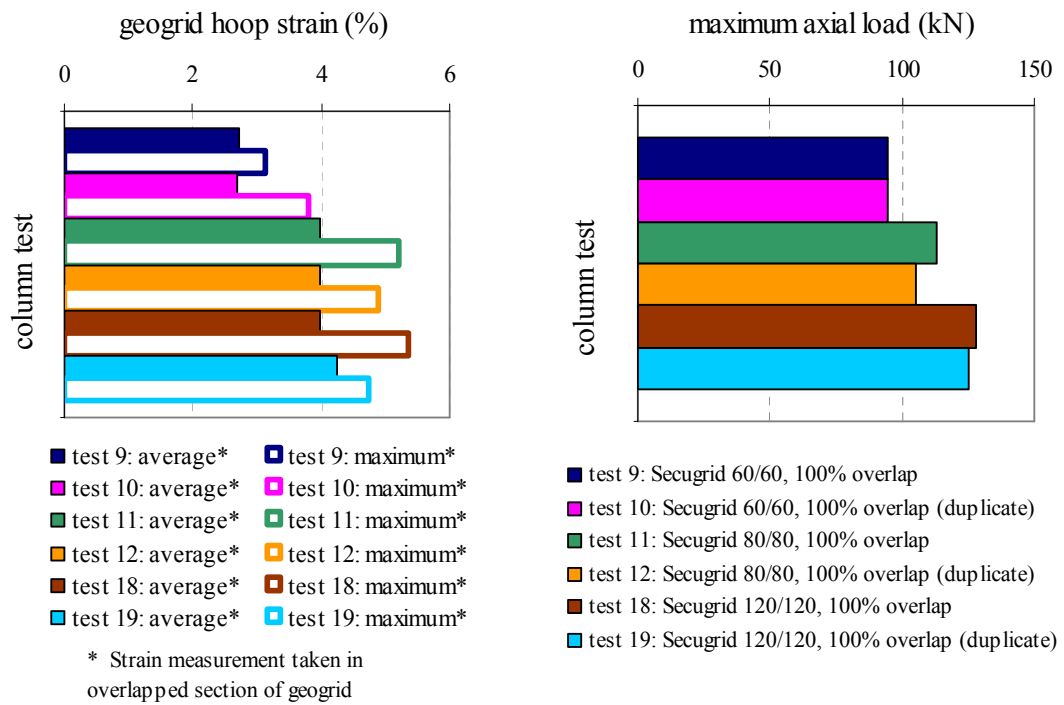


**Figure 5.25:** Strain and maximum load for columns encased with Secugrid Q6 geogrids

The stiffness and capacity of columns encased with biaxial Secugrid generally increased with increasing encasement stiffness. Young's modulus values calculated from medium-scale tests are similar to those reported by Trunk et al. (2004), where large-scale tests were undertaken on unconfined columns encased with welded Secugrid.

#### 5.4.4 14/10 mm gravel and Combigrid tests

Three column tests were undertaken using 14/10 mm gravel rather than the 20/50 mm rubble, as set out in Table 5.4. The first test (test No. 5) comprised encasement constructed from Secugrid 60/60 Q6 with approximately 50% overlap. To retain the smaller aggregate within the encasement, a thin needle-punched geotextile sleeve (151 GRK 3, provided by NAUE) was placed in the geogrid encasement. During loading of this column, the geotextile prevented the gravel from protruding between the geogrid ribs. Little interlock therefore occurred and the section of overlap was observed to progressively slip and slowly unravel as the column was loaded. Based on the deformation of the outer vertical ribs in the overlapped section, hoop forces appeared to be mostly supported by the cable ties. When the cable ties failed simultaneously, the section of overlap completely unravelled, causing column failure. A maximum load of 26 kN was measured prior to failure, with hoop strains of less than 1% also measured. These values were much lower than for column tests where adequate interlock occurred. The geotextile insert was therefore considered unsuitable for the method of overlap. Load-compression and hoop strain plots are presented in Appendix C.1.

Similar behaviour was observed for test No. 7, where Combigrid 60/60 Q6 (with approximately 50% overlap) was used to encase 20/50 mm rubble. Combigrid is manufactured by welding a layer of geotextile between the machine direction and cross-machine direction geogrid ribs. The Combigrid encasement had similar properties to the composite encasement constructed for test No. 5. Even though a coarser aggregate was used than that adopted for test No. 5, the geotextile prevented the rock from adequately protruding between the geogrid ribs, resulting in a similar mode of failure. A similar column capacity (28 kN) and average hoop strain behaviour (less than 1%) was measured. Load-compression and hoop strain plots are presented in Appendix C.1.

It is interesting to note that some vertical ribs were observed to peel away from the horizontal ribs as the Combigrid encasement was compressed. This was not observed in any other test and suggests that the Combigrid welded junctions were of lower strength than the other geogrids tested. However, specifications provided by the manufacturer indicate that Combigrid junction strength is of similar strength to Secugrid, and therefore the material tested was probably not representative of a typical sample (perhaps a bad batch or damage obtained during shipping). Nevertheless, the Combigrid encasement

failed by unravelling and was considered unsuitable for the method of overlap. Photographs of the two columns (after failure) where geotextile encasement was used are presented in Figure 5.26.

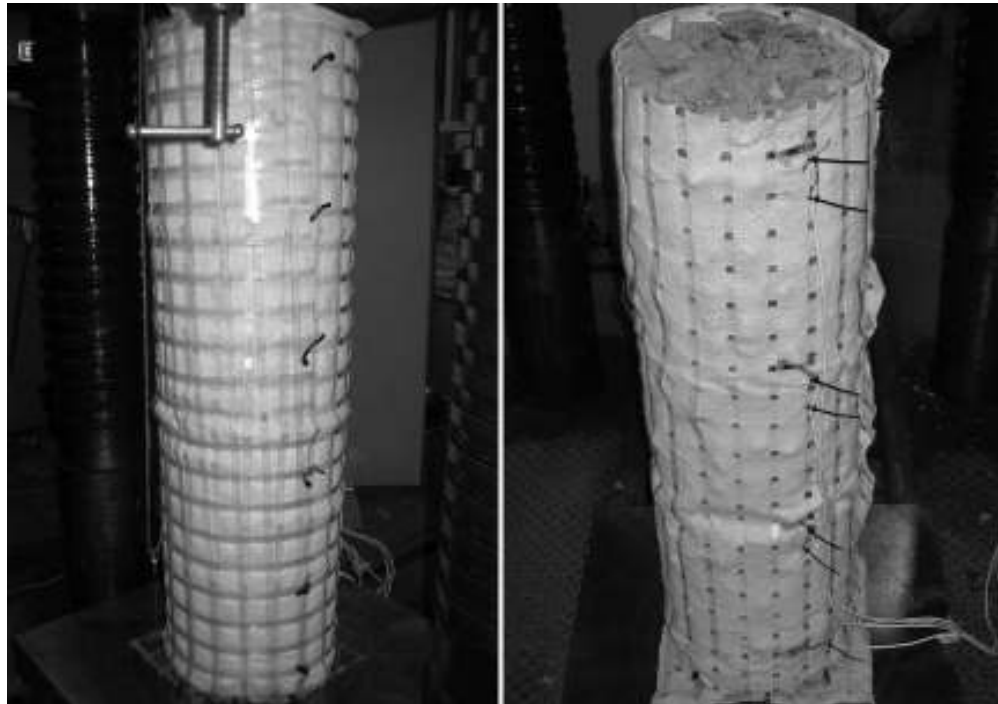


**Figure 5.26:** Failed geotextile encased columns, test No. 5 (left) and test No. 7 (right)

Based on the results of unsuccessful column tests, where geotextile was used to retain and confine the aggregate, another method of retaining 14/10 mm was investigated. A single layer of plastic film, as described in earlier sections, was wrapped around the outside of the geogrid encasement sleeve (which was constructed from Secugrid 60/60 Q6 with 100% overlap). Due to its low strength, the film was not considered to significantly confine the column (at least not to the extent a column would be confined in soil) or significantly impact column capacity. However, it did retain the gravel within the encasement during construction and loading, allowing it to protrude between the ribs to a greater extent than the geotextile encasement. As the plastic film was ductile, it also deformed as the column expanded radially, retaining the gravel throughout loading.

Tests were undertaken on two identical columns, test No. 15 and test No. 16. The load-compression behaviour of these tests is compared to the behaviour of columns constructed from 20/50 mm rubble and encased with Secugrid 60/60 in Figure 5.27. Hoop strains and maximum loads are presented in Figure 5.28, where they are also compared to 20/50 mm rubble tests.

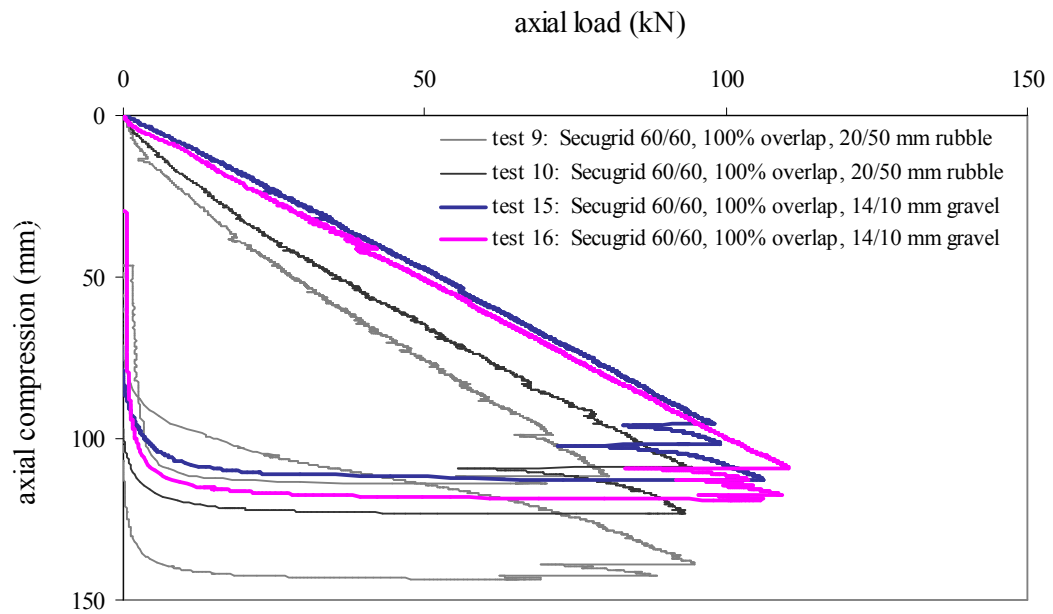


**Figure 5.27:** Load-compression behaviour of columns constructed from 14/10 mm gravel

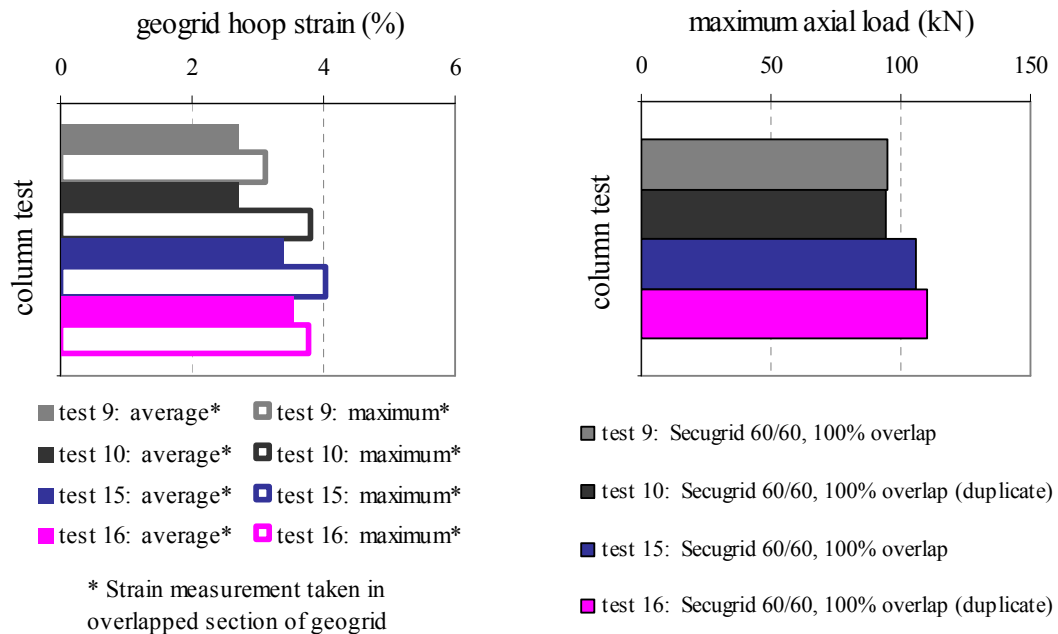


**Figure 5.28:** Strain and maximum load for columns constructed from 14/10 mm gravel

Both columns failed by unravelling of the overlapped section, indicating that sufficient interlock did not occur. Tearing of welded junctions or cutting of the geogrid ribs was not observed in either case. However, columns constructed from 14/10 mm gravel performed better than columns constructed from 20/50 mm rubble (using the same encasement). As indicated in Figure 5.27, columns constructed from 14/10 mm gravel have a greater initial

stiffness than columns constructed from 20/50 mm rubble, possibly due to a greater stiffness of smaller gravel material (although this was not measured). The shape of the load-compression curves are also smoother, probably resulting from less rock breakage using the smaller aggregate.

Columns constructed from 14/10 mm gravel had a greater capacity than columns constructed from 20/50 mm rubble, with greater average and maximum hoop strains in the geogrid also measured. This indicates that although the interlock may not have been as great as for other columns that were tested, the smaller gravel did not damage the ribs like the coarser aggregate. Therefore, at least for Secugrid 60/60 Q6 encasement, the capacity of the geogrid was unlikely to be significantly reduced by cutting.

#### 5.4.4.1 Summary

The results of tests using 14/10 mm gravel and geotextile encasement indicate the following:

- (i) Combigrid or the use of geotextile is not suited to the method of overlap.
- (ii) Finer aggregates generally do not achieve the same level of interlock as coarser aggregates, at least in unconfined conditions. However, finer aggregates appear to cause less damage to the geogrid during loading. The tensile strength of the geogrid is therefore unlikely to be significantly reduced below that measured in the laboratory.

Confinement and friction provided by soils may support additional interlock between aggregates and the overlapped section of encasement. Site testing may therefore show that finer aggregates are better suited to the method of overlap because they can achieve an adequate level of fixity without damaging the geogrid. This potentially important aspect will need to be investigated as part of a site trial, considered outside the scope of the present research.

#### 5.4.5 Secugrid R6 geogrids (uniaxial geogrids)

Three tests were undertaken to investigate the behaviour of 20/50 mm rubble encased with Secugrid R6 geogrids. Secugrid R6 products comprise uniaxial geogrids, where the



strength in the hoop direction is much higher than the strength in the axial (vertical) direction for encasement applications. Secugrid 120/40 and Secugrid 200/40 were both tested. These geogrids have a strength of 120 kN/m and 200 kN/m in the hoop direction, respectively. Furthermore, the aperture spacing of the R6 encasement was about twice that of the Q6 encasement in the hoop direction, a property that may affect interlocking.

The first of the Secugrid R6 column tests was test No. 6, where encasement comprised Secugrid 120/40 constructed from about 60% circumferential overlap. A maximum load of 56 kN was measured prior to column failure, which comprised tearing of the welded junctions in the section of overlap. This indicated that the amount of overlap was insufficient. The average hoop strain of about 1.5% was significantly less than was measured in columns where the amount of overlap was sufficient. Significant deformation of the vertical ribs (comprising twisting and buckling) also occurred during loading.

A second test, test No. 8, was undertaken using the same materials but with 100% overlap. Although a significantly higher capacity of 99 kN was measured, failure comprised tearing of the welded junctions, indicating insufficient overlap. The average hoop strain of 1.3% supported the contention that overlap was not sufficient. As it was not considered practical to increase the amount of overlap above 100%, or test columns with significantly greater diameters (where more welded junctions would be present in the overlap), further testing of Secugrid 120/40 encasement was not undertaken.

A final test, test No. 13, was undertaken using encasement constructed from Secugrid 200/40 (100% overlap). As was observed on the earlier tests, column failure indicated that there was insufficient overlap. Failure loads and strains were slightly less than for test No. 8, even though the geogrid was stiffer in the hoop direction. The reason for this was not further investigated, although the Secugrid 200/40 was more difficult to roll into a cylinder during construction, probably due to the increased stiffness compared to the other geogrids tested. It was therefore considered more likely to unravel in unconfined loading (following breakage of cable ties) when the amount of overlap was insufficient.

The load-compression behaviour of columns constructed using Secugrid R6 encasement is compared to similar tests using Secugrid 60/60 Q6 encasement in Figure 5.29. The average and maximum hoop strains and maximum column loads for the same tests are presented in Figure 5.30.

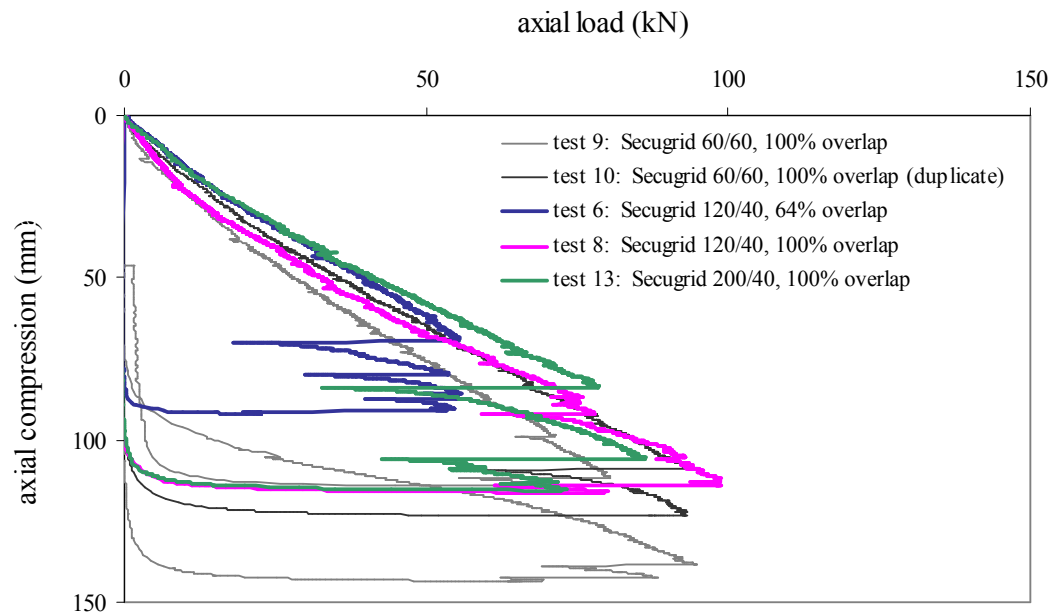


**Figure 5.29:** Load-compression behaviour of columns constructed from Secugrid R6 encasement

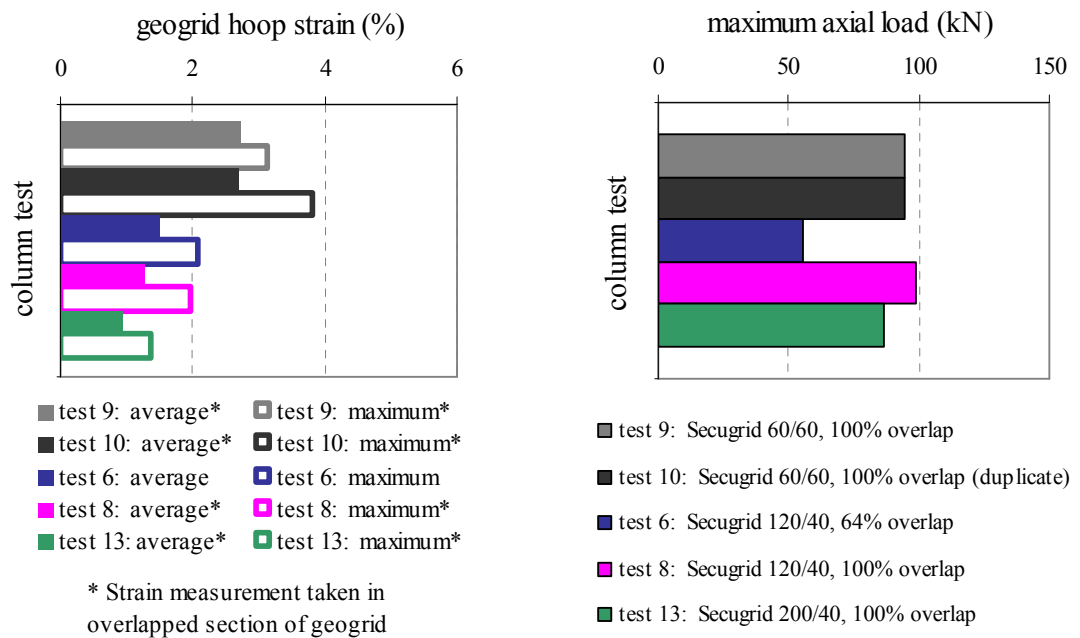


**Figure 5.30:** Strain and maximum load for columns constructed from Secugrid R6 encasement

#### 5.4.4.1 Column stiffness

Of the three tests undertaken, the stiffest response was from the column encased with Secugrid 200/40. However, the stiffness of R6 encased columns was not significantly greater than columns encased with Secugrid 60/60 Q6, even though the strength and

stiffness of the geogrid in the hoop direction was about three times greater. The vertical ribs in the R6 encasement were observed to deform more than in Q6 encasement tests, probably because they were of lower stiffness and strength (tensile strength = 40 kN/m) and at a greater spacing than biaxial geogrids. As a result of vertical rib deformation, the section of overlap was able to slip and unravel to a greater extent than biaxial geogrids, resulting in greater axial strain. The lower stiffness and increased spacing of vertical ribs in uniaxial encasement may account for the reduced axial stiffness observed in tests.

Column behaviour using R6 encasement was not compared to the previous research presented by Trunk et al. (2004) because the overlap slippage resulted in the columns behaving differently to the welded columns tested in the Dessau study.

When considering a welded encasement sleeve constructed from Secugrid, tensile strength is required only in the hoop direction, to limit the radial expansion of the column. The vertical ribs in welded encasement are compressed during loading and therefore the tensile strength is generally not important. However, when using the method of overlap, the sleeve is fixed in position by interlocking of the aggregate and overlapped section of the encasement. The strength of the vertical ribs in tension and bending, as well as the strength of welded junctions are therefore likely to significantly affect the performance of the encasement.

It follows that a biaxial geogrid, where vertical ribs are generally stronger and more closely spaced, will be more effective in locking aggregate in position. This configuration limits the ability of aggregate to move both vertically and circumferentially (at least at the perimeter of the column) and therefore may increase column stiffness. The impact of this interlocking is probably greater for coarser aggregates used in conjunction with smaller column diameters, as was generally the case in the present study. For smaller columns, the ratio of aggregate in contact with the geogrid encasement is likely to be significantly higher than for larger diameter columns.

The behaviour of columns encased with uniaxial geogrid was not investigated further in the present study. However, the role of vertical rib strength in encasement applications may be important and may limit the use of uniaxial geogrids such as the Secugrid R6 range. Further research is recommended to investigate this aspect of encased column behaviour.

#### 5.4.4.2 Location of strain gauges

It is interesting to note that although the capacity of the 100% overlap test was almost twice that of the 60% overlap test, the measured hoop strains were lower. This difference was considered to be a result, in part, of the different locations in which hoop strain was measured. For the column constructed with 60% overlap, strain was measured in the non-overlapped section of the encasement and was considered to represent maximum hoop strain. For encasement constructed using 100% overlap, hoop strains were measured in the section of overlap, albeit in a section closest to the beginning of overlap (near the inner perimeter of geogrid). The locations of the strain gauges in tests No. 6 and No. 8, where different amounts of overlap were adopted, are presented in Figure 5.31.

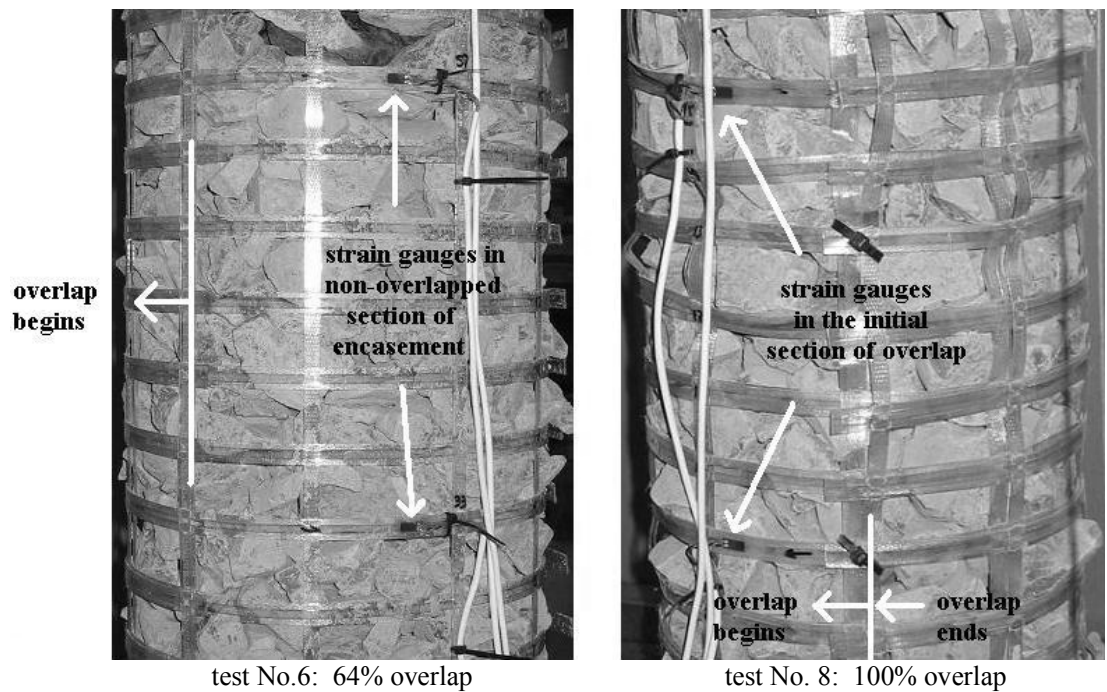


**Figure 5.31:** Location of strain gauges in tests with different amounts of overlap

As hoop strains are likely to decrease the further the section of overlap is from the inner perimeter of geogrid, any measurement of strain taken in this section is likely to be lower than average. This may account for the difference in strain measured in tests with 60% and 100% encasement. This is also supported by testing undertaken on columns constructed from Secugrid 60/60 set out earlier, namely tests No. 4, No. 9 and No. 10. In these tests, the capacity of columns constructed with 100% overlap was higher than for the column constructed with 50% overlap, even though the average circumferential strains

were lower. Although the increased stiffness of the encasement (resulting from more overlap) may have played some role, the difference in strain measurements may be partly attributed to the different locations of the strain gauges.

The possible discrepancy between hoop strains measured in the overlapped and non-overlapped sections may have important implications for design, as it may directly affect any type of strength reduction factor derived from testing. Further column testing undertaken as part of future research should attempt to measure strains in both the inner perimeter and overlapped sections of the encasement.

#### 5.4.4.3 Summary

The Secugrid R6 encasement tests indicate that 100% overlap is insufficient in medium-scale, probably due to the larger aperture size and lower strength of the vertical ribs in the uniaxial geogrid. Larger diameter column tests in confined conditions are probably required to investigate the suitability of the Secugrid R6 range to encasement applications using the method of overlap.

#### 5.4.5 Tensar TX 160 geogrid

A test was undertaken on a column constructed from 20/50 mm rubble encased with Tensar TX 160 geogrid (100% overlap). The TX 160 geogrid has a triangular aperture. The test, No. 17, was undertaken to investigate whether sufficient overlap occurred using a different aperture shape and to investigate the behaviour of encasement that did not comprise welded junctions. As set out earlier, the TX 160 geogrid has a lower stiffness than any of the other geogrids tested, and this had a significant impact on the load-compression behaviour of the column during testing. The load-compression behaviour of this test is compared to two column tests using Secugrid 60/60 encasement (100% overlap) in Figure 5.32.

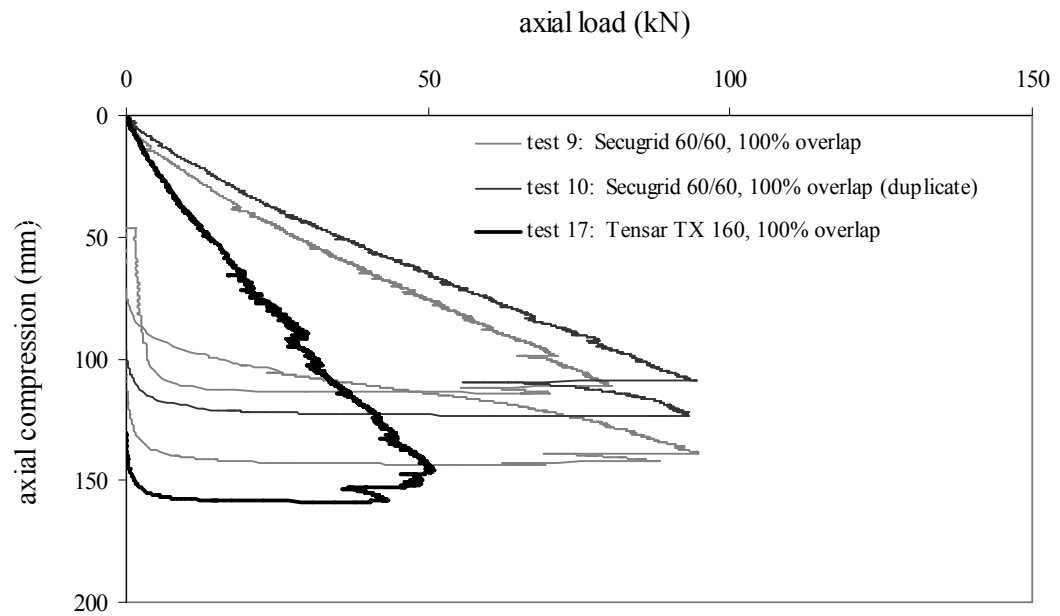


**Figure 5.32:** Load-compression behaviour of column constructed from TX 160 encasement

The results indicate that although a maximum load of 51 kN was measured, it occurred at a much higher axial strain than in other tests. Failure occurred by breakage of the geogrid ribs in the section of overlap (desired failure mode), indicating sufficient overlap and interlock. However, the ribs were significantly more slender than those in biaxial and uniaxial geogrids and therefore less resistant to being damaged by the crushed rock aggregates. Junctions generally remained intact. Hoop strains were not measured because the ribs were too thin to practically instrument.

The test indicates that triangular shaped geogrids can be used to achieve similar interlock to square-shaped geogrids, with the non-welded (integral node) junctions performing adequately. However, the ribs of the TX 160 geogrid were significantly more slender than the other geogrids tested and therefore more susceptible to cutting from angular aggregates. The column stiffness was also significantly less than columns encased with Secugrid, due to the lower stiffness of the TX 160 geogrid (as it was not developed for the type of one-directional circumferential loading that occurs in column encasement). Hence, triangular-shaped geogrids have the potential to be used as encasement material, although would generally require greater stiffness and robustness than the sample tested.

## **5.5 Summary and discussion**

Unconfined medium-scale tests were undertaken on columns constructed from a number of different aggregates and geogrid encasement. Columns were tested to failure. Tests were generally undertaken on columns measuring 0.86 m in height and about 0.24 m in diameter, although this varied in some cases. A test was initially undertaken on a column installed in a tank of kaolin slurry, with the slurry providing some lateral confinement. The test was used to investigate whether encasement could be fixed in position by interlock between the aggregate and overlapped section of the encasement. Although successful, further testing indicated that the method of overlap could be tested in unconfined conditions, and this was adopted in subsequent tests. This increased the number of tests included in the scope of testing and enabled other aspects to be incorporated into the study, including:

- investigating the impact of different aggregates on encased column behaviour, and
- investigating the impact of geogrid stiffness, strength and geometric properties on encased column behaviour.

The impact of different amounts of overlap was also investigated, although this was based more on the outcome of early tests rather than being an initial consideration. The results of medium-scale tests are summarised and discussed in the following sections.

### **5.5.1 Biaxial geogrids (Secugrid Q6 range)**

- Three failure modes have been identified; (i) insufficient overlap – where welded junctions in the section of overlap shear, (ii) insufficient interlock – where the overlapped encasement unravels without damaging the geogrid, and (iii) sufficient interlock and overlap – where horizontal ribs fail in tension.
- The third failure mode is considered the desired failure mode, as tension failure indicates that the available tensile capacity of the geogrid is being used.
- Biaxial geogrids (namely the Secugrid Q6 range) appear to be best suited to encasement applications.
- Using the method of overlap, adequate encasement fixity was achieved when using 20/50 mm rubble encased with Secugrid Q6 geogrid (100% circumferential overlap). 50% circumferential overlap was insufficient in some cases. Testing of

a larger diameter column indicates that a minimum number of welded junctions in the section of overlap may need to be considered in design and construction.

- Encasement sleeves were initially constructed with horizontal ribs located on the inside of the encasement, as this configuration was consistent with the welded encasement used in past studies (refer Section 2.4.5.2). However, in early tests, a higher capacity was measured when horizontal ribs were placed on the outside. Further research is required to investigate the impact of rib location during loading and whether this configuration may cause damage to the encasement during installation.
- Encasement sleeves were fixed in place using cable ties attached along the length of the encasement at spacings of about 170 mm centres. The method appears to provide a cheap and effective technique for constructing encasement on site. As the ties would only be required to support the encasement during installation on site (not during unconfined loading, as was the case in medium-scale tests), spacings can probably be increased to about 0.5 m. However, this would need to be assessed as part of an installation site trial.
- Partial cutting of geogrid ribs occurred during loading of columns constructed from 20/50 mm rubble. Geogrids of higher stiffness and strength were more resistant to cutting (probably because of the wider rib cross-section), supporting higher hoop strains.
- Secugrid 120/120 Q6 encasement was the stiffest of the Q6 products tested and the most resistant to cutting. Although Secugrid 80/80 Q6 is preferred by the manufacturer for encasement construction (as it is more readily manufactured), encasement constructed from Secugrid 120/120 Q6 is considered most suited to an encased column site trial based on performance.
- Based on the observed cutting, a strain or strength reduction factor would need to be applied to the capacity of the geogrid measured in the laboratory. For Secugrid 120/120 used with 20/50 mm rubble, a reduction in strain of about 35% was measured.
- Columns encased with Secugrid 80/80 Q6 and Secugrid 120/120 Q6 have a Young's modulus of approximately 18 MPa and 20 MPa, respectively. This is similar to the range of moduli presented by Trunk et al. (2004), where welded encasement was tested.
- Insufficient interlock occurred for encasement constructed from 14/10 mm gravel. However, higher column capacity and hoop strains were measured because the



finer aggregate did not damage the geogrid ribs like the coarser rubble did. If site testing of smaller aggregates indicates that encasement fixity improves with confinement, smaller aggregates may prove to be more suited to the method of overlap than coarser aggregates.

#### **5.5.2 Uniaxial geogrids (Secugrid R6 range)**

- 100% circumferential overlap was insufficient for uniaxial geogrids (Secugrid R6 range), probably due to the greater aperture spacing in the hoop direction and lower strength and stiffness of the vertical ribs.
- R6 geogrids are generally of higher strength (at least in the hoop direction) than biaxial geogrids, and if sufficient encasement fixity can be achieved in confined testing or site trials, they may provide a high strength option for use on site. However, tests also indicated that the stiffness of columns encased with high strength Secugrid R6 products did not increase significantly above the lower strength biaxial geogrids. This may be due to the observed deformation of the low strength vertical ribs combined with the greater aperture spacing. This effect may be exaggerated by the smaller diameter columns used in testing but may also indicate that uniaxial geogrids are not suited to the method of overlap.
- Further testing of R6 geogrids using the method of overlap under confined conditions with columns of greater diameter than 250 mm should be undertaken. Columns measuring at least 500 mm in diameter are recommended.

#### **5.5.3 Other tests**

- Tests on columns encased with Combigrid and other forms of geotextile indicated that insufficient interlock occurred between the encasement and aggregate. On this basis, Combigrid or geotextile inserts are considered unsuitable for encasement constructed using the method of overlap.
- Testing of a column encased with Tensar TX 160 (a triangular geogrid) indicates that triangular shaped geogrids may be suited to encasement using the method of overlap. However, this type of geogrid was generally not developed for the type of one-directional circumferential loading that occurs in encasement applications.

Hence, a stiffer and more robust geogrid than the one tested in the present study would be required for encasement construction.

#### **5.5.4 Future research**

Although the scope of medium-scale testing undertaken was quite detailed, several aspects of encased column behaviour could not be adequately investigated in the scope of the present research. These aspects were only briefly investigated and will require further testing, particularly in the event that site trials prove successful and the technique of geogrid encasement becomes more widely practiced. These aspects could be investigated as part of a future study comprising both laboratory testing and site testing, including:

- An investigation into the likely reduction in geogrid strength/strain for different combinations of geogrid and aggregate (associated with rock cutting and installation effects).
- Investigating whether smaller aggregates such as fine gravel and coarse sand are suited to the method of overlap in confined conditions (as would occur on site).
- Investigating whether uniaxial geogrids are suited to the method of overlap in confined conditions (as would occur on site). This may include an investigation into the role of vertical rib strength and stiffness for encasement applications using the method of overlap.
- Investigating whether horizontal ribs placed on the outside of the encasement increase the capacity of an encased column and whether this configuration may result in greater damage being caused to the geogrid during installation.
- An investigation into the minimum number of welded junctions required for use with the method of overlap and whether this varies significantly between biaxial and uniaxial geogrids and geogrids of different strength.

Recommendations for the scope of further testing (both laboratory and site) as part of a future study are presented in Chapter 7.

## 6 Extrapolation to full-scale columns

---

The results of medium-scale tests set out in Chapter 5 indicate that the method of overlap can be used to construct geogrid encasement with a level of fixity similar to welding. The technique may also provide a simple method for encasement construction on site. The unconfined medium-scale laboratory tests provide some indication of column stiffness using different geogrids and typical stone column aggregates. However, the performance of full-scale group columns in the confined conditions found on site requires further investigation. Based on the success of the numerical modelling of small-scale laboratory tests set out in Chapter 4, numerical modelling was used to investigate full-scale behaviour.

The numerical analysis set out in Chapter 4 was scaled-up to investigate the behaviour of full-scale geogrid encased stone columns. In particular, the study was used to investigate whether the full-scale behaviour varied significantly from the observations of the small-scale laboratory testing. A parametric study was also undertaken, where material and geometric properties were varied to assess their impact on encased column behaviour. This included the development of design curves that can be used to calculate the performance of full-scale group columns.

### 6.1 Background

The parametric study focussed on group column behaviour because this case was considered the most relevant to site applications. The unit-cell concept was adopted to simplify group column behaviour to that of a single column surrounded by a cylinder of clay within its zone of influence, as set out in Chapter 2. This enabled axisymmetric modelling to be used for calculating approximate group column behaviour.

Based on the results of the small-scale study set out in Chapter 4, the numerical model was scaled up to full-size with some confidence that:

- (i) Models calibrated to the behaviour of laboratory test samples would adequately represent the behaviour of the clay deposit (in stone column applications) from which they were sampled.

- (ii) An idealised method of column installation using a replacement technique could be modelled with reasonable accuracy.

## **6.2 Base model**

A base model was initially developed to study the behaviour of a conventional stone column. The unit-cell geometry used in small-scale modelling was scaled up to a height of 8 m, representing a clay deposit that was 8 m thick. Drained properties were used for all materials because the primary focus of the assessment was on the long-term performance of the columns. Time-rate of consolidation was not assessed. Materials and other important aspects of the base model are discussed in the following sections.

### **6.2.1 Clay**

The base model used in the study assumed the soft clay has properties consistent with Coode Island Silt (CIS), a Quaternary Age clay present in the Yarra River Delta in the Melbourne CBD area. CIS is normally consolidated to slightly over-consolidated and has a similar compressibility to the kaolin used in the small-scale laboratory testing. It is typical of the soft soil deposits in which conventional stone columns are utilised. The properties and behaviour of CIS are well documented (Anantasech 1984; Ervin 1992), making it a suitable material for use in the base model.

The Soft Soil model was used to model the behaviour of CIS in PLAXIS, in the same way kaolin was modelled to replicate small-scale test behaviour. The properties of CIS used in the numerical model are presented in Table 6.1. The properties were based on the average engineering properties presented by Ervin (1992). Initially, a standard oedometer test of the CIS was modelled, the same procedure used for modelling kaolin. The results of the clay compressibility assessed in this model were then compared to CIS standard oedometer test results presented as part of an embankment consolidation case study by Day and Woods (2007). The results of this comparison are presented in Figure 6.1, and include the compressibility of the kaolin obtained from the numerical modelling.

As indicated in Figure 6.1, the assumed compressibility of the soil falls within the range of oedometer test results for CIS, provided by Day and Woods (2007). As these oedometer

tests were considered representative of typical CIS behaviour, the numerical model was therefore considered a satisfactory numerical representation of CIS for the purposes of this study. It should be noted that in Figure 6.1, the pre-consolidation pressures for samples of CIS are generally between about 50 kPa and 100 kPa. Given that the samples were taken at depth, this compares favourably with the pre-overburden pressure of 10 kPa set out in Table 6.1.

**Table 6.1:** Properties of CIS used in numerical model

parameter	unit	value
Unit weight	kN/m <sup>3</sup>	16
Angle of internal friction, $\phi'$	°	30
Dilation, $\psi$	°	0
Cohesion, $c'$	kPa	2
Initial void ratio, $e_0$	-	2.0
Compression index, $C_c$	-	0.8
Recompression index, $C_r$	-	0.08
Pre-overburden pressure	kPa	10

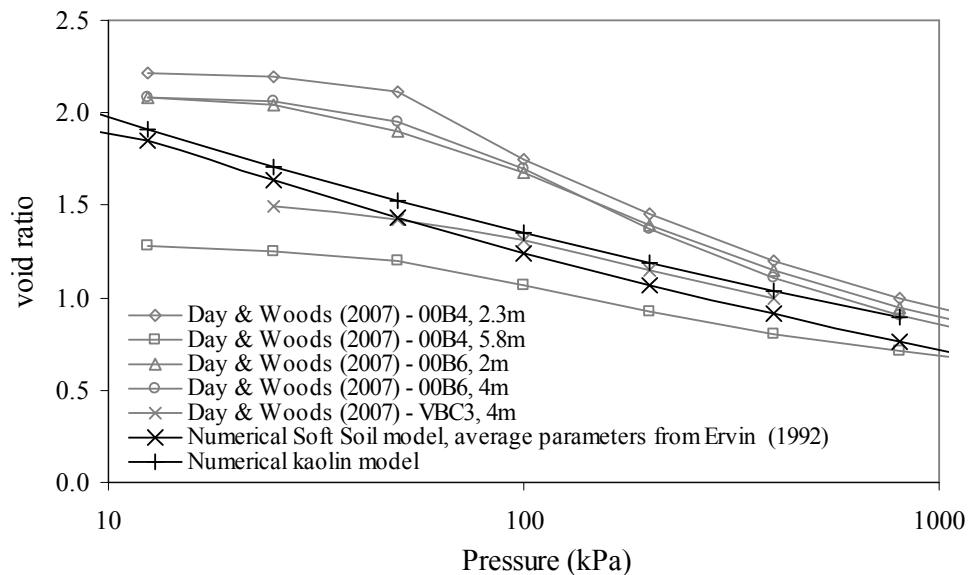


**Figure 6.1:** Compressibility of numerical CIS model compared to oedometer test results

The CIS properties in Table 6.1 were then assumed for the 8 m deep unit-cell model. An 8 m thick deposit is quite common for CIS and represents a typical depth to which stone

columns may be installed. It is also a similar thickness to the case study presented by Day and Woods (2007). The full-scale unit-cell was loaded with 8 m of fill (about 160 kPa surcharge) to compare consolidation settlements with those presented in the case study. Although there were small differences in stratigraphy and surcharge, the unit-cell model produced similar settlements to those outlined in the case study (about 1.6 m). This indicated that the full-scale unit-cell provides a reasonable approximation of the settlement behaviour of CIS and was therefore adopted to represent the clay component of the base model.

### **6.2.2 Stone column**

A literature review was undertaken to determine suitable deformation parameters for the rockfill used in conventional stone columns. The review concentrated on deformation parameters measured from large-scale one-dimensional consolidation tests undertaken on samples of rockfill, including coarse gravels and railway ballast. Rockfill was considered to best represent the material used in conventional stone columns. Large-scale oedometer tests were generally the most readily available tests presented in the literature and are able to approximately reproduce the confining conditions provided by adjacent columns in group column applications. A summary of some of these tests is provided below.

#### Adikari (1981)

One-dimensional consolidation tests were undertaken on rockfill in a cell measuring 635 mm in diameter and 610 mm in height. The samples had a particle size ranging between about 1 mm and 50 mm and were densely compacted, with a peak friction angle of about 45°. Two tests were undertaken, one using a floating ring (designated ‘dense – floating’) and one using a fixed ring (designated ‘dense – fixed’).

#### Oldecop and Alonso (2001)

A one-dimensional consolidation test was undertaken on quartzitic slate rockfill in a cell measuring 300 mm in diameter and 200 mm in height. The sample was compacted to a relative density of about 100% and saturated prior to testing. The average particle size ranged between about 5 mm and 30 mm.

### Ionescu (2004)

One-dimensional consolidation tests were undertaken on railway ballast in a cell measuring 450 mm in diameter. The ballast comprised dry, crushed basalt rock with particle size generally between 20 mm and 60 mm (coarse). Two tests were undertaken:

- (i) a sample with a relative density of 19% (designated 'loose – coarse'), and
- (ii) a compacted sample with relative density = 75% (designated 'dense – coarse')

### Kim et al. (2005)

One-dimensional consolidation tests were undertaken on saturated samples of granitic gneiss rockfill in a cell measuring 980 mm in diameter and 1000 mm in height. The rockfill was compacted to a relative density of about 90%, with a peak friction angle ranging between about 40° and 44°. The two tests of most relevance comprised:

- (i) a fine sample with particle size generally ranging between about 0.5 mm and 20 mm (designated 'very dense – fine').
- (ii) a coarse sample with particle size generally ranging between about 5 mm and 80 mm (designated 'very dense – coarse').

The results of the above tests are presented in pressure – axial strain space in Figure 6.2.

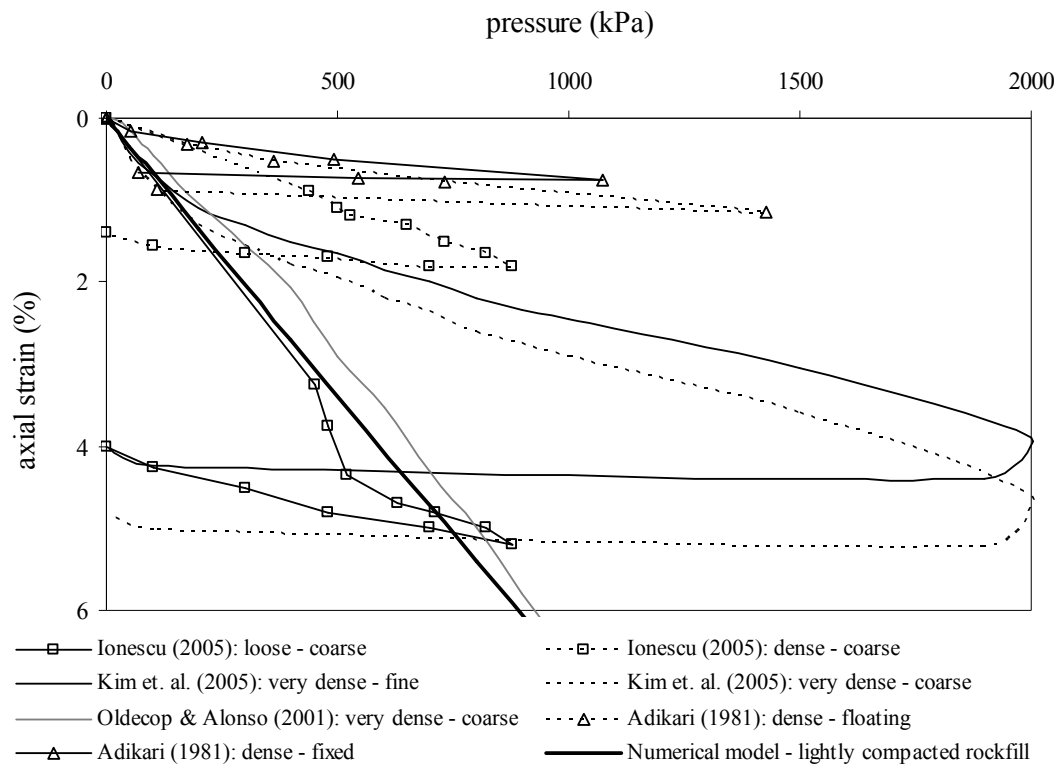


**Figure 6.2:** Summary of one-dimensional consolidation tests undertaken on rockfill

Figure 6.2 indicates that the stiffness or constrained modulus ( $E_{oed}$ ) of the rock fill generally increases with higher relative density (as would be expected). The  $E_{oed}$  ranges from 10 MPa for loose samples up to about 60 MPa for dense to very dense samples, with these values averaged across the range of confining pressures.

As for the PLAXIS modelling of the small-scale laboratory tests described in Chapter 4, the Hardening Soil model was initially adopted for the modelling of the large-scale oedometer tests. However, when applied to the full-scale unit-cell geometry in combination with the Soft Soil model (for the clay component), divergence occurred during the iteration process and a solution could not be obtained. This was attributed to using two highly non-linear models together in full-scale. Adjustments were made to the calculation controls to assist the program to seek a solution more effectively. However, this was only achieved by significantly increasing the calculation time, well beyond the timeframe available for undertaking a parametric study. Because of this, the Mohr-Coulomb model was subsequently used to represent the stone column material (the Soft Soil model was adopted for the clay component). The Mohr-Coulomb model is a more simplistic elastic, perfectly plastic soil model which provides a reasonable and practical solution to the modelling problems encountered using the more complex constitutive models.

The Mohr-Coulomb model is not capable of replicating the non-linear behaviour of some materials. However, the stress-strain relationship for many granular materials, including those used in small-scale tests and those presented in Figure 6.2, can be roughly approximated as linear, at least at lower stresses. As such, the Mohr-Coulomb model may provide a reasonable substitute. To confirm this, a small-scale sand column test was analysed using the Mohr-Coulomb model and the results compared to those obtained from the more sophisticated Hardening Soil model.

Initially, the laboratory sand oedometer tests were modelled using the Mohr-Coulomb model. The model underestimated the gradient of the stress-strain curve at lower stresses and overestimated it at higher stresses. The average stiffness across the range of applied stresses was adopted. The Mohr-Coulomb model was then used in the numerical model of the non-encased sand column test (GC-2) and results were compared to the analysis using the Hardening Soil model. The results of this comparison are presented in Figure 6.3 and indicate close agreement between the two models. The Mohr-Coulomb model calculated



slightly higher deformations at higher stresses. Based on the above relatively good correlation, it was concluded that the Mohr-Coulomb model was reasonable (and practical) for use in the parametric study of encased stone columns.

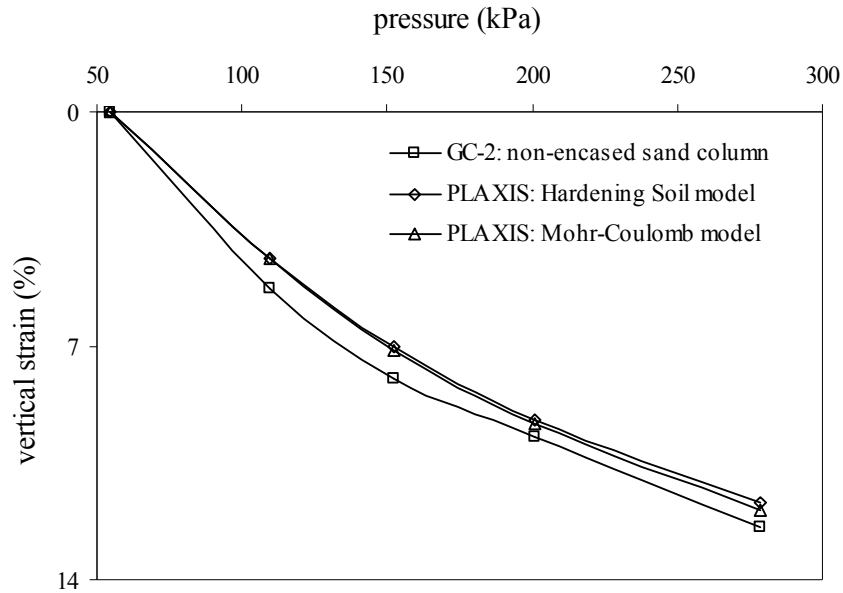


**Figure 6.3:** Comparison of Mohr-Coulomb model to Hardening Soil model in small-scale test

As geogrid encased stone columns are likely to receive less compaction than conventional stone columns, the properties of a lightly compacted granular fill were used in the base model. The stiffness of the stone column was taken from the lower end of the range of oedometer tests presented in Figure 6.2. The stress-strain relationship for the adopted Mohr-Coulomb model is included in this Figure. The parameters used for numerical modelling of the lightly compacted stone column are presented in Table 6.2.

**Table 6.2:** Properties of lightly compacted stone column material used in numerical model

parameter	unit	Value
Unit weight	kN/m <sup>3</sup>	21
Angle of internal friction, $\phi'$	°	37
Dilation, $\psi$	°	6
Cohesion, $c'$	kPa	0.1
Constrained modulus, $E_{oed}$	MPa	15
Poisson's ratio, $\nu$	-	0.3

### 6.2.3 Column installation

Column installation was modelled by replacing the clay material that occupied the column space with the properties of the stone column. This meant that the ‘at rest’ or  $K_0$  lateral earth pressure condition was initially modelled in both the clay and sand. This was the same method used to model installation in the small-scale tests and comprised an idealised replacement technique. For installation on site, both replacement and displacement techniques may be adopted, although it is more likely that a replacement technique would be used in Australia given that bottom-feed systems may not be readily available. Replacement techniques are likely to require the support of steel casing, due to the low strength and high groundwater table on sites generally suited to the technique. The method would probably comprise:

- (i) Pushing or vibrating casing down to the foundation level.
- (ii) Removing material from within the casing using an auger.
- (iii) Placing the geogrid encasement within the casing and filling it with rock fill from the surface or a greater height when additional compaction is required.
- (iv) Possibly providing further compaction using a vibroflot.
- (v) Removing the casing by vibration, providing additional compaction.

It is difficult to envisage significant lateral expansion of the column occurring during this process (due to the confinement provided by the geogrid), or significant lateral relaxation occurring in the surrounding clay. The occurrence of either of these events would need to be assessed and back-calculated following a site trial or laboratory investigation. As this type of research is yet to be undertaken on geogrid encased columns, numerical modelling using an idealised replacement technique was considered satisfactory for the purposes of the parametric study. The impact of increasing the lateral earth pressure coefficient in the clay as part of soil displacement during installation is further explored in the parametric study and described later in this chapter.

### 6.2.4 Effect of column diameter

The base model was used to investigate the impact of varying replacement ratio on the behaviour of stone column treated ground. Three different replacement ratios were modelled,  $A_r=15\%$ ,  $25\%$  and  $35\%$ . These were considered to cover the range in which

stone column ground improvement would be used. To model the change in replacement ratio, it was considered simpler to maintain a constant column diameter and vary that of the unit-cell. However, varying the column diameter (and maintaining a constant unit-cell diameter) may affect the stress state in the column and lead to differences in the cell behaviour. As such, both methods were compared, using the cell geometry presented in Table 6.3.

**Table 6.3:** Unit-cell geometry for constant column and cell diameter approaches

	<b>constant column diameter approach</b>		<b>constant cell diameter approach</b>	
<b>replacement ratio</b>	<b>column diameter (mm)</b>	<b>cell diameter (mm)</b>	<b>column diameter (m)</b>	<b>cell diameter (m)</b>
15%	0.80	2.07	0.77	2.00
25%	0.80	1.60	1.00	2.00
35%	0.80	1.35	1.18	2.00

Both cell types were loaded using an 80 kPa and 160 kPa surcharge. The resulting settlements for the three different replacement ratios were compared to the untreated clay settlement (CIS). Vertical or axial strain reduction was then calculated by comparing the reduction in axial strain of treated soil with that of the untreated soil, a concept similar to the improvement factor used by Priebe (1995). As an example, if untreated settlement is 1 m and treated settlement is 0.5 m (for an 8 m deep deposit), then the strain reduction is 50%. Likewise, if untreated settlement is 1 m and treated settlement is 0.25 m, then strain reduction is 75%. If columns of the same length are compared, percent strain reduction can be considered the same as percent settlement reduction. The results of this assessment are presented in Figure 6.4, where the strain reduction is plotted against replacement ratio for the two modelling approaches that were adopted. The results of the assessment indicate that there is less than 0.5% difference between the two approaches. Based on this, the constant column diameter approach was used for varying the replacement ratio. The 0.8 m column diameter was considered representative of the column diameter that would likely be adopted for encased columns.

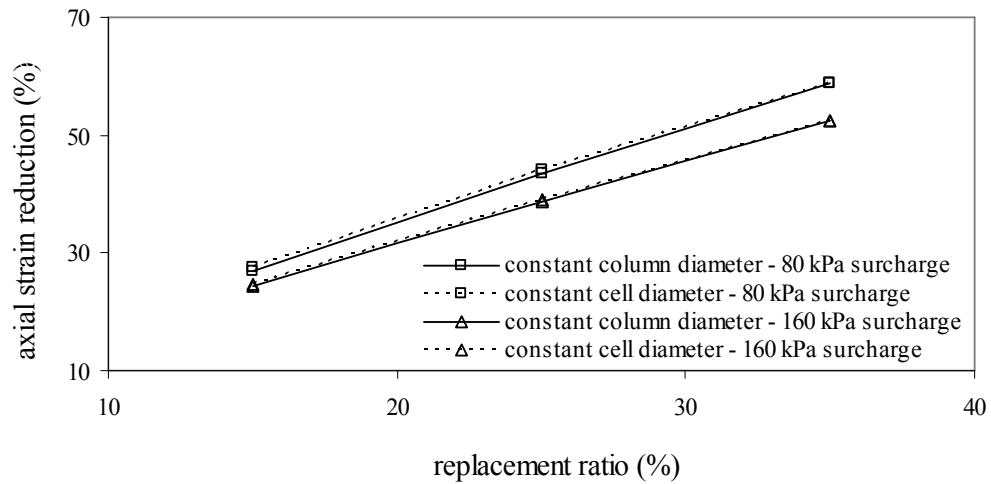


**Figure 6.4:** Comparison of cell behaviour for constant column and cell diameter approaches

### 6.2.5 Effect of mesh size

An assessment was also undertaken to investigate the impact of mesh size on the results of the study. At a replacement ratio of 25%, the base model was assessed using a very coarse mesh (175 elements), coarse mesh (321 elements), medium mesh (453 elements) and fine mesh (854 elements). 15-noded triangular shaped elements were used in the assessment. The results of this assessment are presented in Figure 6.5, where strain reduction is plotted against surcharge pressure.

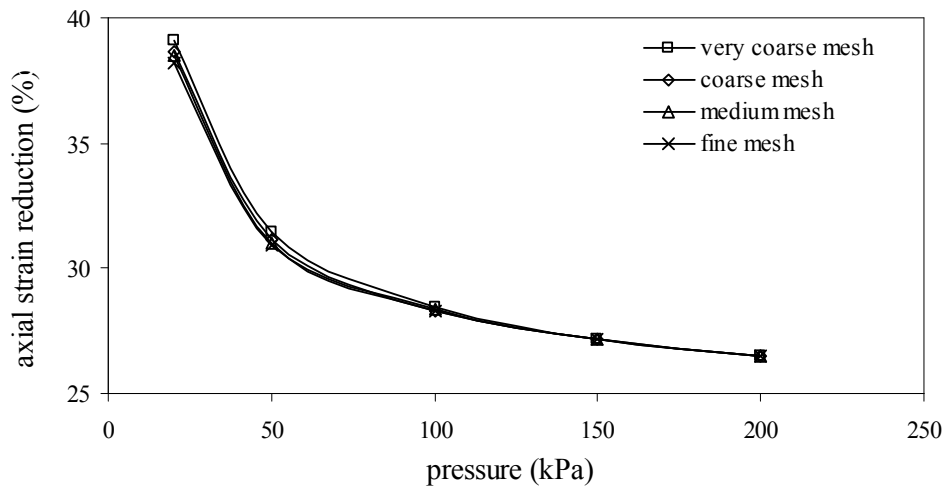


**Figure 6.5:** Impact of mesh size on strain behaviour of unit-cell

There was very little difference between the behaviour of the four models, with less than 1% difference between the very coarse model and the fine model. This indicated that the numerical base model was not mesh dependent (over the range of meshes considered). However, there was a significant increase in calculation time associated with each reduction in mesh size, to the point that the use of a fine mesh would have significantly reduced the number of models that could be assessed as part of the parametric study. Based on this, a coarse mesh was adopted for the base model.

#### **6.2.6 Loading of the unit-cell**

The base model was loaded in increments of 40 kPa, corresponding to about 2 m of soil fill. As a drained model was adopted, no excess pore pressures were present upon application of the next load stage. The model was loaded to a maximum of 160 kPa surcharge (8 m soil fill), close to the maximum load typically applied to stone column foundations. Results were assessed for the cases of 4 m high soil fill (80 kPa surcharge) and 8 m high soil fill (160 kPa surcharge).

#### **6.2.7 Base model performance**

The axial stress-strain behaviour of the base model was consistent with that of conventional stone columns in soft clay. The relationship between replacement ratio and axial strain reduction for the base model is presented in Figure 6.6. To check the sensibility of the result, the numerical relationship was compared to results of well documented studies of lightly compacted columns in soft clay, including design methods, case studies and centrifuge tests. These included:

- Design curves based on the Priebe method for a modular ratio,  $E_{column}/E_{clay} = 10$  (Priebe 1995).
- Empirical curves for stone columns installed in uniform soft clay where  $c_u=20$  kPa (Greenwood and Kirsch 1983).
- Centrifuge test results on columns with a modular ratio,  $E_{column}/E_{clay} = 7$  (Craig and Al-Khafaji 1997).

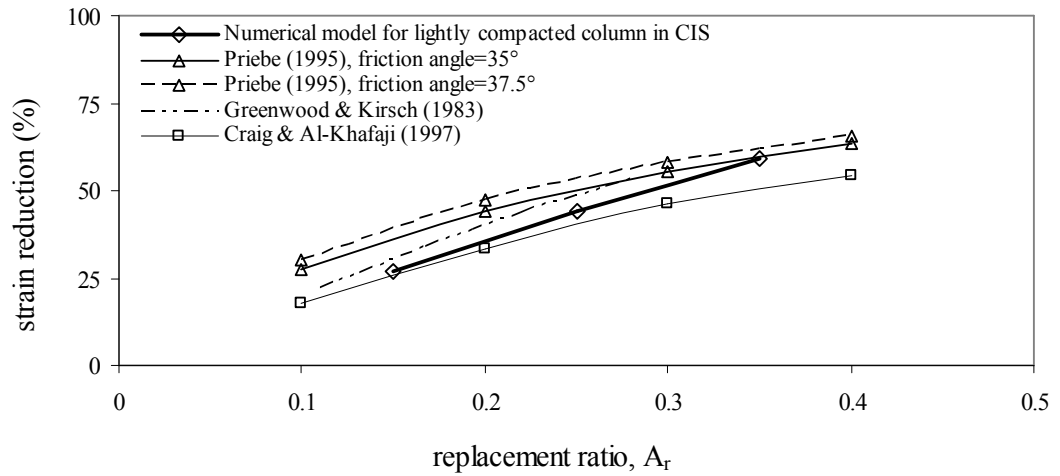


**Figure 6.6:** Behaviour of lightly compacted stone column installed in CIS

The performance of the base model is within the range generally reported for lightly compacted, vibro-replaced stone columns in soft clay. The parameters used in the base model were therefore considered reasonable, providing the basis for further investigation into the behaviour of full-scale encased stone columns using a parametric study.

### 6.3 Parametric study

The parametric study was undertaken in two stages; primary and secondary. In the primary study, parameters that were considered to be of most importance to encased stone column behaviour were varied in all models. In the secondary study, parameters that were either considered to be of less significance or more difficult to accurately model were varied in the base model only.

#### 6.3.1 Primary parametric study

Parameters used in the primary study are summarised below and described in detail in Appendix D.1.

- (i) Replacement ratio – replacement ratios of  $A_r=15\%$ ,  $25\%$  and  $35\%$  were used in the base model and therefore the parametric study.
- (ii) Column stiffness – a heavily compacted column was modelled in addition to the lightly compacted column used in the base model. The heavily compacted

column was assumed to have properties consistent with medium-dense to dense crushed rock and was considered to represent the stiffest material type that would generally be used in encased columns. Relevant properties are presented in Appendix D.1.

- (iii) Soil stiffness – very soft clay was modelled in addition to the soft clay (CIS) used in the base model. The two materials of different stiffness were considered to cover the range of soils in which encased columns would be used. Properties are presented in Appendix D.1.
- (iv) Geogrid stiffness & strength – three types of geogrid with different stiffness and strength were modelled. The properties were based on the range of Secugrid® products supplied by NAUE GmbH, considered most suited to column encasement. The ultimate tensile strength (UTS) of the geogrids adopted for the study are 60 kN/m, 100 kN/m and 200 kN/m, with elastic axial stiffness values of 1030 kN/m, 1670 kN/m and 3440 kN/m, respectively.
- (v) Percent encased length – non-encased columns and columns with the upper 25%, 50% and 100% of their length encased with geogrid were modelled.
- (vi) Surcharge pressure – columns were loaded with a 4 m high soil fill (80 kPa surcharge) and 8 m high soil fill (160 kPa surcharge).

The number of models required to assess the impact of the primary parameters is summarised in Table 6.4.

**Table 6.4:** Parameters investigated in the primary study

No.	parameter	unit	variables	models required
1	Replacement ratio, $A_r$	15%, 25%, 35%	3	3
2	Column stiffness	loosely compacted densely compacted	2	$3 \times 2 = 6$
3	Soil stiffness	soft clay very soft clay	2	$2 \times 6 = 12$
4	Geogrid stiffness and strength	Secugrid UTS=60 kN/m Secugrid UTS=100 kN/m Secugrid UTS=200 kN/m	3	$3 \times 12 = 36$
5	Percent encased length	0%, 25%, 50%, 100%	4	$4 \times 36 = 144$
6	Surcharge pressure	80 kPa, 160 kPa	2	$2 \times 144 = 288$

Although column length was also considered an important parameter, inclusion of this into the primary study would have doubled the number of models from 288 to 566. Due to time constraints, column length (as well as other parameters) was investigated in the limited secondary study.

### **6.3.2 Secondary parametric study**

A secondary study was undertaken to investigate the impact of other parameters on the base model. These parameters were generally not included in the primary study due to time constraints or because they were considered difficult to accurately model. The parameters investigated in the secondary study comprised:

- (i) Column depth – investigating the difference in behaviour between 4 m, 8 m and 12 m long columns.
- (ii) Soil stiffness – comparing the behaviour of columns installed in firm clay to the soft and very soft clay materials modelled in the primary parametric study. The properties of the firm clay model are compared to soft and very soft clay properties in Table 6.5.
- (iii) Method of column installation – a method of column installation where soil was partially displaced was compared to the replacement method adopted in the primary parametric study. Partial displacement was modelled by increasing the lateral earth pressure coefficient in the surrounding clay to  $K_0=1$ . This value has little theoretical basis but was used to assess the impact of increasing the lateral earth pressure coefficient (as would occur during lateral soil displacement) had on column behaviour.



**Table 6.5:** Properties of soil models used in the secondary parametric study

parameter	unit	Value		
		very soft clay	CIS	firm clay
Unit weight	kN/m <sup>3</sup>	14	16	17
Angle of internal friction, $\phi'$	°	25	30	30
Dilation, $\psi$	°	0	0	0
Cohesion, $c'$	kPa	1	2	1
Initial void ratio, $e_0$	-	3.5	2.0	1.2
Compression index, $C_c$	-	1.5	0.8	0.5
Recompression index, $C_r$	-	0.2	0.08	0.05
Pre-consolidation pressure	kPa	5	10	15

### 6.3.3 Results of primary parametric study

#### Axial strain reduction results

The results of the primary parametric study are presented in the form of charts, where percent strain reduction (described earlier and used in the base model) is plotted against replacement ratio, forming curves for columns with 0%, 25%, 50% and 100% encasement. A separate chart was produced for the three different strength geogrids modelled in the following cases:

- 4 m soil fill (80 kPa surcharge) on lightly compacted columns in soft clay (CIS)
- 8 m soil fill (160 kPa surcharge) on lightly compacted columns in soft clay (CIS)
- 4 m soil fill (80 kPa surcharge) on heavily compacted columns in soft clay (CIS)
- 8 m soil fill (160 kPa surcharge) on heavily compacted columns in soft clay (CIS)
- 4 m soil fill (80 kPa surcharge) on lightly compacted columns in very soft clay
- 8 m soil fill (160 kPa surcharge) on lightly compacted columns in very soft clay
- 4 m soil fill (80 kPa surcharge) on heavily compacted columns in very soft clay
- 8 m soil fill (160 kPa surcharge) on heavily compacted columns in very soft clay

The charts present the 6 parameters and 288 combinations investigated in the primary parametric study in a simple form. An example of these charts is presented in Figure 6.7, representing the strain reduction for the case of a 80 kPa surcharge applied to lightly

compacted columns in soft clay (CIS). In this example, the properties of Secugrid® with UTS=100 kN/m in the hoop direction were used.

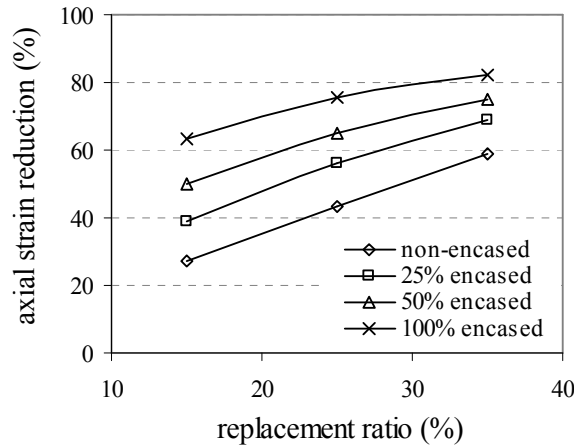


**Figure 6.7:** Example chart of strain reduction plotted against replacement ratio

For the case presented in Figure 6.7, axial strain steadily reduces in the four different encased states analysed (0%, 25%, 50% and 100% encased) by increasing the replacement ratio. For the fully-encased state, at  $A_r=35\%$ , this corresponds to a strain reduction of greater than 80%. This means that if untreated strain is 20%, the treated strain would be less than 4%. For an 8 m deep column, this corresponds to settlement being reduced from 1.6 m to about 0.3 m. This assessment indicates that for fully encased columns, a greater level of ground improvement is achieved than for the non-encased column and partially encased columns.

The trend of reduced axial strain with increasing encased length identified in the full-scale numerical assessment matches the same trend observed in small-scale laboratory testing and the numerical modelling of these tests (described earlier). This would appear to support the use of small-scale testing in assessing encased column behaviour, particularly when used in conjunction with numerical modelling. Site testing of partially encased columns is proposed to provide final confirmation of the technique, although such testing is outside the scope of this study.

### Hoop force results

For the same case set out above, the hoop forces generated in the encasement were plotted against depth for the three replacement ratios (15%, 25% and 35%). These hoop forces are presented in Figure 6.8. To give an indication of how close the geogrid was to tensile

failure, the forces are compared to the UTS of the geogrid in the same chart. The results are presented for the fully encased state only, and indicate that geogrid hoop forces are highest for columns with the lowest replacement ratio. This is to be expected, as columns at lower replacement ratios are required to support higher stresses due to the smaller diameter or greater column spacing.

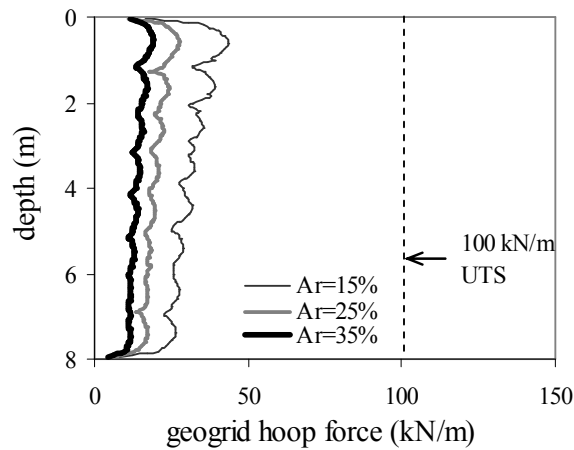


**Figure 6.8:** Example chart of hoop forces generated in geogrid encasement

The hoop forces for partially encased columns are compared to the fully encased column in Figure 6.9 and indicate that for partial encasement, peak hoop forces are either equal to or only slightly less than for the fully encased state. This same observation was made for all of the other cases analysed in the primary parametric study.

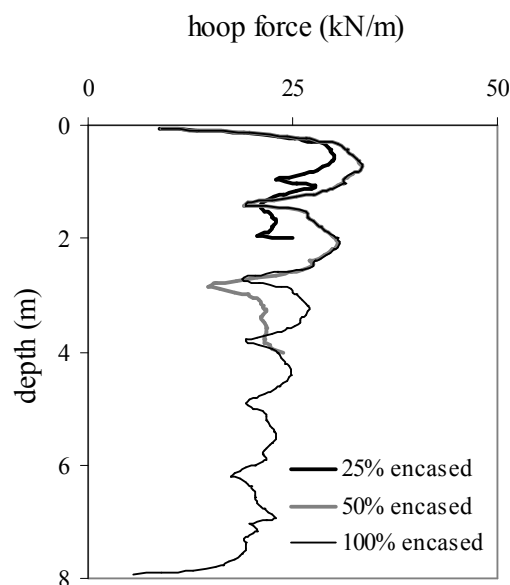


**Figure 6.9:** Hoop forces for partially encased columns

Based on this, charts of hoop force versus depth for the fully encased state can be considered to represent a reasonable upper bound for hoop forces in partially encased columns. The study also supported the observations made from modelling of small-scale tests, where for a given surcharge pressure, hoop forces were only slightly less for columns with reduced encased length.

#### Charts – primary study

Charts for all of the cases investigated in the primary parametric study are presented in Appendix D.2. The impact of each parameter on encased column behaviour is presented in the following sections.

##### 6.3.3.1 Replacement ratio

As set out earlier, increasing the replacement ratio from 15% to 35% significantly reduces axial strain. This was the same for non-encased, partially encased and fully encased columns. In the base model, for replacement ratios between 15% and 35%, strain is reduced from about 30% to 60%, respectively. With the addition of the highest strength, full-length encasement (Secugrid<sup>®</sup>, UTS=200 kN/m) and heavily compacted columns, strain is reduced by between 90% and 95% across the same range. The reduction in strain with increased replacement ratio can be attributed to the greater volume of stiffer column material supporting the load and therefore reducing deformation. This also acts to reduce hoop forces in the geogrid encasement as was observed in all cases assessed in the parametric study.

##### 6.3.3.2 Column stiffness

For lightly compacted columns in soft soil (base model), axial strain is reduced from about 30% to 60% across the range of replacement ratios. For heavily compacted columns, axial strain is reduced from about 40% to 70% across the same range, providing a significant increase in cell stiffness when compared to lightly compacted columns. A similar increase in stiffness is observed for heavily compacted columns with partial and full geogrid encasement, in both soft and very soft clay.

For lightly compacted columns fully encased with Secugrid® (UTS=200 kN/m) and loaded with an 80 kPa surcharge, the maximum hoop force is about 45 kN/m at  $A_r=15\%$ . For heavily compacted columns, the corresponding hoop force is about 35 kN/m. This reduction in load supported by the geogrid is consistent with expectations because the greater stiffness and higher friction angle of the heavily compacted crushed rock enables the column to support higher stresses with less deformation. The same observation applies to fully and partially encased columns at higher replacement ratios and with lower strength geogrid.

### Summary

Column strength and stiffness appear to have a significant impact on unit-cell behaviour. Columns compacted to a greater relative density may reduce settlement and reduce the load supported by the geogrid, perhaps reducing the strength of geogrid needed for a specific application. Whether an encased column can be compacted to the density modelled in the parametric study will need to be confirmed by site trials.

#### 6.3.3.3 Soil stiffness

For non-encased columns, there is little difference in the behaviour between columns in soft clay (CIS) and very soft clay. However, as encasement is increased, particularly to the fully-encased state, strain is reduced by a greater amount in the very soft clay. For example, when full encasement (using Secugrid®, UTS=100 kN/m) is applied to the base model, strain reduction at a replacement ratio of 25% is about 75%. For the same case in very soft clay, the strain reduction is about 85%. This result is consistent with expectations, because in very soft clay, the relative stiffness of the column when compared to the surrounding clay is higher. It follows that strain reduction would be greater in this case.

There is a small reduction in the hoop forces for encased columns in soft clay, compared to columns in very soft clay. This is most likely due to the greater lateral confinement provided to the column by the soft clay, and the higher effective lateral earth pressures resulting from the higher unit weight. Furthermore, the hoop forces decrease with depth in the soft clay to a greater extent than the very soft clay, probably due to the greater effective lateral stress at depth in the soft clay providing greater confinement.

### Summary

The numerical results indicate strain reduction is generally greater for fully and partially encased columns in very soft clay compared to soft clay, although there is little difference in behaviour for non-encased columns. Geogrid hoop forces are generally lower in the soft clay, a likely result of the higher stiffness and higher effective lateral earth pressures.

#### 6.3.3.4 Geogrid stiffness and strength

The study indicated that by increasing the stiffness of the geogrid encasement, axial strain is significantly reduced. For example, when the geogrid of lowest stiffness (Secugrid®, UTS=60 kN/m) is used to fully encase a column in the base model, a strain reduction of 70% is calculated for  $A_r=15\%$ . For the same  $A_r$ , this increased to about 75% for geogrid of medium stiffness (UTS=100 kN/m) and greater than 80% for geogrid of high stiffness (UTS=200 kN/m). The same trend is observed for all cases analysed in the study.

It follows that encasement of greater stiffness is likely to attract higher load and this is observed in the case presented above. For the base model, at  $A_r=15\%$ , the maximum hoop force in the geogrid of lowest stiffness is about 35 kN/m. For the medium and high stiffness geogrids, this value is about 40 kN/m and 45 kN/m, respectively. A similar trend is observed in the other cases analysed in this study.

In some cases analysed, the hoop forces in the encasement exceed the ultimate tensile strength of the geogrid. This generally occurred when a 160 kPa surcharge was applied to columns encased with the geogrid of lowest stiffness at  $A_r=15\%$ . However, for the case of lightly compacted columns in very soft clay, it also extended to columns at  $A_r=25\%$ , and to columns encased with the geogrid of medium stiffness (for  $A_r=15\%$ ). Where hoop forces exceed the UTS, a geogrid of higher strength or columns at higher replacement ratios would need to be adopted.

### Summary

The numerical analyses indicate that geogrids of higher stiffness increase the stiffness of the encased column, reducing axial strain and therefore settlement. The increased stiffness results in greater load being supported by the geogrid. Careful consideration should be given to the use of lower strength geogrids in applications with higher stresses.

### 6.3.3.5 Percent encased length

For all cases assessed in the primary parametric study, increasing the encasement length acted to steadily increase unit-cell stiffness and therefore reduce axial strain. The largest strain reductions for an incremental increase in encased length occurs for cases where an 80 kPa surcharge is applied to columns at low replacement ratios ( $A_r=15\%$ ), using geogrid of high stiffness. With increasing replacement ratio and heavily compacted columns, the impact of both partial and full encasement becomes less significant, most likely because the column material is able to support more of the applied load.

### 6.3.3.6 Surcharge

Although not considered in many analytical design approaches, the numerical analyses indicate surcharge pressure appears to significantly affect the behaviour of stone columns. For the base model at  $A_r=25\%$ , the strain reduction was about 45%. For a 160 kPa surcharge, this was reduced to below 40%. Reductions of similar, or greater magnitude were calculated in most other cases, including for partially and fully encased columns. Axial strain reduction is plotted against pressure for the four different encased states in Figure 6.10. In this Figure, pressure refers to surcharge pressure, where 40 kPa corresponds to about 2 m of soil fill, 80 kPa to about 4 m of soil fill, and so on.

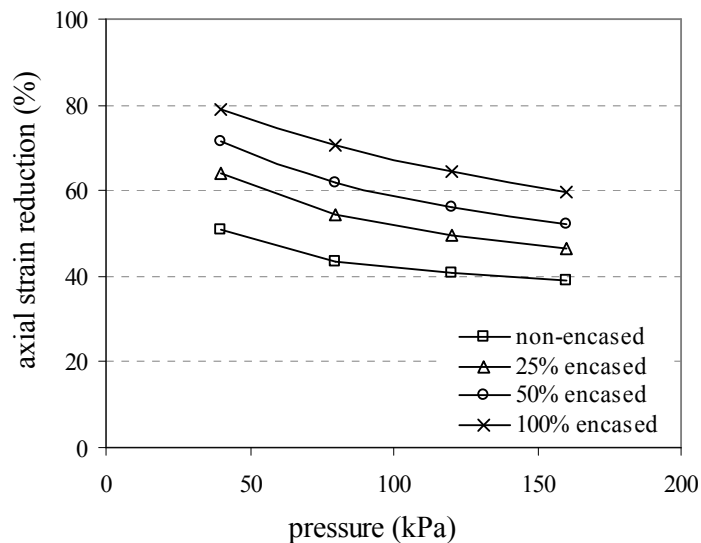


**Figure 6.10:** Axial strain reduction versus pressure for encased columns in base model

Results indicate that strain reduction decreases with increasing surcharge pressure. The rate of this reduction is significant for lower surcharge pressures but tends to reduce for higher surcharge pressures. This observation was made for all of the cases assessed in the study and is most likely due to the stiffness of the adopted clay models being stress dependent. As stresses are increased in the soil, the soil becomes stiffer (through consolidation and use of the Soft Soil model in PLAXIS), supporting more of the load and reducing the impact of the stiffening column.

### Summary

The study indicates that greater benefit may be gained from using conventional and encased stone column ground improvement at lower stresses than at higher stresses (higher surcharges). The impact of applied surcharge is often neglected in conventional stone column assessments and this study indicates that it should be considered when assessing the performance of conventional or encased stone columns.

#### **6.3.4 Results of secondary parametric study**

The secondary parametric study was limited to varying parameters within the base model only, and was therefore not as comprehensive as the primary study. The parameters that were investigated are described separately in the following sections.

##### **6.3.4.1 Column depth**

The impact of column depth was assessed in the base model by modelling columns that were 4 m, 8 m and 12 m deep. The limited study was undertaken using a geogrid of medium stiffness ( $UTS=100$  kN/m). Charts presenting axial strain reduction and hoop forces for columns installed to different depths are presented in Appendix D.3. The study indicates a greater strain reduction for shorter columns. Furthermore, the impact of full encasement is greater for shorter columns while the impact of partial encasement is greater for longer columns. This is probably due to greater effective lateral earth pressures for deeper columns acting to confine the non-encased section more so than for shorter columns.



There is little difference in the maximum hoop force generated in the geogrid for columns at different depths. However, there is a significant decrease in hoop forces with depth for columns deeper than 4 m. This is most likely due to the increased lateral support for deeper columns.

#### 6.3.4.2 Soil stiffness

The differences in behaviour for columns in soft and very soft clay was discussed in the primary study. However, columns in firm clay were modelled as part of the secondary study. The limited study was undertaken using a geogrid of medium stiffness, with charts of axial strain reduction and hoop forces presented in Appendix D.3. The study indicates that strain reduction decreases significantly using the firm clay model when compared to the very soft clay and soft clay models. This is most likely due to the firm clay model being stiffer than the two softer models, and hence, the firm clay supported more of the surcharge, reducing the impact of the stiffening column. The hoop forces within the geogrid are also significantly reduced for the firm clay.

#### 6.3.4.3 Method of column installation

By increasing the lateral earth pressure coefficient to  $K_0=1$ , additional confinement is provided to the column, resulting in a slight increase in strain reduction. Little change is observed in the geogrid hoop forces. A more detailed assessment of the impact of column installation is required once an appropriate technique for site installation is developed. This may include assessment of the lateral stress state in the soil following column installation.

### 6.4 Discussion

Several parameters were considered likely to affect the behaviour of geogrid encased stone columns, several of which were investigated in the parametric study. These parameters are summarised in Table 6.6, where they are ranked in order of their impact on axial strain reduction and geogrid hoop forces, as assessed from the numerical analyses.

**Table 6.6:** Summary of the impact of parameters on encased column behaviour

	axial strain reduction	geogrid hoop forces
high impact	replacement ratio	surcharge pressure
	column stiffness	replacement ratio
	% encased length	soil stiffness
	surcharge pressure	geogrid strength - stiffness
	geogrid strength – stiffness	column stiffness
	soil stiffness	column length*
	column length*	installation method*
low impact	installation method*	% encased length

\* limited study (secondary parameter)

The study indicates that parameters such as replacement ratio and soil stiffness have a significant impact on column behaviour. This has been well documented in previous studies. Additionally, increasing the encased length of a column significantly reduces axial strain, an observation also made in the small-scale laboratory tests presented in Chapter 3. The surcharge pressure has a significant impact on column deformation, an aspect that is often overlooked in stone column design and is probably the most important parameter in the assessment of geogrid hoop forces. The study indicates that parameters such as column length and installation method may have only a small impact on encased column behaviour, although these aspects were only investigated in a limited study.

The charts presented in Appendix D.2 and Appendix D.3 provide an estimate of the behaviour of geogrid encased stone columns under various conditions. Although a site trial is required to confirm the accuracy of such models, they could potentially provide a useful tool for assessing the impact of material and geometric properties on encased column behaviour. Before the charts can be used as a design tool, the following should be addressed:

- The base model compares favourably with typical results for conventional stone columns, but no modelling of site load testing has been undertaken to confirm the behaviour of encased models.
- Hoop forces for low strength geogrids are exceeded when high stresses are applied and would need to be substituted by higher strength geogrids for such conditions.

- The strength of the geogrid would need to be reduced by an appropriate factor of safety. This factor of safety chosen should account for the damage sustained by the encasement during installation and the ultimate tensile strength of the material that can be realised during loading. The available tensile strength may be reduced by factors such as welding, environment and friction/cutting from column material. The results of the medium-scale laboratory testing, presented in Chapter 5, provide some guidance to the selection of an appropriate factor.

## 6.5 Summary

The successful modelling of small-scale tests set out in Chapter 4 gave confidence that full-scale behaviour could be modelled using the same technique, where individual soil models calibrated to full-scale material behaviour were combined. Unit-cell idealisation was used to simplify the case of group columns to a single column surrounded by a cylinder of clay within its zone of influence. The unit-cell geometry was selected to model 0.8 m diameter columns installed at typical replacement ratios.

A base model was initially analysed, where the behaviour of non-encased columns were compared to well documented cases of conventional stone columns installed in clay of a similar consistency. The behaviour of the full-scale base model compared favourably to these cases. A parametric study was then undertaken to investigate the impact of different properties on encased column behaviour. Parameters used in the study comprised:

- Replacement ratio
- Column stiffness
- Soil stiffness
- Geogrid stiffness and strength
- Percent encased length
- Surcharge pressure
- Installation method

Charts which present axial strain reduction and geogrid hoop force for the different cases investigated in the parametric study are presented in Appendix D.2 and D.3. The study indicates that parameters such as replacement ratio, percent encased length and surcharge pressure have a significant impact on encased column behaviour while properties such as

soil stiffness have less impact. Trends identified in full-scale modelling, such as reduced strain with increased encased length, compared favourably with measurements from small-scale tests. This supports the approach of using small-scale testing in combination with numerical modelling to investigate encased column behaviour. The charts that have been produced as part of the parametric study may provide a useful tool for assessment of encased column behaviour, although the results of full-scale testing and site trials are needed for validation.

## **7 Research findings and practical applications**

---

The research presented in this thesis was undertaken to investigate geogrid encased stone column behaviour, with practical aspects of construction and performance considered a primary focus. The findings of this research are summarised in this chapter, together with discussion on possible practical applications, construction methods and proposals for future research and testing.

### **7.1 Research summary**

A summary of the testing and modelling undertaken as part of the geogrid encased stone column investigation is presented in this section.

#### **7.1.1 Background**

Geotextile encased columns (GECs) have been used successfully in recent times to extend the use of conventional stone columns to very soft soils (Raithel et al. 2005). The technique provides a practical method of ground improvement, but its use can be limited in some cases by:

- The requirement for fine column aggregates that do not damage the geotextile during loading, such as sand and fine gravel. Fine aggregates may not be available on some projects.
- The minimal compaction provided to the GEC during installation. This is typically done to reduce potential damage caused to the geotextile but can result in significant densification during loading and therefore settlement.
- The relatively high circumferential strains required to mobilise hoop forces in the geotextile. This can result in significant radial expansion during loading and therefore settlement.

Due to the potential limitations of geotextile and to broaden the use of geosynthetics for encasement construction, an alternative material was investigated. Geogrid was

considered to be a suitable alternative because of its increased robustness, relatively high stiffness and the low strains required to mobilise tension forces. These properties were likely to enable the geogrid encasement to be used with typical stone column aggregates such as crushed rock and to be compacted to a greater extent than GECs. Geogrid encased stone columns are also likely to show greater stiffness than GECs, providing an alternative ground improvement option in some cases.

### **7.1.2 Research aims**

Limited research into the use of geogrid encasement has been undertaken in the past. Previous research has comprised testing of geogrid encased columns constructed using the technique of welding (Trunk et al. 2004), a method now considered too costly to implement (Heerten 2006). Smaller studies have also been undertaken which have included limited small-scale testing of fully-encased isolated columns. This type of testing has generally formed part of a broader theoretical study into geosynthetic encasement. The research presented in this thesis was undertaken with the practical aspects of geogrid encasement being a primary consideration. The aims of the research included:

- (i) To investigate if the method of geogrid encasement provided a suitable alternative to geotextile encasement.
- (ii) To investigate the types of soils, geogrids and column aggregates best suited to the technique.
- (iii) To investigate the likely performance of geogrid encased stone columns and the properties that had the greatest impact on column behaviour.
- (iv) To investigate practical methods of column construction.

### **7.1.3 Components of research**

To fulfil the aims of the project, research comprised investigation into the following aspects of encased stone column behaviour:

- Group column behaviour and how it differed from isolated column behaviour. Group column applications form the majority of stone column projects and group column testing is considered paramount to understanding encased column

behaviour. Much of the previous published research has focussed on isolated columns, and although considered more simple to test and analyse, fail to adequately address group column conditions.

- Whether partial circumferential encasement of the upper section of a column produced similar behaviour to a fully-encased column. It is well documented that radial expansion is greater in the upper section of columns during loading. By encasing only this section, thereby limiting radial expansion, behaviour of a partially encased column may be similar to a fully-encased column. Research into this particular aspect may help to reduce the amount of geogrid required for encasement.
- Whether the method of overlap used to construct an encasement sleeve provided a similar level of fixity to welding. Geogrid encasement has been constructed in the past by rolling geogrid into a sleeve and mechanically welding the narrow overlapped seam. The method is unlikely to be adopted on site due to the high cost of equipment mobilisation. The method of overlapping the encasement by at least a half circumference was therefore investigated. The method of overlap relies on interlock between the aggregate and geogrid in the overlapped section to fix the encasement in position.
- The impact of different material properties on geogrid encased column behaviour. These included geogrid stiffness, strength and geometric properties, the stiffness and size of column aggregate and the stiffness of the surrounding soil.

#### **7.1.4 Methodology and observations**

The research presented in this thesis comprised a four-stage approach. Small-scale laboratory testing, numerical simulation of the small-scale tests, medium-scale testing and scaled-up numerical modelling were used to assess full-scale performance. The four-stage approach was considered an effective and efficient method of fulfilling the aims of the research. The methodology and results of the four stages are summarised in the following sections.

#### 7.1.4.1 Small-scale laboratory testing

Small-scale laboratory testing was undertaken to investigate encased column behaviour. The controlled nature of testing enabled the behaviour of columns encased with materials of different stiffness and encased lengths to be compared. The method of overlap and interlock was also tested. Testing predominantly focussed on simulating group column behaviour using unit-cell idealisation although isolated columns were also tested.

Testing was undertaken in three custom-made consolidation cells, measuring about 150 mm in diameter. Samples of very soft kaolin clay measuring about 310 mm in height were consolidated from slurry in each cell. A full-depth frozen sand column was installed at the centre of the sample using a replacement technique. Columns measured 51 mm in diameter. Where encasement was used, fibreglass or aluminium mesh was wrapped around the outside of the column during construction, with welding simulated using an epoxy-resin adhesive. The aluminium mesh was about twice as stiff as the fibreglass and the meshes generally provided a small-scale representation of full-size geogrid. Other aspects of testing including column geometry, height and sand particle size were scaled down where practical. For group column tests, a piston was used to load the sample, creating the unit-cell conditions that approximated group column behaviour. Isolated columns were loaded using a small footing equal in diameter to the column. Staged loading was adopted for all tests, with consolidation generally completed between stages. The methodology and results of column testing are described in detail in Chapter 3.

Observations from small-scale column tests included the following:

- For both group and isolated columns, steadily increasing the encased length generally increased column stiffness. For isolated columns, it also resulted in increased capacity.
- Fully-encased columns were observed to be significantly stiffer than partially-encased columns.
- Isolated columns failed by rapid radial bulging of the non-encased section of the column, accompanied by visible uplift at the clay surface in some cases. The bulge zone was confined to a length of about 2 column diameters (in the upper section of the non-encased section). Mesh capacity was not exceeded in any isolated column test.



- Mesh failure occurred in most group column tests. In these tests, the confinement provided by the unit-cell boundary conditions acted to constrain the column, enabling it to be loaded to higher stresses and to mesh capacity. Column bulging generally occurred along the full length of the non-encased section.
- The behaviour of aluminium mesh encased columns differed little from fibreglass encased columns, even though the stiffness of the aluminium was double that of the fibreglass. This was considered a result of the insufficient contrast in stiffness between the two meshes in small-scale.
- Encasement constructed using the method of overlap (which relies on interlock from the sand and the overlapped section of mesh) provided a level of fixity similar to bonding the mesh with epoxy-resin.
- Columns acted as effective vertical drains, with sample consolidation times in testing being reduced by a factor of between 2 and 7, with values of 3 and 4 being typical. The ability of columns to act as drains was reduced with ongoing consolidation, attributed to the observed ingress of clay into the column cross-section (by up to 6 mm, corresponding to about 40% of the column cross-sectional area) after consolidation.

#### 7.1.4.2 Numerical modelling of small-scale tests

Numerical analysis is commonly used to model laboratory test results, usually leading to a better understanding of the engineering problem at hand. Numerical analysis was used in this case to model the results of the small-scale tests, providing insights into encased column behaviour. The analyses were undertaken using the well established geotechnical finite element software, PLAXIS.

Initially, numerical models that represented small-scale test materials were calibrated to the behaviour of laboratory strength and deformation tests undertaken on the materials. A geometric representation of the test cell was then developed, with the relevant stress histories applied to the materials. Column installation was modelled using a replacement technique, with the same load stages that were adopted in testing applied to the models. Numerical results closely matched the laboratory test results, including aspects such as load-settlement behaviour, radial column expansion and time rate of consolidation. The analysis also investigated the development of hoop forces within the meshes,

supplementing the observations and conclusions made from the small-scale tests. The adopted method of numerical analysis was considered an effective method of simulating encased column behaviour. The modelling process is described in Chapter 4.

#### 7.1.4.3 Medium-scale laboratory testing

Medium-scale tests were undertaken using typical stone column materials to investigate whether encasement could be fixed in position using the method of overlap. A column test was initially undertaken in the partial-confinement provided by a tank filled with kaolin slurry. However, further testing indicated that the columns constructed using the method of overlap could be tested in unconfined compression. This increased the number of tests that were undertaken in the allocated timeframe and broadened the scope of testing. The increased scope included investigating the impact of different geogrids (with different strength, stiffness and geometric properties), different aggregates and different amounts of overlap on encased column behaviour.

Tests were generally undertaken on columns measuring 0.86 m in height and about 0.25 m in diameter. Columns were tested to failure. Encasement was constructed from biaxial geogrid (Secugrid Q6), uniaxial geogrid (Secugrid R6) and Combigrid provided by NAUE GmbH. A test was also undertaken using a triangular geogrid (Tensar TX 160) manufactured by Tensar International. Encasement sleeves were fixed in place using cable ties spaced at about 170 mm centres. This supported the column during construction and initial loading but provided little structural support after interlock had occurred. Encasement was generally filled with “20/50 mm rubble”, comprising crushed basalt graded between 20 mm and 50 mm (considered to be representative of typical stone column aggregates). The rubble was generally compacted to a relative density between 60% and 70%. Several tests were also undertaken on columns constructed using “14/10 mm gravel”, a finer aggregate.

Observations from medium-scale column tests included the following:

- Three failure modes occurred; (i) insufficient overlap – where welded junctions in the section of overlap sheared, (ii) insufficient interlock – where the overlapped encasement unravelled without damaging the geogrid, and (iii) sufficient interlock and overlap – where horizontal ribs failed in tension.
- Biaxial geogrids (namely the Secugrid Q6 range) were best suited to encasement.

- About 0.5% circumferential strain was required to significantly mobilise hoop forces in the Secugrid Q6 encasement.
- Sufficient encasement fixity occurred when 20/50 mm rubble was encased with Secugrid Q6 geogrid (100% circumferential overlap).
- A minimum number of welded junctions in the section of overlap were required to prevent shearing of the welded junctions and unravelling of the encasement.
- Horizontal ribs placed on the outside of the encasement generally increased column capacity when compared to ribs placed on the inside.
- Partial cutting of geogrid ribs occurred during loading of columns constructed from 20/50 mm rubble. Higher strength geogrids were more resistant to cutting.
- Secugrid 120/120 Q6 encasement was the stiffest of the Q6 geogrids tested and the most resistant to cutting. Based on testing, it was considered the most suitable geogrid for encasement construction on site.
- The average axial Young's modulus of columns encased with Secugrid 120/120 Q6 was approximately 20 MPa, comparing favourably to previous studies on columns constructed using welded encasement.
- For columns constructed from 14/10 mm gravel, the amount of interlock was generally less than for the coarser 20/50 mm rubble, although the gravel did not damage or cut the geogrid like coarse aggregates.
- 100% circumferential overlap was insufficient for uniaxial geogrids (Secugrid R6 range), probably due to the greater aperture spacing in the hoop direction and lower strength and stiffness of the vertical ribs.
- Unconfined loading of small diameter columns was probably not an effective method of testing uniaxial encasement.
- Combigrid and geotextile encasement were not suited to the method of overlap.
- Encasement constructed from triangular geogrid may be suited to the method of overlap but requires geogrid of greater stiffness and robustness than the sample used in testing.

#### 7.1.4.4 Extrapolation to full-scale columns

The numerical modelling technique adopted to simulate small-scale test results was scaled-up to investigate the behaviour of full-scale geogrid encased stone columns. Numerical modelling was undertaken to investigate the impact of a variety of column,

geogrid and clay properties on encased column behaviour, as part of a parametric study. Numerical modelling enabled the impact of these properties to be investigated without the significant time and resources typically required for such an investigation using laboratory and site testing.

An 8 m high unit-cell was modelled using a 0.8 m diameter column. Different cell diameters were modelled to represent different replacement ratios. Properties consistent with Coode Island Silt, a soft clay found in the Yarra River Delta region of the Melbourne CBD, were adopted for the clay component of the model. Properties consistent with lightly compacted gravel were used for the stone column component. The soil models were calibrated to the behaviour of laboratory compression tests in the same way they were for the numerical analysis of small-scale tests. The load-settlement behaviour of this base model was then compared to that of well documented case studies and centrifuge tests undertaken on stone columns in soft clay. The results of the modelling provided a close match to the published data.

With some confidence that the base model adequately modelled full-scale stone column behaviour, geogrid encasement was added as part of the parametric study. The properties of the three different types of geogrid used in the study were consistent with geogrids supplied by NAUE GmbH and adopted in the medium-scale tests set out in Chapter 5. Other parameters that were varied in the study comprised encasement length, column stiffness, clay stiffness, surcharge pressure, column length and the method of column installation. The methodology and results of the parametric study are presented in Chapter 6. Observations from the scaled-up numerical modelling included the following:

- Parameters were divided into two categories, their impact on reducing vertical strain and their impact on reducing circumferential hoop forces in the geogrid.
- Increasing the replacement ratio (from 15% to 35%), improving the engineering properties of the column (greater compaction, higher friction angle) and increasing the percent encased length reduced vertical strain most effectively.
- Column length and soil stiffness had the least impact on reducing vertical strain.
- Increasing the surcharge (from 80 kPa to 160 kPa), reducing the replacement ratio (from 35% to 15%) and reducing the soil stiffness increased hoop forces within the geogrid most significantly.
- Column length and the percent encased length had the least impact on geogrid hoop forces.

- For densely compacted columns installed at replacement ratios above 25% and fully-encased with a geogrid of medium to high stiffness, settlement may be reduced by 90%.
- Charts produced from the parametric study may provide a useful tool for assessing encased column behaviour but verification with site testing is recommended.

## **7.2 Discussion**

Small-scale testing, numerical modelling and medium-scale testing were combined in a four-stage approach to investigate various aspects of geogrid encased stone column behaviour. The scope of this study was considered to fulfil the research aims outlined earlier in this chapter. The results of the research, also summarised earlier in this chapter, generally indicate that geogrid encased stone columns can provide an alternative method of ground improvement. As practical aspects of the technique are a primary consideration, construction and installation methods, together with performance will form the focus of further discussion in the following sections.

### **7.2.1 Group and isolated columns**

The costs associated with equipment mobilisation and shipment of geogrid materials to site are likely to make group column applications more economical than isolated column applications. Group column behaviour was therefore considered the primary focus of this research. Although geogrid encased stone columns are unlikely to be used in isolation, the practical aspects discussed in the following sections generally apply to both column types.

### **7.2.2 Partial encasement**

Although subject to scale errors, small-scale testing indicates that by steadily increasing the percent encased length of a column, column stiffness is increased and therefore settlement may be steadily reduced. This contention is further supported by numerical modelling, firstly by replication of the small-scale laboratory test results and secondly, by a full-scale parametric study.

#### 7.2.1.1 Isolated columns

Testing indicated that for isolated columns, failure occurred rapidly and was therefore dependent on the undrained shear strength of the soil in the non-encased section of the column. Although unlikely to be adopted in practice, careful testing would need to be undertaken to accurately measure the strength of the soil in the non-encased section of an isolated column prior to the technique being adopted.

#### 7.2.1.2 Group columns

The method of partial encasement is likely to be suited to some practical group column applications, some of which are discussed later in this chapter. Furthermore, the stiffness of natural soil tends to increase with depth, along with lateral confining pressures. These conditions could not easily be simulated in the laboratory. On this basis, the non-encased section of a column may be confined to a greater extent in real soils than was measured in the laboratory. This may result in greater reductions in settlement being achieved on site using partial encasement than were measured in the laboratory.

### 7.2.3 Full-length encasement

All forms of modelling and testing undertaken in the present study indicate that columns of high stiffness can be constructed using full-length geogrid encasement. In the small-scale tests, an 80% reduction in settlement was measured prior to mesh failure, at a relatively low replacement ratio of about 11%. In numerical modelling, settlement reduction ranged from as low as 50% to greater than 95% depending on replacement ratio and geogrid stiffness. Although medium-scale testing was unconfined and did not simulate the confining conditions present at site, column stiffness was observed to increase with increasing geogrid stiffness. The Young's moduli calculated from column tests increased from about 13 MPa for Secugrid 60/60 encased columns up to about 20 MPa for Secugrid 120/120 encased columns. This compared favourably with research presented from previous studies.

#### 7.2.2.1 Likely site performance

Based on the results of the present research, it is considered that by varying the replacement ratio and geogrid stiffness, column stiffness can be tailored to suit a range of settlement criteria. With a replacement ratio of about 25% and geogrid of medium to high stiffness, settlement reduction (when compared to the behaviour of the untreated soil) is likely to be in the order of 80% to 90%. This type of performance brings the method in line with stiffer forms of ground improvement such as soil mixing.

#### 7.2.2.2 Limitations

Based on the behaviour of unconfined medium-scale column tests in the laboratory, columns are likely to undergo some shortening prior to hoop forces being mobilised in the geogrid. This may result in significant settlement occurring during the construction stage of a project, and on this basis, the method is probably not suited to structures (such as buildings) that are sensitive to total and differential settlement. However, with confinement from soil, columns are likely to perform with greater stiffness than measured in unconfined tests. Columns may also be compacted to a greater density on site compared to that undertaken in laboratory studies.

Column relative densities ranged between about 60% and 70% in testing, achieved by shaking the geogrid sleeve during construction. With columns likely to be installed to depths of up to about 12 m in practice, crushed rock will receive additional compaction energy from the fall height during placement and through vibration. Column construction practices are discussed later in this chapter.

#### 7.2.4 Method of overlap

The method of overlap has been shown to provide a potentially effective and economical method for encased stone column construction on site. The method of overlap was effective in small-scale testing, providing a level of fixity similar to welding (simulated using epoxy-resin adhesive). It was also effective in medium-scale column tests, where the behaviour of encasement constructed using the method of overlap compared

favourably to previous studies where encasement was welded. The method of fixing the geogrid encasement sleeves using cable ties is likely to be easily adopted on site.

#### 7.2.3.1 Required overlap

The medium-scale testing of full-scale geogrid encasement and typical stone column aggregates indicates that a minimum number of welded junctions may be required in the section of overlap to prevent the encasement from unravelling. Below this number, high stresses are likely to be placed on welded junctions, causing them to shear or tear. However, further testing is required to confirm this contention and if correct, to quantify the number of welded junctions required for different geogrids in different conditions. It is recommended that any full-scale on-site testing of encased stone columns following this study should comprise encasement constructed from a full circumference of overlap, as this was shown to be effective in medium-scale tests. Future testing and research is discussed later in this chapter.

#### 7.2.3.2 Materials and geogrid cutting

Medium-scale testing indicates that biaxial geogrids (Secugrid Q6 range) are best suited to the method of overlap, with aggregate graded between 20 mm and 50 mm providing the best interlock. However, the angular crushed rock used in testing (considered representative of typical stone column material) tended to partially cut the geogrid ribs during column loading, reducing the tensile strength of the geogrid. Further testing is required to confidently assess this strength loss and provide a suitable factor of safety for design.

The method of overlap may also be suited to other aggregate types, particularly smaller crushed rock gravel, when used in the confined conditions found on site (the impact of rounded gravel was not investigated in this study). Confinement provided from the surrounding soil may enable the smaller aggregate to interlock better with the encasement. Furthermore, shear between the expanding geogrid sleeve and surrounding clay may reduce the ability of the encasement to unravel, increasing column capacity. As the smaller aggregate is not likely to damage the geogrid during loading, site testing may show that it is more suited to the practice of geogrid encasement than coarser aggregate.



### 7.2.5 Geogrid properties

In small-scale testing, the behaviour of columns encased with aluminium mesh could not be differentiated from columns encased with fibreglass mesh, even though the fibreglass mesh had half the stiffness of the aluminium. This was probably because the scaled stiffness of each mesh was likely to be greater than for typical geogrid, providing insufficient contrast. However, numerical analyses (based on geogrid properties consistent with Secugrid) indicate that increased geogrid stiffness may significantly increase column stiffness and therefore reduce settlement. The impact of geogrid stiffness and strength was measured in medium-scale testing of columns encased with Secugrid Q6 geogrids. By increasing the ultimate tensile strength of the geogrid from 60 kN/m, to 80 kN/m and then 120 kN/m, the stiffness and capacity of the encased column increased. The impact of aggregate cutting was also reduced for geogrids of higher stiffness (higher strength), most likely due to the greater cross-sectional area of the ribs.

#### 7.2.4.1 Strength

The numerical analyses indicate that the selection of a geogrid with a suitable strength may be critical for certain applications. Lower strength geogrids may not be suited to applications with relatively high column loads. In addition, if a significant factor of safety is applied to the geogrid, the lowest strength geogrid assessed in the parametric study (Secugrid 60/60) may not be a suitable encasement material. Medium-scale laboratory testing of this particular geogrid indicated that due to cutting, the tensile strain of the geogrid was halved (from 6.2% down to about 3%). Therefore, a significant strength reduction factor would be required when using this product with coarse, angular aggregates and its use would be limited to applications with very low surcharge pressures.

#### 7.2.4.2 Geogrids best suited to encasement construction

Of the products tested and assessed numerically, Secugrid 120/120 Q6 appears to be best suited to geogrid encasement construction. Its use is recommended for future site trials and full-scale testing. It is considered to be a medium to high strength geogrid and due to current manufacturing processes, is the highest strength biaxial geogrid available from

NAUE at this time. It is also a new product and where availability is a problem, Secugrid 80/80 Q6 may provide a suitable alternative (based on testing set out in Chapter 5).

If a higher strength geogrid is required, uniaxial Secugrids may be capable of providing this strength, at least in the hoop direction. However, medium-scale testing indicates that the suitability of Secugrid R6 geogrids to encasement applications is required to be assessed using confined testing, probably site testing.

#### 7.2.4.3 Limitations

Based on hoop forces assessed in numerical modelling, the strength of different geogrids currently available on the market may limit the use of geogrid encased stone columns to surcharges of less than about 160 kPa or about 8 m of soil fill. This, however, would need to be assessed on an individual project basis.

### 7.2.6 Practical applications

Although a site trial is required for final confirmation of the potentially successful practical use of geogrid encasement, the outcomes of this research indicate that the technique has significant potential to provide an alternative ground improvement option. The technique is probably suited to many of the same applications as GECs, conventional stone columns and many other methods of soft soil ground improvement. In addition, it may lend itself to a range of new and practical applications. Some of these applications are described in this section.

#### 7.2.6.1 Fully encased columns

Based on the outcomes of this research, full-length geogrid encased stone columns are likely to be suited to supporting many lightly and moderately loaded structures in a range of weak soils. These may include embankments supporting motorways and railways, dykes, bridge abutments, large diameter storage tanks, as part of land reclamation, car parking facilities, large warehouse and storage type facilities and many more. Due to the high stiffness of the encased column relative to the surrounding clay, a geogrid reinforced

bridging layer that acts to transfer load evenly between columns would most likely be required as part of any project. This, however, would need to be assessed on an individual project basis.

#### Very soft and extremely soft soils

Like GECs, geogrid encased stone columns are primarily suited to very soft and extremely soft soils – the type of soil in which conventional stone columns and other forms of ground improvement are generally not suited. Testing and numerical modelling undertaken as part of the present research indicates that geogrid encased stone columns are likely to behave with greater stiffness than GECs, for several reasons including:

- The hoop strain required to mobilise hoop forces is about 0.5%, less than the 1% to 4% needed for geotextile encasement. This may reduce the initial radial expansion of the column and therefore reduce settlement.
- Geogrid is more robust than geotextile and can therefore be used in combination with typical stone column aggregates such as crushed rock, which may increase column stiffness.
- Increased robustness may also enable the column to be compacted to a greater extent during installation, increasing column stiffness and reducing settlement.

#### Conventional stone column projects

There appears to be no significant impediment to the use of geogrid encasement for conventional stone column projects. Encased columns would provide increased stiffness when compared to conventional columns and may further improve the properties of the treated soil mass, as indicated by the numerical parametric study set out in Chapter 6. Where geogrid encasement is added to a conventional stone column project, the engineering behaviour of the treated soil may be significantly improved, with little additional cost or change to the installation method required. Both aspects are discussed later in this chapter.

Geogrid encased stone columns may be used to reduce total and differential settlement, increase stability and accelerate consolidation. If full-length encasement was to be adopted on a conventional stone column project, settlement reduction could be increased from about 30% or 40% up to about 90%. This reduction in settlement may apply to both primary consolidation settlements and creep settlements (although creep settlement reduction was not investigated in the present research), the latter being particularly

important for projects with a longer design life. This range of performance may appeal to a client or contractor.

Alternatively, geogrid encasement may be used to reduce the number of columns used on a conventional stone column project. If a similar settlement performance to a conventional stone column foundation is desired, the number of columns required using full encasement may be halved (based on the results of the parametric study presented in Chapter 6). The cost saving associated with reducing the volume of material used to construct each column may outweigh the additional cost of the geogrid and construction. Finally, as set out earlier, the stiffness of the geogrid encasement and replacement ratio may be varied to tailor settlement to design requirements in some cases.

#### 7.2.6.2 Partially encased columns

As varying the encasement stiffness and replacement ratio of fully-encased columns may be used to alter the treated soil stiffness, partial encasement may provide another method for tailoring settlement to design requirements. By changing the encased length of a column, settlement may be altered significantly. This characteristic may be utilised to solve some common engineering problems in soft soils.

##### Progressive settlement reduction

One such case is the “step” in differential creep settlement that often occurs between a rigid piled structure (such as a bridge abutment) and areas of soft ground (such as beneath a motorway embankment). Even if conventional stone columns have been used to improve the properties of the soil beneath the embankment, a step in creep settlement can occur at the interface of the rigid structure over time. This may be reduced to some extent by decreasing the spacing between columns on the lead up to the interface, but may still require a program of resurfacing and maintenance throughout the design life of a project to manage the problem. By steadily increasing the length of encasement on the lead-up to the piled structure, settlement can be steadily and progressively reduced, limiting the step in differential settlement at the interface. The concept is illustrated in Figure 7.1.

The technique may significantly reduce the need for resurfacing at the interface during the life of the project. Furthermore, if stone columns are already being used on the project,

there would be little additional cost, except that associated with the geogrid. This cost may be offset by a reduction of stone columns in the lead-up to the piled structure.

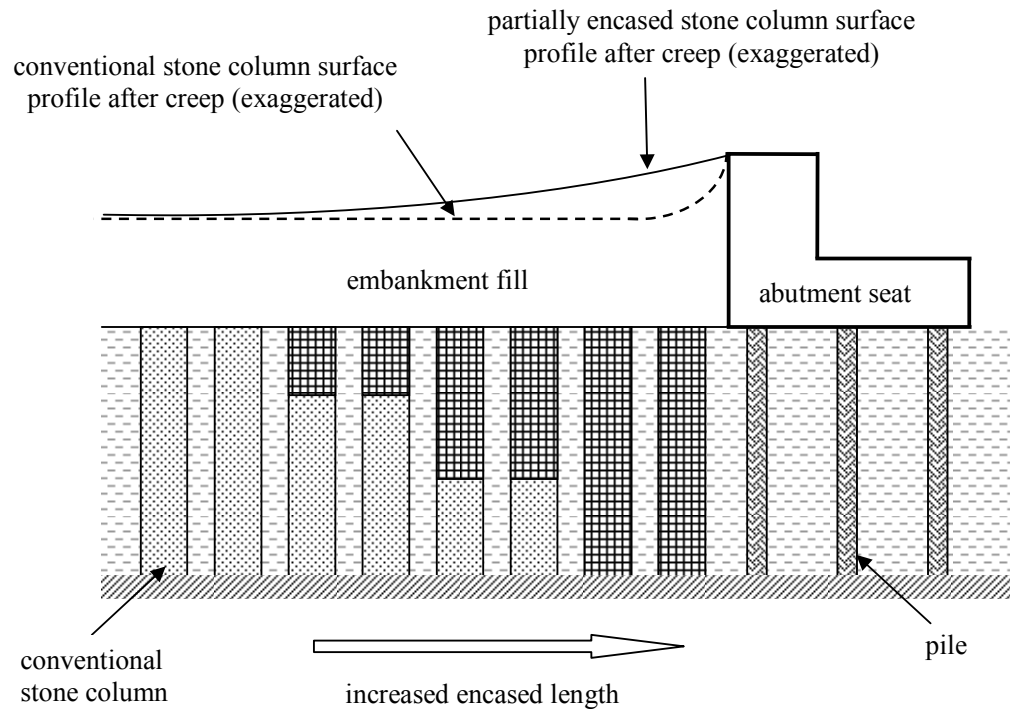


**Figure 7.1:** Reducing the step in differential settlement

### Layered soils

Another use for partially encased stone columns would be on sites where a younger deposit of weaker material overlies an older deposit of stiffer material (layered stratum). This may comprise a very soft or extremely soft clay overlying a firm clay, a common occurrence in alluvial deposits. In such conditions, geogrid encasement would only be required in the weaker material to provide the required lateral confinement. The concept is illustrated in Figure 7.2.

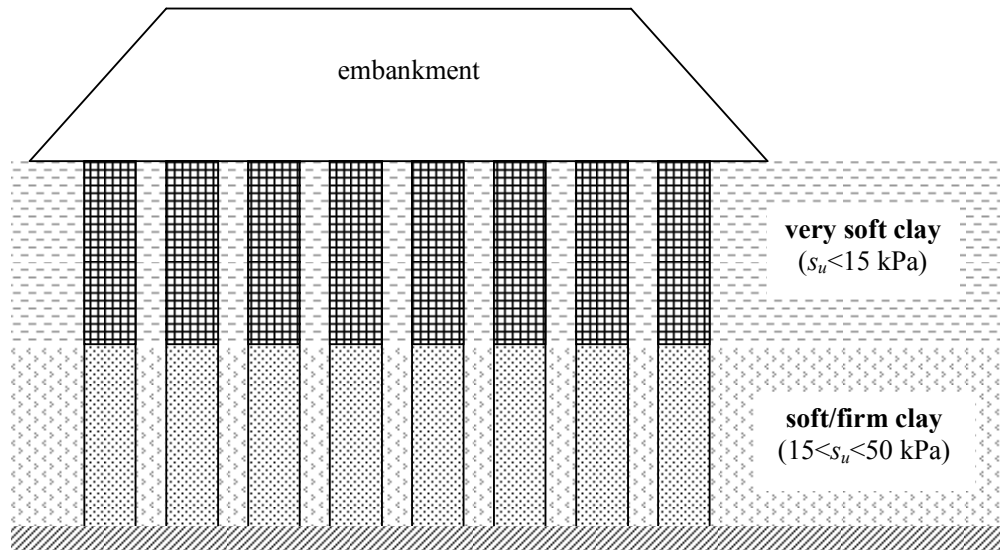


**Figure 7.2:** Partial encasement for sites with layered stratum

### 7.2.7 Construction methods

This section outlines the methods that may be adopted for constructing geogrid encased stone columns on site. Recommendations and suggestions are generally based on testing undertaken as part of this research and are made with the intention of providing guidance for an initial site trial. Further laboratory testing and site testing may improve and refine the material types and construction methodology set out here. A scope for such testing is presented at the end of this chapter.

#### 7.2.7.1 Materials

As outlined in earlier sections, angular crushed rock aggregate graded between about 20 mm and 50 mm appears best suited to geogrid encased stone columns. Secugrid 80/80 Q6 geogrid performed adequately in testing and is likely to provide a suitable encasement material in many cases. It is also readily available. However, Secugrid 120/120 Q6 geogrid was the best performed of the geogrids tested, and on this basis, is most suited to encasement construction.

#### 7.2.7.2 Encasement construction

Encasement should be constructed to the required diameter using a full circumference of overlap. For example, a 0.7 m diameter column has a perimeter of about 2.2 m and therefore a 4.4 m wide roll of geogrid is required. NAUE supplies geogrid in roll widths of up to 4.75 m and lengths of up to about 100 m. If a uniaxial geogrid is used, where the strength is generally much higher in the machine direction, column height may be restricted to the roll width (4.75 m). Alternatively, uniaxial geogrid may need to be custom-made with the higher strength ribs in the cross-machine direction.

The encasement may be fixed in the shape of a cylindrical sleeve using cable ties, probably at 0.5 m spacings along the length of the column. The cable ties provide little structural support to the column during loading and would therefore be used to temporarily support the encasement during installation. Cable ties were used at closer intervals in medium-scale testing because columns were generally unconfined during construction and loading.

#### 7.2.7.3 Replacement installation

Replacement installation may comprise a method similar to that currently used to install conventional stone columns and GECs. Steel casing would be vibrated down to the founding layer, somewhere between about 4 m and 12 m deep. The material inside the casing would then be removed using an auger. The geogrid encasement, only slightly smaller in diameter than the internal diameter of the casing, would then be placed inside the empty casing. The encasement may initially have to be lifted by winch and some consideration will need to be given to lifting the encasement without damaging the welded junctions. Once lowered inside the casing, the encasement can be filled with aggregate.

Aggregate may be dropped from higher than ground level to increase the energy of placement and therefore increase compaction effort. The column may be overfilled by a small amount so that when the casing is slowly vibrated out of the ground, the reduction in column height with densification is accounted for. A possible replacement installation technique is illustrated in Figure 7.3.

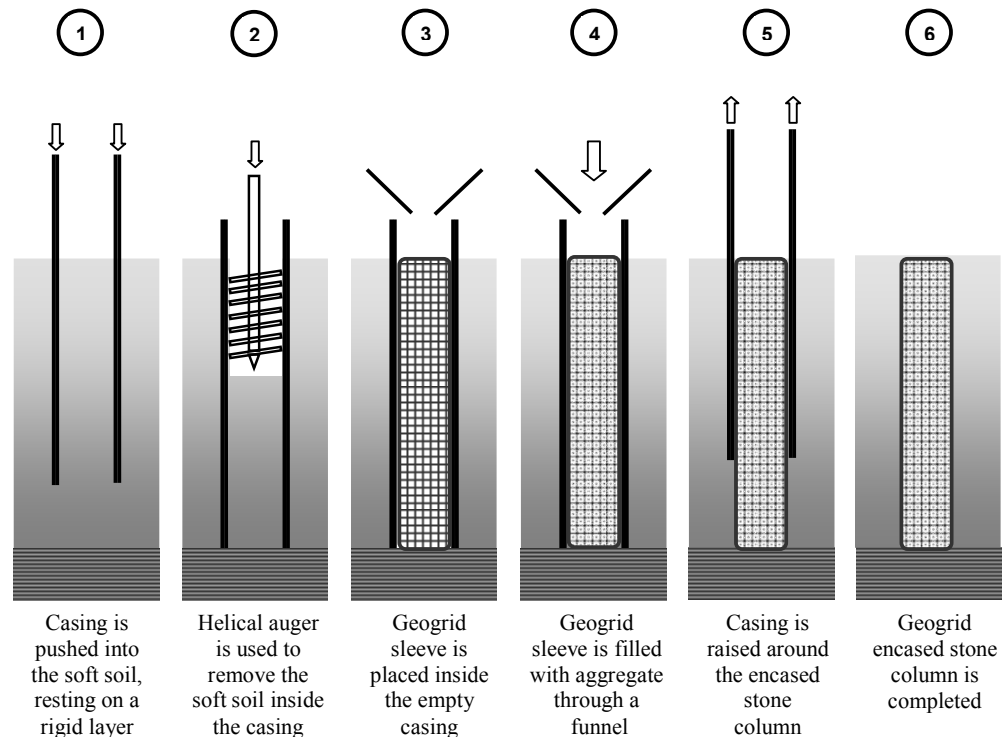


**Figure 7.3:** Replacement installation of geogrid encased stone columns

#### 7.2.7.4 Displacement installation

A displacement method of installation has been successfully trialled in the past as part of the laboratory column testing and installation trial presented by Trunk et al. (2004). The method comprised bottom-feed column installation, undertaken by contractor Keller Grundbau GmbH. Welded geogrid encasement sleeves were closed at the base (or toe), by welding extra flaps of geogrid together. A photograph of these prefabricated geogrid encasement sleeves is presented in Figure 7.4.

The vibroflot was then raised, allowing the sleeve to be placed around it. Following this, the encased vibroflot was lowered on top of a thin steel plate resting on the ground, which acted to protect the base of the encasement from any debris as it was vibrated into the ground. Once the encasement had been pushed to the founding level, it was filled in lifts with aggregate. Photographs of this installation process (with closed-toe encasement) are presented in Figure 7.5. It should be noted that using this technique, little protection was provided to the perimeter of the encasement during penetration. Horizontal ribs were



located on the inside of the sleeve to prevent them being torn away from the vertical ribs as the encasement was pushed into the ground during installation.



**Figure 7.4:** Prefabricated geogrid sleeves (welded)

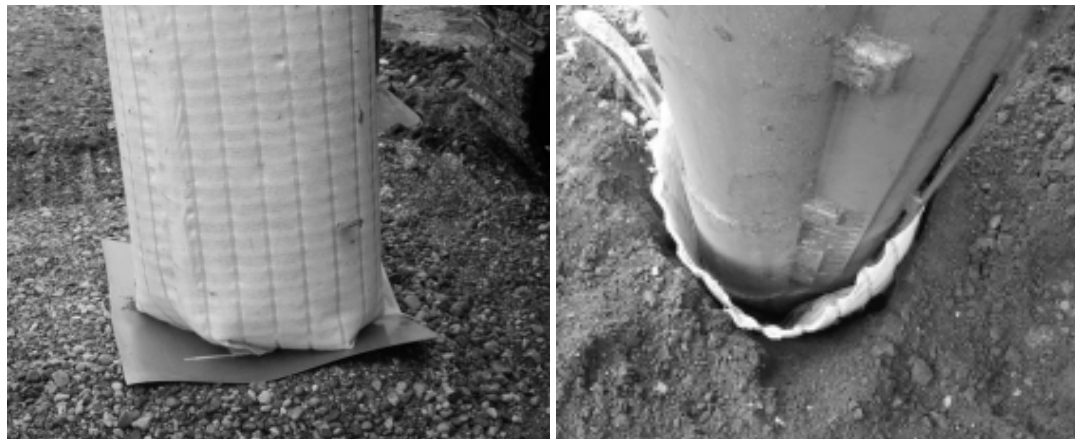


**Figure 7.5:** Displacement installation method during site trial

To extend this method to use with overlapped encasement, rather than welded, the base of the encasement would need to be closed. This could be done in a similar manner to the welded sleeves, where extra flaps of geogrid or a geogrid base plate could be joined using cable ties. However, the method requires a bottom-feed system. It also requires that the column diameter is only slightly larger than the vibroflot diameter, generally about 0.45 m. This may not be suitable in some cases.

Alternatively, a displacement method similar to that used for installing GECs may be adopted to install geogrid encased stone columns. The technique is outlined in Chapter 2. However, it is likely that specialised equipment would need to be developed specifically for use with geogrid encased stone columns.

#### 7.2.7.5 Installation of partially encased columns

Partial encasement is probably not suited to the displacement method of column installation using the bottom-feed system. It is difficult to envisage the encasement being placed around only the upper section of the vibroflot without it being damaged during penetration. Partial encasement could be used in conjunction with a replacement method with relative ease. Rather than placing the encasement in the casing before it is filled, the casing would be partially filled with aggregate (to a level dependent on the length of partial encasement). The encasement sleeve would then be placed inside the casing and the remainder filled with aggregate.

#### 7.2.8 Cost

At the time of writing this thesis, it was estimated that geogrid suited to encasement applications may cost about AUD \$5/m<sup>2</sup> – AUD \$10/m<sup>2</sup> shipped to site (depending on supplier, order size, etc.). On this basis, full-length column encasement may add additional costs to a medium-size stone column project in the order of 10% to 15%. These additional costs are likely to be reduced on larger projects and may be offset by a reduction in the number of stone columns required.

### 7.3 Further research

Further research is required to investigate various aspects of encased stone column behaviour not covered in the present research. In particular, a site trial is required to confirm that geogrid encased stone columns can be successfully installed and loaded. It is recommended that a site trial comprising installation of crushed rock columns encased with Secugrid 120/120 Q6 geogrid is undertaken, as set out in earlier sections.

### 7.3.1 Scope of further research

Although several aspects of encased column behaviour could not be adequately investigated in the present study, further investigation may provide greater understanding of encased column behaviour and help to refine encased column design. Most aspects considered to require further investigation arose from the medium-scale tests and are summarised below:

- (i) Cutting from angular rock during loading, and damage caused to the encasement during installation may reduce geogrid tensile capacity. The magnitude of this reduction is likely to depend on the types of geogrid and stone aggregate used. The reduction in capacity should therefore be investigated for the different combinations of materials likely to be used in practice. This would need to be assessed with some confidence for design purposes.
- (ii) Investigating whether smaller aggregates such as fine crushed rock gravel and coarse sand are suited to the method of overlap in confined conditions. Provided that sufficient interlock is achieved, smaller aggregates may be preferred to coarser aggregates because they are less likely to damage the geogrid. Furthermore, smaller aggregates may be more readily available on some sites. This research may be extended to include rounded gravels (although they are typically more difficult and expensive to source).
- (iii) Investigating whether uniaxial geogrids are suited to the method of overlap in confined conditions. This may include an investigation into the role of vertical rib strength and stiffness for encasement applications using the method of overlap. Uniaxial geogrids generally have greater strength than biaxial geogrids (at least in the hoop direction) and may provide a high strength option for encasement applications.
- (iv) Investigating whether horizontal ribs placed on the outside of the encasement increase the capacity of an encased column, as was observed in initial medium-scale tests. Trials using this configuration may also be used to investigate whether damage is caused to the encasement during installation.
- (v) An investigation into the minimum number of welded junctions required in the section of overlap and whether this varies significantly between biaxial and uniaxial geogrids and geogrids of different strength.

Should the method of geogrid encasement be regularly implemented on site, future research may also be directed at investigating whether geogrid encasement is sensitive to certain soil types and environmental conditions. Research may also be directed at the long-term strain behaviour of geogrid encasement and how this may affect encased column performance and design.

### 7.3.2 Scope of proposed testing

For the aspects of encased column behaviour identified in the scope of further research, such research may comprise laboratory testing, site testing or a combination of both. Further testing may be undertaken following the successful completion of a site trial. Alternatively, if the scope of the initial site trial is sufficient, these aspects may be incorporated into it. The proposed scope of testing used to investigate these aspects is presented in Table 7.1.

**Table 7.1:** Proposed future laboratory and site testing

aspect	proposed testing	
	laboratory	site*
Strength reduction from cutting and installation effects	Further medium-scale tests using 20/50 mm rubble to develop confidence intervals. May comprise tests with Secugrid 80/80 and 120/120 Q6 products.	Isolated columns installed using replacement and displacement methods and loaded to failure, including: <ul style="list-style-type: none"> <li>• 20/50 mm rubble column encased with Secugrid 120/120 Q6 (100% overlap).</li> <li>• 14/10 mm gravel column encased with Secugrid 120/120 Q6 (100% overlap).</li> <li>• Sand column encased with Secugrid 120/120 Q6 (100% overlap).</li> <li>• Rounded gravel column encased with Secugrid 120/120 Q6 (100% overlap).</li> </ul> The same tests may also be undertaken using Secugrid 80/80 Q6 encasement for comparison.

aspect	proposed testing	
	laboratory	site*
Suitability of small aggregates to the method of overlap	Not practical unless columns are confined.	Included in site testing outlined above (testing of strength reduction associated with installation damage).
Suitability of uniaxial geogrids to the method of overlap	Not practical unless columns are confined.	<p>Isolated columns installed using replacement and displacement methods and loaded to failure, including:</p> <ul style="list-style-type: none"> <li>• 20/50 mm rubble column encased with Secugrid 200/40 R6 (100% overlap).</li> <li>• 20/50 mm rubble column encased with Secugrid 120/40 R6 (100% overlap).</li> <li>• 14/10 mm gravel column encased with Secugrid 200/40 or 120/40 R6 (100% overlap), provided smaller aggregates are effective with biaxial geogrids.</li> </ul>
Effect of horizontal ribs on outside for both column capacity and installation	<p>Further medium-scale testing using 20/50 mm rubble.</p> <p>Identical columns should be prepared using Secugrid 120/120 or 80/80 Q6 encasement (100% overlap).</p> <p>One set should have ribs on the outside and the other set have ribs on the inside. Behaviour of the two sets can then be compared.</p>	<p>Isolated column installation tests using both replacement and displacement techniques. Identical columns (say 20/50 mm rubble encased with Secugrid 120/120 Q6) should be installed with horizontal ribs on the inside and outside of the encasement. Soil around the upper section of the column should then be excavated to observe any damage to the encasement. Columns should not be loaded prior to excavation so that installation damage can be separated from that sustained during loading. Secugrid R6 products (uniaxial) may also be tested depending on the results of load tests.</p>

aspect	proposed testing	
	laboratory	site*
Minimum number of welded junctions	<p>Further medium-scale testing using 20/50 mm rubble.</p> <p>Column diameter, height and percent overlap should be varied to assess the minimum number of welded junctions required.</p> <p>Tests should be undertaken using Secugrid Q6 products, probably 80/80 and 120/120.</p> <p>Data on the junction strength of different geogrids will be required.</p>	Isolated column tests are dependent on the results of further laboratory testing.

---

\* All site tests to be conducted on fully encased columns

### 7.3.3 Instrumentation

For the initial site trial or for the site testing outlined above, isolated column load tests are proposed. This is because they are typically cheaper to perform than load tests on a larger group of columns (which generally require construction of an embankment or load platform). Isolated columns may be loaded to failure using a variety of techniques. Instrumentation of an isolated column may comprise strain gauging of horizontal ribs in the upper section of the column, attached by excavating adjacent to the column after installation. The method used to measure column load would be dependent on the method of column loading adopted. Settlement may be measured by accurate survey.

Column groups are unlikely to be tested to failure and therefore instrumentation would need to be more comprehensive. Group columns may be loaded with soil fill, in the form of an embankment. Depending on the scale of the trial area, instrumentation may comprise the following:

- Strain gauging in the upper section of the column, installed by excavating adjacent to the upper section of the column. The strain gauges may provide an indication of the hoop forces supported by the encasement.

- Load cells in the upper section of several columns to measure the proportion of the surcharge pressure supported by each column.
- Load cells at several (near-surface) locations in the surrounding clay to measure the proportion of the surcharge pressure supported by the clay.
- Pore pressure transducers installed at several different locations and depths in the surrounding clay to measure the rate of excess pore pressure dissipation.
- Settlement plates located at the surface of several columns and the surface of the clay to measure total settlement and to assess the load-settlement behaviour of columns.
- Magnetic extensometers at several locations in the surrounding clay to measure the depth at which most settlement is occurring.

Following successful site testing of geogrid encased stone columns, further testing may also be used to confirm the results of the numerical parametric study set out in Chapter 6 and to confirm that the method of partial encasement is effective in steadily reducing settlement.

## 8 Conclusions

---

The research presented in this thesis was used to investigate whether geogrid encased stone columns may provide a practical method of ground improvement, particularly in very soft and extremely soft soil. A similar method using geotextile encased columns (GECs) has been used on numerous projects in recent years and is well established in Europe. However, the technique can result in relatively large settlements and is limited to use with certain material types. Investigation into the use of geogrid encasement may provide an alternative to GECs and broaden the appeal of geosynthetic encased columns.

The research focussed on the practical aspects of encased column construction and performance, with the aims including:

- (i) To investigate if the method of geogrid encasement provided a suitable alternative to geotextile encasement.
- (ii) To investigate the types of soil, column aggregate and geogrid best suited to the technique.
- (iii) To investigate the likely performance of geogrid encased stone columns and the properties that had the greatest impact on column behaviour.
- (iv) To investigate practical methods of column construction.

These aims were investigated using a four-stage approach which combined small-scale laboratory testing, numerical simulation of the small-scale tests, medium-scale laboratory testing and scaled-up numerical modelling. The findings of this four-stage investigation are described and discussed in Chapter 7, with consideration also given to possible construction techniques, practical applications and further research and testing. The conclusions of this research, related to the project aims, are listed below.

1. Geogrid encased stone columns are likely to provide a practical and effective method of ground improvement in extremely soft to soft soils ( $s_u$  less than about 15 kPa). Columns tested in small-scale significantly stiffened the behaviour of very soft clay, a result that was replicated using numerical analysis. Medium-scale testing indicated that the technique was effective with real geogrid



materials and the type of crushed rock typically used in conventional stone column applications.

2. Numerical analysis indicates that geogrid encasement may also be used to improve the performance of conventional stone columns in stiffer soils.
3. The method of geogrid encasement is likely to provide a stiffer alternative to GECs. Hoop strains (about 0.5%) required to mobilise tension forces in the geogrid are generally lower than for GECs. In addition, coarser aggregates may be more heavily compacted using the more robust geogrid encasement.
4. Full-length geogrid encasement may be suited to both group and isolated column applications, although isolated column use may be limited by cost.
5. A site trial is recommended for confirmation of the encasement technique, in particular, to investigate aspects such as installation and load-settlement behaviour.
6. Geogrid encased stone columns may be constructed using the method of overlap, where the circumference of the encasement is overlapped by a certain amount. Interlock between the aggregate and overlapped section of the encasement is likely to provide a level of fixity similar to welding. The encasement may be temporarily held in position (for installation) by using cable ties.
7. The method of overlap provides a simple and practical method for encasement construction on site, and is likely to be significantly cheaper than the alternative of mechanically welding encasement (where a welding frame would generally need to be mobilised to site).
8. The method of overlap appears to be primarily suited to biaxial geogrids. The best performed columns were constructed from Secugrid® 120/120 Q6 geogrid (with 100% circumferential overlap) and crushed rock aggregate graded between 20 mm and 50 mm. These materials (depending on availability) and encasement configuration are recommended for use in an initial site trial.
9. A minimum number of welded junctions may be required in the section of overlap to prevent the encasement from unravelling. Further research is required to confirm and better investigate this aspect. For the proposed site testing, 100% circumferential overlap appears to be sufficient in most cases.
10. Other geogrids (including uniaxial and triangular-shaped geogrids) and smaller aggregates may also be suited to the method of overlap but were not as effective in unconfined testing. These materials should be tested on site to determine their suitability.

11. Angular crushed rock may damage the encasement by cutting into the ribs during column loading, thereby reducing geogrid strength. The impact of cutting was reduced for higher strength geogrids, probably because of the thicker rib cross-sections. For Secugrid 120/120 Q6, tension capacity was reduced by up to about 35%. A factor of safety would need to be considered in design, based on the results of further testing.
12. Although smaller aggregates did not interlock as well with the overlapped encasement in unconfined tests, they did not cause damage to the geogrid like coarser aggregates. Site testing is recommended to investigate whether interlock using gravels and coarse sands improves in confined conditions. If so, smaller aggregates may provide a suitable column material.
13. Combined geotextile/geogrid encasement (such as Combigrid<sup>®</sup>) is not suited to the method of overlap.
14. Settlement of geogrid encased stone columns groups is likely to be reduced most effectively by increasing the replacement ratio, increasing the column stiffness and strength (through greater compaction and increased friction angle) and increasing the encasement stiffness. By changing these properties, settlement may be tailored to meet different design requirements.
15. Encasement hoop forces are likely to be reduced most effectively by reducing the surcharge or column load, increasing the replacement ratio, using encased columns in stiffer soils or using stiffer column materials.
16. When compared to the behaviour of the untreated soil, fully encased stone columns may reduce settlement by between about 50% and 95%, depending on properties such as replacement ratio and geogrid stiffness. For columns encased with material of similar strength and stiffness to Secugrid 120/120 Q6, at a replacement ratio of about 25%, settlement reduction is likely to be in the order of 90%. This behaviour may bring the performance of the technique in line with stiffer ground improvement techniques such as soil mixing.
17. The reduction in settlement (when compared to untreated soil) achieved using geogrid encased stone columns is likely to be significantly greater than that achieved using conventional stone columns.
18. The method of partial encasement, where the percent encased length of a column is reduced, may be used to vary column stiffness. This may be used to tailor settlement to design requirements, in a similar manner to changing replacement ratio and geogrid stiffness. It is probably not suited to isolated columns.

## References

---

- Adikari, G. S. N. (1981). "Investigations into the behaviour of earth and rockfill dams." *PhD Thesis*, Monash University.
- Al-Joulani, N. (1995). "Laboratory behaviour of sleeve-reinforced stone columns." *Proceedings of Geosynthetics '95*, Nashville, Tennessee, USA, 3, 1111-1123.
- Alexiew, D., Brokemper, D., and Lothspeich, S. (2005). "Geotextile Encased Columns (GEC): Load capacity, geotextile selection and pre-design graphs." *Proceedings of GeoFrontiers 2005*, Austin, Texas, United States, 497-510.
- Alexiew, D., Horgan, G. J., and Brokemper, D. (2003). "Geotextile encased columns (GEC): load capacity and geotextile selection." *Proceedings of BGA International Conference on Foundations: Innovations, observations, design and practice*, Dundee, Scotland, 81-90.
- Anantasech, C. (1984). "Stress-deformation and strength of soft alluvial clay." *PhD Thesis*, Monash University.
- Ayadat, T., and Hanna, A. M. (2005). "Encapsulated stone columns as a soil improvement technique for collapsible soil." *Ground Improvement*, 9(4), 137-147.
- Balaam, N. P., and Booker, J. R. (1981). "Analysis of rigid rafts supported by granular piles." *International Journal for Numerical and Analytical Methods in Geomechanics*, 5, 379-403.
- Balaam, N. P., and Booker, J. R. (1985). "Effect of stone column yield on settlement of rigid foundations in stabilized clay." *International Journal for Numerical and Analytical Methods in Geomechanics*, 9, 331-351.
- Balaam, N. P., Brown, P. T., and Poulos, H. G. (1977). "Settlement analysis of soft clays reinforced with granular piles." *Proceedings of 5th SouthEast Asian Conference on Soil Engineering*, Bangkok, Thailand, 81-92.
- Balaam, N. P., and Poulos, H. G. (1983). "The behaviour of foundations supported by clay stabilised by stone columns." *Proceedings of 8th European Conference on Soil Mechanics and Foundation Engineering*, Helsinki, Finland, 1, 199-204.

- Barksdale, R. D., and Bachus, R. C. (1983). "Design and construction of stone columns: Final Report SCEGIT-83-104." Federal Highway Administration, Washington D.C. 20590.
- Baumann, V., and Bauer, G. E. (1974). "The performance of foundations on various soils stabilized by the vibro-compaction method." *Canadian Geotechnical Journal*, 11, 509-530.
- Bjerrum, L. (1972). "Embankments on soft ground: State of the art report." *Proceedings of ASCE Specialty Conference on Performance of Earth and Earth-supported Structures*, Lafayette, IN, 2, 1-54.
- Brinkgreve, R. B. J., and Broere, W. (2004). "PLAXIS 2D - Version 8 (User Manual)." Technical University Delft, Netherlands.
- Cai, F., and Li, G.-X. (1994). "Granular piles reinforced with geosynthetics." *Proceedings of 5th International Conference on Geotextiles, Geomembranes and Related Products*, Singapore, 1, 347-350.
- Charles, J. A. (2002). "Ground improvement: the interaction of engineering science and experience-based technology." *Geotechnique*, 52(7), 527-532.
- Charles, J. A., and Watts, K. S. (1983). "Compressibility of soft clay reinforced with granular columns." *Proceedings of 8th European Conference on Soil Mechanics and Foundation Engineering*, Helsinki, Finland, 1, 347-352.
- Cheung, K. C. (1998). "Geogrid reinforced light weight embankment on stone columns." *NZGS Symposium Roding Geotechnics*, 273-278.
- Clemente, J. L. M., and Davie, J. R. (2000). "Stone columns for settlement reduction." *Proceedings of International Conference on Geotechnical and Geological Engineering, GeoEng 2000*, Melbourne, Australia.
- Craig, W. H., and Al-Khafaji, Z. A. (1997). "Reduction of soft clay settlement by compacted sand columns." *Proceedings of 3rd International Conference on Ground Improvement Geosystems*, London, England, 219-224.
- Day, R., and Woods, P. (2007). "Verification of consolidation parameters of a near-normally consolidated clay by back analysis of an instrumented, wick-drained

reclamation." *Proceedings of 10th ANZ Conference on Geomechanics*, Brisbane, Australia, 105-111.

De Mello, L. G., Mondolfo, M., Montez, F., Tsukahara, C. N., and Bilfinger, W. (2008). "First use of geosynthetic encased sand columns in South America." *Proceedings of 1st Pan-American Geosynthetics Conference*, Cancun, Mexico, 1332-1341.

Duncan, J. M., and Chang, C.-Y. (1970). "Nonlinear Analysis of Stress and Strain in Soil." *ASCE, Journal of the Soil Mechanics and Foundation Division*, 96, 1629-1653.

Ervin, M. C. (1992). "Engineering properties of Quaternary Age sediments of the Yarra Delta." *In: Engineering Geology of Melbourne*, A.A. Balkema, Rotterdam, 245-259.

Gachet, P., Klubertanz, G., Vulliet, L., and Laloui, L. (2003). "Interface Behaviour of Unsaturated Soil with Small-scale Models and Use of Image Processing Techniques." *Geotechnical Testing Journal*, 26(1), 1-10.

Ghionna, V., and Jamiolkowski, M. (1981). "Colonne di ghiaia." *X Ciclo di conferenze dedicate ai problem di meccanica dei terreni e ingegneria delle fondazioni metodi di miglioramento dei terreni*, Politecnico di Torino Ingegneria, atti dell'istituto di scienza delle costruzioni(507).

Gohl, W. B., Jefferies, M. G., Howie, J. A., and Diggle, D. (2000). "Explosive compaction: design, implementation and effectiveness." *Geotechnique*, 50(6), 657-665.

Goughnour, R. R. (1983). "Settlement of vertically loaded stone columns in soft ground." *Proceedings of 8th European Conference on Soil Mechanics and Foundation Engineering*, Helsinki, Finland, 1, 235-240.

Goughnour, R. R., and Bayuk, A. A. (1979). "Analysis of stone column-soil matrix interaction under vertical load." *Proceedings of International Conference on Soil Reinforcement*, Paris, France, 271-277.

Gray, D. H., and Al-Refeai, T. (1986). "Behaviour of fabric-versus-fibre reinforced sand." *Journal of Geotechnical Engineering Division*, 112(8), 804-820.

Greenwood, D. A. (1970). "Mechanical improvement of soils below ground surface." *Ground Engineering Conference*, Inst Civ Eng, London, 11-22.

- Greenwood, D. A. (1991). "Load tests on stone columns." *Deep Foundation Improvements: Design, Construction and Testing*, Las Vegas, Nevada, USA, 148-171.
- Greenwood, D. A., and Kirsch, K. (1983). "Specialist ground treatment by vibratory and dynamic methods: State of the art." *Proceedings of Advances in Piling and Ground Treatment for Foundations*, Institute of Civil Engineers, London, England, 17-45.
- Han, J., and Ye, S. L. (2001). "Simplified method for consolidation rate of stone column reinforced foundations." *Journal of Geotechnical and Geoenvironmental Engineering*, 127(7), 597-603.
- Heerten, G. (2006). "Personal communication, 16/08/2006 (NAUE GmbH)."
- Heerten, G., and Ewert, W. F. (2004). "Welded geogrids as new generation of reinforcing products in geotechnical applications." *Proceedings of ECI International Conference on the use of Geosynthetics in Soil Reinforcement and Dynamics*, Dresden, Germany, 85-102.
- Heerten, G., Paul, A., Reuter, E., and Volzke, B. (2004). "(In German) Geogitterummantelte Mineralstoffsäulen - ein neues System für Gründung und Baugrundverbesserung." *Vorträge der Baugrundtagung*, Leipzig, Germany(205-212).
- Holtz, R. D., and Kovacs, W. D. (1981). "An introduction to geotechnical engineering." *Prentice-Hall, Inc.*, New Jersey.
- Hughes, J. M. O., and Withers, N. J. (1974). "Reinforcing of soft cohesive soils with stone columns." *Ground Engineering* (May), 42-49.
- Hughes, J. M. O., Withers, N. J., and Greenwood, D. A. (1975). "Field trial of the reinforcing effect of a stone column in soil." *Geotechnique*, 25(1), 31-44.
- Ionescu, D. (2004). "Evaluation of the engineering behaviour of railway ballast." *PhD Thesis*, University of Wollongong.
- Kim, B.-J., Kim, Y.-S., and Shin, D.-H. (2005). "Shear strength and one-dimensional compression characteristics of granitic gneiss rockfill dam material." *Journal of the KGS*, 21(7), 31-42.

- Madhav, M. R., Alamgir, M., and Miura, N. (1994). "Improving granular column capacity by geogrid reinforcement." *Proceedings of 5th International Conference on Geotextiles, Geomembranes and Related Products*, Singapore, 1, 351-356.
- Malarvizhi, S. N., and Ilamparuthi, K. (2007). "Comparative study on the behaviour of encased stone column and conventional stone column." *Soils and Foundations - Japanese Geotechnical Society*, 47(5), 873-885.
- McKelvey, D., and Sivakumar, V. (2000). "A review of the performance vibro stone column foundations." *Proceedings of Third International Conference on Ground Improvement Techniques*, Singapore, 245-254.
- McKelvey, D., Sivakumar, V., Bell, A., and Graham, J. (2004). "Modelling vibrated stone columns in soft clay." *Geotechnical Engineering*, 157(3), 137-149.
- McKenna, J. M., Eyre, W. A., and Wolstenholme, D. R. (1975). "Performance of an embankment supported by stone columns in soft ground." *Geotechnique*, 25(1), 51-59.
- Mitchell, J. K. (1981). "Soil Improvement: State of the art report." *10th International Conference on Soil Mechanics and Foundation Engineering*, Stockholm, Sweden, 4, 509-565.
- Mitchell, J. M., and Jardine, F. M. (2002). *A guide to ground treatment*, CIRIA publication C573, London.
- Muir-Wood, D., Hu, D., and Nash, D. F. T. (2000). "Group effects in stone column foundation: model tests." *Geotechnique*, 50(6), 689-698.
- Munfakh, G. A., Abramson, L. W., Barksdale, R. D., and Juran, I. (1987). *In-situ ground reinforcement*, Soil Improvement – A Ten Year Update: Geotechnical Special Publication No. 12.
- Murugesan, S., and Rajagopal, K. (2006). "Numerical analysis of geosynthetic encased stone column." *Proceedings of 8th International Conference on Geosynthetics*, Yokohama, Japan, 1681-1684.
- Murugesan, S., and Rajagopal, K. (2007). "Model tests on geosynthetic-encased stone columns." *Geosynthetics International*, 14(6), 346-354.

- Nods, M. (2002). "Put a sock in it " *Ground Engineering* (Dec), 25.
- Oldecop, L. A., and Alonso, E. E. (2001). "A model for rockfill compressibility." *Geotechnique*, 51(2), 127-139.
- Paul, A., and Ponomarjow, A. (2004). "The bearing behaviour of geogrid reinforced crushed stone columns in comparison to non-reinforced concrete pile foundations." *Proceedings of Third European Geosynthetics Conference; Geotechnical Engineering with Geosynthetics*, Munich, Germany, 1, 285-288.
- Priebe, H. J. (1976). "Abschätzung des setzungsverhaltens eines durch stopfverdichtung verbesserten baugrundes (In German)." *Die Bautechnik* 53(Heft 5), 160-162.
- Priebe, H. J. (1995). "Design of vibro replacement." *Ground Engineering*, 28(10), 31-37.
- Pulko, B., and Majes, B. (2005). "Simple and accurate prediction of settlements of stone column reinforced soil." *Proceedings of 16th International Conference on Soil Mechanics and Geotechnical Engineering*, Osaka, Japan, 1401-1404.
- Raithel, M., and Kempfert, H.-G. (1999). "Bemessung von geokunststoffummantelten Sandsäulen (In German)." *Die Bautechnik*, 76(Heft 11), 983-991.
- Raithel, M., and Kempfert, H.-G. (2000). "Calculation Models for Dam Foundations with Geotextile Sand Columns." *Proceedings of International Conference on Geotechnical and Geological Engineering, GeoEng 2000*, Melbourne, Australia.
- Raithel, M., and Kempfert, H.-G. (2002). "Experiences on Dike Foundations and Land Fills on Very Soft Soils." *Proceedings of International Workshop ISSMGE - Technical Committee TC 36 "Foundation in Difficult Soft Soil Conditions"*, Mexico City, Mexico, 176-181.
- Raithel, M., Kirchner, A., Schade, C., and Leusink, E. (2005). "Foundation of construction on very soft soils with geotextile encased columns – state of the art." *Proceedings of GeoFrontiers 2005*, Austin, Texas, United States.
- Raju, V. R. (1997). "The behaviour of very soft soils improved by vibro replacement: Technical paper 12-64E." *Ground Improvement Conference*, London, England.



- Schanz, T., Vermeer, P. A., and Bonnier, P. G. (1999). "Formulation and verification of the Hardening-Soil Model." *R.B.J. Brinkgreve: Beyond 2000 in Computational Geotechnics*, Balkema, Rotterdam, 281-290.
- Sharma, J. S. (1998). "A study of the behaviour of geogrid reinforced stone columns." *Proceedings of Sixth International Conference on Geotextiles, Geomembranes, related products and associated technologies*, Atlanta, United States, 877-882.
- Sharma, R. S., Phani Khumar, B. R., and Nagendra, G. (2004). "Compressive load response of granular piles reinforced with geogrids." *Canadian Geotechnical Journal*, 41(187-192).
- Sidak, N., Strauch, G., and Wehr, J. (2004). "Installation of geotextile covered stone columns by the Keller depth vibrator techniques." *ASEP GI, International symposium on ground improvement*, Paris, France, 269-284.
- Sivakumar, V., McKelvey, D., Graham, J., and Hughes, D. (2004). "Triaxial tests on model sand columns in clay." *Canadian Geotechnical Journal*, 41(2), 299-312.
- Sivakumar, V., McNeill, J., and Coyle, A. (2002). "Performance of vibro stone column foundations under triaxial loading." *Proceedings of 4th International Conference on Ground Improvement Techniques*, Kuala Lumpur, Malaysia, 683-688.
- Sloan, S. W., and Randolph, M. F. (1982). "Numerical prediction of collapse loads using finite element methods." *International Journal for Numerical and Analytical Methods in Geomechanics*, 6, 47-76.
- Stark, T. D., and Yacyshyn, B. M. (1991). *Specifications for constructing and load testing stone columns in clays*, Deep Foundation Improvements: Design, Construction and Testing, ASTM Special Technical Publication 1089.
- Tan, S. A. (2007). "Personal communication, 18/04/2007."
- Tan, S. A., and Oo, K. K. (2005). "Finite element modeling of stone columns - a case history." *Proceedings of 16th International Conference on Soil Mechanics and Geotechnical Engineering*, Osaka, Japan, 1425-1428.
- Tan, S. A., Tjahyono, S., and Oo, K. K. (2008). "Simplified Plane-Strain Modeling of Stone Column Reinforced Ground." *Journal of Geotechnical and Geoenvironmental Engineering*, 134(2), 185-194.

- Taylor, D. W. (1948). "Fundamentals of Soil Mechanics." *New York*, John Wiley.
- Trunk, U., Heerten, G., Paul, A., and Reuter, E. (2004). "Geogrid wrapped vibro stone columns." *Proceedings of Third European Geosynthetics Conference; Geotechnical Engineering with Geosynthetics*, Munich, Germany, 1, 289-294.
- Van Impe, W., and De Beer, E. (1983). "Improvement of settlement behaviour of soft layers by means of stone columns." *Proceedings of 8th European Conference on Soil Mechanics and Foundation Engineering*, Helsinki, Finland, 309-312.
- Van Impe, W. F. (1989). *Soil improvement techniques and their evolution*, A.A Balkema, Rotterdam, Netherlands.
- Van Impe, W. F., and Rouck, J. D. (1985). "Soil Improvement in Belgium." *Proceedings of 3rd International Geotechnical Seminar: Soil Improvement Methods*, Singapore, 201-228.
- Vermeer, P. A. (2008). "Personal communication, 04/09/2008, (2nd International Workshop on Soft Soils - Focus on Ground Improvement)."
- Vermeer, P. A., and Brinkgreve, R. B. J. (1998). "Plaxis finite element code for soil and rock analyses." Balkema, Rotterdam.
- Vesic, A. S. (1972). "Expansion of cavities in infinite soil mass." *Journal of the Soil Mechanics and Foundation Division*, SM3, 265-290.
- Wallays, M., Delapierre, J., and Van Den Poel, J. (1983). "Load transfer mechanism in soils reinforced by stone or sand columns." *Proceedings of 8th European Conference on Soil Mechanics and Foundation Engineering*, Helsinki, Finland, 313-317.
- Wehr, J. (2008). "Personal communication, 04/09/2008 (Keller Grundbau GmbH)."
- Zhigang, Z., Qisens, Z., and Jianlong, Z. (2001). "Analysis of improved ground with geonet reinforced stone columns: Landmarks in Earth Reinforcement." *Proceedings of International Symposium on Earth Reinforcement*, Fukuoka, Japan, 635-638.

## APPENDICES

**APPENDIX A.1**  
**(small-scale test objectives and considerations)**

## **1 Column groups**

Stone column groups are commonly installed beneath embankments, tank bases and other lightly loaded structures with large footprints. Column group applications form the majority of stone column projects. Towards the centre of such applications, stone columns are laterally confined by adjacent columns, creating roughly oedometric conditions. As a result, the unit-cell concept is commonly adopted to simplify group column behaviour to that of a single column surrounded by clay within its zone of influence. A single sand column installed at the centre of a cylindrical test cell and surrounded by clay are generally considered to represent the boundary conditions imposed by unit-cell idealisation. A rigid, circular footing equal in diameter to that of the cell is used to load the column and surrounding soil.

A primary aim of this study was to investigate column group behaviour. Two cells were constructed to simulate column group behaviour using unit-cell idealisation. The cells were constructed from stainless steel measuring approximately 155 mm in internal diameter. A sand column measuring 51 mm in diameter was installed at the centre of the cell. The geometry of the cell and column were dependent on the availability of suitable materials. A 51 mm diameter column within a 155 mm diameter cell equated to a replacement ratio,  $A_r$ , of about 11%. This was at the lower end of the range generally adopted for full-scale stone columns, but due to the controlled nature of laboratory testing, was considered adequate for assessment of column behaviour. Following the completion of testing, numerical modelling was undertaken to further explore the impact of replacement ratio on column behaviour.

## **2 Isolated columns**

In site applications, isolated columns are rarely used for ground improvement, particularly in Australia. However, stone columns may occasionally be used to support small pad footings and strip footings. In addition, columns located at the edge of groups may behave more like isolated columns than unit-cell idealised columns. The behaviour of isolated columns is also well documented and although it may have little practical significance, the behaviour of isolated columns was investigated for comparison to previous research.

Based on research undertaken by Hughes and Withers (1974), model sand columns act independently when placed more than 2.5 diameters apart. Due to material availability, a Perspex cell measuring 143 mm in internal diameter was used for isolated column testing. A sand column measuring 51 mm in diameter was installed at the centre of the cell, equating to a column spacing of about 2.8 diameters. This geometry was considered sufficient to prevent the cell boundary impacting on column behaviour.

To ensure that only the model sand column was loaded, a circular footing measuring 51 mm in diameter was used (the same diameter as the column). This prevented the clay from being loaded, thereby providing additional confinement to the column.

### **3        Staged construction**

Due to time constraints, loading of laboratory models is commonly undertaken using constant displacement techniques. To model a drained state with reasonable accuracy, the load must be advanced at a sufficiently slow rate to prevent the build-up of excess pore pressure within the cohesive material. This rate can be justified theoretically but may be difficult to confirm in practice. However, the most common stone column applications are for the support of structures such as embankments, where construction is completed in stages. Full or partial excess pore pressure dissipation generally occurs between stages, allowing strength gains in the founding materials to be utilised for further loading. In order to replicate this type of construction, staged loading was used for model column tests, allowing complete dissipation of excess pore pressure between stages.

For the unit-cell condition, where column failure was considered unlikely, loading was advanced in increments of about 50 kPa, up to a maximum surcharge pressure of about 300 kPa (roughly corresponding to the maximum surcharge that would be applied to a stone column foundation). This range in stress resulted in about 5 load stages, enabling adequate assessment of the relationship between applied stress and vertical strain. For isolated columns, staged loading was continued until column failure occurred. Due to the nature of isolated column loading, smaller and more frequent load stages were used.

#### **4 Length of geogrid encasement**

As conventional stone columns are loaded, they tend to expand radially. Depending on whether a column acts as part of a group or in isolation, this lateral deformation may vary in magnitude and location. Full-length geosynthetic encasement provides additional lateral confinement to columns, reducing radial deformation and therefore vertical settlement. However, little research has been undertaken to investigate whether partial encasement of only the upper section of a column (where radial expansion may be greater) may provide a similar reduction in settlement. In this study, column tests were undertaken using different percentages of encased length to investigate the impact of partial encasement on column deformation. Tests comprising encasement of the upper 25%, 50% and 75% of the column were undertaken. These tests were compared to results for non-encased and fully-encased columns, for both isolated and group cases.

#### **5 Geogrid properties**

The properties of geogrid, namely the tensile strength and stiffness, are likely to affect the radial deformation of columns and therefore their vertical stress-strain behaviour. To investigate the impact of varying these properties, two different types of material were used. Fibreglass and aluminium were used to simulate the geogrid. The two materials have different stiffness and strength properties.

#### **6 Bonding of the geogrid**

Unlike geotextile encasement, geogrid cannot be extruded to form a seamless cylindrical sleeve during the manufacturing process. To create the geogrid sleeve, rolls of geogrid would need to be shipped to site, cut and shaped into a cylinder and then welded along the overlapped seam. Welding would have to be undertaken using a specialised welding frame that would also have to be shipped to site. The cost associated with shipping the welding frame is likely to limit its use to larger projects. The development of an alternative method to welding was therefore investigated. One alternative option was to create a geogrid sleeve with approximately a half circumference of sacrificial overlap. It was hypothesized that interlock from crushed rock aggregate protruding between

overlapped geogrid ribs may prevent the sleeve from unravelling, providing a level of fixity similar to welding.

To replicate the welding process in small-scale, aluminium and fibreglass meshes were formed into a cylindrical sleeve and bonded using epoxy-resin. The weld was tested to ensure it was of suitable strength. For the method of overlap, the mesh was overlapped by an amount equal to half the column circumference and stitched in place at several locations to maintain shape. It was not known whether interlock could be replicated in small-scale tests but the mesh size and sand particle size were scaled down from full-scale conditions.

## **7 Scale effects**

For the development of a scale-model, all dimensions and stress conditions need to be reduced by an appropriate scale factor. While it was possible to scale down many stone column properties, it was difficult to scale down in-situ earth pressures without using a centrifuge. Even with a centrifuge, it may still have been difficult to accurately model aspects such as column installation. Nevertheless, many authors have previously used scale models to observe stone column behaviour and derive methods for predicting full-scale behaviour. It was expected that a detailed program of small-scale testing combined with numerical modelling would enable adequate assessment of encased column behaviour. Various aspects of scale modelling are described in this section.

### Ratio of column length to column diameter

For field applications, the ratio of column length to column diameter ( $L/D$  ratio) is typically in the range of 3 to 20, with values of about 10 being most common. For this study, columns measuring 51 mm in diameter and about 310 mm long were used, resulting in a  $L/D$  ratio of about 6.

### Replacement ratio

A replacement ratio of about 11% was used for small-scale testing of column groups. This was at the lower end of the 10% to 35% range typically adopted in construction, but was considered suitable given the controlled nature of testing.



#### Ratio of column diameter to average particle size

For field applications, the diameter of a stone column typically ranges from 0.4 m to 1.2 m. The granular column material generally has an average particle size of between 25 mm and 75 mm. This results in a *column diameter – average particle size* ratio of 5 to 50, with values of 20 to 30 being more common. A ratio of about 30 was used for small-scale testing.

#### Ratio of geogrid aperture size to average particle size

The ratio of geogrid aperture size to average particle size is likely to be close to unity. For encased columns, some of the stone column aggregate is likely to protrude from between geogrid ribs. The small-scale mesh was selected with aperture size roughly equal to the average particle size of the sand.

#### Soil strength and stiffness

Geosynthetic encasement is generally suited to cohesive soils, where  $s_u \leq 15$  kPa. A material of similar strength and stiffness to very soft clay was expected to provide a suitable scale-model material. The undrained shear strength of the consolidated kaolin clay was about 5 kPa. In addition, it has similar stiffness, compressibility and void ratio to natural soft clay.

#### Column friction angle and particle shape

Medium dense to very dense crushed rock aggregate is typically used to form stone columns, with a relative density ranging between 60% and 100%. Dense sand (relative density of 90%) with a peak internal friction angle of about  $40^\circ$  was used to replicate the properties of crushed rock in small-scale. The sub-angular sand particles were also considered to adequately represent typical stone column aggregates.

### **8 Stress concentration**

For column groups, the stress concentration ratio represents the ratio of vertical stress in the stone column compared to the vertical stress in the surrounding clay. It is an important design parameter, particularly for the ‘Equilibrium Method’, outlined earlier. In order to measure this parameter, miniature pressure cell transducers were attached to the load plate of one of the steel consolidation cells for some of the column tests. The transducers measured the stress at the surface of the clay and the sand.

**APPENDIX A.2**  
**(cell manufacture, instrumentation and safety)**

## 1 Construction materials and manufacture

The following section describes the materials and manufacturing process undertaken. All fabrication was undertaken within the Monash University Civil Engineering Workshop unless otherwise specified. Based on available construction materials and the proposed end use, two types of cells were developed. The first cell was constructed from Perspex and used to test isolated columns. The second type of cell, of which two were assembled, was constructed from stainless steel and used to test column groups using unit-cell idealisation.

### Perspex cell

The Perspex cell comprised the following components:

- Perspex cylinder measuring 550 mm long and 143 mm in internal diameter (with 9 mm wall thickness). The Perspex cylinder was bored and polished to ensure constant diameter along the full length.
- Aluminium base plate measuring 260 mm diameter and 30 mm thick. A 10 mm deep groove was machined into the base plate to house an O-ring on which the Perspex cylinder would be seated and sealed. A single drainage channel with tap was fitted to the base plate to control drainage. 6 No. holes 11 mm in diameter were drilled and threaded to accommodate tie rods.
- Aluminium top plate measuring 260 mm diameter and 30 mm thick. A 5 mm deep groove was machined within the plate to house an O-ring. The plate was seated on the Perspex cylinder and sealed. Holes were drilled and threaded within the plate to accommodate a pressure relief valve and air pressure inlet tap. A 25 mm diameter hole was machined at the centre of the plate to house the piston shaft. 6 No. holes were also drilled to accommodate tie rods.
- Brass guide which was bolted to the upper side of the top plate and used to guide movement of the piston shaft. The guide had an internal diameter of 25 mm. Grooves were machined at the base of the guide and within the internal surface to house O-rings used to seal the top plate and piston shaft, respectively.
- Aluminium piston measuring 143 mm in diameter and 40 mm thick. 2 No. grooves were machined into the side of the piston to house O-rings used to seal the piston against the internal surface of the Perspex cylinder. A 19 mm hole was drilled at the centre of the piston to allow drainage through the centre.

- Hollow stainless steel piston shaft measuring 400 mm long, 25 mm outside diameter with 3 mm wall thickness. The shaft was welded to a plate which was bolted to the piston and sealed with an O-ring. The top of the shaft was threaded internally. A Swagelock tap was fixed to the top to control drainage.
- 2 No. brass porous plates measuring 143 mm in diameter and 4.5 mm thick. One plate was placed on the aluminium base plate and one plate was bolted to the underside of the piston.
- Solid Stainless steel tie rods measuring 580 mm long and 11 mm diameter. Tie rods were threaded at each end. The top end of each tie rod was threaded and glued into steel reinforced plastic knobs.
- Steel bracket bolted to the aluminium top plate. The bracket was used to mount a string potentiometer (stringpot) gauge, used to measure piston displacement.
- Solid steel rod measuring 5 mm in diameter and 150 mm long. The rod was attached to the top end of the piston shaft and used to fix the retractable string connector of the stringpot gauge.
- Stainless steel small footing measuring 50 mm long and 51 mm diameter. A 19 mm hole was machined at the centre of the footing for drainage. 2 No. bolt holes were drilled down the length of the footing allowing the footing to be attached to the base of the piston or piston shaft when required (weights were used to load the column for small pressures so that the piston was not required).
- 1 No. brass porous plate measuring 51 mm in diameter and 4.5 mm thick. The plate was bolted to the underside of the footing.
- A steel load plate that could be fixed to the top of the piston shaft. The plate enabled the cell to be loaded with weight rather than pressure when necessary.

#### Stainless steel cells

2 No. stainless steel cells were designed to initially perform the same task as the Perspex cell and were therefore constructed with similar components. Exceptions included:

- Stainless steel cylinder measuring 155 mm in internal diameter (with 7 mm wall thickness). The cylinders were bored and polished by a specialist contractor.
- No small footing or small footing connections as these were not required for column group testing (samples were loaded with the piston).
- 2 No. hexagonal brass ports measuring 25 mm wide and 40 mm long. The brass ports were screwed into the sides of the steel cylinder at distances of 100 mm and 150 mm from the base plate and used to house pore pressure transducers.

## **2 Instrumentation**

### Datalogger

Instrumentation was monitored and logged using a 10 Channel DataTaker (D600 Series 2 data logging system). The DataTaker was connected to a computer with data acquisition software and battery backup support.

### Settlement measurement

A string potentiometer transducer (Stringpot) was attached to each cell to measure the displacement of the piston as a sample was tested. The displacement of the piston enabled measurement of sample strain. Stringpot transducers measure displacement via a thin cable that extends from a spring loaded drum. A rotary sensor is attached to the drum and the electrical output is proportional to cable travel. For typical applications, the drum is mounted to a fixed position and the cable is attached to a moving object. In this case, the drum was fixed to the top plate of the cell using a steel bracket. The cable was hooked to the steel rod, attached to the top of the piston shaft. During consolidation, the cable remained in a vertical position at all times. The Stringpot transducers (LX-PA Series) were supplied by UniMeasure Inc. and had a 15" (375 mm) travel. In practice, the transducers were generally accurate to  $\pm 0.1$  mm.

### Pore pressure measurement

Two pore pressure transducers were connected to the side-walls of each steel cell at distances of 100 mm and 150 mm above the base plate, respectively, and aligned at 90° from each other horizontally. The transducers were used to measure the excess pore pressure and pore pressure dissipation in the clay during loading. The different locations of the transducers were used to confirm that stress was evenly distributed throughout the sample and to observe the impact of drainage path length on consolidation rate. The pore pressure transducers had a range of 6 bar (600 kPa), and were supplied by Druck Ltd.

### Stress concentration

Two miniature stress transducers were attached to the porous plate on the underside of the piston in one of the steel cells. They were attached using a thin layer of adhesive rubber such that the stiffness of the connection would not affect the stress measurement. The diaphragm transducers were supplied by TML Japan (Model PDA-PA) and measured 6.5 mm in diameter. The two transducers had a range of 500 kPa and 3000 kPa, and measured

the stress in the clay and sand, respectively. The transducers operated by measuring strain in the miniature diaphragm, with voltage output calibrated to pressure.

### **3        Safety**

As part of the Occupational Health, Safety and Environment (OHS&E) policy at Monash University, all aspects of laboratory work were assessed for potential hazards prior to commencement. This assessment comprised the development of *Safe Work Instructions* for laboratory testing of model sand columns. It incorporated:

- Identification of hazardous activities associated with the testing.
- Assessment of the risk associated with these hazards.
- Measures that could be adopted to minimise or eliminate these hazards.
- Waste disposal procedures with consideration to environmental impact.
- After hours access procedures.
- Emergency Procedures.

**APPENDIX A.3**  
**(weld testing of mesh)**

## 1      **Testing of weld strength**

To create geogrid encasement sleeves on site, the geogrid may be welded using a specialised frame. To replicate this process in small-scale, a cylindrical sleeve was formed by overlapping the mesh by about 10 mm and bonding the overlapped section (seam) with adhesive. It was important that the strength of this seam was at least equal to the strength of the mesh itself, so that a point of weakness was not introduced. Samples were prepared to test this by cutting 200 mm long strips in half and bonding a 10 mm overlapped seam (about 7 strands) with adhesive. Restricting the width of overlap to 10 mm was expected to limit the impact of this seam on encasement stiffness. Two types of adhesive were tested, epoxy-resin and a resin specifically developed for use with fibreglass.

Each adhesive was tested twice on both types of mesh, equating to 8 tests in total. The load-strain relationship for seam testing of fibreglass and aluminium meshes are presented in Figure 1 and Figure 2, respectively. Results indicated that the behaviour of mesh bonded with epoxy-resin was similar to the behaviour of the mesh itself. Failure occurred within the mesh strands, indicating that the bond strength of the epoxy-resin was at least equal to the strength of the non-bonded mesh. However, the bond strength of the fibreglass specific resin to the fibreglass mesh was significantly less than the strength of the fibreglass strands, as highlighted in Figure 1. Failure occurred by fibreglass strands progressively peeling away from the resin during loading, perhaps a result of the adhesive failing to bond properly to the thin paint coating on the mesh strands.

For the aluminium mesh, the tensile strength of the samples bonded with fibreglass resin was similar to the strength of the mesh itself. However, as highlighted in Figure 2, the strain was significantly higher, perhaps indicating slippage of the bonded strands. As a result, the epoxy-resin (Selleys Araldite) was deemed to be the most suitable adhesive for bonding both meshes. The nominal width of overlap (10 mm) used in the uniaxial testing was adopted for construction of the mesh sleeves.



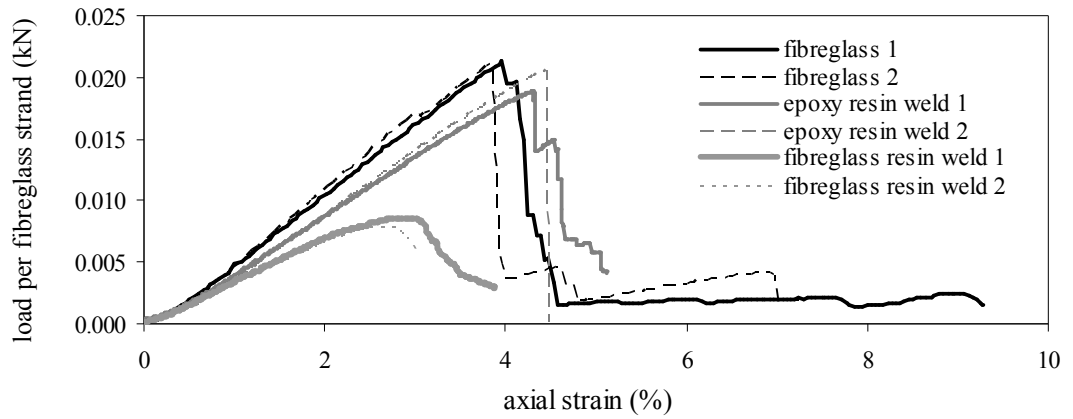


**Figure 1:** Load-strain relationship for seam testing of fibreglass mesh

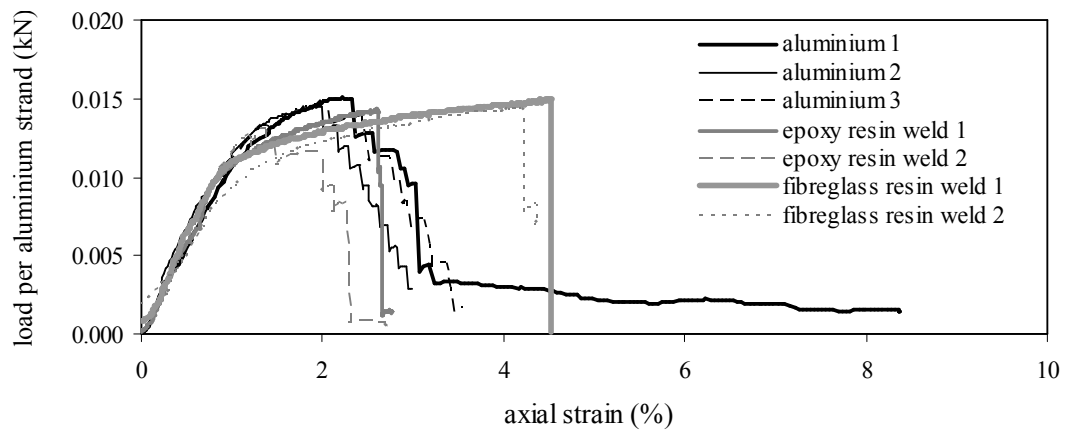


**Figure 2:** Load-strain relationship for seam testing of aluminium mesh

## 2 Soaked testing

Soaked testing was undertaken to confirm that there was no strength loss in the epoxy-resin weld after being submersed in water. Typically, the geogrid encased model columns were tested in a submersed environment over a period of 3 to 4 weeks. Based on this, samples of mesh with epoxy-resin welding were soaked in kaolin slurry for 28 days prior to testing. Samples were then rinsed and immediately tested in the uniaxial test apparatus.

Three bonded samples of fibreglass and two bonded samples of aluminium were tested. The load-strain behaviour for 28-day soaked samples of bonded fibreglass and aluminium mesh are compared to non-soaked samples in Figure 3 and Figure 4, respectively. Although the initial stiffness of each sample was not significantly affected by soaking (indicated by the gradient of the initial linear section of the load-strain plot), there was a

significant loss in tensile strength. The average reduction in tensile strength ranged from about 25% in the aluminium mesh to 35% in the fibreglass mesh. Failure generally occurred within the mesh strands and not within the bonded section, indicating that the meshes were sensitive to saturation rather than the resin.

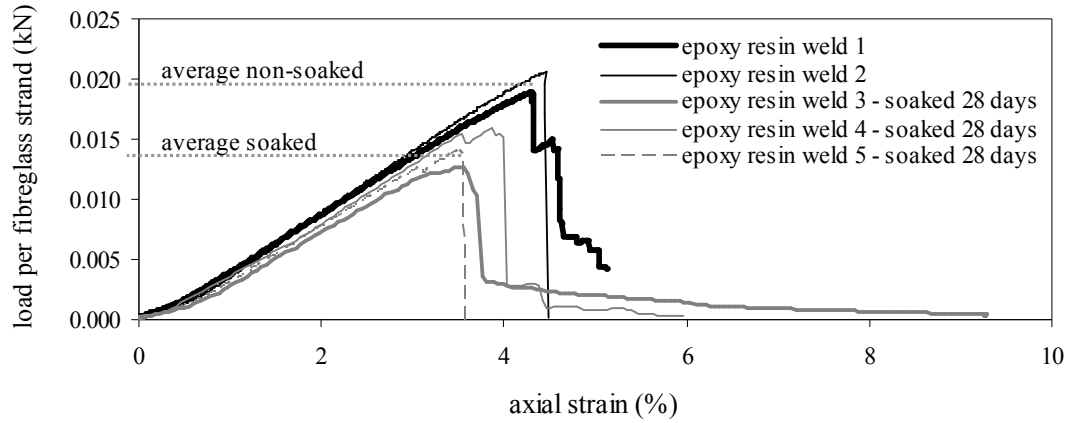


**Figure 3:** Load-strain relationship for seam testing of fibreglass mesh (28-day soaked)

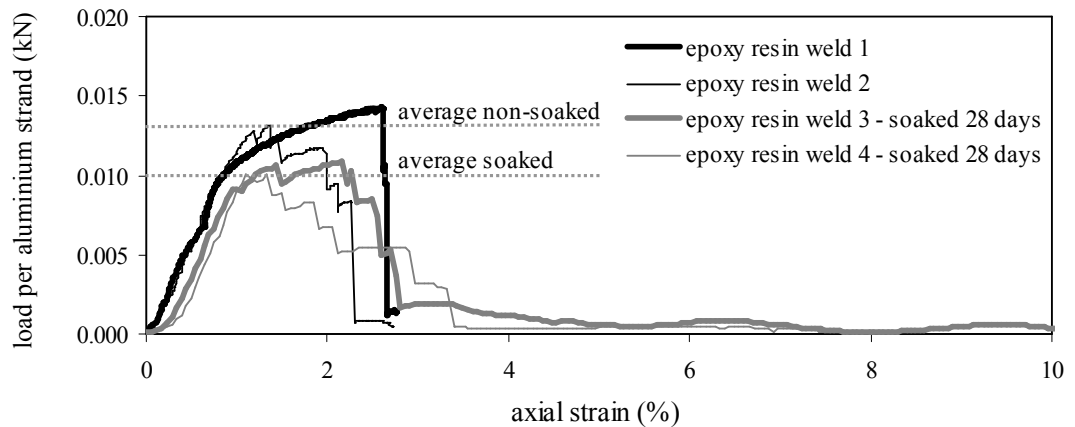


**Figure 4:** Load-strain relationship for seam testing of aluminium mesh (28-day soaked)

As the meshes were primarily manufactured for outdoor use (in potentially wet environments), it was considered unlikely that submersion alone would account for the reduction in strength. It was also considered possible that the environment provided by the kaolin slurry may have been mildly corrosive to the mesh. Although meshes that were sensitive to the surrounding environment were not desired, the time and testing required to find more suitable meshes could not be justified in this component of research. As mesh stiffness was not significantly affected by saturation, and the properties of the meshes had been well defined by testing, both meshes were retained for encased column testing.

## **APPENDIX A.4**

### **(cell calibration)**

## 1 Perspex cell

### 1.1 Assessment of side-wall friction

Gachet et al. (2003) investigated the effectiveness of various lubricants on reducing side-wall friction in consolidation cells. They showed that of the lubricants tested, silicone was the most effective, significantly reducing side-wall friction. Based on their findings, three tests were undertaken to reduce cell friction. The tests comprised consolidating a 470 mm high sample of kaolin slurry (with initial moisture content of 115%) within the Perspex cell under constant stress and comparing the vertical strain to that observed in a conventional oedometer test. Three tests were undertaken using the following lubrication:

- (i) no lubrication
- (ii) lubrication using *Inox* – a commercially available oil based lubricant
- (iii) lubrication using silicone

A thin coat of the lubricant being tested was applied to the inside surface of the Perspex cell prior to the cell being filled with slurry. The cell was then pressurised to 57 kPa, with the slurry receiving only a percentage of this pressure due to O-ring resistance. Each test was continued until primary consolidation had been completed. This was determined from settlement measurements, where settlements of less than 1 mm/day were generally considered to indicate the completion of primary consolidation. This generally took a minimum of 12 days.

### 1.2 Assessment of O-ring friction

Prior to consolidation testing, the friction associated with O-rings was measured. A load cell was placed directly beneath the piston and the base of the cell was used for reaction. As the chamber above the cell was pressurised with air, the load and therefore pressure beneath the piston was recorded. This testing was only undertaken for the case where the internal wall of the cell was lubricated with silicone.

Testing indicated that little pressure was transferred to the load cell (and therefore the sample) until the upper chamber was pressurised to about 8 kPa. This pressure differential

increased slightly as the cell pressure was increased to 50 kPa and then 100 kPa. A pressure of 100 kPa was considered to be the maximum cell pressure likely to be adopted in isolated column testing. Based on this, the friction associated with O-rings was estimated to range between 8 kPa and 11 kPa across the range of working stresses. Although O-ring friction for the unlubricated cell was not measured, observations from early consolidation trials indicated that the piston did not move downwards until a pressure of 18 kPa was applied to the upper chamber. This was significantly higher than for the lubricated case.

### 1.3 Impact of lubricant on side-wall friction

Vertical strain for the cell consolidation tests undertaken with three different side-wall lubricants are plotted against time in Figure 1. Based on the O-ring friction testing undertaken for the case of silicone lubrication, a cell pressure of 57 kPa equated to a pressure of about 48 kPa being transferred to the kaolin (9 kPa friction loss). The equivalent strain for a standard oedometer test undertaken on the same material, at a vertical pressure of 48 kPa, is also indicated.

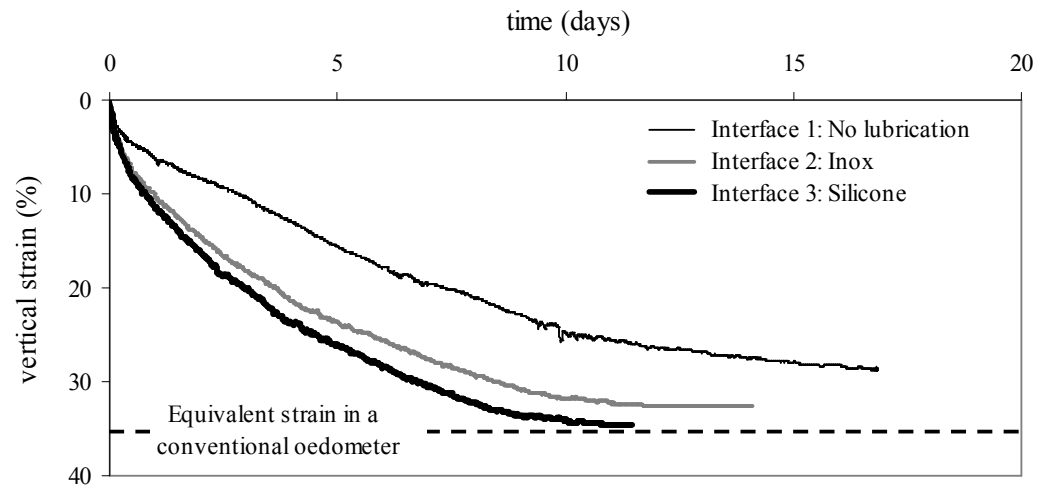


**Figure 1:** Comparison of vertical sample strain using different side-wall lubricants

For the sample with no lubrication, the 29% strain observed at the completion of primary consolidation was significantly less than the equivalent 36% strain for a standard oedometer test. With the application of *Inox* and then silicone, sample strain was increased to about 33% and 35%, respectively. It is likely that the increase in vertical

sample strain with the use of lubricants was a result of both reducing the friction at the slurry–Perspex interface and providing lubrication for the piston O-rings. Testing also indicated that for the unlubricated sample, significant delay occurred in the consolidation process when compared to the lubricated samples. This may be the result of a ‘stick-slip’ mechanism acting between the O-rings and unlubricated Perspex surface, a common occurrence at an unlubricated interface.

After accounting for the friction associated with the O-rings, the use of silicone lubrication was considered to reduce side-wall friction to the point where the vertical stress-strain behaviour of the cell was similar to that of a standard oedometer.

#### 1.4 Further testing

Shear box testing was undertaken to further quantify the reduction in shear stress at the kaolin-Perspex interface associated with the use of silicone lubricant. Samples of kaolin clay consolidated at a vertical stress of 100 kPa were sheared in a conventional shear box measuring 60 mm x 60 mm, under drained conditions (shear rate of 0.3 mm/hour). Three tests were undertaken, comprising (i) kaolin clay, (ii) kaolin clay against an unlubricated Perspex block, and (iii) kaolin clay against a Perspex block lubricated with silicone.

The shear stress-displacement relationship for samples sheared with a vertical confining pressure of 50 kPa are presented in Figure 2.

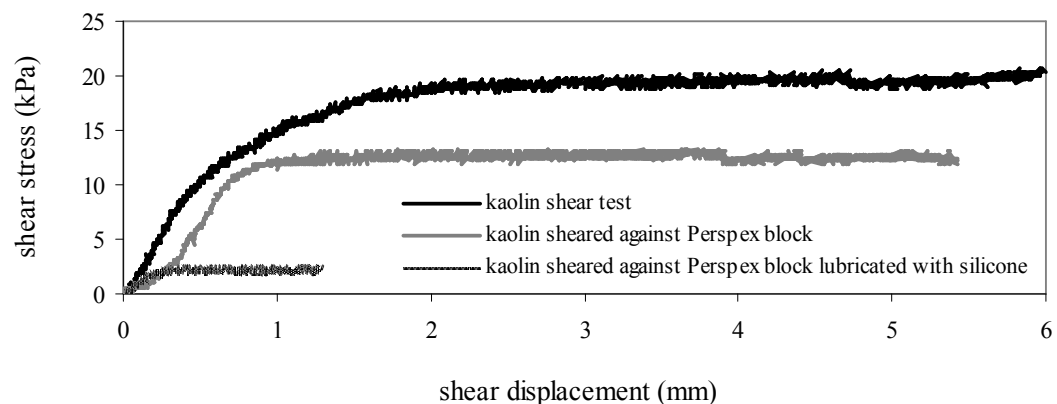


**Figure 2:** Shear stress – displacement relationship for interface testing

Results indicated a reduction of shear stress at the kaolin-Perspex interface of about 85% when lubricated with silicone, equating to a friction angle of approximately  $\phi=2^\circ$  at the lubricated interface. Undrained testing (shear rate of 0.6 mm/minute) indicated a reduction in interface shear stress in the order of 92%, equating to an interface shear strength of 0.4 kPa.

Based on the testing undertaken, it was considered that the application of silicone lubrication to the internal surface of the consolidation cell brought the performance of the cell approximately in line with that of a standard oedometer. The side-wall friction within the cell was therefore considered negligible for the purposes of isolated column testing.

## **2 Stainless steel cells**

Consolidation testing of kaolin was also undertaken in the two stainless steel cells to assess the impact of friction when lubricated with silicone. Results of the testing undertaken are described in this section.

### **2.1 Assessment of side-wall friction**

A consolidation test was undertaken in Steel cell #1 to investigate the impact of side-wall friction on the vertical stress-strain behaviour of kaolin samples. The test was also undertaken to provide base data for comparing model column tests. Kaolin slurry measuring 477 mm high (with an initial moisture content of about 115%) was consolidated in several stages, with primary consolidation completed between each stage. The results of the consolidation cell test are plotted in the vertical strain-log pressure plane and compared to standard oedometer tests in Figure 3. Results indicated that the compressibility of the kaolin sample in Steel cell #1 closely matched the compressibility of kaolin in standard oedometer tests.

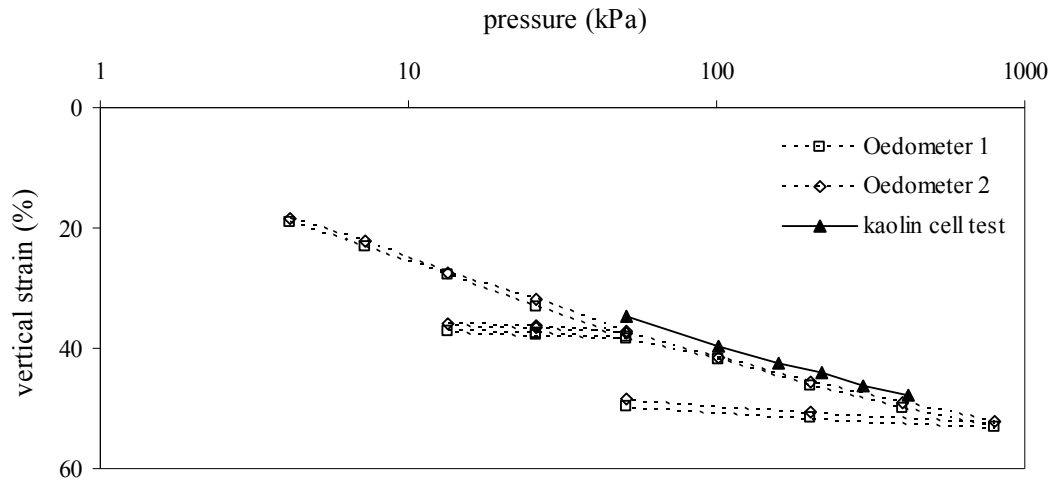


**Figure 3:** strain-log pressure behaviour of kaolin slurry in Steel cell #1

## 2.2 Assessment of O-ring friction

Two pore pressure transducers were attached to the side walls of each steel cell and used to measure excess pore pressure during loading. By comparing air pressure in the upper chamber to excess pore pressure within the sample, a measurement of the O-ring friction was possible. An initial calibration test was undertaken in each cell to measure O-ring friction. Each cell was filled with water. Air pressure was then applied to the upper chamber in 50 kPa increments up to a maximum of 400 kPa. Pore pressure transducers measured water pressure for each increment. The difference between the cell pressure and the water pressure represented O-ring friction. Results of the calibration test for Steel cell #1 are presented in Figure 4, along with measurements of O-ring resistance taken from column tests (the results of which were presented later in this chapter). Results for Steel cell #2 are presented in Figure 5.



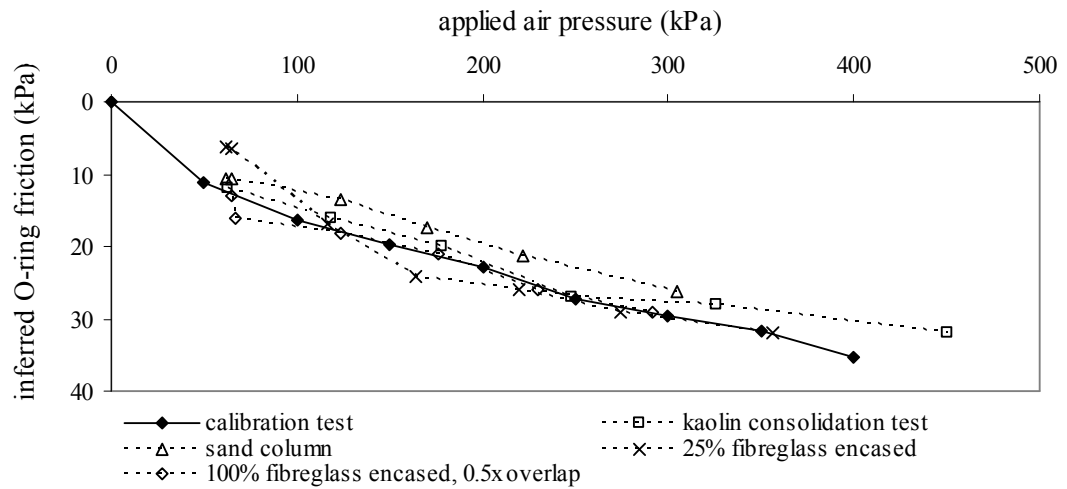


**Figure 4:** Inferred O-ring friction derived from cell tests in Steel cell #1

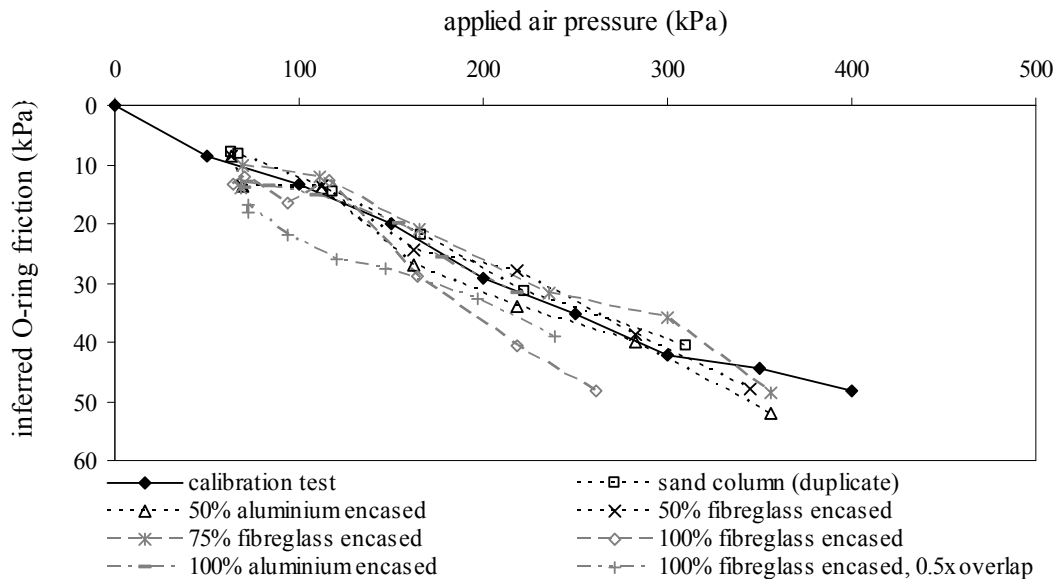


**Figure 5:** Inferred O-ring friction derived from cell tests in Steel cell #2

Testing indicated that although there was some minor variability, resistance increased roughly linearly over the range of applied vertical stresses (50 kPa to 400 kPa). Load resistance was slightly lower for Steel cell #1 compared to Steel cell #2, most likely due to minor differences established during cell construction. Based on these results, it was concluded that between 85% and 90% of the applied pressure was transferred to the sample when the internal surface of the cells were lubricated with silicone.

**APPENDIX B.1**  
**(PLAXIS Soft Soil model)**

In the Soft Soil model, a logarithmic relationship exists between the volumetric strain,  $\varepsilon_v$ , and the mean effective stress,  $p'$ . For primary isotropic loading (virgin consolidation), this can be expressed as:

$$\varepsilon_v - \varepsilon_v^0 = -\lambda^* \ln\left(\frac{p'}{p^0}\right) \quad (1)$$

Where  $\lambda^*$  is the modified compression index. The expression plots as a straight line in log-pressure space.

For isotropic unloading and reloading, the expression can be written as:

$$\varepsilon_v - \varepsilon_v^0 = -\kappa^* \ln\left(\frac{p'}{p^0}\right) \quad (2)$$

Where  $\kappa^*$  is the modified swelling index. The soil behaviour during unloading and reloading is considered to be elastic.

Basic input parameters for the for the Soft Soil model include the following:

$\lambda^*$	Modified compression index
$\kappa^*$	Modified swelling index
$c$	Cohesion
$\phi$	Peak angle of internal friction
$\psi$	Angle of dilatancy

However, in engineering practice and throughout this research, soil compressibility is generally expressed in terms of the compression index,  $C_c$ , and the re-compression or swelling index,  $C_r$ . The expressions used to relate modified compression index to compression index and modified swelling index to swelling index can be formulated as:

$$\lambda^* = \frac{C_c}{2.3(1+e)} \quad (3)$$

$$\kappa^* \approx \frac{C_r}{2.3(1+e)} \quad (4)$$

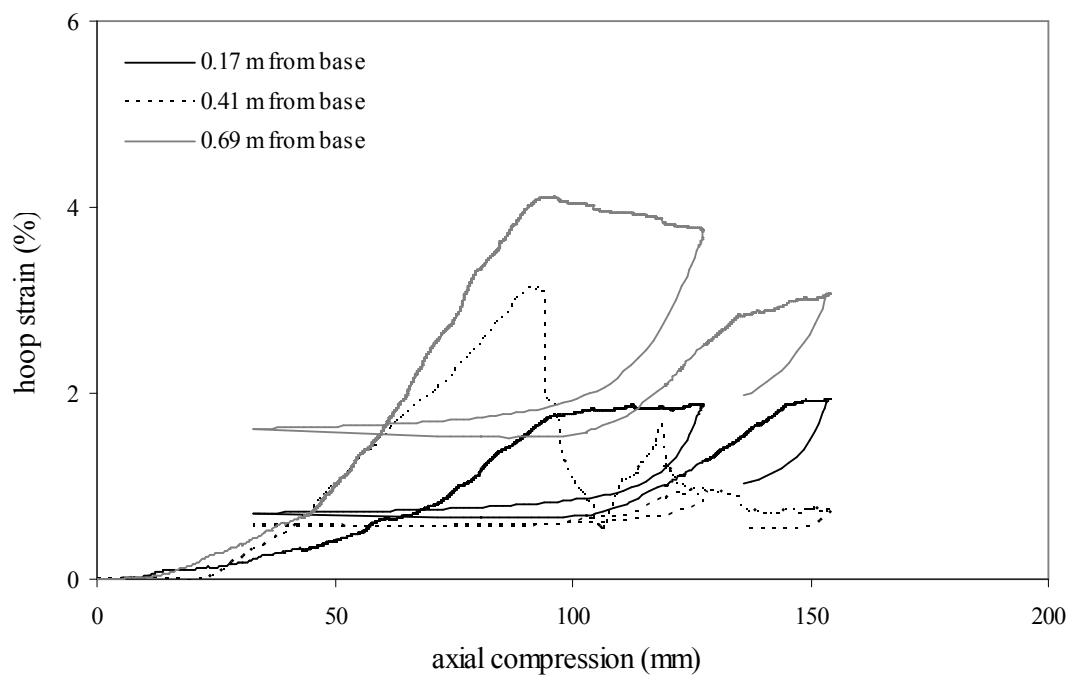
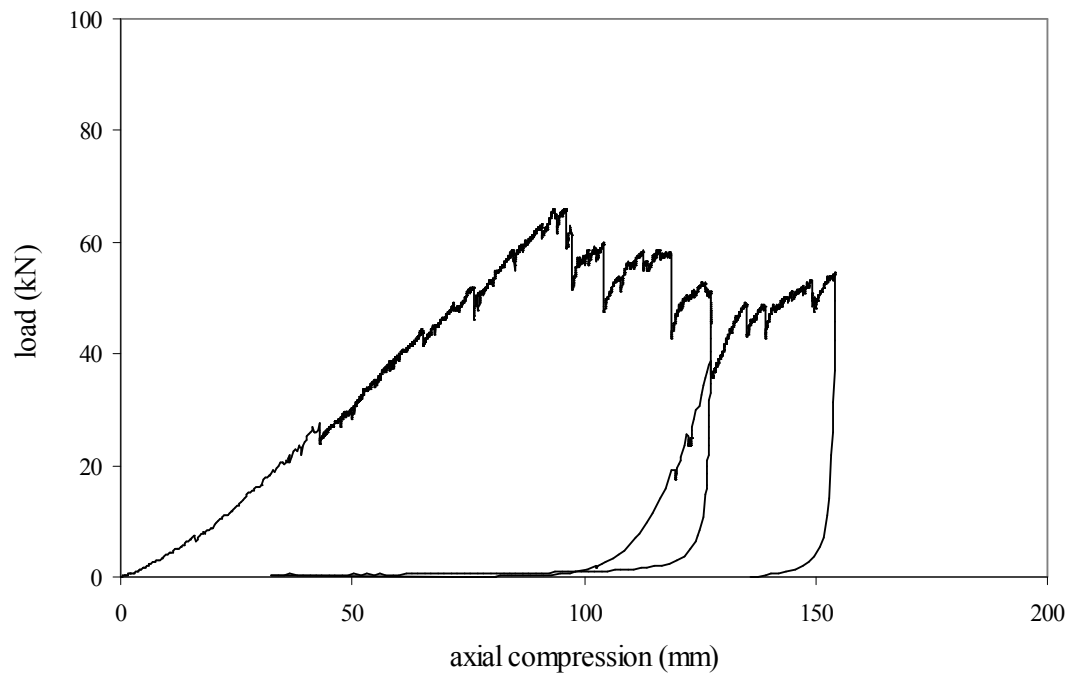
Where  $e$  is the void ratio of the soil.

In the Soft Soil model, the yield function describes the irreversible volumetric strain in primary compression. A perfectly-plastic Mohr-Coulomb yield function is used to model the failure state.

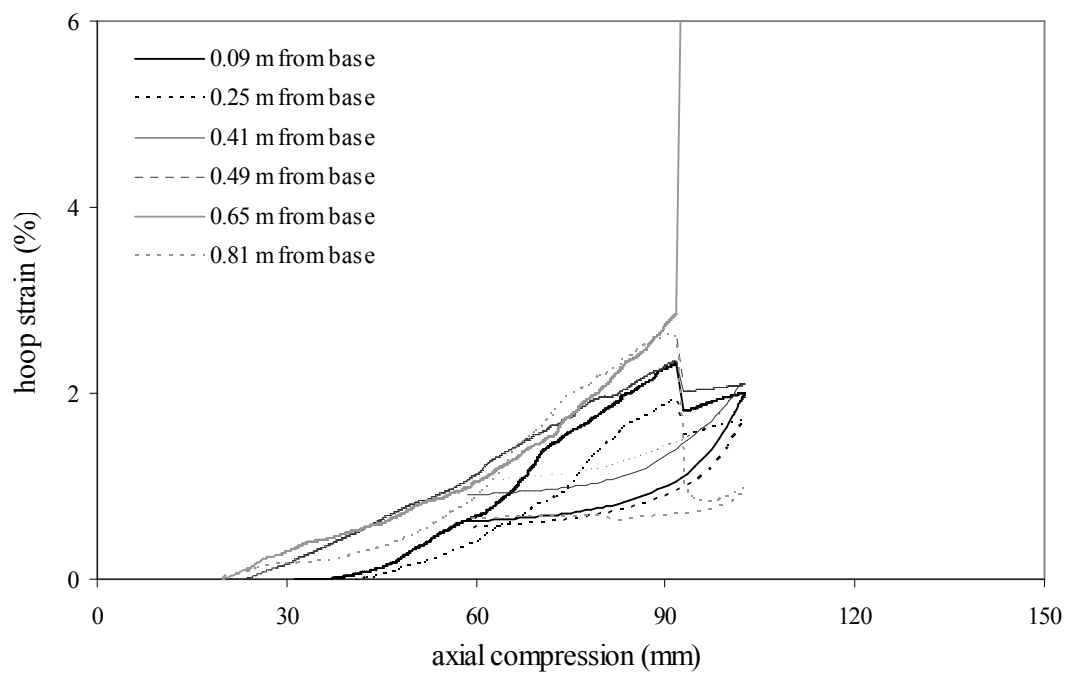
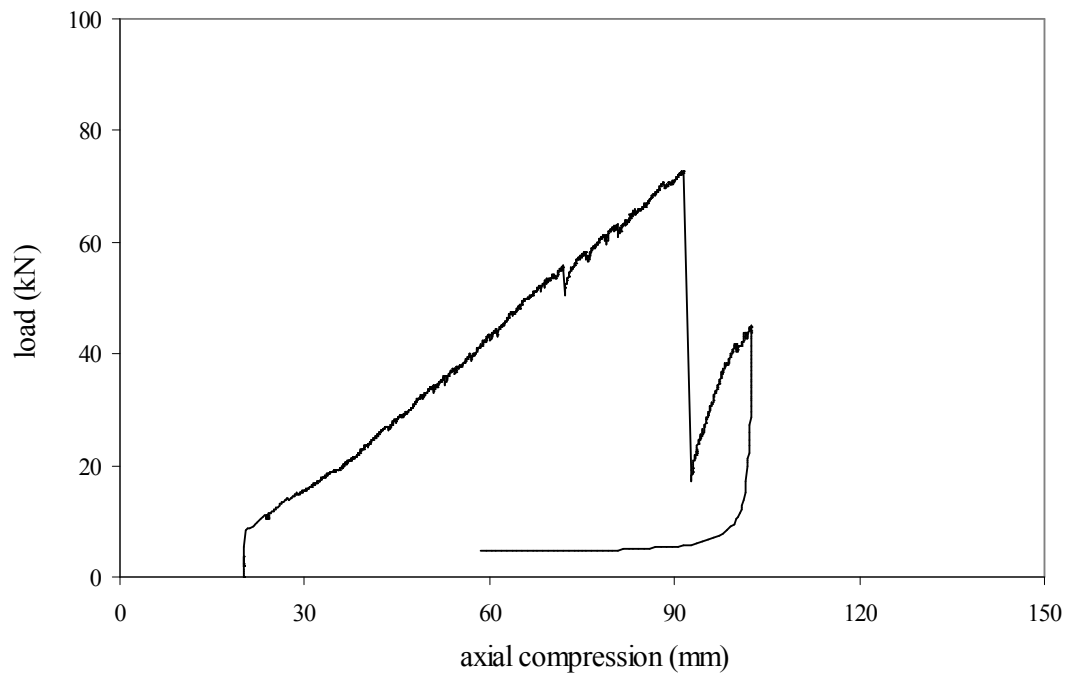
## **APPENDIX C.1**

**(medium scale tests – load-compression and strain measurements)**

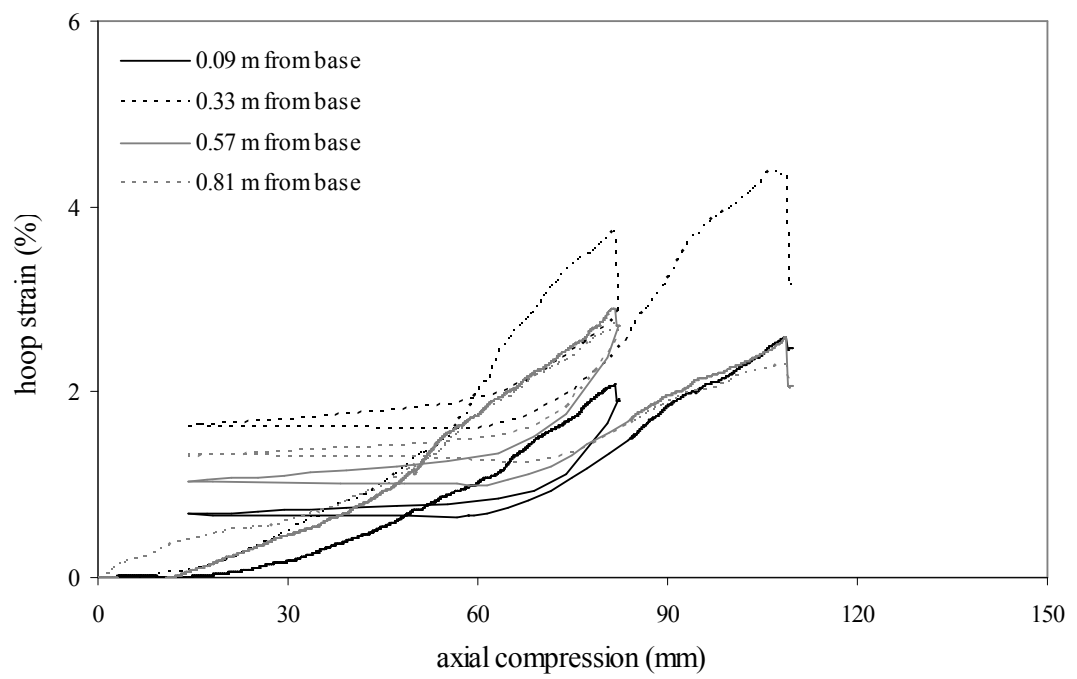
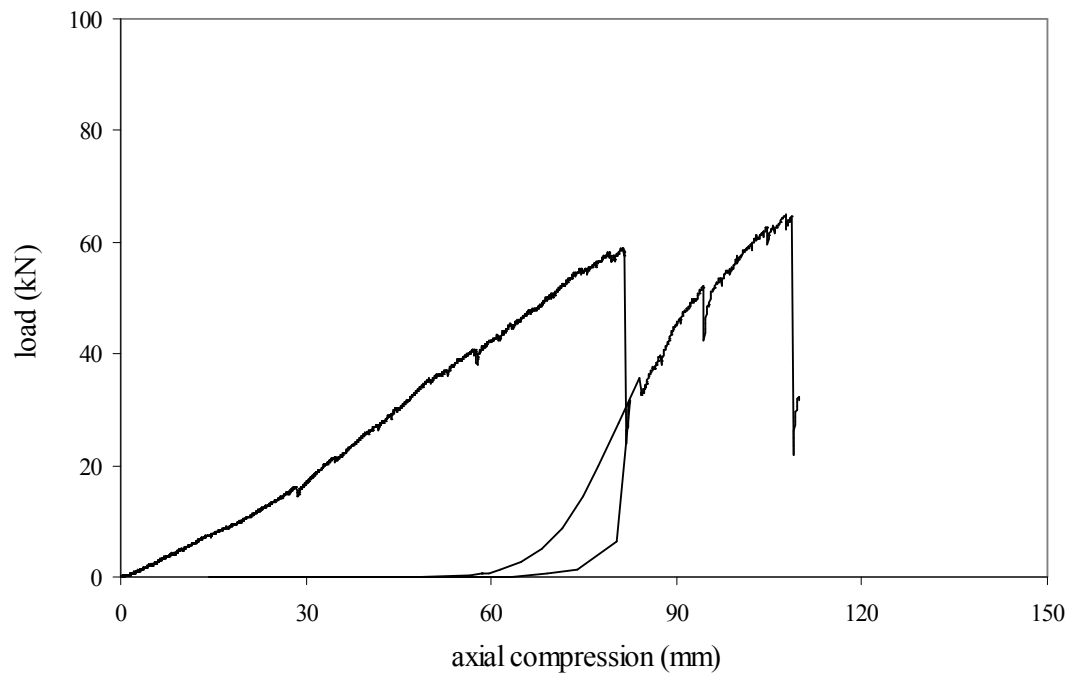
## Test No. 1



## Test No. 2

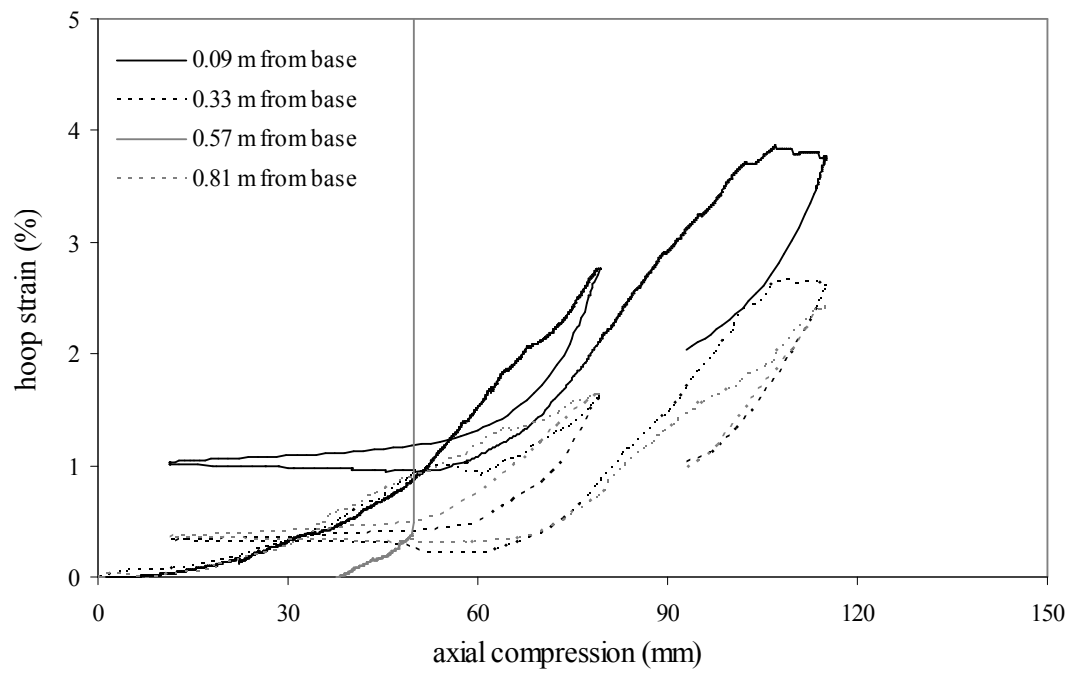
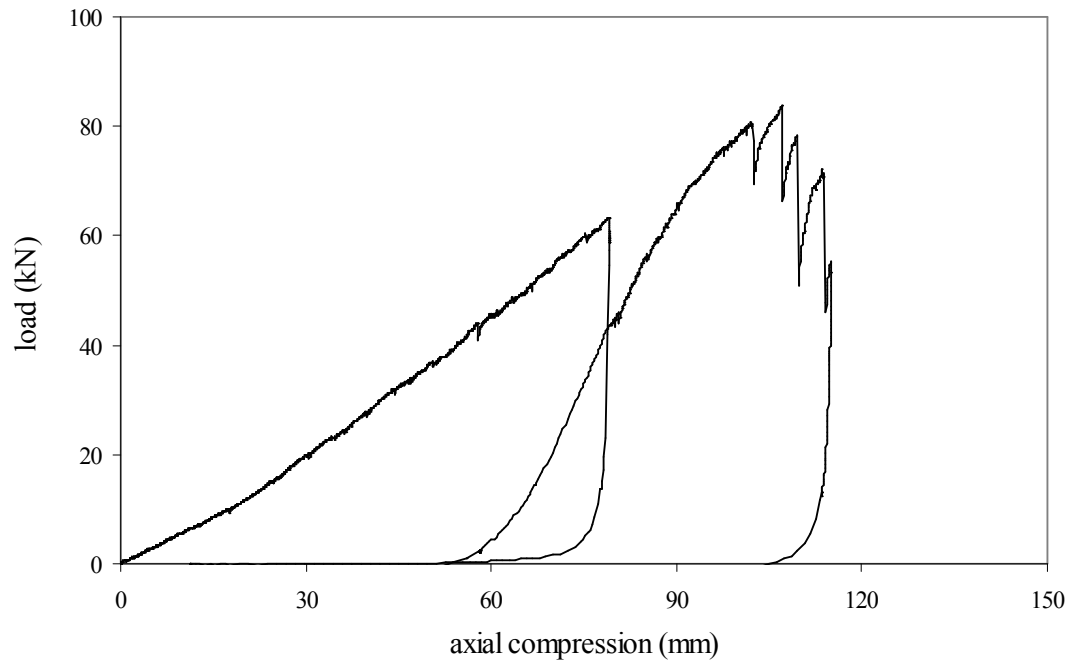


### Test No. 3

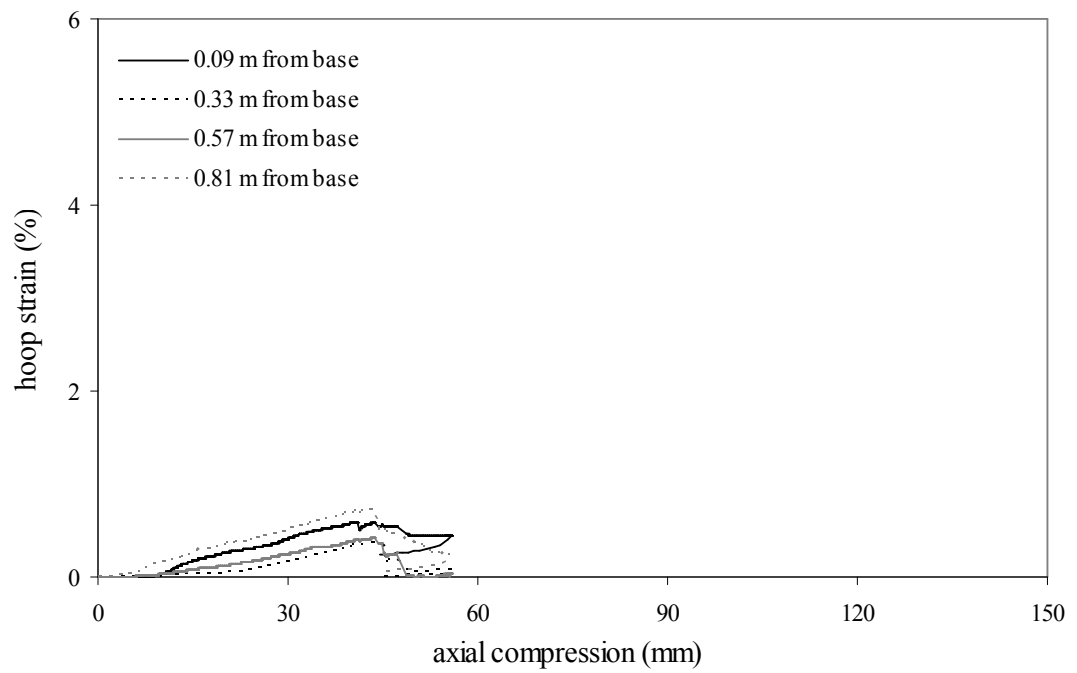
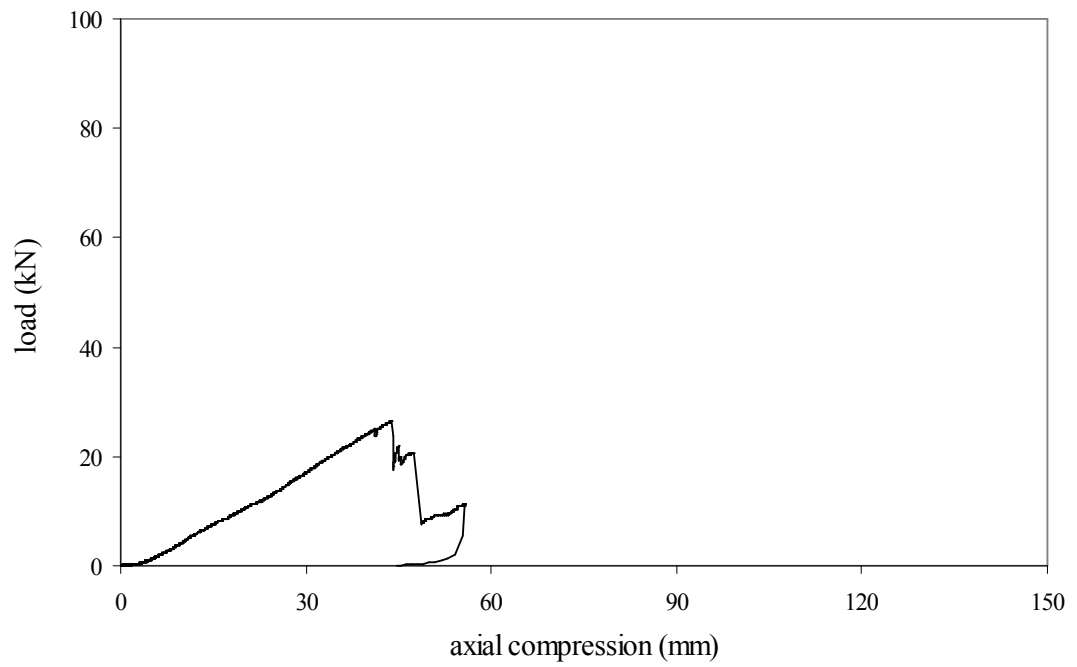




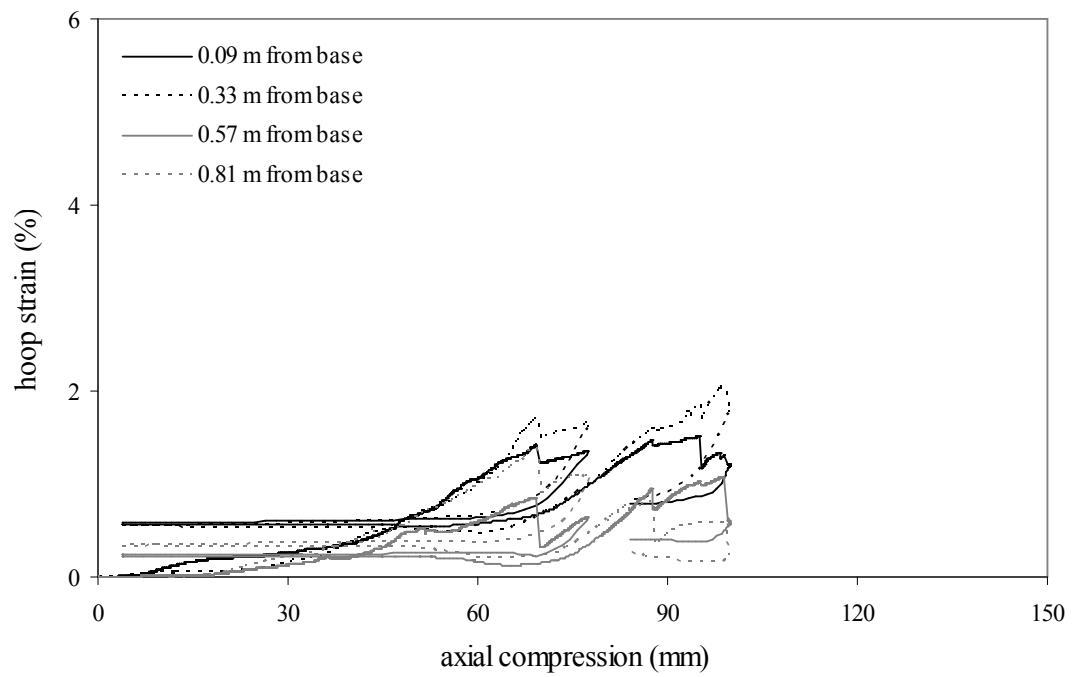
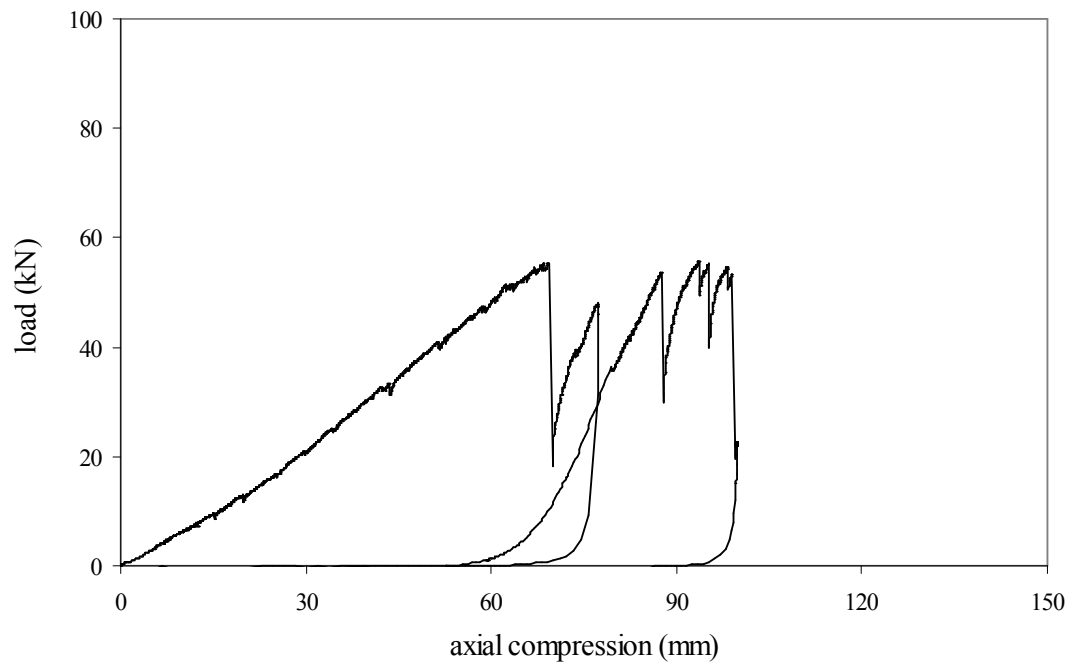
# Test No. 4



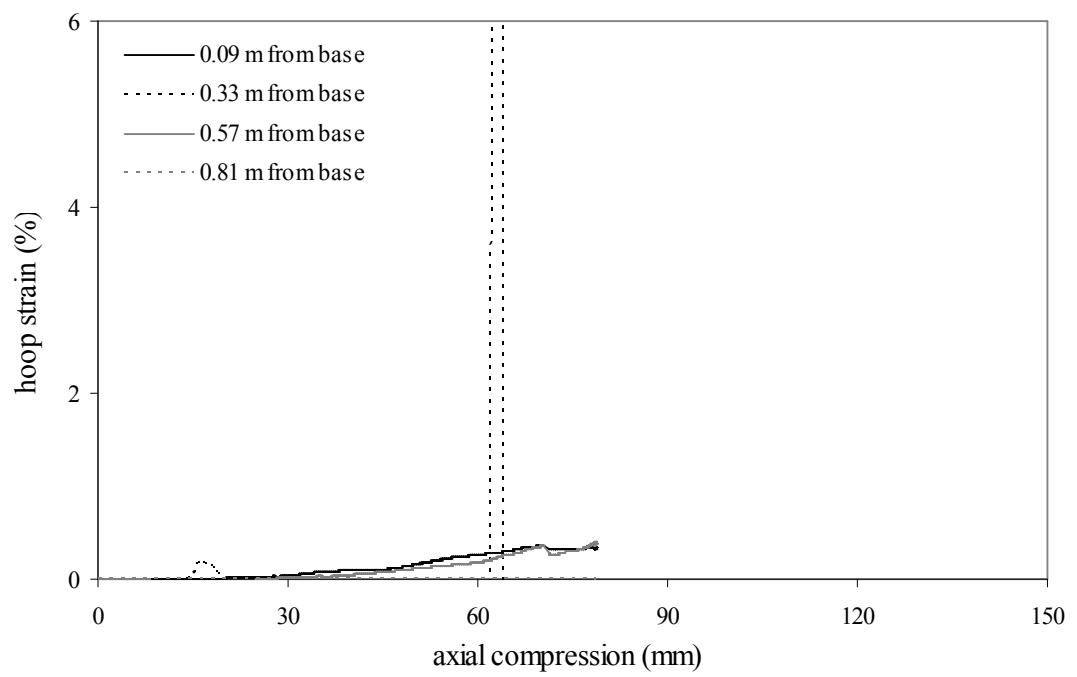
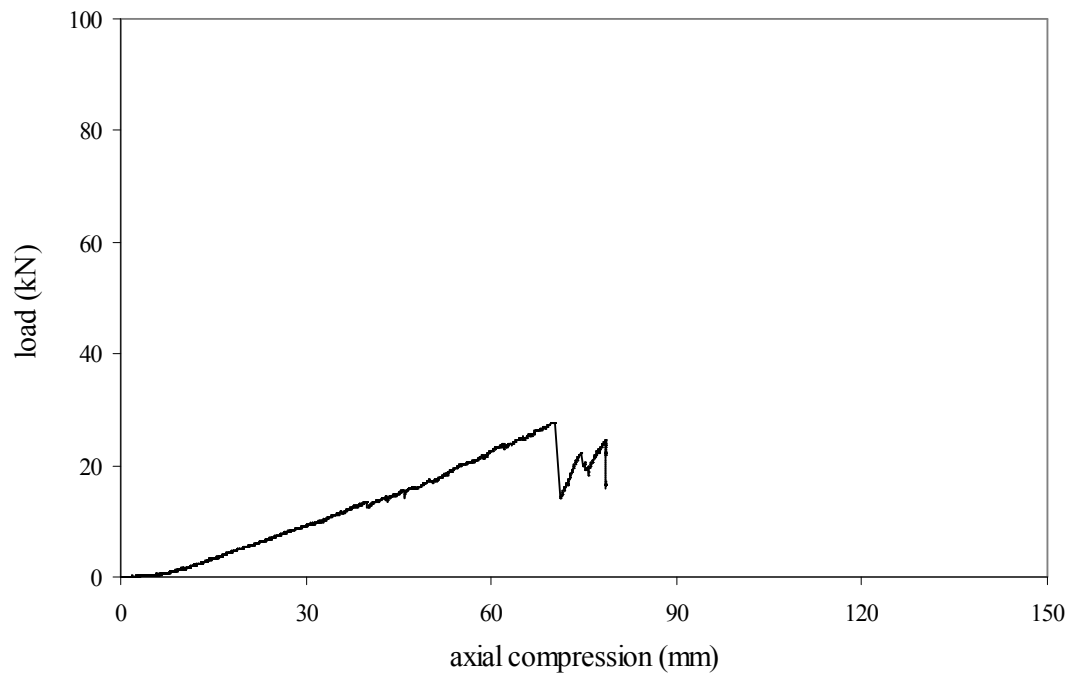
## Test No. 5



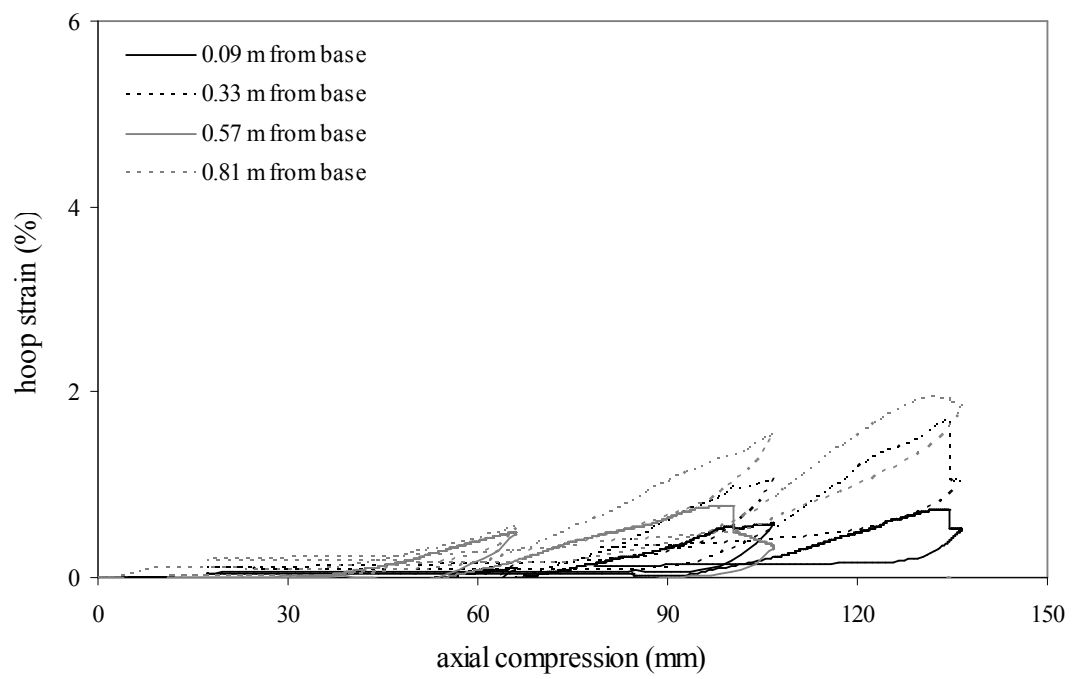
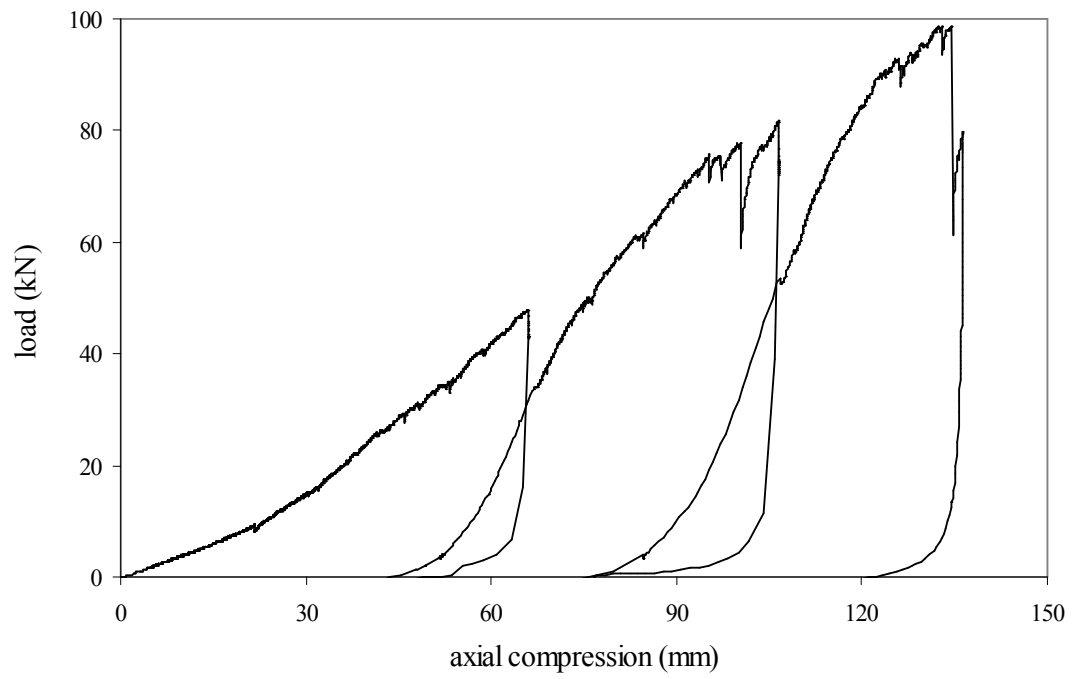
## Test No. 6



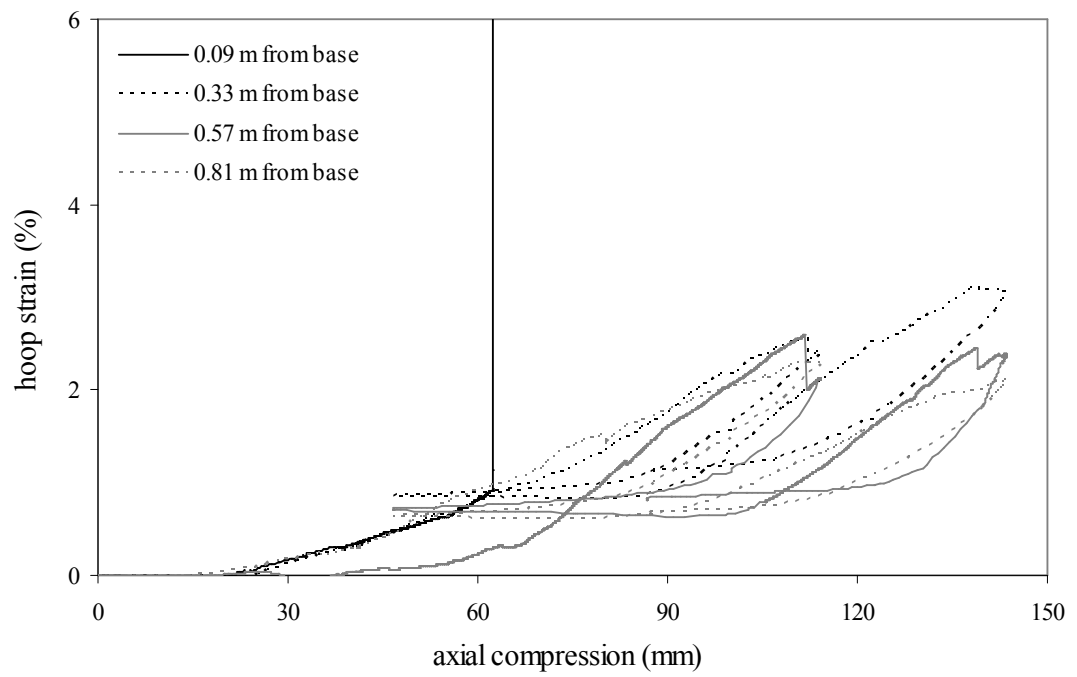
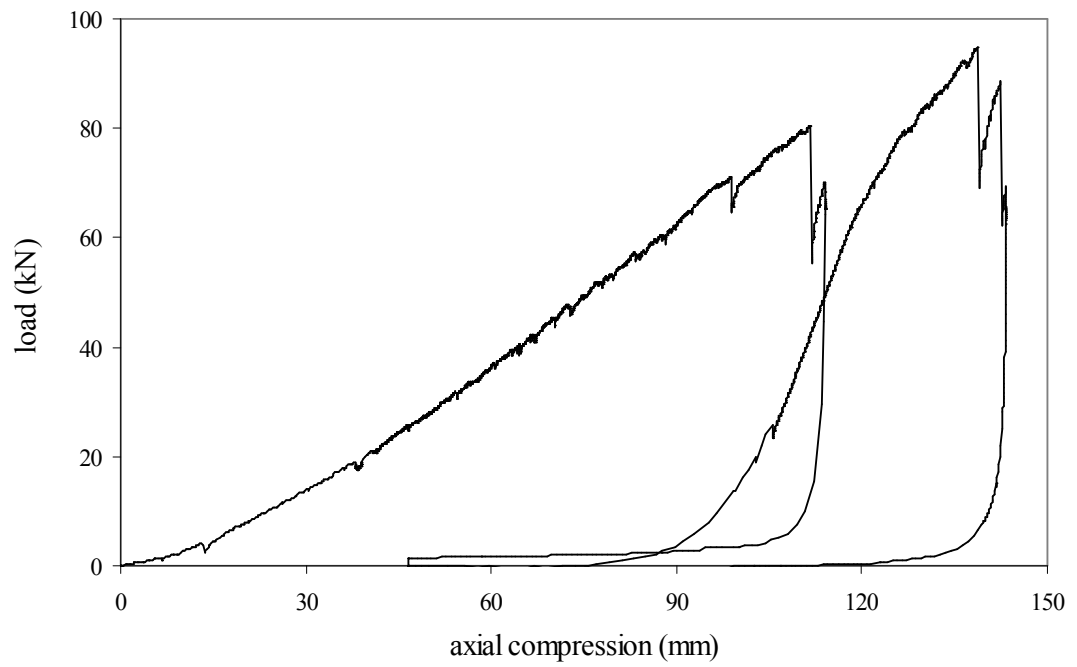
### Test No. 7



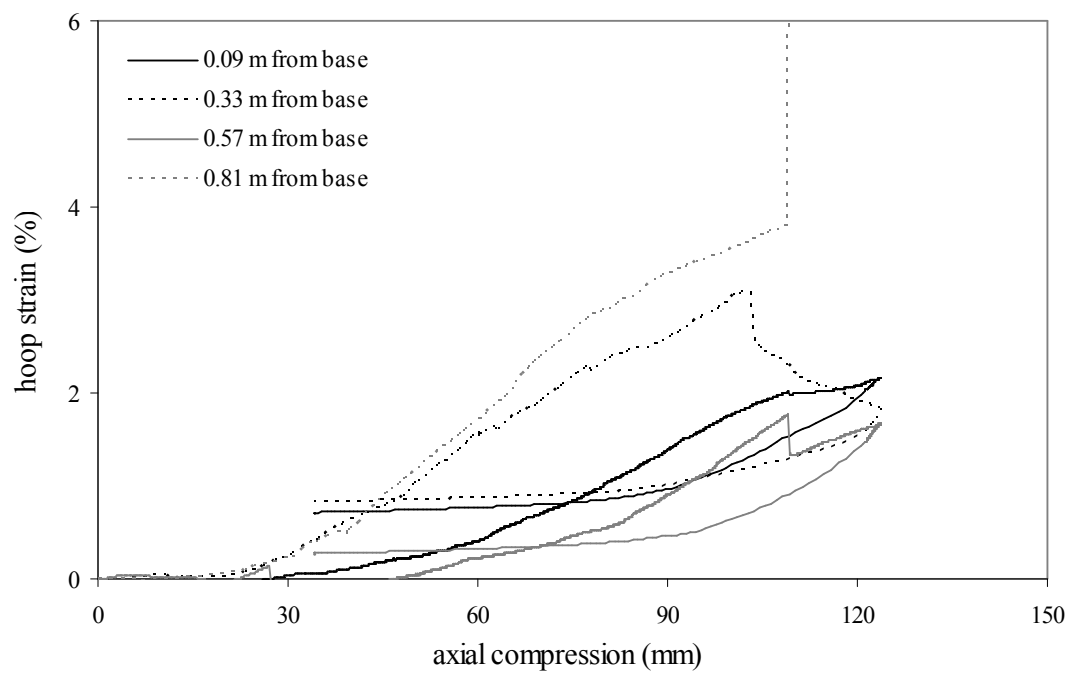
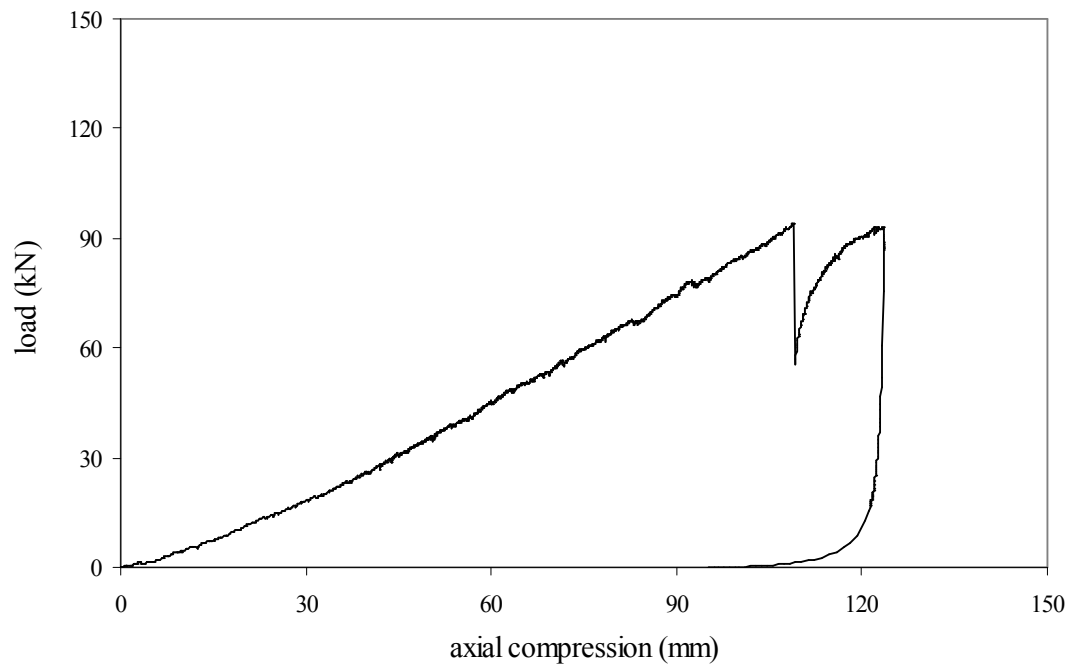
## Test No. 8



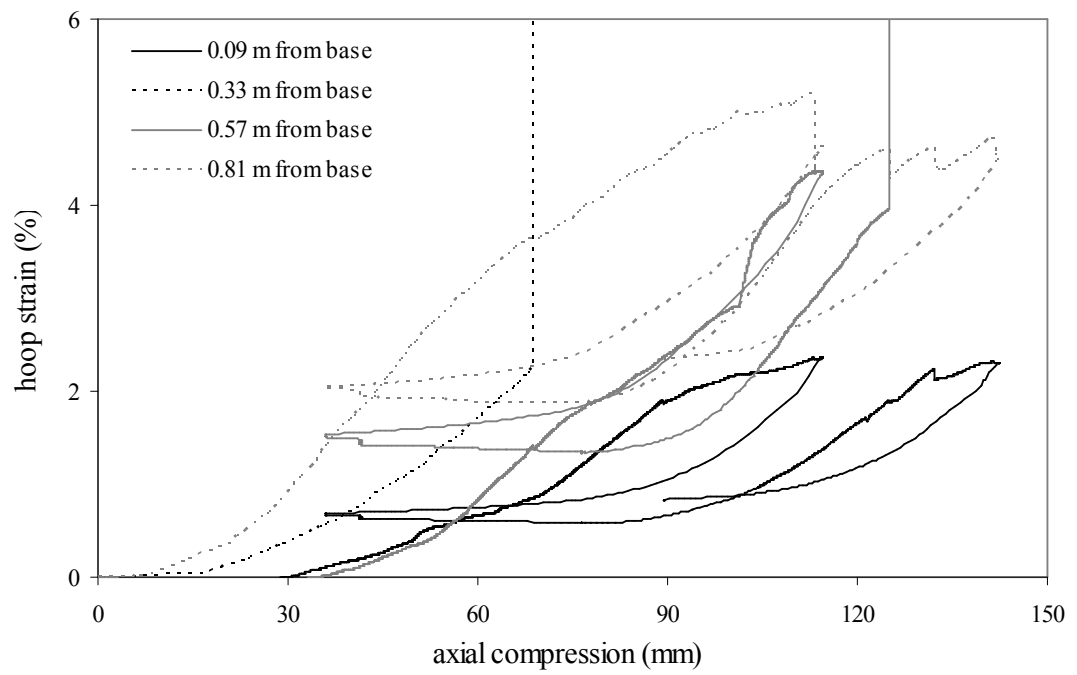
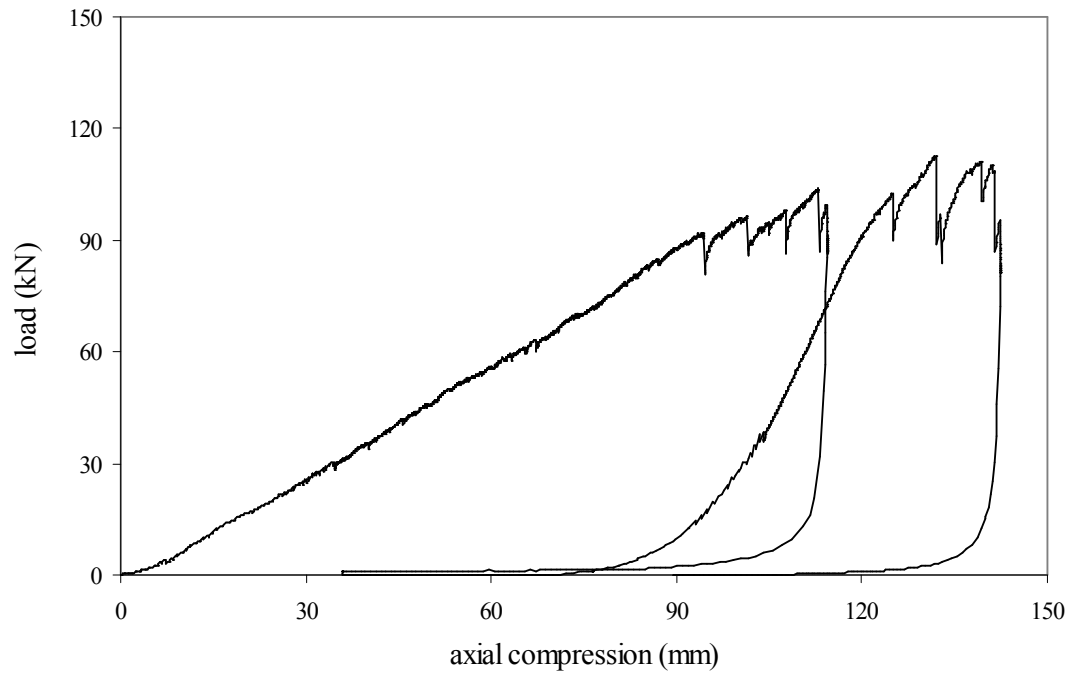
### Test No. 9



**Test No. 10**

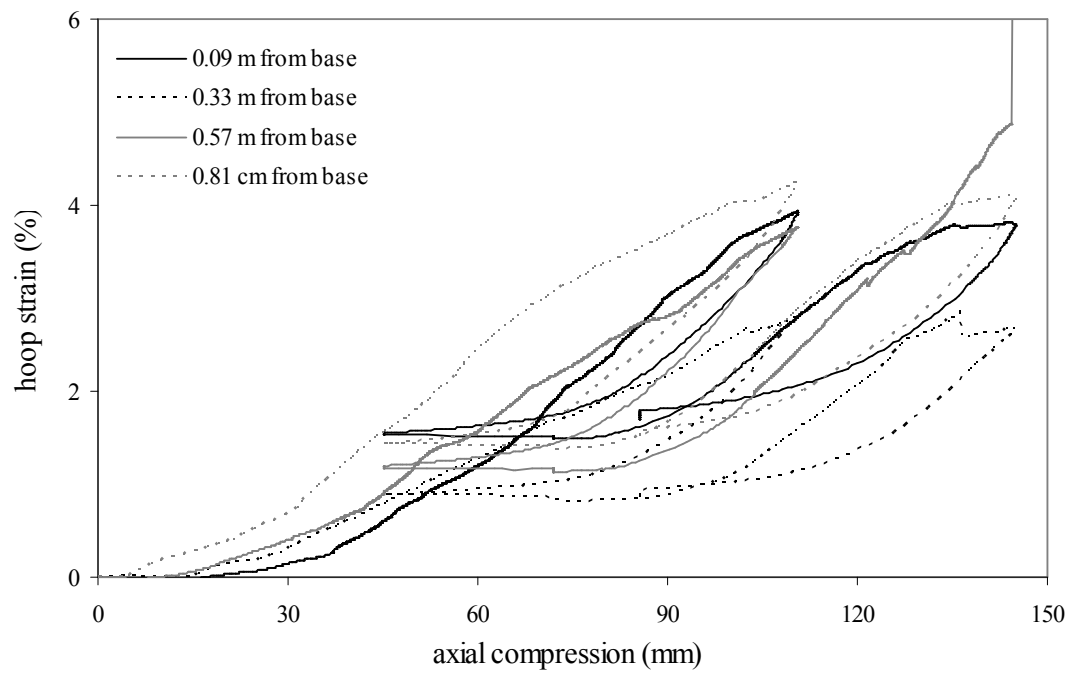
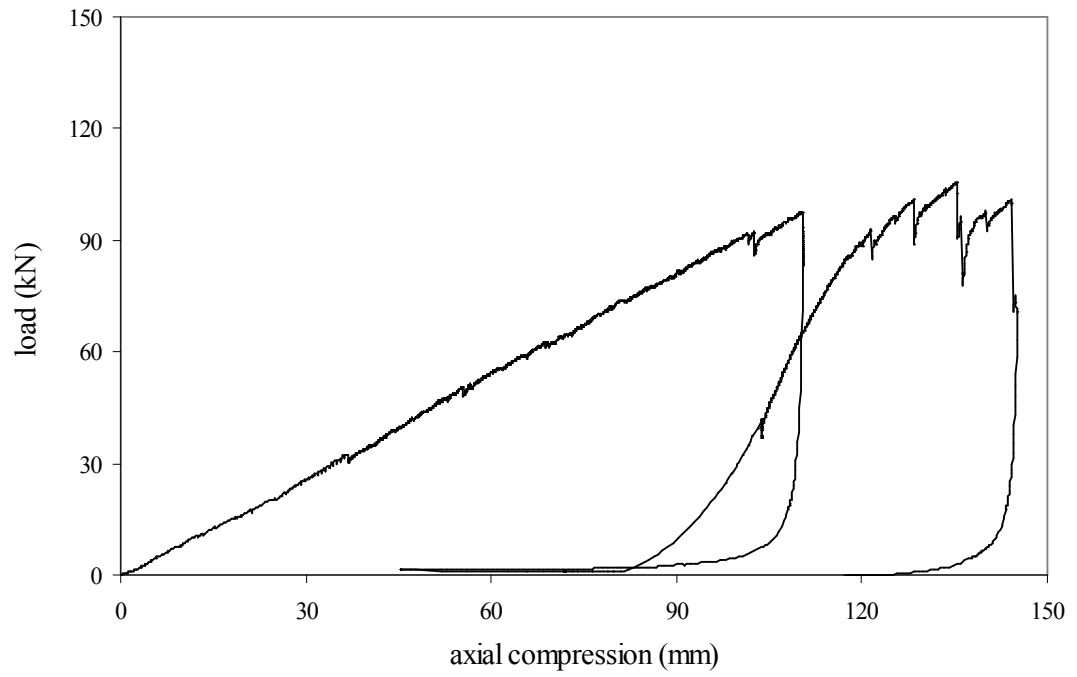


**Test No. 11**

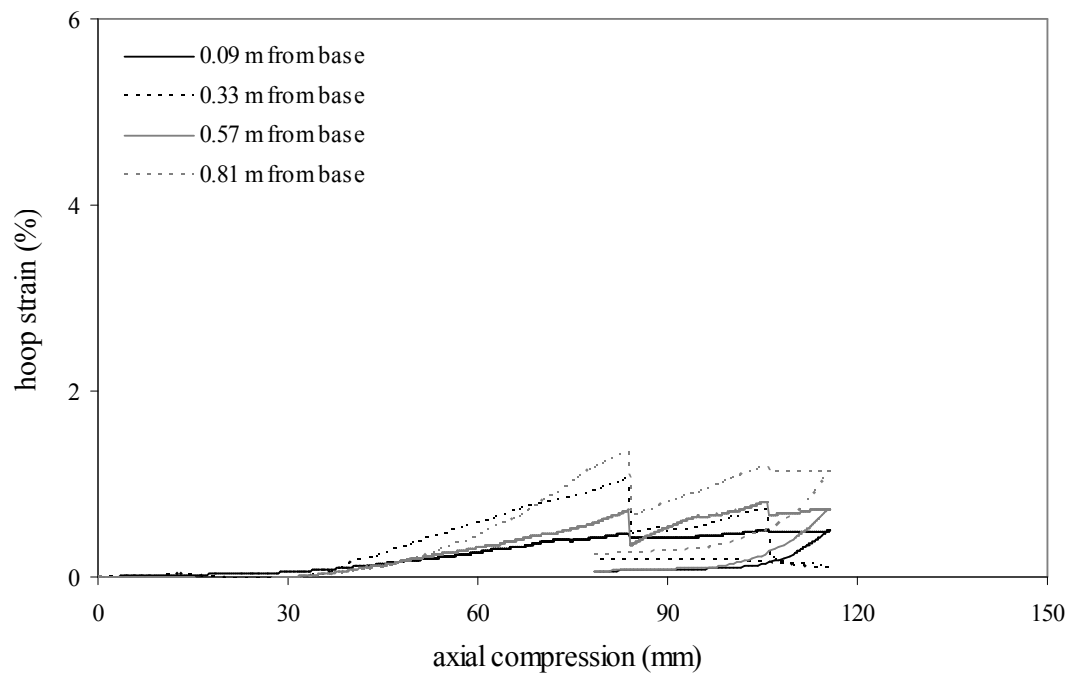
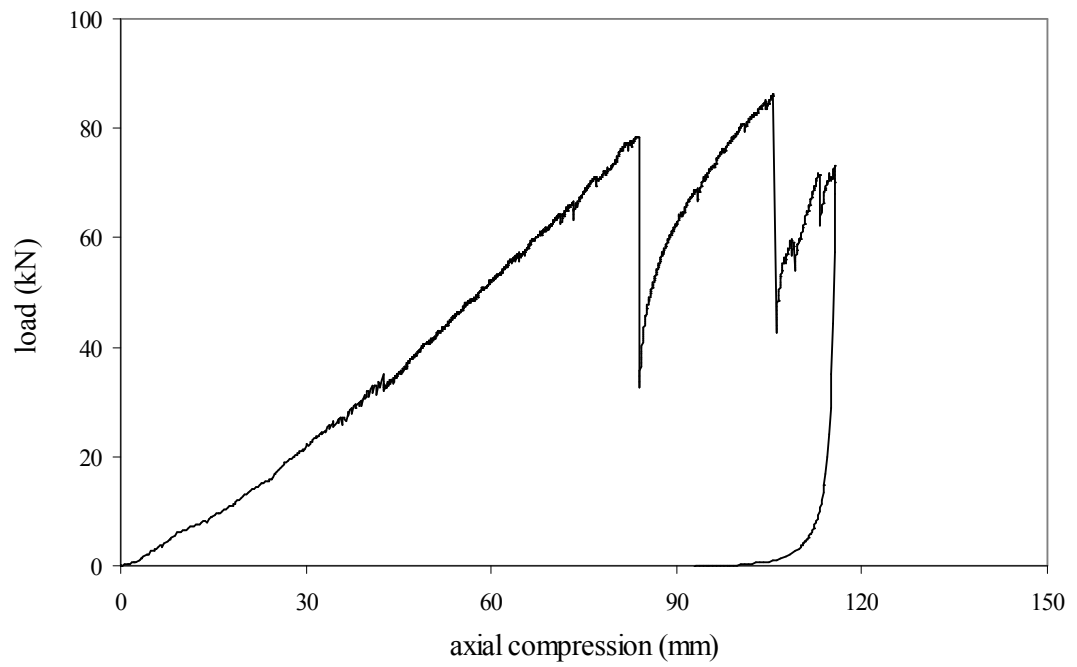




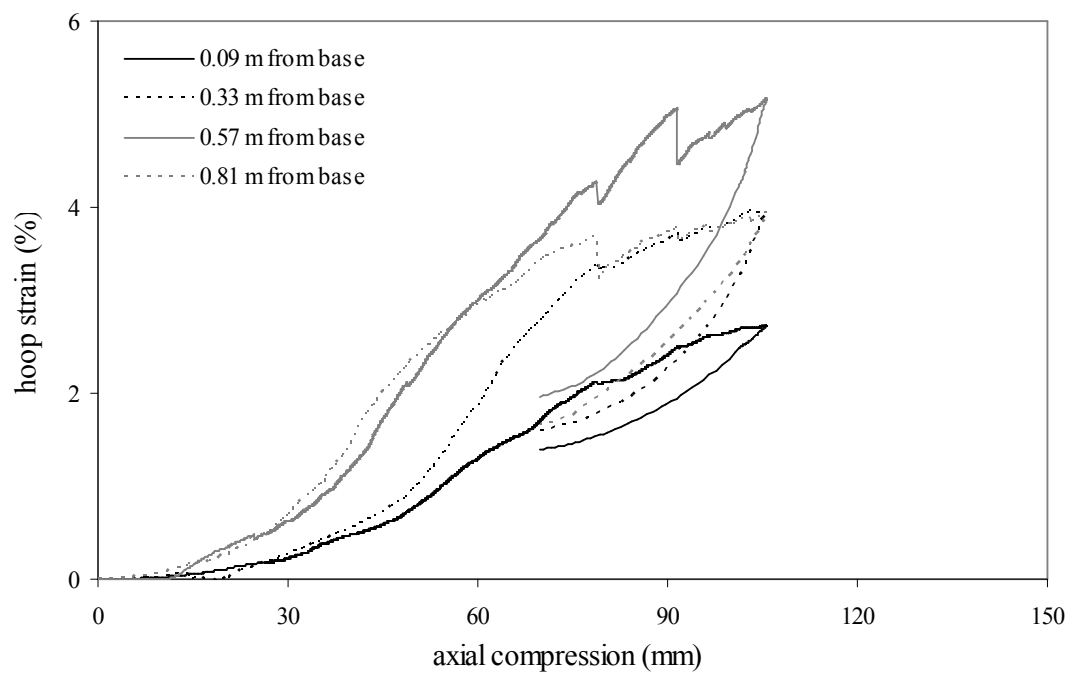
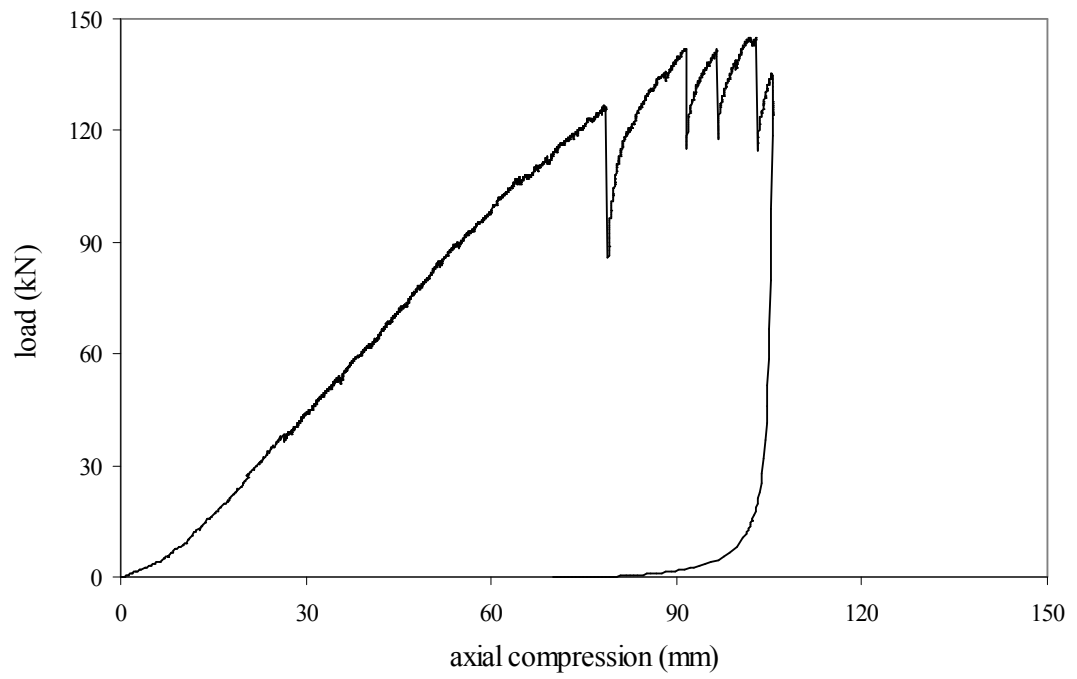
**Test No. 12**



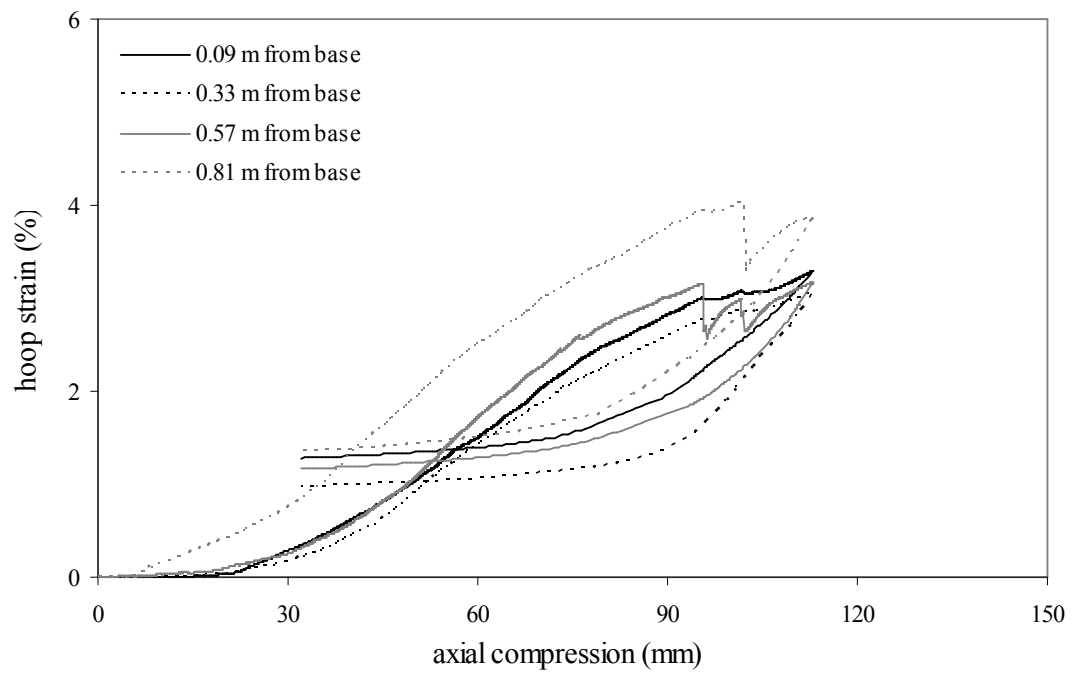
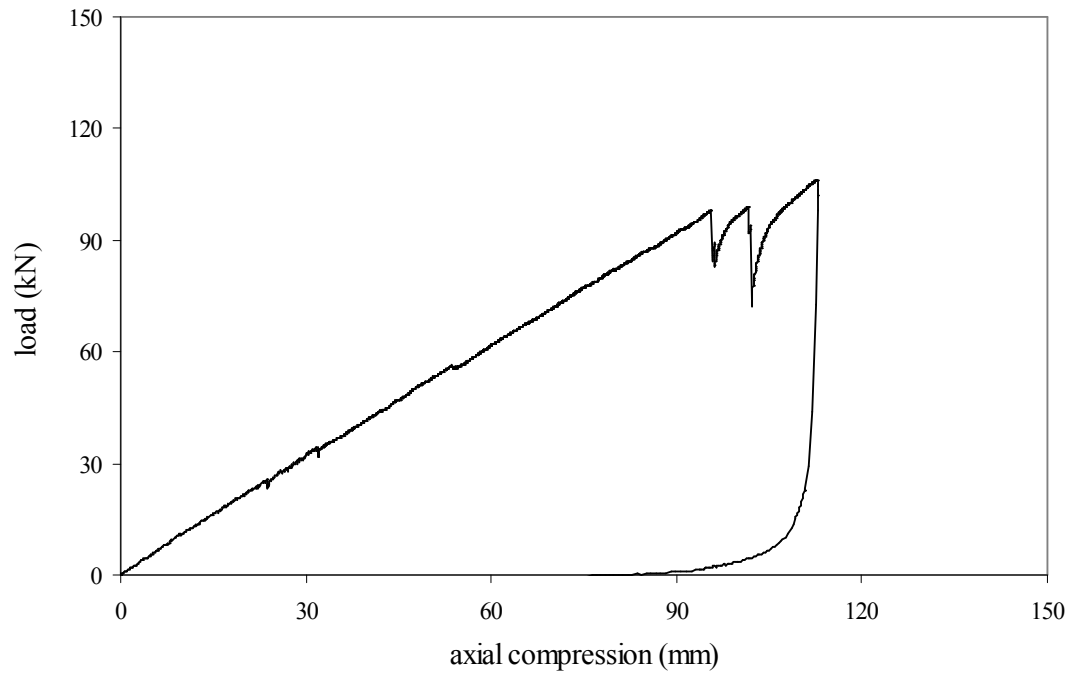
**Test No. 13**



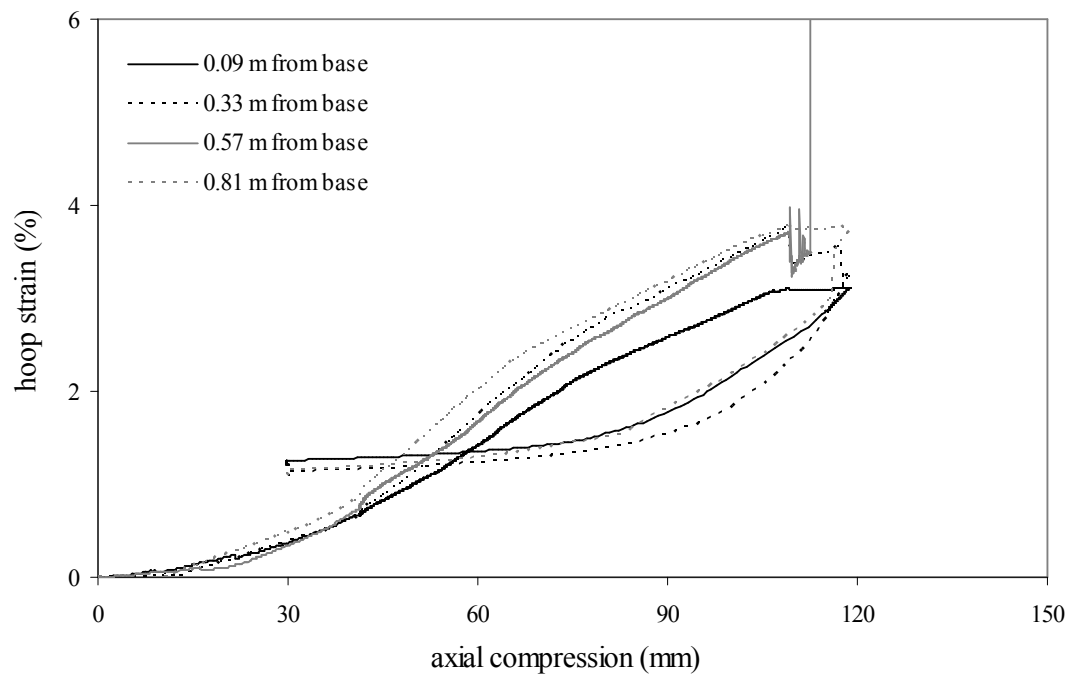
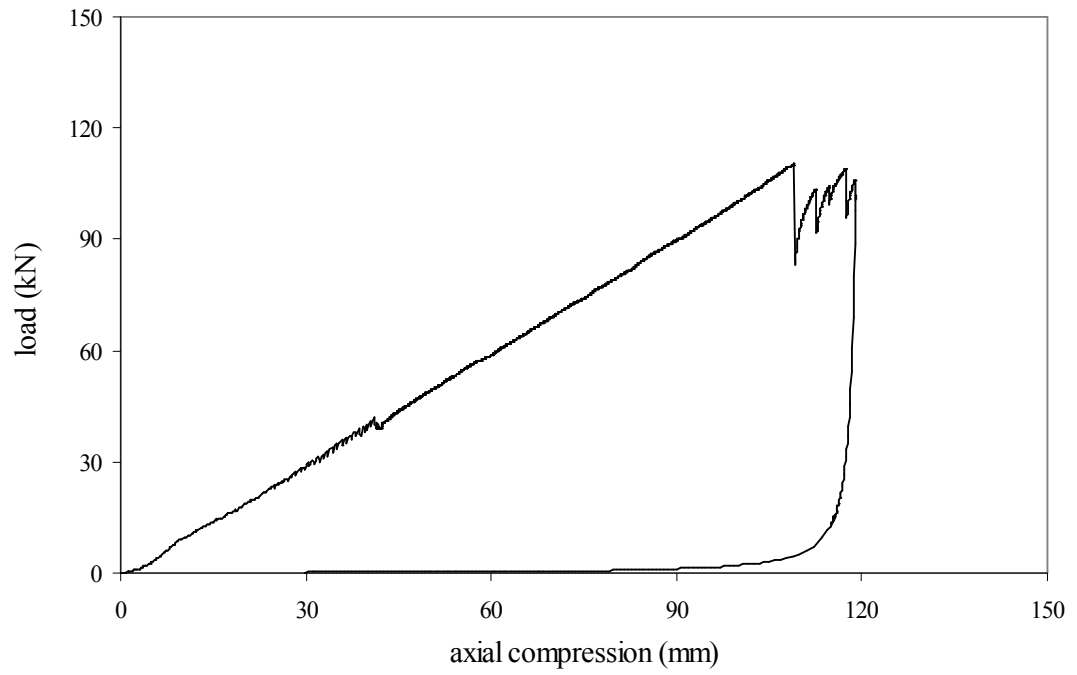
**Test No. 14**



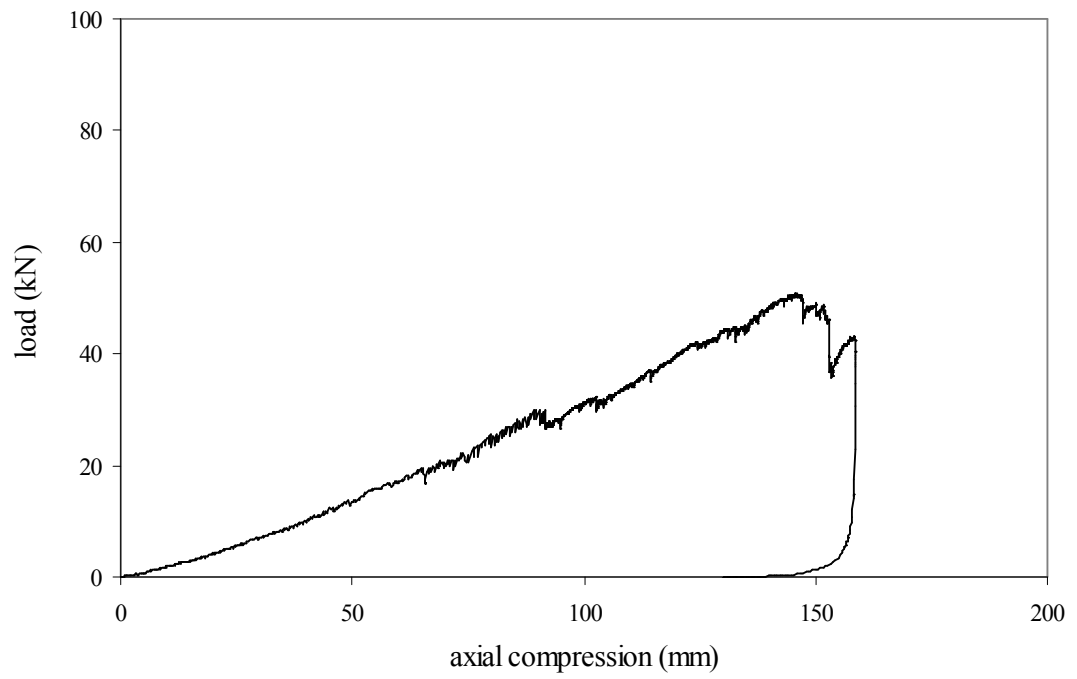
**Test No. 15**



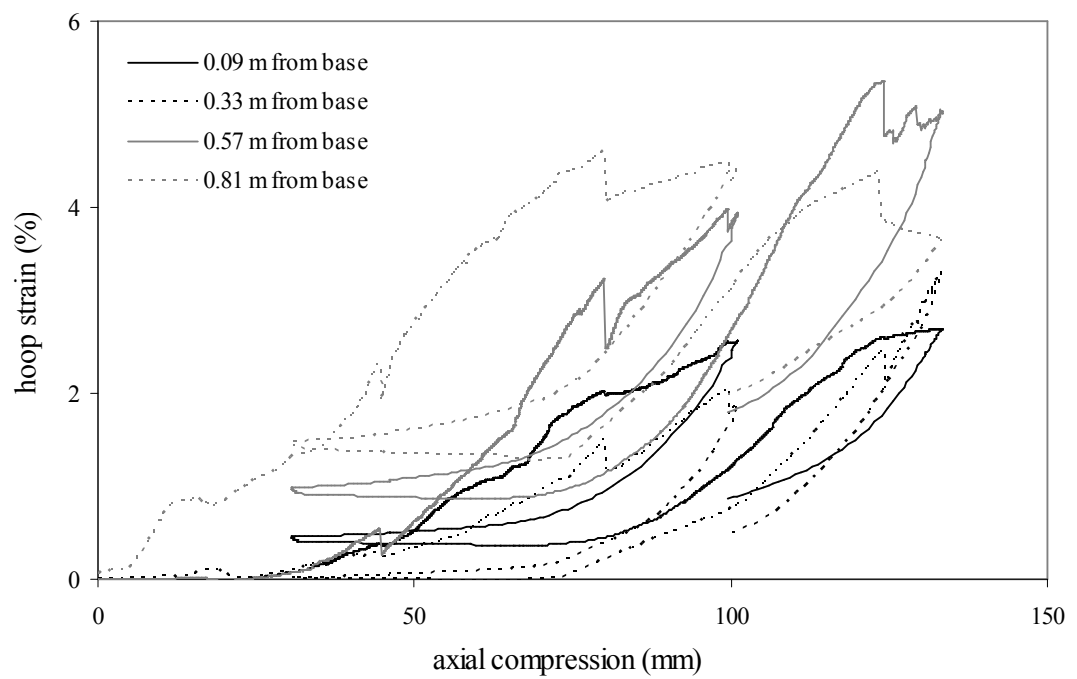
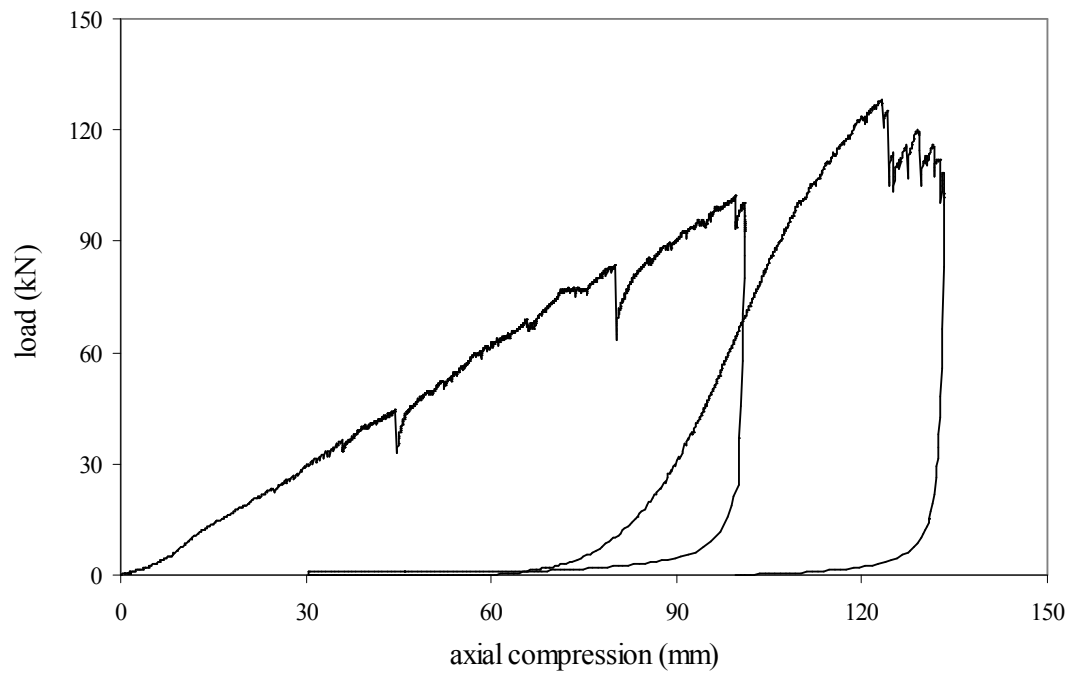
**Test No. 16**



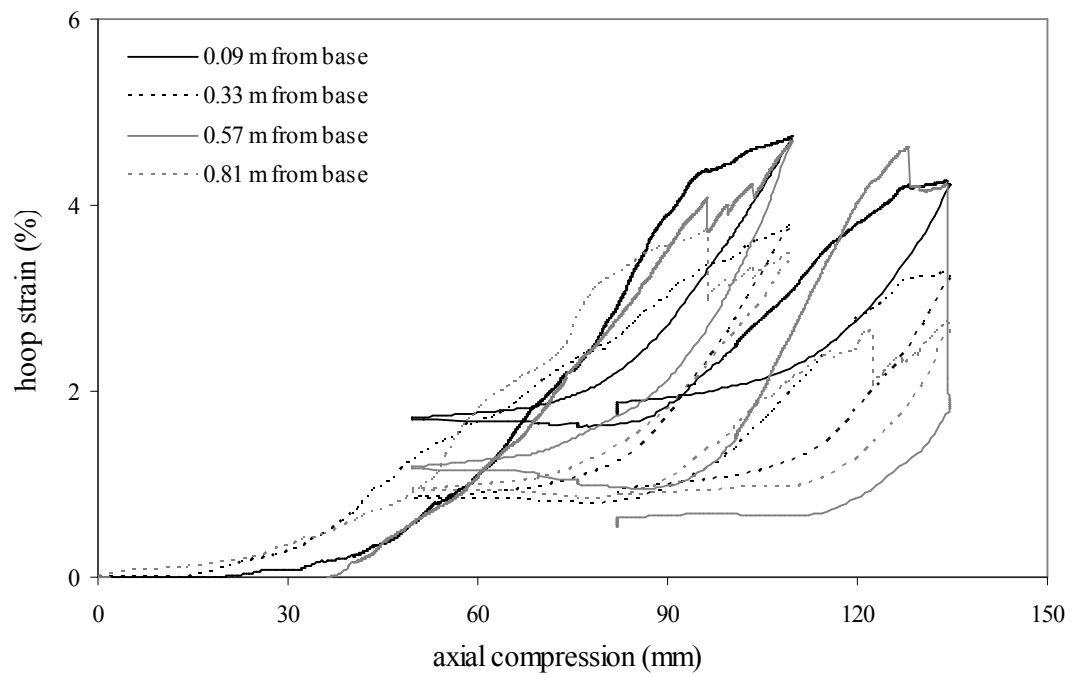
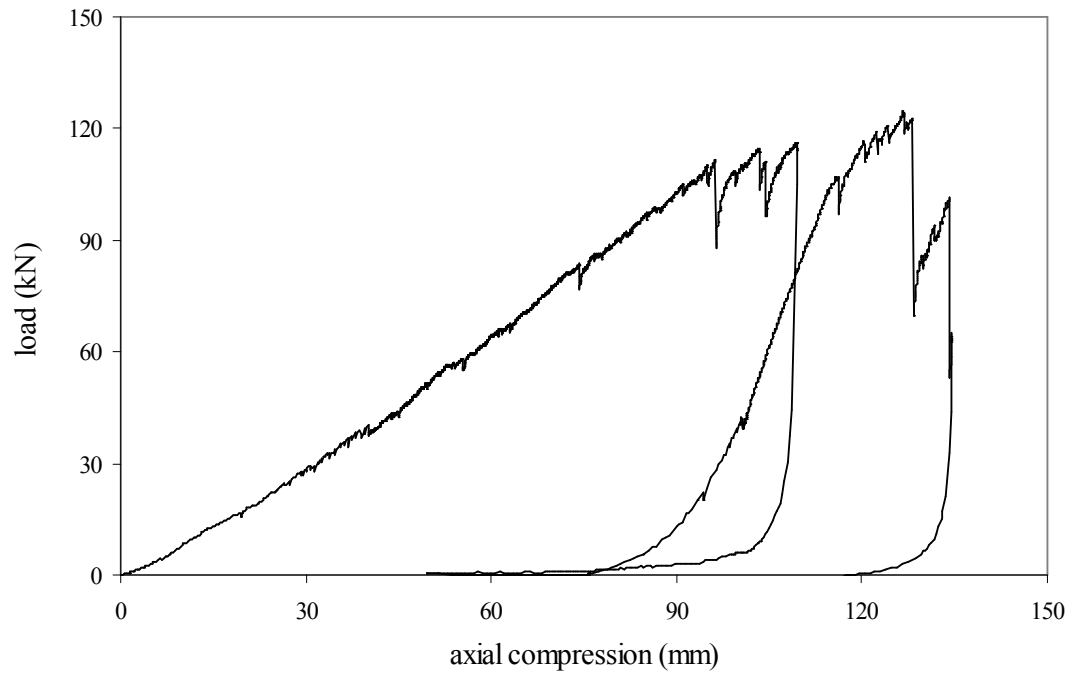
**Test No. 17**



**Test No. 18**



**Test No. 19**





**APPENDIX D.1**  
**(primary parametric study – parameters)**

## 1 Replacement ratio

Replacement ratios of  $A_r=15\%$ ,  $25\%$  and  $35\%$  were used in the base model and therefore parametric study. This range was considered to adequately cover most stone column applications.

## 2 Column stiffness

In addition to the lightly compacted stone column used in the base model, a heavily compacted column was modelled to investigate the impact on encased column behaviour. Like the lightly compacted column, the heavily compacted column was modelled as a Mohr-Coulomb material. The lightly compacted column was adopted to represent a loose gravel or sandy gravel material while the heavily compacted column was adopted to represent a medium-dense to dense, coarse crushed rock material (considered typical of stone column aggregates).

The strength parameters of the heavily compacted column were adjusted in accordance with those typical of medium-dense to dense crushed rock. The constrained modulus was double that of the lightly compacted material, in line with the large-scale oedometer test results presented in Figure 6.2 for dense rockfill and the modulus values calculated for columns in Chapter 5. Properties for the lightly and heavily compacted granular materials are presented in Table 1.

**Table 1:** Properties for lightly and heavily compacted column material

parameter	unit	value	
		lightly compacted column	heavily compacted column
Unit weight	kN/m <sup>3</sup>	21	22
Angle of internal friction, $\phi'$	°	37	45
Dilation, $\psi$	°	6	12
Cohesion, $c'$	kPa	0.1	0.1
Constrained modulus, $E_{oed}$	MPa	15	30
Poisson's ratio, $\nu$	-	0.3	0.3

### 3 Soil stiffness

Two types of soil were modelled in the primary parametric study:

- (i) CIS, considered representative of soft clay, and
- (ii) a material considered representative of a very soft clay.

The materials were likely to represent the range of soils in which encased columns were likely to be installed. The properties of these soils are presented in Table 2.

**Table 2:** Properties for very soft and soft soil (CIS)

parameter	unit	value	
		very soft soil	CIS
Unit weight	kN/m <sup>3</sup>	14	16
Angle of internal friction, $\phi'$	°	25	30
Dilation, $\psi$	°	0	0
Cohesion, $c'$	kPa	1	2
Initial void ratio, $e_0$	-	3.5	2.0
Compression index, $C_c$	-	1.5	0.8
Recompression index, $C_r$	-	0.2	0.08
Pre-consolidation pressure	kPa	5	10

### 4 Geogrid stiffness and strength

Three types of geogrid with different stiffness and strength were used in the primary parametric study to investigate the impact of geogrid properties on encased column behaviour. The properties were based on three different geogrids supplied by NAUE GmbH. The geogrids were selected from the Secugrid® range of products, which comprise geogrid ribs formed from polyester. The ribs are mechanically welded to form junctions arranged in square or rectangular geometric patterns. Q6 and R6 products generally comprise biaxial and uniaxial geogrids, respectively, with R6 products generally having the highest strength and stiffness.

Secugrid® products were considered most suited to use as encasement material and the properties of the three geogrids used in this study are presented in Table 3. The typical load-strain behaviour of these geogrids is presented in Figure 1, and indicates varying stiffness during loading for both products. As non-linear behaviour of the geogrid could

not easily be incorporated into the PLAXIS model, an average elastic axial stiffness was used to approximate the geogrid behaviour.

**Table 3:** Properties of geogrid used in parametric study

geogrid	tensile strength (kN/m)	EA (kN/m)
Secugrid UTS=60 kN/m (Q6)	60	1030
Secugrid UTS=100 kN/m (Q6)	100	1670
Secugrid UTS=200 kN/m (R6)	200	3440

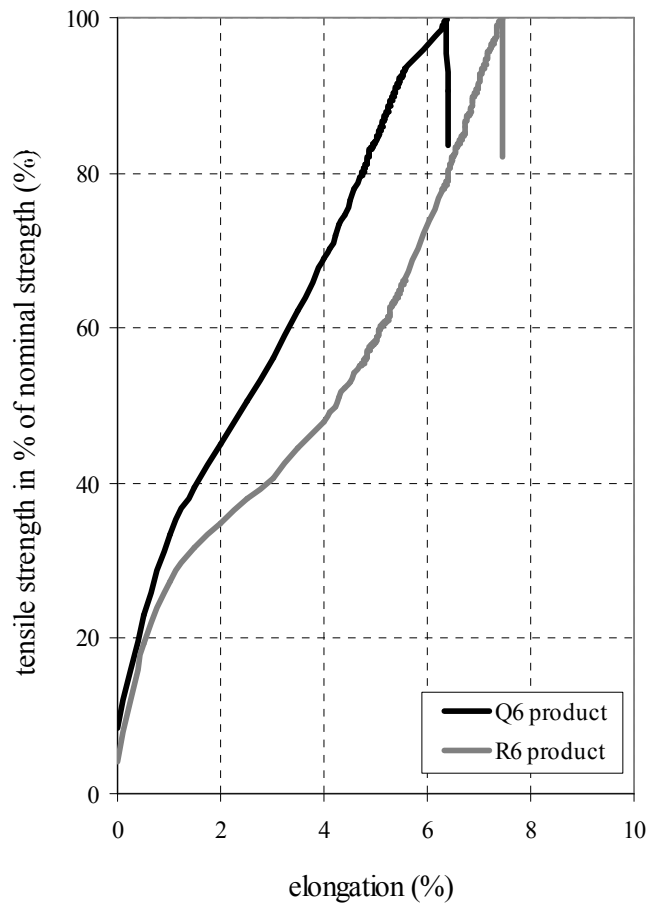


**Figure 1:** Typical load-strain behaviour of Secugrid® products

## 5 Percent encased length

Partial encasement of geogrid encased columns was investigated in small-scale laboratory testing, presented in Chapter 3. The impact of encasing the upper 25%, 50% and 100% (fully encased) of the column was investigated in the primary parametric study.

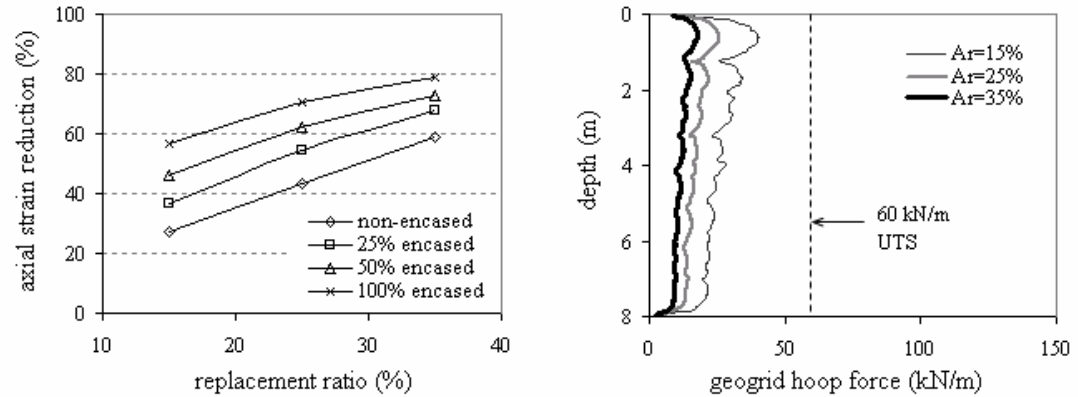
## **6            Surcharge pressure**

The height of soil fill, or surcharge pressure, was likely to affect the confinement provided to the columns and therefore their stress state. The impact of surcharge pressure was investigated in the primary parametric study by using two load cases. The first was application of 4 m of soil fill (corresponding to about 80 kPa surcharge) and the second was an 8 m of soil fill (corresponding to about 160 kPa surcharge).

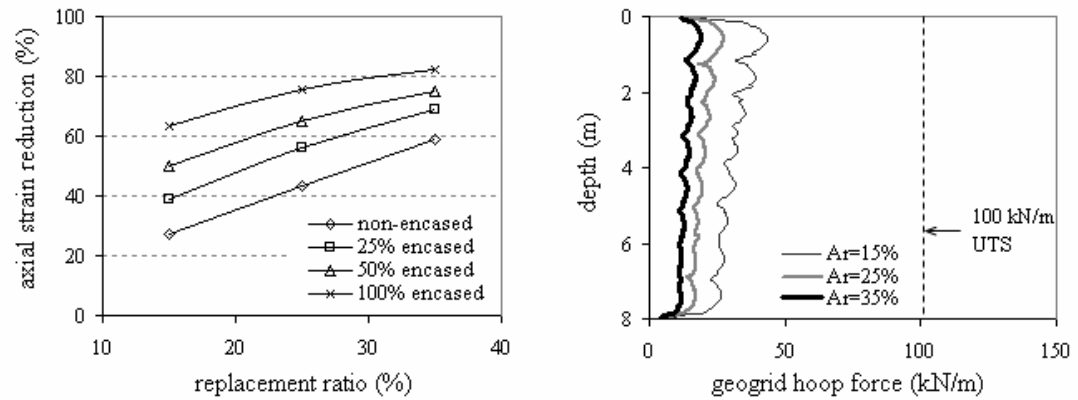
**APPENDIX D.2**  
**(primary parametric study – charts)**

**Load:** 80 kPa surcharge (4 m soil fill)  
**Soil:** Soft clay (Coode Island Silt)  
**Column:** Lightly compacted

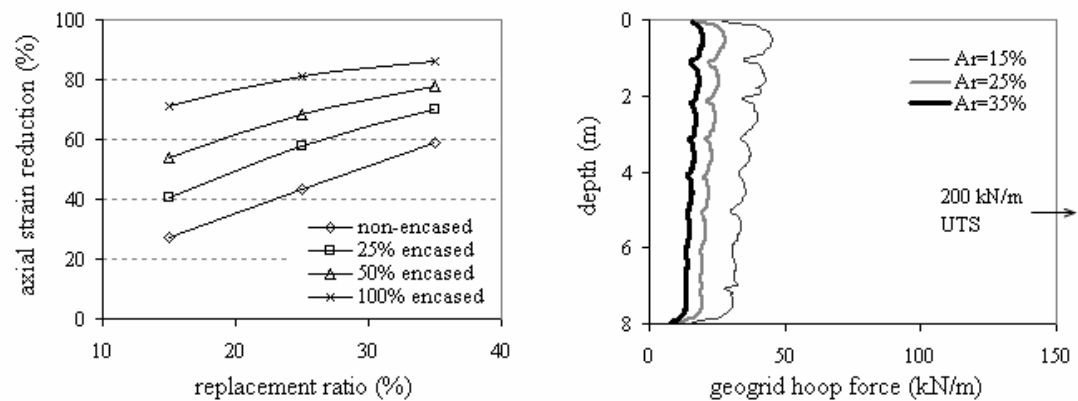
Geogrid #1: Secugrid with 60 kN/m UTS in hoop direction



Geogrid #2: Secugrid with 100 kN/m UTS in hoop direction

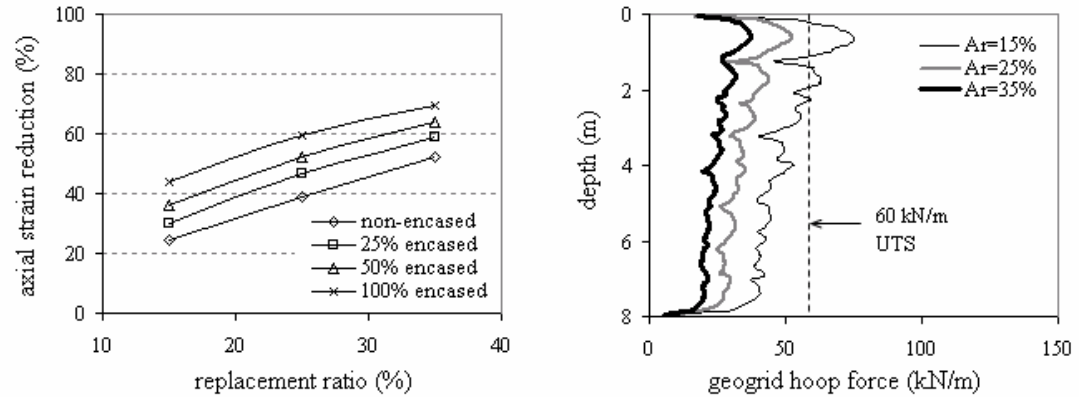


Geogrid #3: Secugrid with 200 kN/m UTS in hoop direction

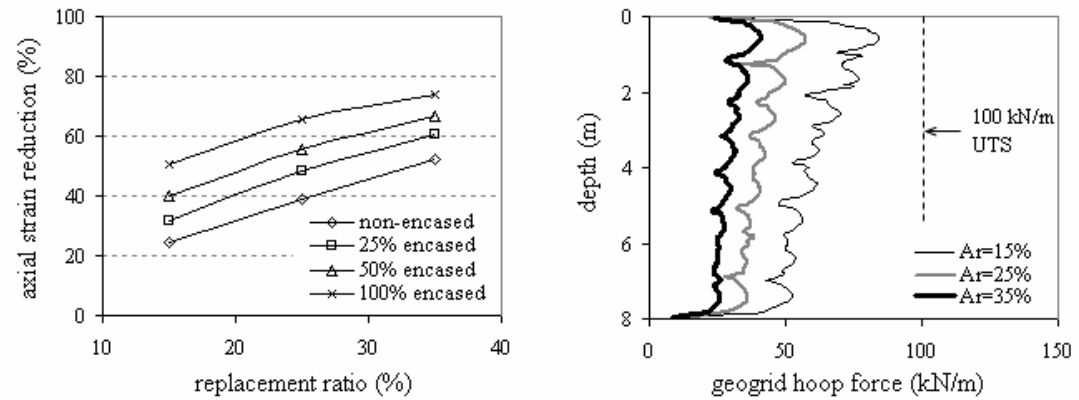


**Load:** 160 kPa surcharge (8 m soil fill)  
**Soil:** Soft clay (Coode Island Silt)  
**Column:** Lightly compacted

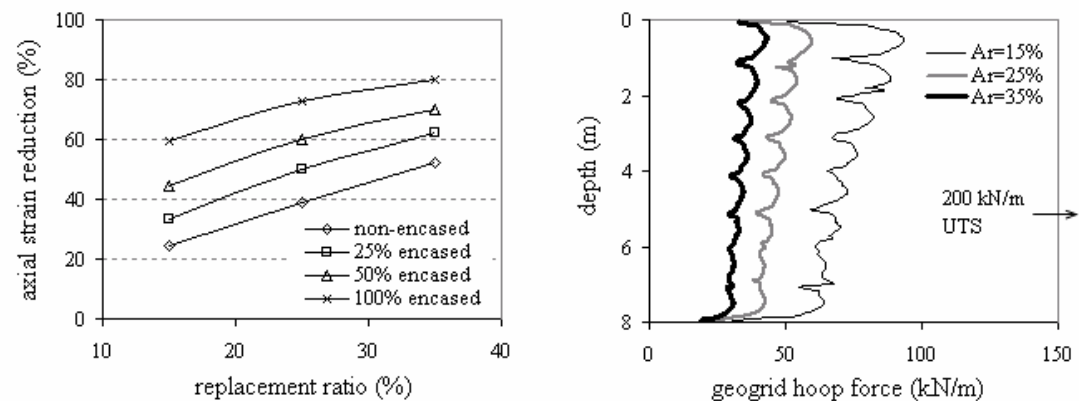
Geogrid #1: Secugrid with 60 kN/m UTS in hoop direction



Geogrid #2: Secugrid with 100 kN/m UTS in hoop direction



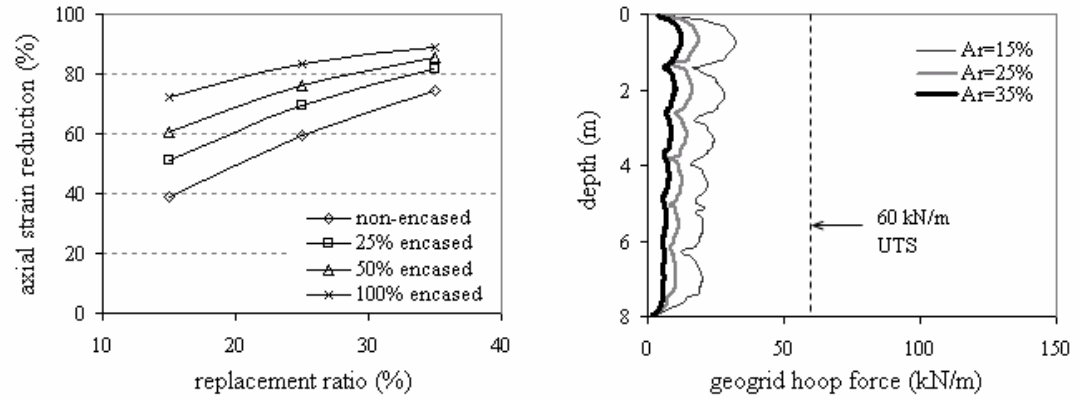
Geogrid #3: Secugrid with 200 kN/m UTS in hoop direction



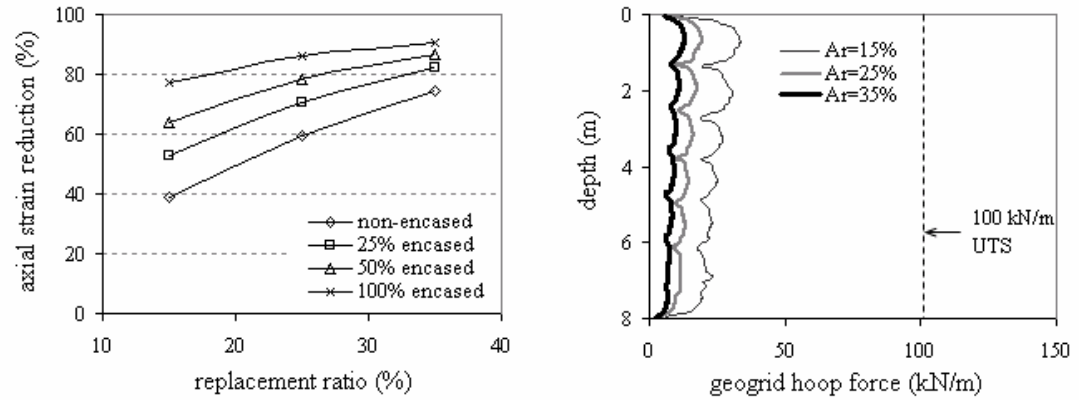


**Load:** 80 kPa surcharge (4 m soil fill)  
**Soil:** Soft clay (Coode Island Silt)  
**Column:** Heavily compacted

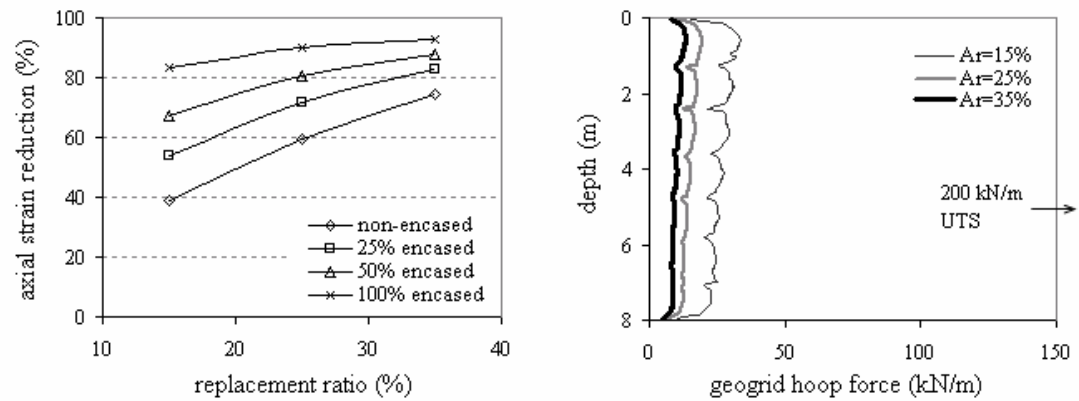
Geogrid #1: Secugrid with 60 kN/m UTS in hoop direction



Geogrid #2: Secugrid with 100 kN/m UTS in hoop direction

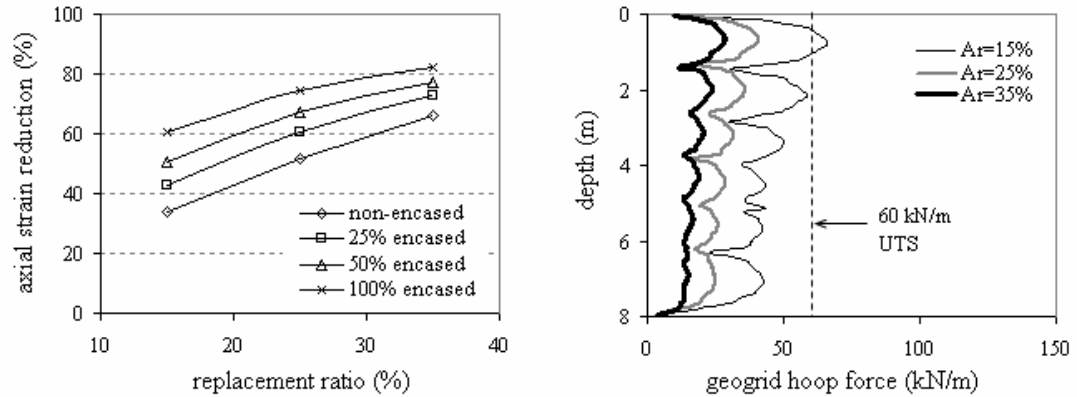


Geogrid #3: Secugrid with 200 kN/m UTS in hoop direction

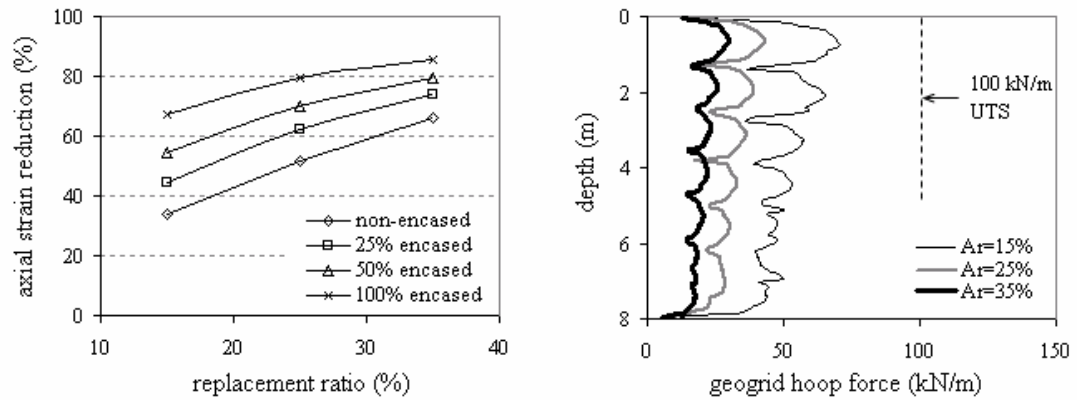


**Load:** 160 kPa surcharge (8 m soil fill)  
**Soil:** Soft clay (Coode Island Silt)  
**Column:** Heavily compacted

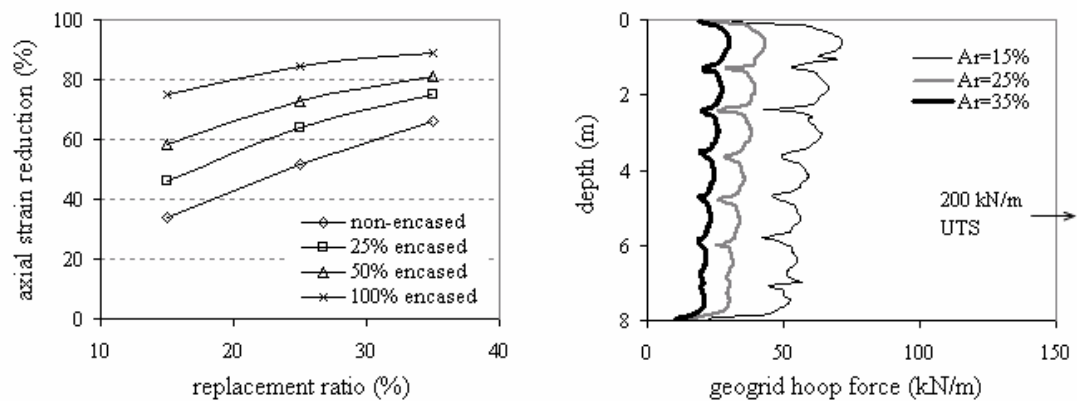
Geogrid #1: Secugrid with 60 kN/m UTS in hoop direction



Geogrid #2: Secugrid with 100 kN/m UTS in hoop direction

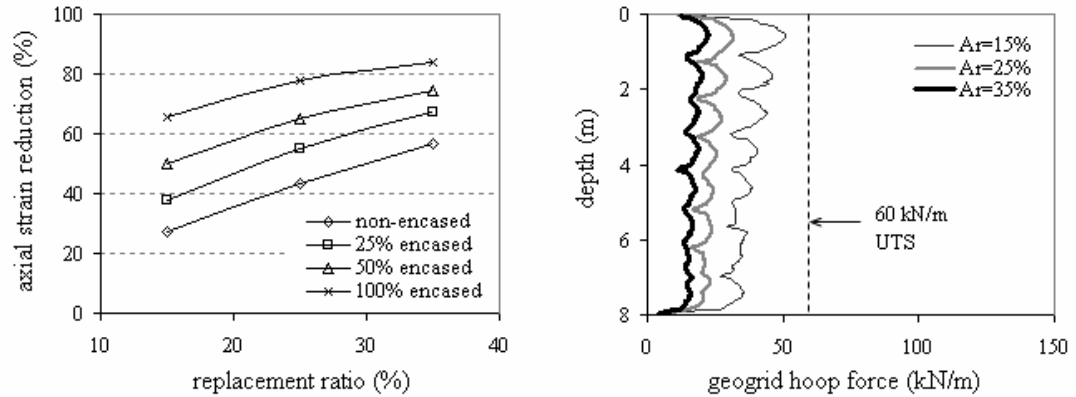


Geogrid #3: Secugrid with 200 kN/m UTS in hoop direction

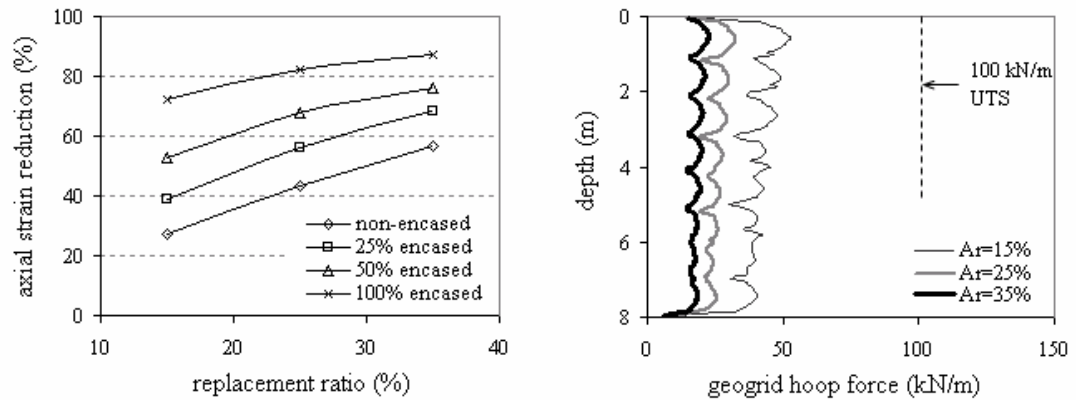


**Load:** 80 kPa surcharge (4 m soil fill)  
**Soil:** Very soft clay  
**Column:** Lightly compacted

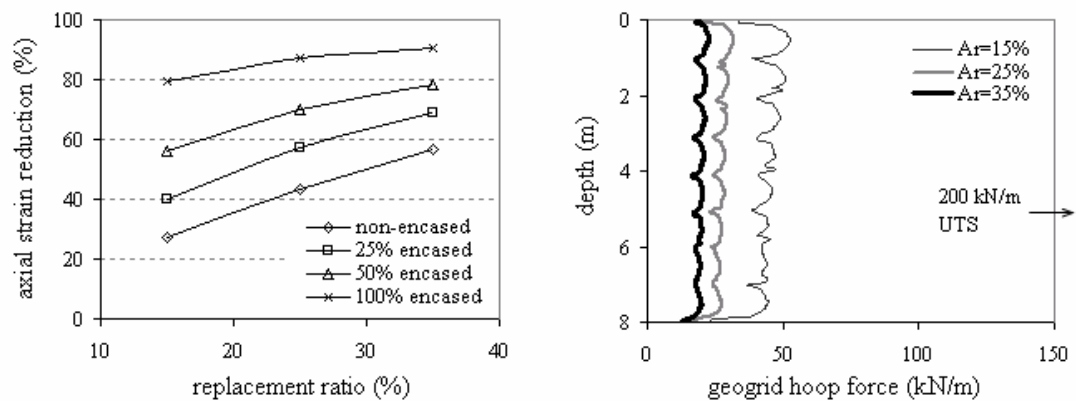
Geogrid #1: Secugrid with 60 kN/m UTS in hoop direction



Geogrid #2: Secugrid with 100 kN/m UTS in hoop direction

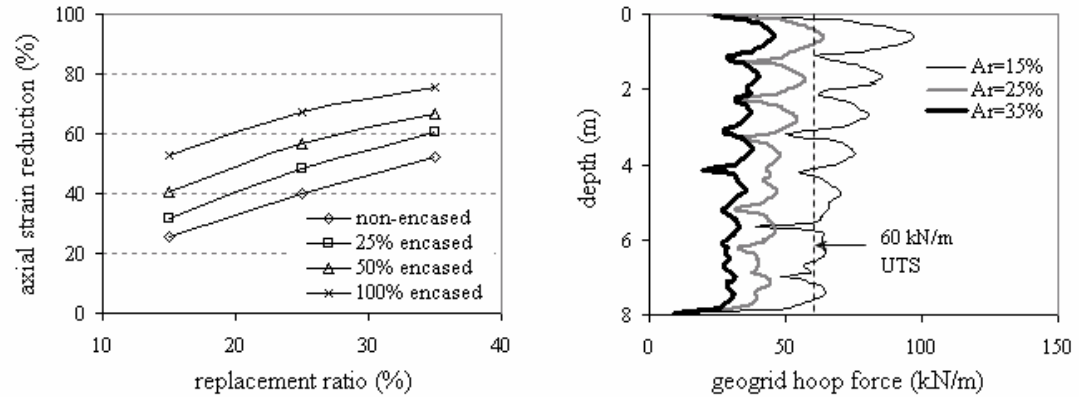


Geogrid #3: Secugrid with 200 kN/m UTS in hoop direction

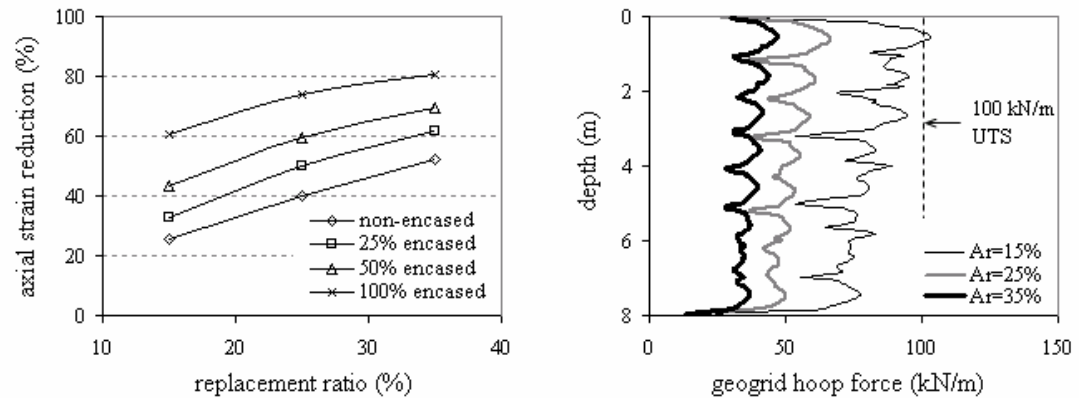


**Load:** 160 kPa surcharge (8 m soil fill)  
**Soil:** Very soft clay  
**Column:** Lightly compacted

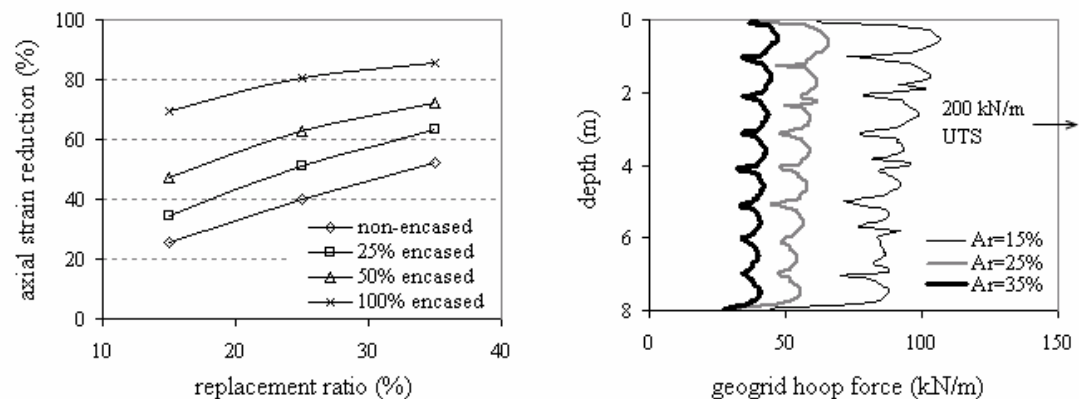
Geogrid #1: Secugrid with 60 kN/m UTS in hoop direction



Geogrid #2: Secugrid with 100 kN/m UTS in hoop direction

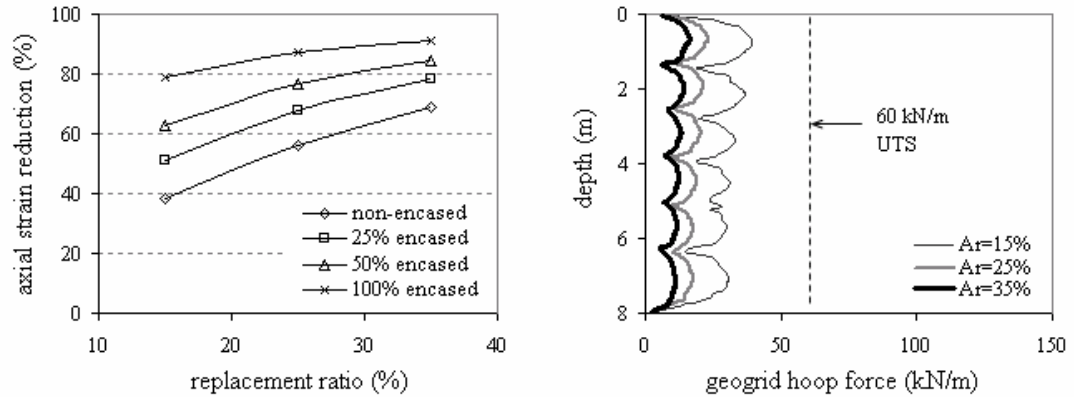


Geogrid #3: Secugrid with 200 kN/m UTS in hoop direction

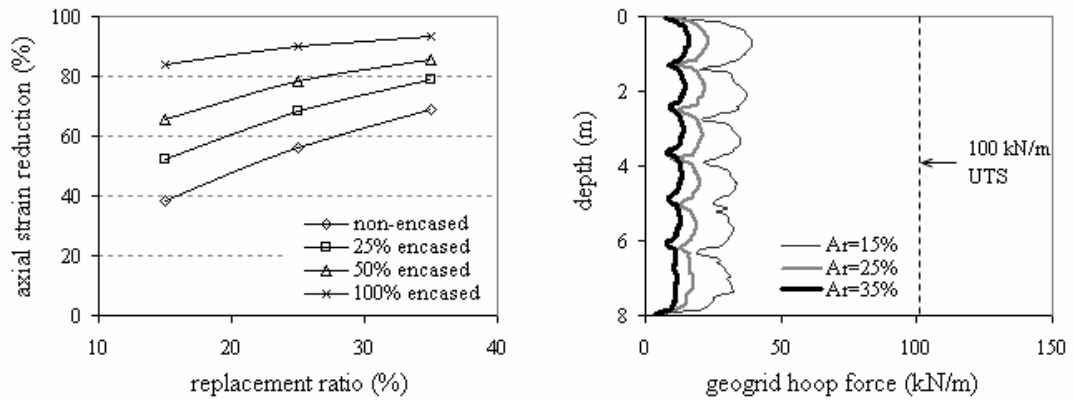


**Load:** 80 kPa surcharge (4 m soil fill)  
**Soil:** Very soft clay  
**Column:** Heavily compacted

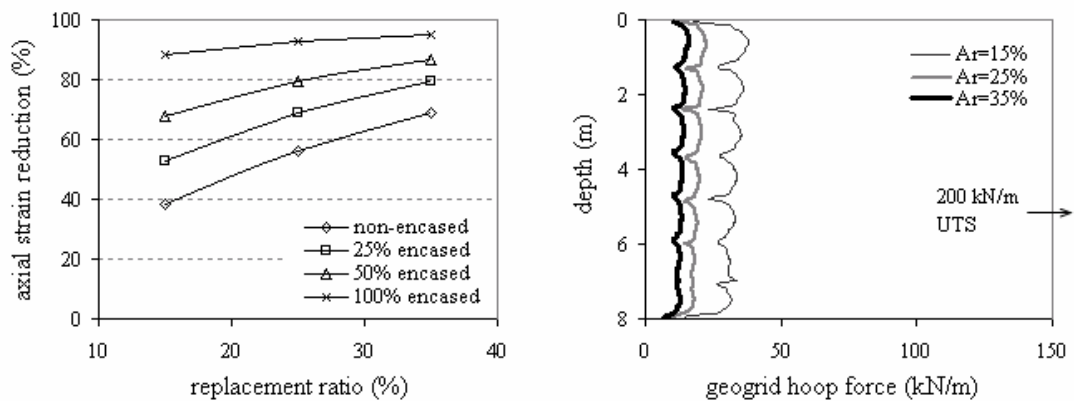
Geogrid #1: Secugrid with 60 kN/m UTS in hoop direction



Geogrid #2: Secugrid with 100 kN/m UTS in hoop direction

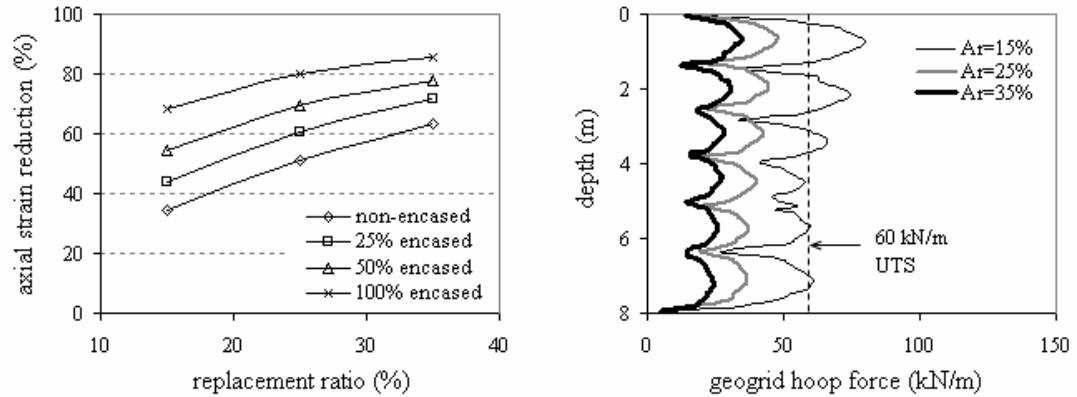


Geogrid #3: Secugrid with 200 kN/m UTS in hoop direction

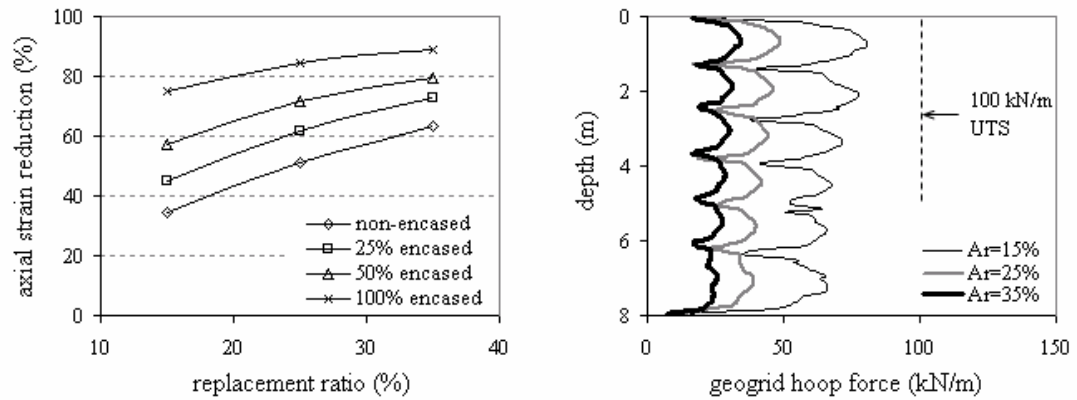


**Load:** 160 kPa surcharge (8 m soil fill)  
**Soil:** Very soft clay  
**Column:** Heavily compacted

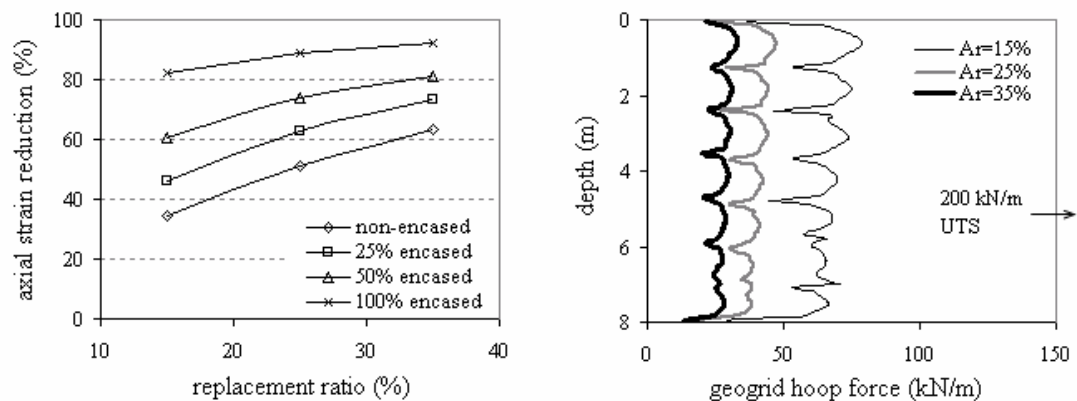
Geogrid #1: Secugrid with 60 kN/m UTS in hoop direction



Geogrid #2: Secugrid with 100 kN/m UTS in hoop direction



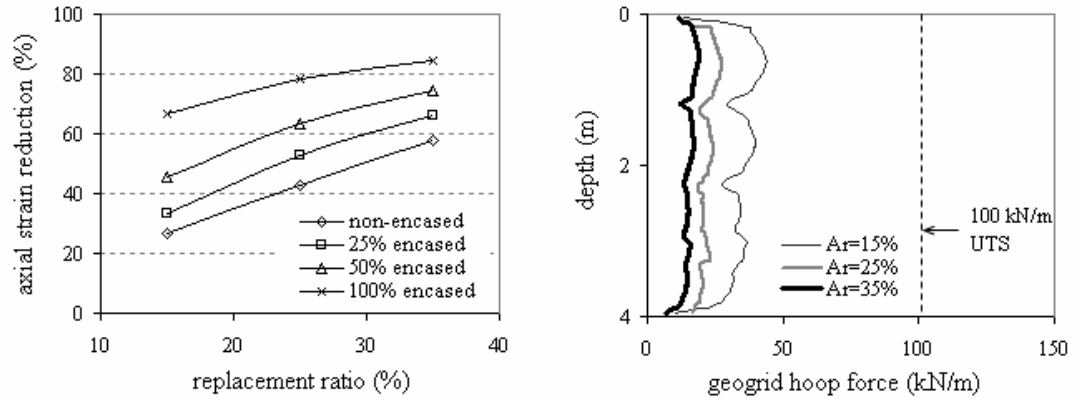
Geogrid #3: Secugrid with 200 kN/m UTS in hoop direction



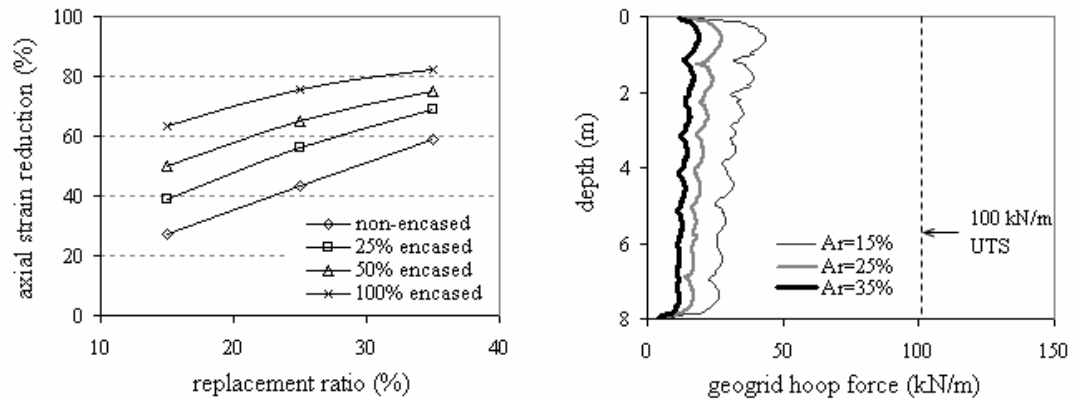
**APPENDIX D.3**  
**(secondary parametric study – charts)**

**Load:** 80 kPa surcharge (4 m soil fill)  
**Soil:** Soft clay (Coode Island Silt)  
**Column:** Lightly compacted  
**Geogrid:** Secugrid with 100 kN/m UTS in hoop direction

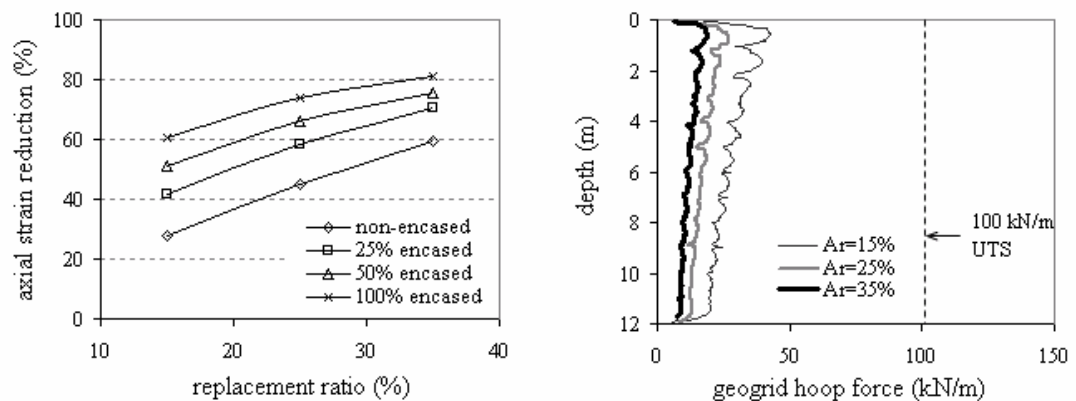
#### 4m deep column



#### 8m deep column



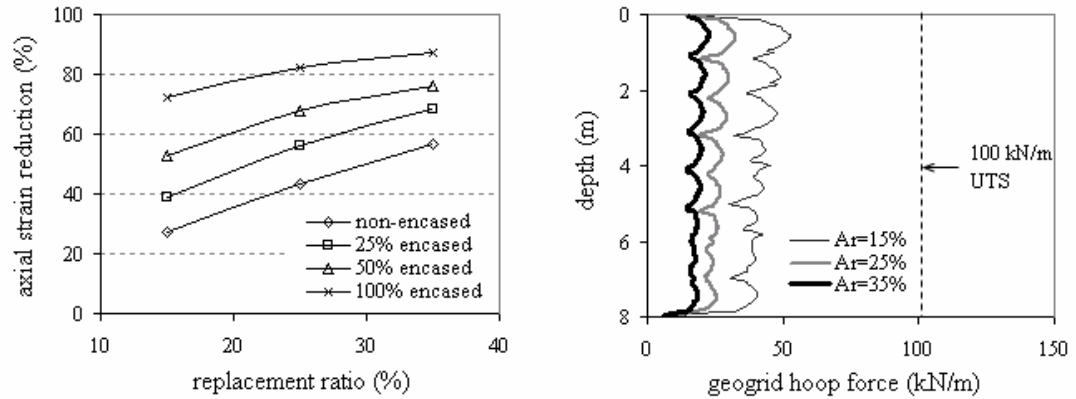
#### 12m deep column



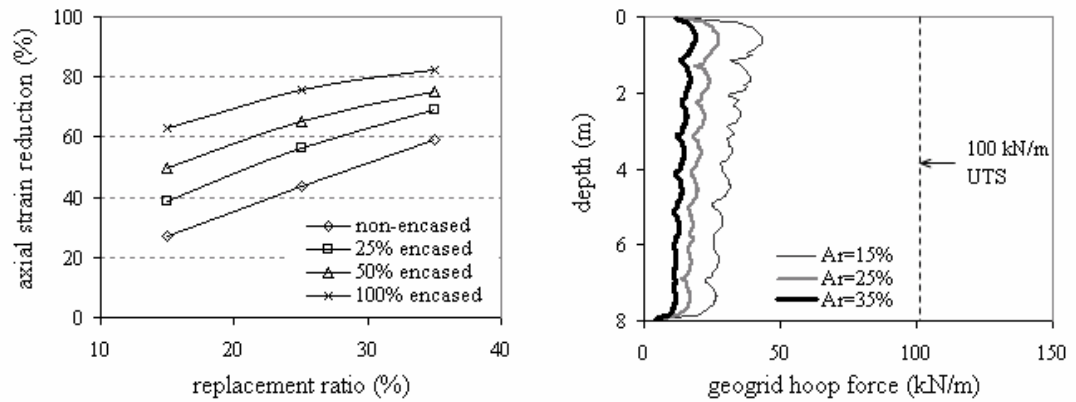


**Load:** 80 kPa surcharge (4 m soil fill)  
**Column:** Lightly compacted  
**Geogrid:** Secugrid with 100 kN/m UTS in hoop direction

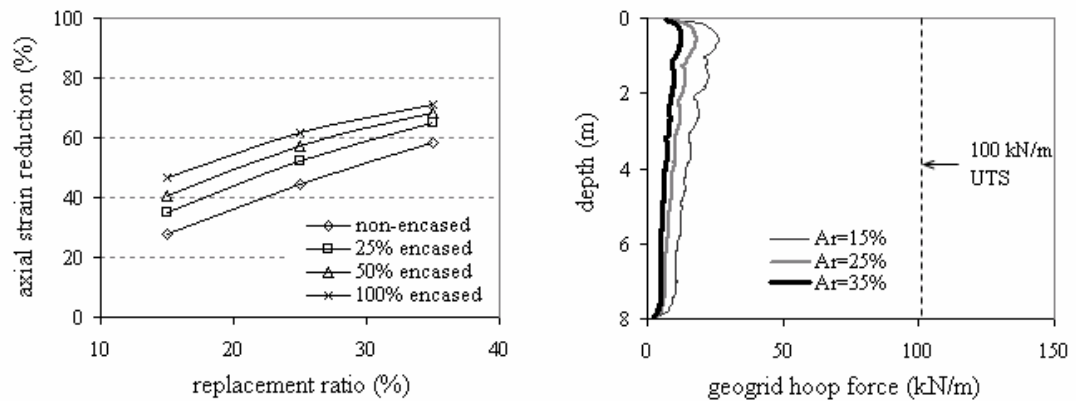
Very soft clay



Soft clay (Coode Island Silt)

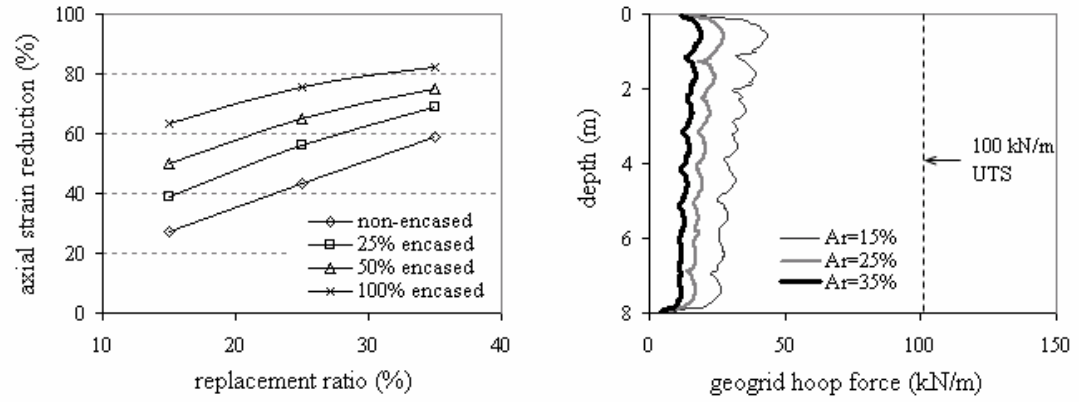


Firm clay



**Load:** 80 kPa surcharge (4 m soil fill)  
**Soil:** Soft clay (Coode Island Silt)  
**Column:** Lightly compacted  
**Geogrid:** Secugrid with 100 kN/m UTS in hoop direction

#### Replacement technique



#### Displacement technique

